NUCLEAR TRACKS

Space Physics
Geophysics
and
Nuclear Physics

Published by

INDIAN ACADEMY OF SCIENCES
BANGALORE

NUCLEAR TRACKS

Cover Photograph:

A mosaic of photomicrographs of nuclear tracks produced by solar flare and galactic cosmic ray heavy nuclei, by fission of uranium, and by heavy ion beam from accelerator in different mineral and plastic detectors.

NUCLEAR TRACKS

(RESEARCHES IN SPACE PHYSICS, GEOPHYSICS AND NUCLEAR PHYSICS)

Edited by

J. N. GOSWAMI

Physical Research Laboratory, Ahmedabad

INDIAN ACADEMY OF SCIENCES

Bangalore 560 080

Reprinted from the Proceedings of the Indian Academy of Sciences
(Earth and Planetary Sciences), Volume 90, pp. 337–460, December 1981

Edited by J. N. Goswami and printed for the Indian Academy of Sciences
by Macmillan India Press, Madras 600 002, India

Foreword

The nuclear track technique, developed by R. L. Fleischer, P. B. Price and R. M. Walker in the early 60's, has found significant application in a wide variety of research fields including Nuclear Physics, Cosmic Rays, Planetary and Space Sciences, Geophysics, Geochronology, Biophysics and several branches of applied sciences. The wide applications of this technique arise from the fact that wide range of natural and artificial detector materials, having very different properties to suit the experimental requirements are available.

Work on nuclear etch-tracks was initiated in India at the Tata Institute of Fundamental Research, Bombay in 1965 coincident with a visit of Prof. P. B. Price. At that time, the work mainly concerned with the study of cosmic ray prehistory using meteorite samples. Work on geochronology using the fission track method was soon followed and was taken up as a major project at the Kurukshetra University. At present, there are more than twenty institutes and universities engaged in different fields of research using the nuclear etch-track technique. They include the Physical Research Laboratory, Ahmedabad; the Tata Institute of Fundamental Research, Bombay; the Bhabha Atomic Research Centre, Bombay; the Kurukshetra University, Kurukshetra; the Indian Institute of Technology, Kanpur; the Aligarh Muslim University, Aligarh; the Banaras Hindu University, Varanasi; the Panjab University, Chandigarh; the Guru Nanak Dev University, Amritsar; the Gauhati University, Gauhati; and the Poona University, Poona, among others.

Considering the involvement of a large number of Indian scientists in the use and application of the nuclear track technique, the Bhabha Atomic Research Centre, organised the first national seminar-cum-workshop on the use and application of solid state nuclear track detectors (SSNTD) in March, 1979. It was decided to hold such seminars on a biennial basis and the second national seminar-cum-workshop was hosted by the Physical Research Laboratory, during 24–26 February, 1981. The scope of this meeting was enlarged to include both topical reviews as well as contributed papers on different subjects. Panel discussions on subjects of current research interest were also organised as a part of the workshop. About eighty scientists from different institutes and universities, participated in the seminar. The seminar was also vitalised by the active participation of several scientists from USA, France and USSR, including Prof. R. M. Walker, who alongwith Profs. P. B. Price and R. L. Fleischer pioneered the development and application of the nuclear track technique.

Prior to the organisation of this seminar at PRL, it was proposed that the key papers presented at this seminar should be published for the benefit of the research

workers involved in this field in India. The idea was to have a volume that can be used as a reference or as a source book by the research workers in this field. Accordingly, the organizers have solicited articles from several of the participating scientists and have also approached the Indian Academy of Sciences for help in publishing such a volume. It is opportune to acknowledge gratefully the acceptance of this proposal by the General Editor, Publications, Indian Academy of Sciences.

The present volume contains seven key papers presented in the various sessions and the panel discussions organized during the seminar-cum-workshop. These papers authored by Indian and foreign scientists cover a wide spectrum of topics including researches in lunar and meteorite samples, geochronology, contemporary and ancient energetic particles in the interplanetary space and studies on nuclear fission. All the papers were refereed following the usual procedures adopted for publication in the *Proceedings of Indian Academy of Sciences*.

The scope for carrying out research work in the field of space sciences, geochronology and nuclear physics in India using the nuclear track technique is enormous. The current work being carried out at the Tata Institute of Fundamental Research in the field of solar physics, specially the study of solar flare elemental composition using plastics as detectors has contributed significantly towards our understanding of the acceleration and propagation mechanisms of solar flare particles. Collaborative work between the TIFR and PRL scientists, specifically the analysis of cosmic ray tracks recorded in a lexan detector stack exposed in space during 1973–74 during the SKYLAB-III mission led to the observation of the anomalous cosmic ray component in near earth orbit. Prof. Biswas and his colleagues have discussed the possible source and origin of this component in an article in this volume. Further work in this direction using the SPACELAB platform has already been planned and a plastic detector payload is scheduled to be flown during the SPACELAB-III mission in 1984.

Studies of meteorite and lunar samples, using the nuclear etch-track technique have provided valuable insight into a wide variety of topics that include cosmic ray prehistory, exposure and evolutionary history of lunar samples and meteorites, thermal history of meteorite parent bodies, early irradiation and accretionary history of solar system objects, and atmospheric ablation processes. Some of these aspects are dealt with in three articles in this volume by Drs. G. Crozaz, N. Bhandari and J. N. Goswami. Additional information based on radionuclide and mass-spectrometric studies which complement the track-based studies are also discussed in these articles. In spite of the large volume of data available, certain aspects, particularly those related to early evolutionary history of the solar system, deserve further attention.

Application of nuclear track technique in fission studies covers a wide spectrum of subjects e.g. determination of extremely short half-lives, reaction cross-section studies, properties of fission isomers and search for the still elusive superheavy nuclei. The present status of these studies, have been reviewed in an article in

this volume by Dr. R. H. Iyer. Opportunities for pursuing research problems in the field of nuclear physics will definitely increase with the variable energy cyclotron at Calcutta reaching routine operational phase.

Fission track geochronology is an attractive field for many researchers since it is a simple and straightforward method, and involves minimum requirements of instrument and other facilities, apart from a thermal neutron source. With the Bhabha Atomic Research Centre providing routine facilities for thermal neutron irradiation, it is not surprising that a majority of research workers in India involved in nuclear track studies are actively pursuing this field of research. Prof. K. K. Nagpaul has highlighted the significant aspects of the fission track geochronology of the Indian sub-continent in his article. The problem of proper interpretation of fission track data, which was the theme of a panel discussion during the seminar, has been thoroughly treated in the article by Dr. G. Poupeau. It is important for the research workers in this field to be aware of these problems and make sure that proper care is taken in interpretation of the fission track data in terms of the geological evolutionary history of a given region.

It is interesting to note that in spite of the vast amount of information obtained through the use of SSNTD, we do not yet know the track formation mechanism and even the basics of track etching processes. Understanding these basic processes should lead to a whole new range of applications of SSNTD. Much more work remains to be done in several fields in which SSNTD has found its application. For example, quantitative understanding of track annealing behaviour in minerals should prove valuable for extracting meaningful information from fission track studies. Development of new detectors with improved response and charge resolution will also be an important step forward. The developments in the field of SSNTD in India has been rather slow in recent years primarily due to a lack of freshness in approach but it is hoped that the present volume as well as the February, 1981 biennial get together of the Indian trackologists to exchange views and ideas will go a long way in changing this trend.

D. LAL

Physical Research Laboratory
Ahmedabad.

Group photograph of the participants in the second national seminar-cum-workshop on SSNTD held at the Physical Research Laboratory, Ahmedabad.
(February 24-26, 1981)

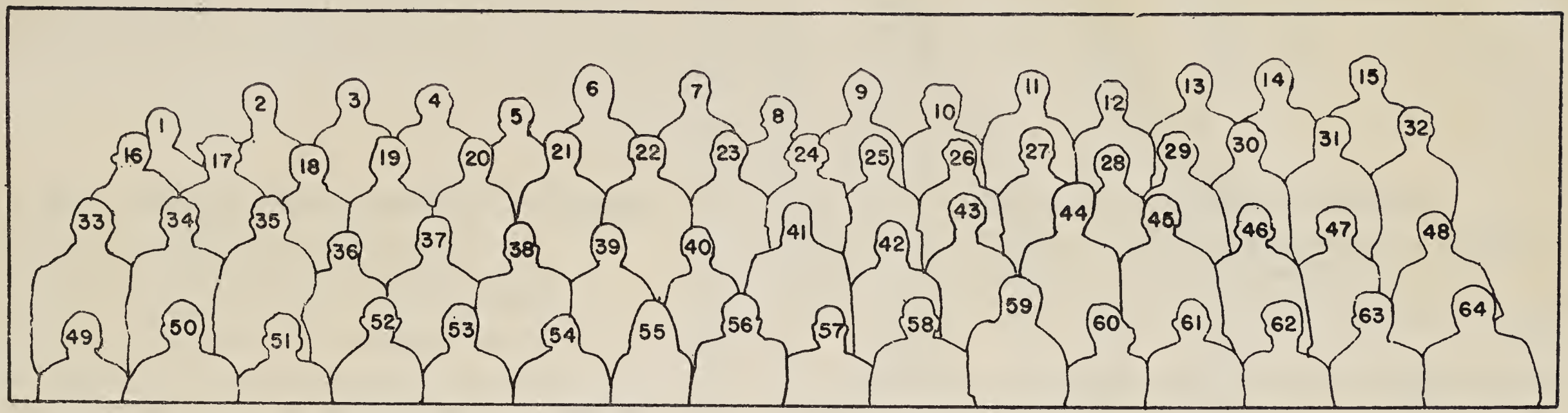

Participants

1. P. Das, Gauhati University, Assam
2. K. Patgiri, Gauhati University, Assam
3. O. P. Sharma, Wadia Institute Dehradun
4. P. N. Shukla, Physical Research Laboratory, Ahmedabad
5. N. Lal, Kurukshetra University, Haryana
6. S. Singh, Guru Nanak Dev University, Amritsar
7. P. Sharma, Physical Research Laboratory, Ahmedabad
8. N. Hussain, Physical Research Laboratory, Ahmedabad
9. R. S. Waraich, Kurukshetra University, Haryana
10. P. Sharma, Kurukshetra University, Haryana
11. K. D. Bal, Kurukshetra University, Haryana
12. C. M. Nautiyal, Physical Research Laboratory, Ahmedabad
13. M. M. Sarin, Physical Research Laboratory, Ahmedabad
14. S. P. Bhatnagar, Gujarat University, Ahmedabad
15. M. N. Vahia, Tata Institute of Fundamental Research, Bombay
16. P. K. Karmakar, Saha Institute of Nuclear Physics, Calcutta
17. L. Chand, Aligarh Muslim University, Aligarh
18. M. B. Potdar, Physical Research Laboratory, Ahmedabad
19. R. Ramesh, Physical Research Laboratory, Ahmedabad
20. V. M. Choubey, Wadia Institute, Dehradun
21. K. K. Sharma, Wadia Institute, Dehra Dun
22. B. L. K. Somayajulu, Physical Research Laboratory, Ahmedabad
23. M. Bhaskaran, Physical Research Laboratory, Ahmedabad
24. R. Korisettar, Physical Research Laboratory, Ahmedabad
25. T. R. Venkatesan, Physical Research Laboratory, Ahmedabad
26. R. Rangarajan, Physical Research Laboratory, Ahmedabad

27. T. D. Goswami, Gauhati University, Assam
28. S. K. Bhattacharya, Physical Research Laboratory, Ahmedabad
29. J. N. Goswami, Physical Research Laboratory, Ahmedabad
30. D. Sengupta, Physical Research Laboratory, Ahmedabad
31. K. Gopalan, Physical Research Laboratory, Ahmedabad
32. A. M. Awasthi, Physical Research Laboratory, Ahmedabad
33. A. K. Choudhury, Physical Research Laboratory, Ahmedabad
34. J. R. Trivedi, Physical Research Laboratory, Ahmedabad
35. R. Jha, Physical Research Laboratory, Ahmedabad
36. M. M. Dhawan, Kurukshetra University, Haryana
37. A. K. Ganguly, Saha Institute of Nuclear Physics, Calcutta
38. D. S. Srivastava, Aligarh Muslim University, Aligarh
39. V. Sinha, Gujarat University, Ahmedabad
40. S. Trivedi, Tata Institute of Fundamental Research, Bombay
41. A. P. Sharma, Kurukshetra University, Haryana
42. S. K. Chakravarthy, Kurukshetra University, Haryana
43. I. M. Talwar, Kurukshetra University, Haryana
44. H. S. Virk, Guru Nanak Dev University, Amritsar
45. V. P. Singh, Kurukshetra University, Haryana
46. A. B. Chakranarayan, Poona University, Poona
47. P. K. Panchal, Poona University, Poona
48. V. L. Bhat, Physical Research Laboratory, Ahmedabad
49. N. Durgaprasad, Tata Institute of Fundamental Research, Bombay
50. N. Bhandari, Physical Research Laboratory, Ahmedabad
51. R. H. Iyer, Bhabha Atomic Research Centre, Bombay
52. A. Ivliev, Vernadsky Institute of Geochemistry and Analytical Chemistry, USSR Academy of Sciences, Moscow, USSR
53. G. Poupeau, Centre des Faibles Radioactivities, Laboratoire Mixte, CNRS/CEA, 91190, Gif-sur Yvette, France
54. S. P. Pandya, Physical Research Laboratory, Ahmedabad
55. G. Crozaz, The McDonnel Centre for the Space Sciences, Washington University, Missouri, 63130, U.S.A.
56. D. Lal, Physical Research Laboratory, Ahmedabad
57. K. R. Ramanathan, Physical Research Laboratory, Ahmedabad
58. V. L. Ginzberg, P. N. Lebedeev Institute of Physics, Moscow, USSR
59. R. M. Walker, Washington University, St. Louis, Missouri, 63130, U.S.A.
60. G. Ustinova, Vernadsky Institute of Geochemistry and Analytical Chemistry, USSR Academy of Sciences, Moscow, USSR
61. S. Biswas, Tata Institute of Fundamental Research, Bombay
62. K. K. Nagpaul, Kurukshetra University, Haryana
63. M. N. Rao, Physical Research Laboratory, Ahmedabad
64. S. D. Verma, Gujarat University, Ahmedabad

CONTENTS

On the origin of the low energy cosmic rays from stellar sources

S BISWAS, N DURGAPRASAD and SUSHMA S TRIVEDI
Tata Institute of Fundamental Research, Bombay 400 005, India

Abstract. The model of stellar origin of the anomalous component in the low energy cosmic rays for He to Fe ions observed in space vehicles is studied in the light of recent results. The model of heliospheric origin by Fisk *et al* which has several attractive features cannot explain the long-term variations of intensity observed during 1974 to 1978 as pointed out by Nagashima and Morishita. The stellar origin model of Durgaprasad and Biswas, on the other hand, can easily account for the sudden appearance of the anomalous component in 1972 and its large decrease in intensity in 1978 on the basis of polarity reversal of the solar magnetic field as discussed by Nagashima and Morishita (1980). In this work, we show that in the stellar model energetic ions of He, C, N, O, etc. could originate in O-type stars which manifest very strong stellar wind with mass loss rate of $3 \cdot 10^{-6}$ $M_{\odot}$ per year. These have terminal velocities of about 1200 to 4000 km/sec and are typically a few times their escape velocity. These velocities correspond to ion energies of 10 to 100 keV/amu. These ions are in partly ionised state and are accelerated in the interstellar shock fronts to about 1 to 50 MeV/amu and thus account for the observed anomalous component of low energy cosmic rays.

Keywords. Cosmic rays; anomalous component; stellar sources; Novae; O-type stars.

1. Introduction

In recent years a new component in low energy cosmic rays (1–30 MeV/amu) was discovered in the vicinity of earth and at distances upto 18 A. U. (Hovestadt *et al* 1973; McDonald *et al* 1974; Garcia-Munoz *et al* 1975; Chan and Price 1974; Mewaldt *et al* 1975a; Webber *et al* 1975; Biswas *et al* 1975; Biswas and Durgaprasad 1980; and Webber 1979). The component has anomalous He, N, O and Ne abundances, that are quite different from solar and galactic cosmic rays. The IMP 7 & 8, Pioneer 10 & 11 and Voyager 1 & 2 spacecrafts have provided new and interesting information on the composition, time variation, radial and perpendicular gradient of this component. Pioneer 10 was at 20 A.U. in mid 1979 and travelling at the rate of 3 A.U. per year is likely to reach close to the heliospheric boundary at 50 A.U. by about 1985. The data from these spacecrafts are expected to give additional information about this new component.

The origin of these particles is not definitely known at present. Several attempts have been made to explain its origin (Fisk *et al* 1974; Durgaprasad 1977; Durgaprasad and Biswas 1977; Biswas *et al* 1981). The model of Fisk *et al* (1974) have some attractive features which could partly account for the composition of the anomalous component. However, recent results show very large time variation of this component and the intensity reached very low value in early 1979 (Hovestadt *et al* 1979). Nagashima and Morishita (1979, 1980) discussed in detail the long-term modulation of the anomalous component and they pointed out that the heliospheric

model of Fisk *et al* (1974) cannot account for the long-term variations observed recently and these variations can be easily understood from the stellar model of Durgaprasad and Biswas (1977). They interpret the modulation as occurring due to the polarity reversal of the polar magnetic field of the Sun, one such reversal having occurred in the period of 1969–71. This interpretation is based on the hypothesis that when polar magnetic field of the Sun is nearly parallel to the galactic magnetic field, they both could easily connect with each other, and hence the low energy galactic cosmic rays could penetrate more easily into the heliosphere along the magnetic lines of force, as compared with those in the antiparallel state of the magnetic fields. This leads to a 22-year variation in cosmic ray intensity because polarity reversal occurs around every solar maximum. These authors point out that the sudden appearance of the anomalous component in 1972 and its absence in 1975 could be easily understood by the hypothesis of Durgaprasad and Biswas (1977) as a polarity reversal. Further, these authors point out that the observation presented by the Chicago group (McKibben *et al* 1979) that the anomalous component has abnormally large density gradient perpendicular to the solar equatorial plane can also be understood by the stellar origin model of Durgaprasad and Biswas (1977).

2. Novae model of the origin

Firstly, we discuss some of the significant aspects of the model of Durgaprasad and Biswas (1977) (Paper 1) as follows:

2.1 *Abundance of elements of some novae envelopes*

It is assumed that the sources of these particles are relatively close and particles emitted from novae explosion may be possible candidates. This was arrived at from some similarities in the abundances of He, C, N and O abundances in the anomalous

Table 1. Relative abundances in low energy cosmic rays and in some novae envelopes

Elements	Low energy cosmic rays measured at 10 MeV/amu (a)	Low energy cosmic rays demodulated (b)	Novae envelope HR Del (c)	Galactic cosmic rays (> 1 GeV/amu) (d)	Sun (e)
He	60—200	120—400	150—700	35	180
C	1	1	1	1	1
N	5	4	5	0·25	0·25
O	25	18	20	0·9	1·67
Ne	1	0·7	—	0·16	0·22
Mg	0·4	0·25	0·04	0·18	0·09
Si	0·5	0·3	0·04	0·12	0·10
Fe	0·1	0·1	0·05	0·1	0·08

(a) Webber *et al* (1979)
(b) Durgaprasad and Biswas, (1977)
(c) Antipova, (1974)
(d) Webber *et al* (1972)
(e) See *e.g.* Biswas and Durgaprasad (1980).

component and in some novae envelopes (table 1). It may be noted that because the spectral shapes of He, C, N, O, etc. for the anomalous component of the low energy cosmic rays are different from each other, the relative abundances are dependent on energy. For example, O/C ratio is 4·4 and 4·7 at 9-30 and 8-20 MeV/amu energy intervals respectively (McDonald *et al* 1974; Biswas and Durgaprasad 1980), whereas at 10 MeV/amu, the ratio is 25 (Webber 1979). The demodulated spectra and abundances are calculated using ' forced-field ' potential and the measured spectra at interplanetary space at a few A.U. It may also be noted that the measured abundances of some elements of some of the novae envelopes show some similarities whereas other elements such as Mg, Si do not. After emission from the source during the propagation and acceleration stages the relative abundances of the ions will undergo changes which would depend on a number of parameters including the ionization states of the ions. The ion states are important properties of these particles as discussed in the following sections.

2.2 *Ionization states*

In this model it is assumed that ions are emitted from the source regions with energies of the order of 100 keV/amu. At these energies the charged states of the ions, *e.g.* of carbon and oxygen are mostly C^{+1}, C^{+2} and O^{+1}, O^{+2}, for equilibrium values of charge states in interstellar space.

The average charge, (i) carried by an ion moving through matter depends upon the atomic number Z of the ion, its velocity, v, and on the nature of the medium. For velocity much greater than the electron velocity, the ion is fully stripped of its electrons and is completely ionised. For lower velocities and energies, it will retain some electrons and be partially ionised. In paper-1, calculations were made on the average charge i carried by an ion of atomic number Z and energy E moving through interstellar space, which is assumed to consist mainly of hydrogen. In table 2, we give the values of i for various values of Z (C, N, O, Ne, Mg, Si and Fe ions) and E (varying from 100 keV/amu to 10 MeV/amu) calculated according to the procedure described in paper 1. These charge states are estimated to be accurate upto 10%. Compared to the dimension 10–50 A.U. of the heliosphere it can then be concluded that these charge states are still preserved in the interplanetary medium in the vicinity of the

Table 2. Average equilibrium values i of charged states of ions in interstellar space (composed mainly of hydrogen) (taken from Durgaprasad and Biswas 1977)

Atomic number	Kinetic energy (eV/amu)			
	10^5	5×10^5	10^6	10^7
6	1·8	4·3	5·4	6
7	1·8	4·7	5·9	7
8	1·9	5·0	6·4	8
10	2·1	5·7	7·3	10
12	2·3	6·2	8·2	12
14	2·5	6·7	8·9	14
26	3·3	8·8	12·5	25

earth. Even after acceleration to about 10 MeV/amu from 0·1 MeV/amu, the charge states given in table 2 represent the values of i in the interplanetary medium.

As regards modulation in interplanetary medium, it is noted that ions having energies around 10 MeV/amu and in partly ionized states will be modulated in the region 50 to 1 A.U. quite differently than the ions of fully stripped nuclei with the same energy/amu. This is because the magnetic rigidity, R, of an ion is given by $R = (APc/i)$, and the lesser the value of i/A, the greater is the rigidity of the particle for the same value of Pc. The oxygen and neon ions have higher rigidities than the carbon ions and will be hence less modulated. Thus oxygen and neon ions are relatively enhanced in the inner solar system.

The differential modulation of C, O, Ne, Mg and Si ions have been calculated as described in paper 1. For this purpose, the calculations of Garcia-Munoz *et al* (1975) are taken to be representative of the modulation for the 1973–74 period. Also using the ' force-field ' solution of Gleeson and Axford (1968) it was estimated that for this period the force-field potential is around 270 MeV/amu. Using these data, the differential modulation of oxygen and carbon ions is estimated to be a factor of 1.3. The relative modulation factors of He, N, Ne, Mg, Si and Fe ions with respect to carbon ions thus calculated are 0·5, 1·2, 1·4, 1·5, 1·6 and 2·2 respectively. In this paper, it is shown that during propagation in interstellar space, the charge states are preserved as these are equilibrium values and hence the ions can travel fairly long paths in interstellar space.

2.3 *Acceleration process*

The ions with equilibrium charge states having kinetic energies about 100 keV/amu were assumed, in paper 1, to be accelerated at the heliospheric boundary. On the basis of recent astronomical observations it seems more likely that interstellar shock fronts would be capable of accelerating these ions from 100 keV/amu to the energy range of 1 to 50 MeV/amu quite efficiently. This is discussed in more detail in the recent model of the stellar origin of the anomalous cosmic rays as given later.

2.4 *Propagation in interplanetary space*

Next we examine the question, what are the charge states of these ions in interplanetary space? It is shown in paper 1 that the mean free path for stripping of these ions (*e. g.* C, O) in interplanetary space are 2×10^4 A. U. and 3×10^5 A. U. at energies of 10^5 eV and 10^7 eV respectively. These values are several orders of magnitude higher compared to the dimensions of about 50 A. U. of the heliosphere. It can then be concluded that these charge states are preserved in interplanetary medium and in the vicinity of 1 A.U.

2.5 *Relative abundances*

In table 1, the demodulated abundances are compared to the abundance values for novae DQ Her 1934 obtained by absorption method by Antipova (1974), who observed that abundances of C, N, O were abnormal as compared to those of normal stars and of solar system. Abundance in another novae HR DEL 1967 was also

abnormal, but oxygen was very depleted, as given in paper 1. From these observations, it is clear that novae abundances show, peculiarities as well as variations. Emission processes and interstellar acceleration mechanism are also expected to modify the abundances of the ions accelerated to ~10 MeV/amu. It can thus be concluded from table 1 that peculiarities of the He, C, N, O, Ne abundances observed in the anomalous component of low energy cosmic rays could partly exist in astrophysical objects such as novae.

3. Stellar model of O-type stars with strong stellar wind as source of low energy cosmic rays

As discussed in the last section, it was suggested in paper 1 that novae type objects having peculiar composition may act as the sources of injecting particles. While this possibility exists, a number of new astrophysical results have been obtained in recent years which provide new clues on the origin of low energy cosmic rays from stellar sources. The new model of Biswas *et al* (1981) is based on these recent observations.

In this model, it has been proposed that O-type stars with strong stellar winds act as the source of injection of low energy cosmic rays. These ions, of energies 10-100 keV/amu, are in partly ionised state such as $C^{+1,+2,+3}, \ldots$, $O^{+1,+2,+3}, \ldots$, etc. and hence these have very low rate of Coulombian energy loss in hot, thin interstellar plasma of $T \approx 5{\cdot}10^5$ °K and $N_e \approx N_p \approx 3 \times 10^{-3}$ cm^{-3} which fills 70–80% of interstellar medium (see *e. g.* Melrose 1979). As a result the ions can travel fairly long distances in interstellar medium. During interstellar propagation a fraction of the ions will interact with shock fronts of supernovae remnants and gain energy by Fermi mechanism. Several authors (Blanford and Ostriker 1978; Ostriker 1979) have recently worked out the efficient mechanism of acceleration of galactic cosmic rays in interstellar shock fronts. It is suggested that low energy ions can be accelerated to 1–50 MeV/amu energy range in such shock fronts in interstellar medium and thus low energy cosmic rays are generated. These cosmic ray ions enter the heliosphere from interstellar medium and are channelled by the interstellar magnetic field and large scale magnetic field in the heliosphere (Nagashima and Morishita 1979, 1980). The general outline of the model of the stellar origin of low energy cosmic rays is given in figure 1. We shall briefly discuss some significant aspects of this model.

3.1 *O-type stars*

It is now well established that O-type stars with $20\ M_\odot < M < 100\ M_\odot$ manifest very high mass loss rates (see Conti and Deloore 1979; Conti and McCray 1980). The mass loss occurs in the form of very strong stellar winds and these account for high rate of mass loss of $3{\cdot}10^{-6}\ M_\odot$ per year. This can be compared to the normal mass loss of the Sun of $10^{-14}\ M_\odot$ per year in the form of solar wind. In the spectral classification O-type stars have the highest surface temperature of $T > 30{,}000$°K and the largest masses in the main sequence phase. The luminosities of O-type stars are very high which are on the average about 10^{39} ergs sec^{-1} *i.e.* $\sim 10^6\ L_\odot$ These

Figure 1. Model of the origin of low energy cosmic rays from stellar wind (Biswas *et al* 1981)

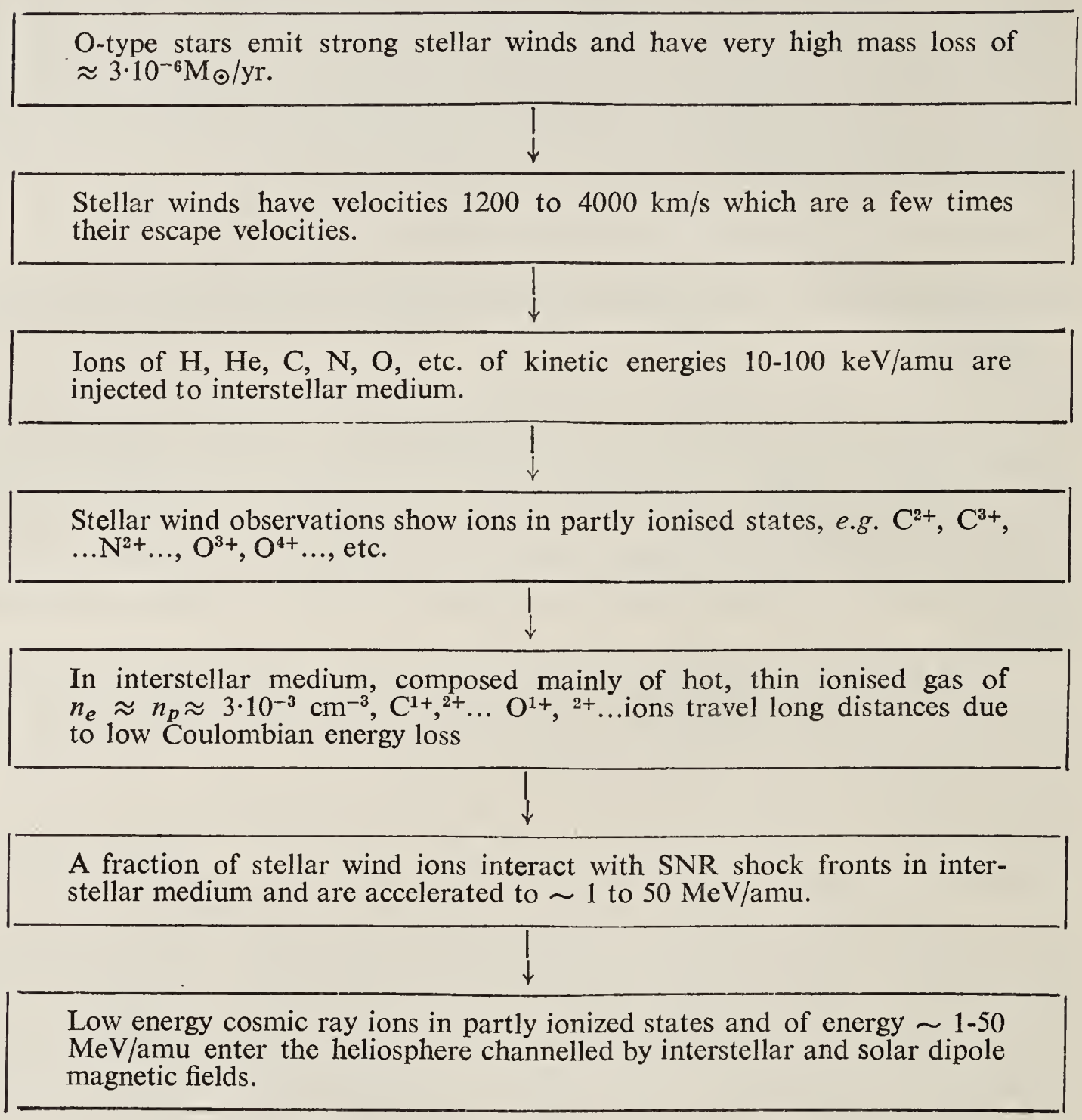

stars consequently have short life time of $\sim 10^6$ years. As a result O-type stars are rare and there are about 3×10^5 such stars in the galaxy, *i.e.* a fraction of 10^{-6} of the total number of stars. Because of the short lifetime they have gone through about 10^4 generations during the lifetime of the galaxy. Their high mass loss rate contributes to a large fraction of new matter injected into the interstellar space.

The terminal velocities of stellar winds from O-type stars range from 1200 to 4000 km/sec and these are typically a few times their escape velocities. These velocities correspond to ion energies of 10-100 keV/amu. Because of very high velocities exceeding the escape velocities, these ions are considered in the present model as good candidate for the source of injection of low energy cosmic rays.

3.2 *Ion states and propagation in interstellar medium*

Observational data show that ions of the stellar wind are injected in the interstellar medium in partly ionized state such as C^{+2}, $^{+3}$..., N^{+2}, $^{+3}$..., O^{+2}, $^{+3}$.... It seems likely that such elements exist in many ion states. The recent observation of interstellar medium has dramatically changed our picture of the interstellar medium.

From soft x-ray and interstellar ultraviolet studies it is now indicated that a large fraction (70–80%) of interstellar medium is filled with ionized gas of high temperature, $T \approx 5{\cdot}10^5$ K and of low density $n_e \approx n_p \approx 3 \times 10^{-3}$ cm^{-3} (see *e.g.* Melrose 1979). It is estimated that repeated SN explosions maintain the interstellar medium at high temperature.

We have calculated the energy loss of the partly ionized elements of stellar wind in the hot, thin interstellar medium using rigorous equations of Coulombian energy loss of ion in two component plasma according to Butler and Buckingham (1962). From these calculations it is noted that low energy ions such as He^{+1}, C^{+2}, etc. with initial energy of about 100 keV/amu can travel a long distance in hot, thin interstellar medium till their energies are reduced to ~10 keV/amu. This arises from the decreasing energy loss rate with decreasing energy beyond the electron loss maximum. In case of He^{+1} ion this path length is calculated as 4×10^{20} cm. For other elements, the path lengths and the distances travelled would depend on their ionization states and these are expected to be within one order of magnitude of the above.

3.3 *Acceleration in interstellar medium*

It has been calculated by several authors that supernovae remnant shock fronts can travel a large distance in the hot and low density interstellar medium (see *e.g.* Ostriker 1979). The interaction of fast ions with the expanding shock fronts can provide efficient acceleration process through first order of Fermi process. A number of authors have worked out such processes for acceleration of high energy cosmic rays (*e.g.* Ostriker 1979). In this work we propose that nonrelativistic heavy ions can be accelerated from 10 to 100 keV/amu range to 1 to 50 MeV/amu by means of collisions with SNR shock fronts in interstellar medium. In this case, the energy gain requirements are of the order of a factor of 5×10^2. Acceleration efficiency will be dependent on the ion states of the particles and this effect is probably responsible for unusual abundance ratios such as O/C. Further calculations on these aspects of the model are in progress.

3.4 *Entry into heliosphere*

The accelerated heavy ions would then enter the heliosphere and give rise to the observed flux of low energy cosmic ray ions. Depending on the polarity of the sun and the large scale magnetic field direction of the interplanetary mganetic field and the direction of interstellar magnetic field, these cosmic ray ions would be channelled favourably or not, as discussed by Nagashima and Morishita (1979, 1980). Thus the long term variation of the intensity of the low energy cosmic rays may be understood.

4. Concluding remarks

The above model provides a suitable framework in which various properties of low energy cosmic rays may be understood. Detailed calculations of the processes involved are in progress, with a view to obtain more insight into the phenomena relating to the origin of low energy cosmic rays.

References

Antipova L I 1974 *Highlights of astronomy*, ed. G Contopoulos, (Dordrecht: D Reidel) p. 501

Biswas S and Durgaprasad N 1980 *Space Sci. Rev.* **25** 285

Biswas S, Durgaprasad N, Nevatia J, Venkatavaradan V S, Goswami J N, Jayanthi U B, Lal D and Mattoo S K 1975 *Astrophys. Space Sci.* **33** 337

Biswas S, Durgaprasad N and Trivedi Sushma S 1981 *Proc. 17th Int. Cosmic Ray Conf.* Paris **2** (Saclay: CENS) p. 314

Blanford R D and Ostriker J P 1978 *Astrophys. J. Lett.* **221** L229

Butler S T and Buckingham M J 1962 *Phys. Rev.* **126** 1

Chan J H and Price P B 1974 *Astrophys. J.* **190** L39

Conti P S and Deloore C W H (ed) 1979 IAU Symp. No. 83 (Dordrecht: D Reidel)

Conti P S and McCray R 1980 *Nature* (*London*) **208** 9

Durgaprasad N 1977 *Astrophys. Space Sci.* **47** 435

Durgaprasad N and Biswas S 1977 *Proc. 15th Int. Cosmic Ray Conf. Plovdiv* **2** (Plovdiv: Bulgarian Acad. Sci.) p. 103

Fisk L A, Kozlovsky B and Ramaty R 1974 *Astrophys. J.* **190** L35

Gleeson L J and Axford W I 1968 *Astrophys. J.* **154** 1011

Garcia Munoz M, Mason G M and Simpson J A 1975 *Astrophys. J.* **202** 265

Hovestadt D, Klecker B, Gloeckler G, Ipavich F M, Fan C Y and Fisk L A 1979 *Proc. 16th Int. Cosmic Ray Conf.* Kyoto **3** (Japan: Univ. of Tokyo) p. 255

Hovestadt D, Vollmer O, Gloeckler G and Fan C Y 1973 *Phys. Rev. Lett.* **31** 650; and *Proc. 13th Int. Cosmic Ray Conf.* Denver **2** (Colorado: Univ. of Denver) p. 1498

McDonald F B, Teegarden B J, Trainor J H and Webber W R 1974 *Astrophys. J.* **187** L105

McKibben R B, Pyle K R and Simpson J A 1979 *Astrophys. J.* **227** L 147

Melrose G B 1979 *Plasma Astrophys.* Vol. 1. (New York: Gordon and Breach) p. 20

Mewaldt R A, Stone E C, Vider S B and Vogt R E 1975 *Proc. 14th Int. Cosmic Ray Conf.* Munich **2** (Max Planck Instiut, Munich), p. 798

Nagashima G and Morishita I 1979 *Proc. 16th Int. Cosmic Ray Conf.* Kyoto **3** (Japan: Univ. of Tokyo), p. 325

Nagashima G and Morishita I 1980 *Planet. Space Sci.* **28** 195

Ostriker J P 1979 *Proc. 16th Int. Cosmic Ray Conf.* Kyoto 2 (Tokyo: Univ. of Tokyo), p. 124

Webber W R 1979 *Proc. 16th Int. Cosmic Ray Conf.* Kyoto 14 (Tokyo: Univ. of Tokyo), p. 271

Webber W R, Damle S V and Kish J 1972 *Astrophys. Space Sci.* **15** 245

Webber W R, McDonald F B, Trainor J H, Teegarden B J and Von Rossenvinge T T 1975 *Proc. 14th Int. Cosmic Ray Conf.* 12 (Munich: Max Planck Institut) p. 4233

Irradiation history and atmospheric ablation of meteorites: Results from cosmic ray track studies

J N GOSWAMI
Physical Research Laboratory, Ahmedabad 380 009, India

Abstract. The dominant component of nuclear tracks observed in meteoritic minerals poor in uranium is produced by cosmic ray very heavy (VH: $Z > 20$) nuclei. Studies of cosmic ray tracks and other cosmogenic effects in meteorites give us information on the irradiation history of these meteorites and enable us to estimate the extent of ablation during their atmospheric transit, and hence their pre-atmospheric masses. In a specific type of meteorite, known as *gas-rich* meteorite, one finds individual grains and xenoliths that have received solar flare and galactic cosmic ray irradiation prior to the formation of these meteorites. Detailed studies of these exotic components give insight into the accretionary processes occurring in the early history of the solar system. Some of the important results obtained from such studies and their implications to meteoritics are summarized.

Keywords. Tracks; cosmic ray; meteorite; ablation; solar flares; irradiation history; exposure age; accretionary processes.

1. Introduction

The nuclear tracks observed in silicate grains from extraterrestrial samples (*e.g.* lunar samples and meteorites) are produced by one or more of the following components:

(i) stopping solar flare and galactic cosmic ray (GCR) very heavy (VH: $Z > 20$) nuclei,
(ii) spontaneous fission of ^{238}U and, in some cases ^{244}Pu,
(iii) induced fission of U and Th, and
(iv) nuclear reaction-induced spallation recoils.

In the case of uranium-poor silicate grains in meteorites and lunar samples, the dominant source of tracks is the stopping solar flare and GCR heavy nuclei. The spallation recoil tracks have extremely short range ($< 1\mu$) and are relatively unimportant except for lunar samples and meteorites with very long exposure ages. This can also be distinguished from the VH nuclei tracks, which have recordable track lengths of $\geqslant 10\mu$ in common silicate grains. The low-energy (1–100 MeV/amu) solar flare particles have a maximum range of about a millimetre equivalent of silicate material, and as such solar flare VH nuclei tracks can be seen only in soil grains and rocks exposed on the lunar surface. In the case of meteorites, the solar flare track records are completely lost due to the atmospheric ablation processes which remove, on an average, a couple of centimetres of the surfacial material. A specific meteorite type, the *gas-rich* meteorite, is however, an exception, and one can find solar flare track records in silicate grains extracted from the interior of these meteorites, indicating that these grains were exposed to low-energy solar flare radiations prior to their incorporation into these meteorites. The nuclear tracks observed in most of the meteo-

ritic silicate grains are thus produced primarily by VH nuclei in galactic cosmic rays. A detailed study of the track records in meteorites along with studies of other cosmogenic records (*e.g.* noble gas and radionuclide concentrations) gives information on: (i) the exposure and irradiation history of meteorites in space and (ii) the extent of atmospheric ablation and hence their pre-atmospheric masses. The study of individual components in gas-rich meteorites, that have received pre-compaction solar flare irradiation, on the other hand, offers us the unique opportunity to investigate possible changes in solar activity in the past and also to understand the accretionary processes occurring in the early history of the solar system. The present paper deals with some of the important aspects of the above studies and the present status of our understanding in these fields.

2. Irradiation history of meteorites

The cosmic ray exposure history of the meteorites, in general, is considered to be a single stage process involving removal of these objects from their parent bodies at some time in the past, and their exposure in space as small objects before being captured by the earth in recent times. It is generally assumed that while they were present in their parent bodies (the asteroids being the most probable parent bodies of meteorites) the meteorites were well shielded from cosmic rays. Such an assumption is justified since the mean attenuation length of various cosmogenic interactions varies from less than a micron (for solar wind interaction) to, at best, a couple of metres (for production of stable isotopes and radionuclides). There are, however, exceptions to the single stage exposure of meteorites, the gas-rich meteorites being one example. There are also other meteorites that have probably experienced multi-stage exposures, resulting from their presence in the nuclear active zone in the parent bodies, and collisional fragmentation in space after being ejected as small objects from the parent bodies. Exposure histories of each of the above types of meteorites will be discussed separately.

2.1 *Meteorites with single-stage exposure history*

In meteorites with single-stage exposure history, the cosmogenic records observed in them (*e.g.* tracks, spallogenic stable- and radio-nuclides, etc.) can be interpreted in terms of two parameters: (i) the intensity of the galactic cosmic rays, and (ii) the cosmic ray exposure durations. Studies of cosmogenic effects in both lunar and meteorite samples have shown that the long-term average intensity of both the proton and heavy ion components in GCR, responsible for production of cosmogenic nuclides and nuclear tracks respectively, has essentially remained constant for the last few tens of millions years (Arnold *et al* 1961; Lal 1972; Walker 1975; Reedy *et al* 1981). We shall therefore assume a constancy in galactic cosmic ray intensity in the past in the discussion that follows.

Assuming a constancy in GCR intensity it is possible, in principle, to obtain the duration of cosmic ray exposure T of a meteorite by studying the cosmogenic records in it. However, the process of atmospheric ablation, which results in the removal of variable amounts of near surface material in different meteorites, introduces an additional uncertainty regarding the shielding depths of the analysed samples within the

original meteorite, and hence on the exposure age estimates. Also, because of the extremely depth-sensitive production rate of nuclear tracks, the track records in meteorites alone *cannot* be used to estimate the duration of cosmic ray exposure. The problem is less severe in the case of cosmogenic stable- and radio-nuclide studies, since their production rates as a function of depth do not vary too much, and one can use an average production rate, independent of the shielding depth of the analysed samples, to obtain approximate exposure ages of meteorites. Examples of typical production rate profiles for nuclear tracks and stable isotopes and radionuclides in spherical meteroites of different sizes are shown in figure 1. One can immediately note the large difference in the production rate profiles for tracks and cosmogenic nuclides. An added advantage in the case of cosmogenic nuclides is the possibility of studying more than one radionuclide or more than one isotope of the same element in the case of stable-nuclides, which gives an additional clue for introducing shielding depth corrections to the exposure age estimates (Eberhardt *et al* 1966). Studies of exposure age distribution of meteorites, based on measurements of cosmic ray produced stable isotopes using mass-spectrometric techniques, have led to groupings in the exposure age distributions of different meteorite types (Wanke 1966; Crabb and Schultz 1981). These groupings have been attributed to discrete collisional events involving the parent body/bodies of the different meteorite types at different times in the past.

An accurate knowledge of the shielding depths of the analysed samples and the size of the original meteorites is however important for a better understanding of the exposure and irradiation history of individual meteorites, and particularly in the case of small meteorites where the production rates of cosmogenic nuclides vary signi-

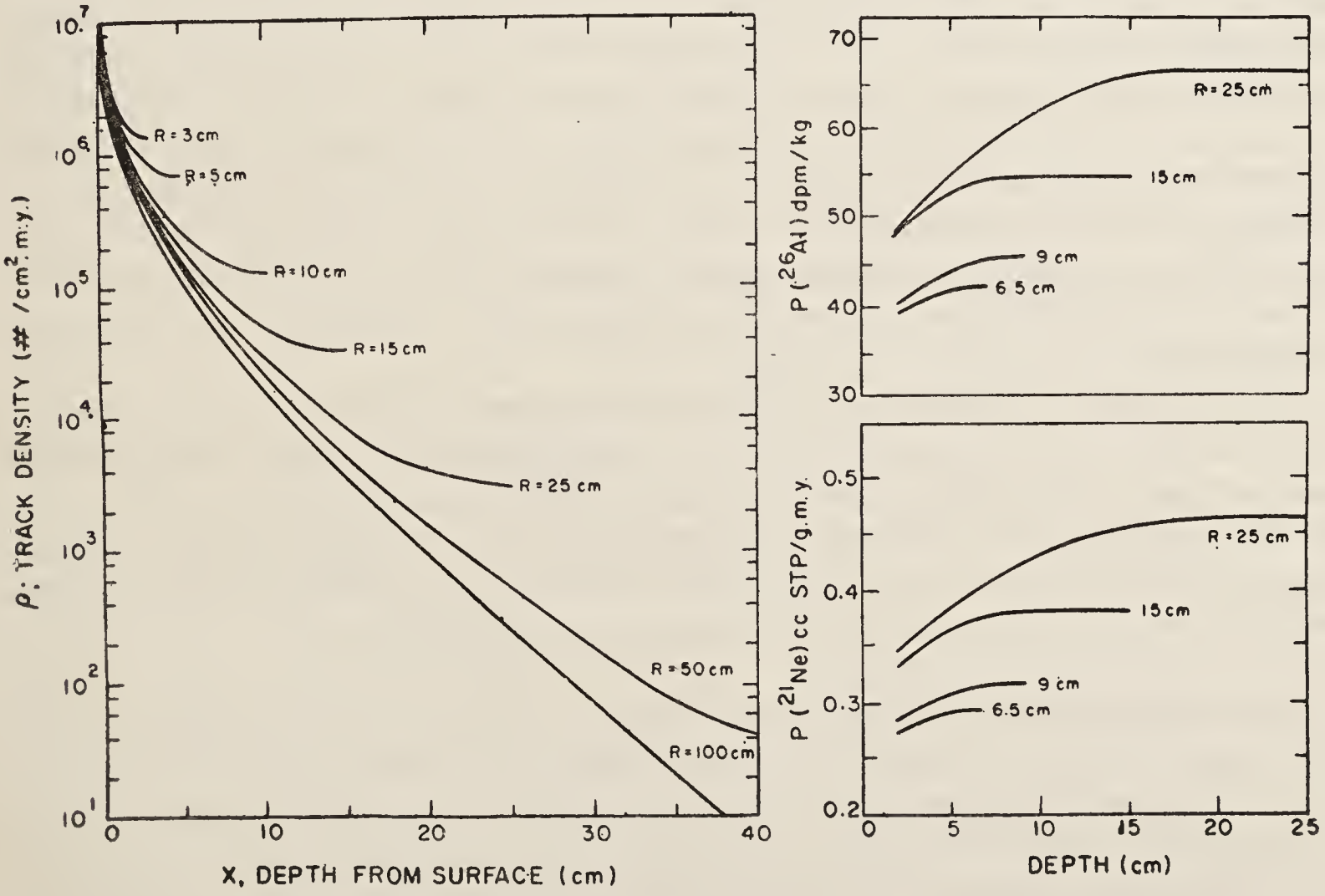

Figure 1. Production rate of cosmic ray produced tracks, radio-nuclide (^{26}Al) and stable isotope (^{21}Ne) in meteorites of chondritic composition. The P (^{21}Ne) values are in the unit of 10^{-8}.

ficantly at a given shielding depth for different sizes of meteorites (figure 1). It is therefore essential to understand the magnitude of atmospheric ablation of meteorites, and for this purpose, the study of nuclear track records would be ideal because of its extremely depth sensitive production rate.

3. Atmospheric ablation of meteorites

The magnitude of atmospheric ablation of meteoroids during their passage through the earth's atmosphere depends on various parameters *e.g.* velocity, angle of entry, mass, density, shape etc. of the meteoroids. Analytical treatment of this problem to determine the dependence of meteoroid ablation on the above parameters has been carried out by various authors (Opik 1958; Baldwin and Sheaffer 1971; Revelle 1978). The discussion in this paper will be confined to studies based on the nuclear track method.

The basic principle involved in determining the extent of atmospheric ablation of meteoroids using the nuclear track method has been discussed by Fleischer *et al* (1967) and Bhattacharya *et al* (1973). The first step is to obtain the values of shielding depths (depth of the sampling point from the original (pre-atmospheric) meteoroid surface) for different sampling points within the recovered (post-atmospheric) meteorite. This involves determination of cosmic ray track densities in silicate grains taken from the sampling locations and evaluation of the rate of production of tracks, TPM (no. of *t*racks *p*er *m*.y.), using the information on cosmic ray exposure age of meteorites obtained from stable isotope and/or radio-nuclide studies. Since the track production rate at a given depth X is not very sensitive to the size of the meteorite (see figure 1), one can easily evaluate the shielding depth ΔX of any given sampling point. Bhattacharya *et al* (1973) have generated a set of graphs, using the track production profile shown in figure 1, which directly gives the shielding depth ΔX as a function of both TPM and *effective* recovered radius of the meteorites and can be used conveniently to obtain ΔX values. In generating these ΔX *vs* TPM graphs, Bhattacharya *et al* (1973) assumed that the ablation is symmetric. However, the error introduced in the estimate of shielding depths, because of this assumption, is not serious since for a $\pm$ 100% error-estimate in the actual radius of the meteorite, the error in shielding depth is less than $\mp$ 10%.

The methods of estimating pre-atmospheric size and radius of the meteorites for different ablation characteristics, based on shielding depth values obtained from nuclear track studies, have been discussed in detail by Gupta and Lal (1978). They have considered cases involving both symmetric and asymmetric ablation, and also survival of meteoroids as single or multiple fragments. The important results obtained in the work of Gupta and Lal (1978) are summarized below:

(i) In the case of a single surviving fragment, it is possible to accurately reconstruct the pre-atmospheric size and shape of the meteorites if the centre of the pre-atmospheric body is contained within the recovered fragment.

(ii) If the centre of the original meteorite is not contained within the recovered body, reconstruction of pre-atmospheric size is not possible in a straight-forward manner. However if a large data set for shielding depths at various points of the recovered fragment can be obtained, one can estimate the pre-

atmospheric size by comparing the expected and observed probability distributions of shielding depths for meteorites of different sizes which have suffered different degrees of ablation.

(iii) In the case of meteorite fall involving multiple fragments one can estimate approximate pre-atmospheric size from the lowest track density value, obtained after extensive analysis of a large number of samples, assuming that the lowest density sample represents the centre of the original meteorite. Another approach is to estimate mass-loss for different track density intervals based on the observed and expected recovered masses for different track density intervals.

Earliest studies of atmospheric ablation of meteorites using the nuclear track method were carried out by Fleischer *et al* (1967), and more extensive studies were carried out to determine pre-atmospheric sizes of different meteorites by Price *et al* (1967), Cantelaube *et al* 1969, Lal *et al* (1969), Lorin and Pellas (1975), Bull and Durrani (1976), Goswami *et al* (1978) and Bagolia *et al* (1977, 1978, 1980). The ablation phenomena in more than 150 meteorites have been studied recently by Bhandari *et al* (1980). Following the methods of Bhattacharya *et al* (1973) and Gupta and Lal (1978), Bhandari *et al* (1980) have obtained ' good ', ' model ' and ' limit ' estimate of pre-atmospheric masses for a large number of meteorites, classified into four sub-groups, based on the frequency distribution of the shielding depths of samples analysed from each meteorite. ' Good ' estimate for pre-atmospheric masses could be obtained only for about 20% of the analysed meteorites, since extensive sampling is necessary to obtain such estimates. They have found that the mass-ablation estimate ranges between 25 to 99·9% of the original mass, with a weighted mean of ~85%. The frequency distribution of pre-atmospheric masses (M_0) was found to follow a distribution of the type $dN \propto M_0^{-1}\, dM_0$. There is also a suggestion in the data that a relation between the mean mass-ablated and the atmospheric velocity of the meteorite exists in the velocity range 14 to 20 km sec^{-1}.

The frequency distribution of minimum shielding depths for different meteorites grouped as a function of percentage mass-ablation, obtained by Bhandari *et al* (1980), is shown in figure 2. The small values of minimum shielding depth, even in the cases of high ablation mass loss, indicate multiple fragmentation in the initial part of the trajectory since the outer regions, corresponding to low ΔX values, will be ablated away in the absence of fragmentation. The results obtained from nuclear track studies of the Dhajala shower (Bagolia *et al* 1977) illustrates such a phenomenon. The frequency distribution of the pre-atmospheric masses for the ' good ' estimate cases is shown in figure 3. The roughly equal populations in the mass interval, $M_0 = 10$–1000 kg, indicate a power law distribution of the type $dN \propto M_0^{-1}\, dM_0$, as noted earlier. Such a distribution is distinctively flatter than the estimated index of about -2 for meteoroids in the mass-range $1 - 10^8$ g (Gault *et al* 1974), and of about $-1{\cdot}6$ for meteoroids in the mass range $10^3 - 10^7$ g (McCrosky 1968). However, as Bhandari *et al* (1980) have noted, the lower efficiency in recovering small meteorites introduces a definite bias in the track based data towards meteorites of larger sizes.

The estimation of shielding depth by the track method has also been proved to be extremely useful in obtaining accurate production rates of cosmogenic nuclides in meteorites of various sizes. A combined study of nuclear track and cosmogenic nuclides in several meteorites, carried out recently by Bhattacharya *et al* (1980),

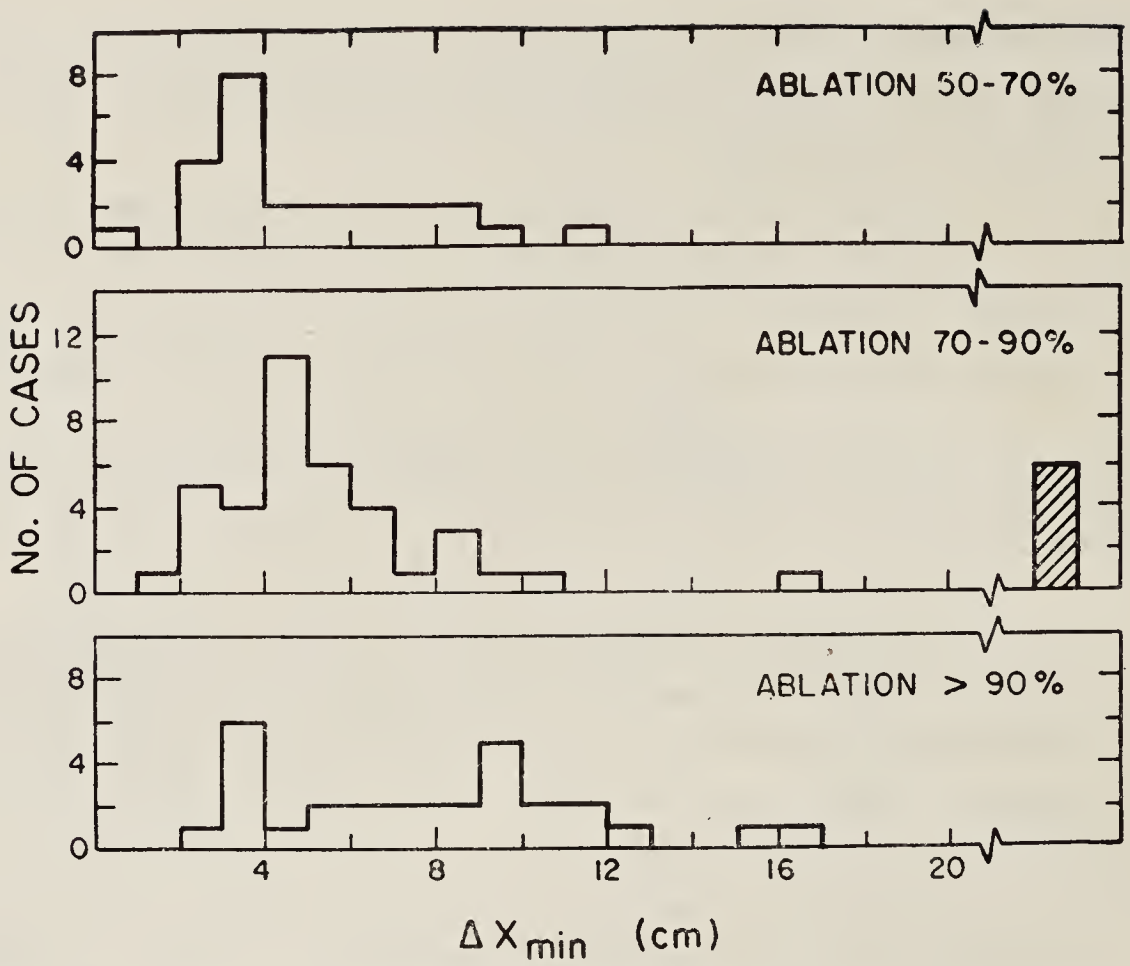

Figure 2. Frequency distribution of *minimum shielding depth* (ΔX_{min}) values for meteorites in three different ablation intervals. The no. of cases for which ΔX_{min} exceeds 20 cm are combined together (from Bhandari *et al* 1980).

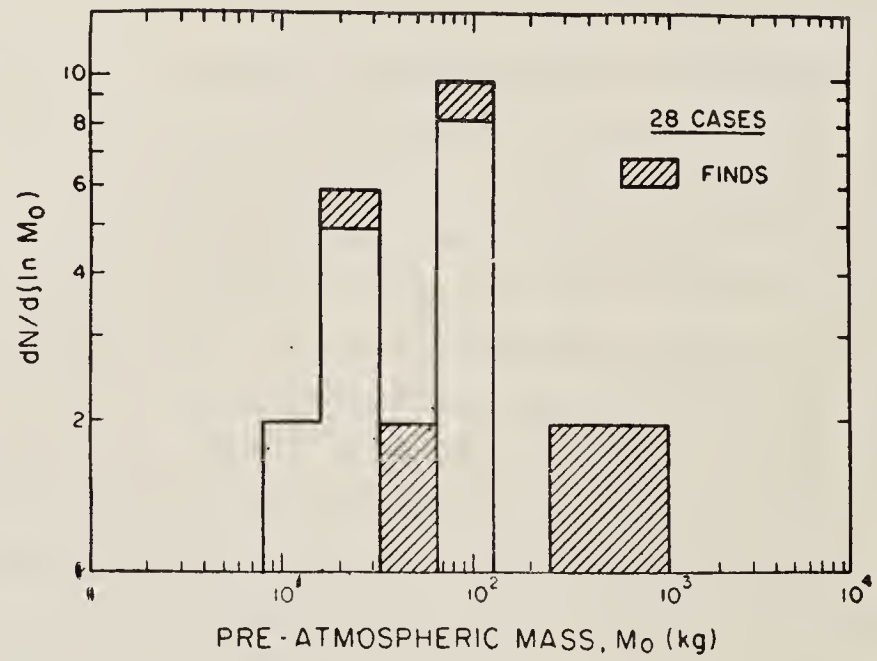

Figure 3. The number of meteorites in equal logarithmic mass interval is shown based on data for 28 meteorites for which reliable estimates of pre-atmospheric masses have been obtained using the nuclear track method (from Bhandari *et al* 1980).

led to the estimation of the parameter defining the hardness of energy spectra of cosmic ray primary and secondary nucleons at different depths within the meteorites of different sizes. This information is crucial in obtaining the production rates of cosmogenic nuclides as a function of depth for meteorites of different sizes.

The temperature gradient within a meteorite generated during the atmospheric ablation process also leads to partial annealing of tracks in the near surface (crusted) region of the recovered meteorite, and partial fading of low-temperature thermoluminescence. Studies of these effects coupled with laboratory data on track annealing and thermoluminescence fading characteristics can, therefore, give valuable insight into the atmospheric ablation process itself. Some work on these lines have recently been initiated (Jha and Lal 1981; Singhvi *et al* 1981).

4. Meteorites with multiple exposure histories

In the preceding discussion on the atmospheric ablation of meteorites it has been assumed that the meteorites have had a simple (one-stage) cosmic ray exposure in space as small objects. However considering the fact that collisional events (both cratering and catastrophic disruption of large objects) play an important role in the generation of meteorites, one expects some of the meteorites to have multiple cosmic ray exposure histories, prior to their exposure in space as a small object in the recent past. Such pre-irradiation could take place if the meteorites resided within the nuclear active zone (the upper few metres) of the first or second generation parent objects from which they were finally removed during collisional events. Monte-Carlo calculations of collision processes taking place among inner solar system objects (Turner 1979; Wetherill 1980) indicate that instances of multiple exposure of meteorites may be quite common. For example, in the case of meteorites with pre-atmospheric masses in the range 10–1000 kg, the probability of multiple exposure could be as high as 50% (Wetherill 1980). This result, however, depends on the assumed values of certain parameters characterizing the number distribution of small-size objects in the inner solar system and the collisional processes involved, and thus may be somewhat uncertain. Nonetheless, an analysis of meteorites with multiple exposure history offers a unique opportunity of studying the finer details in the evolutionary processes of solar system objects.

Although gas-rich meteorites can be cited as a specific case of meteorites with multiple exposure history, pre-irradiation in this case primarily refers to short-duration solar wind and solar flare irradiation of a few percent of the constituent components of these meteorites. Further, the records of solar wind and solar flare irradiations can be easily detected using particle track and mass-spectrometric methods. However, in non-gas-rich meteorites, devoid of solar wind-solar flare irradiation records, it is rather difficult to pinpoint cases of multiple exposure history, since, in the absence of any *a priori* knowledge of probable multiple exposure, the records of any given cosmogenic products (*e.g.* track, spallogenic stable isotopes and radionuclides) could be explained by considering an ' effective ' single stage exposure. A method has been suggested recently by Bhandari and Potdar (1981) to detect cases of meteorites with multiple exposure history from a combined analysis of nuclear track and cosmogenic noble gas data. Based on the calculation of neon isotopic ratio ($^{22}Ne/^{21}Ne$) in meteorites of different sizes, and comparing the results of these calculations with measured values of this ratio in meteorites, whose pre-atmospheric masses have been determined by the track method, Bhandari and Potdar (1981) concluded that for a shielding depth <30 cm, meteorites in all sizes show a (22/21) ratio of $\geqslant 1{\cdot}08$. Thus meteorites with measured (22/21) ratios of $< 1{\cdot}06$ indicate a deep seated (> 30 cm) exposure in larger size parent bodies. Their approach, shown in figure 4, is to study the relationship between cosmogenic neon isotopic ratio and the measured track production rate (assuming an ' effective ' single stage exposure) and to identify meteorites having probable multiple exposures histories. They have reported that $\sim 20\%$ of the meteorites for which data have been analysed so far could have had multiple cosmic ray exposure histories. A more elaborate discussion of this topic will be found in the accompanying paper by Bhandari (1981).

A very strong case for multiple cosmic ray exposure histories of a couple of Antarctic meteorites was presented by Imamura *et al* (1979), based on a combined analysis of

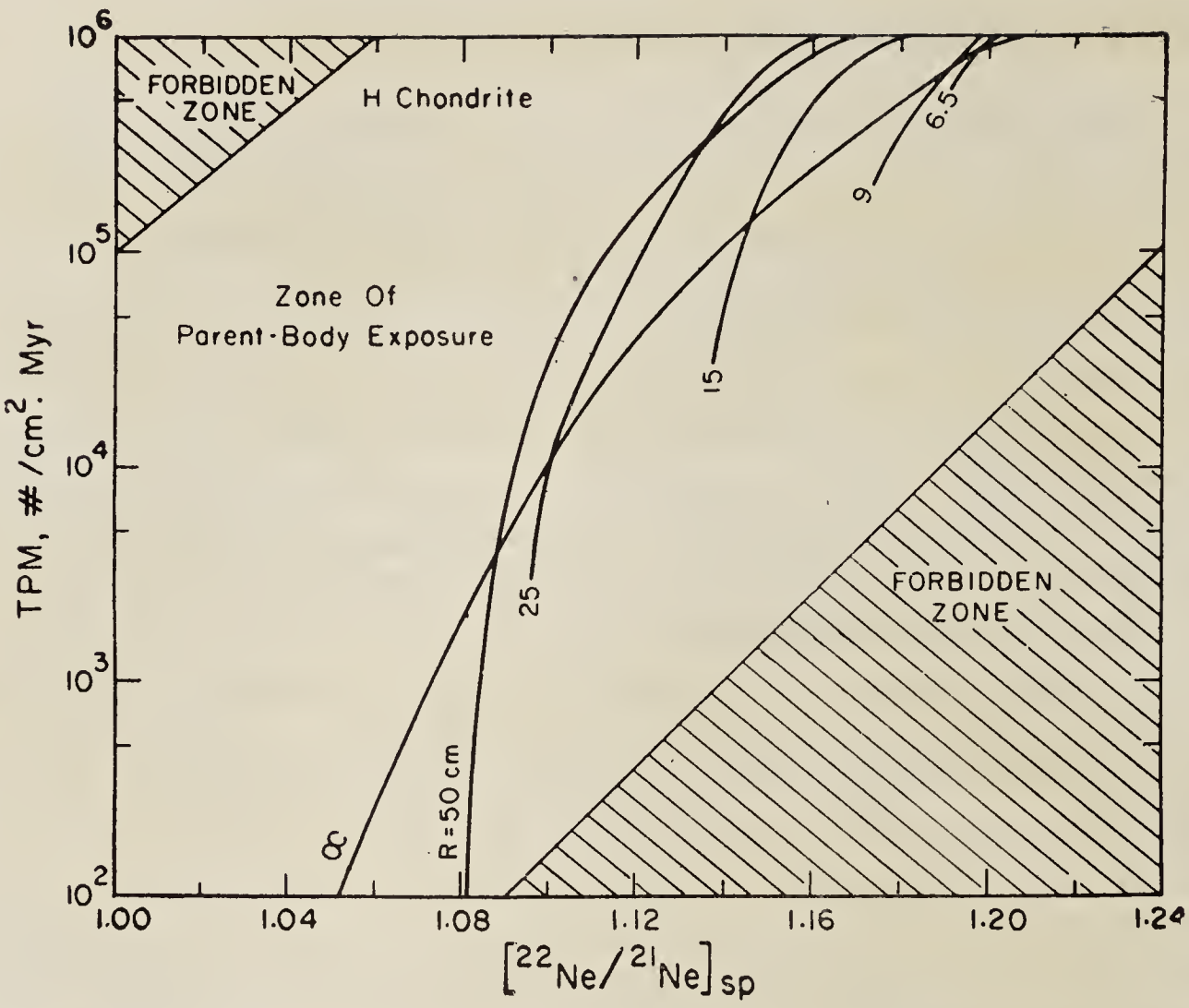

Figure 4. Correlation plot of cosmic ray produced neon isotopic ratio $(^{22}Ne/^{21}Ne)_{sp}$ and track producition rate (TPM) for chondritic meteorites of different sizes and with a simple single stage cosmic ray exposure history. The hatched portion indicates forbidden zones. Data for meteorites with multiple exposure histories should deviate from the trend lines towards the upper left.

radionuclide and stable isotope data. Further work in this direction based on combined studies of nuclear track, noble gas and radionuclides is extremely important for a proper understanding of the collision-controlled evolutionary history of the small objects in the inner solar system.

5. Irradiation and evolutionary history of the gas-rich meteorites

The gas-rich meteorites can be considered as a special meteorite type having multiple exposure history. They contain individual components that have received solar-wind and solar flare irradiation prior to their compaction into the meteorite bodies. The irradiation records survived the compaction/brecciation processes leading to the formation of these meteorites, and can be easily detected using the nuclear track and mass spectrometric methods. In figure 5 are shown tracks due to solar flare heavy nuclei in grains from two gas-rich meteroites. The occurrence of such grains varies from ~ 1 to 20% among the grains present in these meteorites.

Gas-rich meteorites are present in varying proportion in different stony meteorites —both chondrites and achondrites. All the type 1 carbonaceous chondrites (CI), and 65% of the type-2 carbonaceous chondrites (CM) are gas-rich. Among other chondritic type the percentage abundance of gas-rich meteorites varies from zero (C3(0) chondrites) to $\sim 20\%$. Among the achondrites, the aubrites and the howardites have gas-rich members.

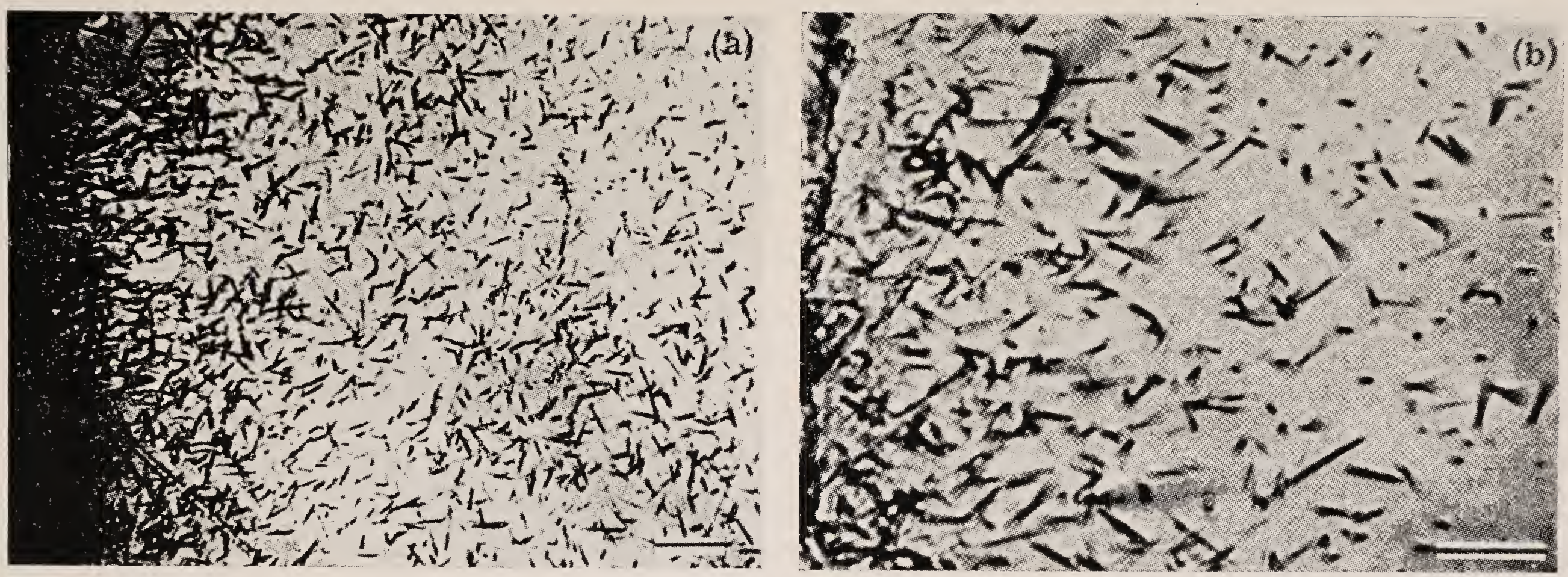

Figure 5. Solar flare tracks in individual grains from the gas-rich Kapoeta howardite (**a**) and the CM chondrite Murchison (**b**). The scale bar is 10 micron in both cases. Note the gradient in track density (with high track density near the edge of the grains to the left), reflecting the steeply falling energy spectrum of the solar flare heavy nuclei.

Since the solar wind and solar flare irradiation of individual components of gas-rich meteorites, comprising both single grains and xenoliths (rock fragments), preceded the compaction of these meteorites, the study of the irradiation records in these components provide the unique opportunity for obtaining information on the solar activity at different epochs in the past. Although it is difficult to obtain information about the time of compaction of the gas-rich meteorites, the available data suggest that the compaction of the CI and CM chondrites took place more than 4 b.y. (billion years) ago (Macdougall and Kothari 1976) and it could be about 1·4 to 3·7 b.y. ago for other types of chondrites and achondrites (Schultz and Signer 1977; Rajan *et al* 1979). Information on the intensity and composition of solar flare particles during the early history of the sun, based on studies of gas-rich meteorites, has been summarized by Rajan (1974), Goswami *et al* (1980) and Crozaz (1980).

Apart from obtaining information about the activity of the ancient sun, studies of nuclear tracks and other cosmogenic effects in samples of gas-rich meteorites also provide valuable insight into the dynamical accretionary and evolutionary process of solar system objects. There is a general consensus at present that most of the gas-rich meteorites are regolithic* breccias from an asteroidal surface, and that the individual components of these meteorites received their solar flare and solar wind irradiation while residing in the asteroidal regolith. This scenario which was postulated quite some time back (Suess *et al* 1964) gained wider acceptance only after the analysis of lunar samples and the observed similarity in the solar wind-solar flare records of the gas-rich meteorites and the lunar soils and soil breccias, which are definitive regolith products, and some of which are gas-rich in character (Lal and Rajan 1969; Pellas *et al* 1969; Wilkening 1971; Pellas 1972; Poupeau and Berdot 1972; Rajan 1974; Poupeau *et al* 1974). Detailed comparison of solar flare irradiation records in lunar soil grains and track-rich grains in gas-rich meteorites and the observed anisotropy in the track irradiation pattern in the track rich grains ruled out the possibility that these grains were irradiated individually in free-space prior to their compaction into these meteorites (such an irradiation would have led to an isotropic track irradiation pattern). As the case for regolith evolution of gas-rich meteorites has been strengthened, attempts have been made to characterize the nature of the asteroidal regolith and the associated impact processes, and model the dynamical evolution of the asteroidal regolith (Anders 1975, 1978; Price *et al* 1975; Housen *et al* 1979; Langevin and Maurette 1980), based on our present understanding of processes taking place in the lunar regolith (Gault *et al* 1974; Arnold 1975; Langevin and Arnold 1977). The effect of several important parameters *e.g.* differences in gravity field and the flux and velocity of bombarding objects etc., in the lunar and asteroidal cases, has to be considered in these calculations. The results obtained indicate much higher values for the regolith thickness on asteroidal objects, extending upto several hundreds of metres, as opposed to about ten metres in the case of the moon. Although there seems to exist a *qualitative* agreement between the observed solar wind-solar flare irradiation features in gas-rich meteorites and those predicted on the basis of regolith evolution models, it must be noted here that in all the attempts made so far to explain the cosmogenic features seen in gas-rich meteorites, the *pre-compaction* exposure

*The term 'regolith' refers to the upper layers of dust and rocklets produced by impact processes on atmosphereless bodies of the solar system (*e.g.* moon, asteroids). The thickness of this layer depends on the physical characteristics of the bodies and the impacting objects, and can vary from a few metres to a few hundred metres.

duration of individual components of these meteorites within the ' nuclear-active ' region in the asteroidal regolith, has been considered as a free parameter or equated to the total cosmic ray exposure duration. Based on a re-evaluation of this problem Goswami and Lal (1979) postulated that the regolith irradiation scenario for gas-rich meteorites is not compatible at least in the case of the CI and CM (carbonaceous type 1 and 2) chondrites. They have based their argument on the fact that the pre-compaction irradiation durations, during which the individual components of the gas-rich meteorites must have received their solar flare and solar wind irradiation, is extremely short ($< 10^5$ yr) in the case of CI and CM chondrites, and have shown that such short duration irradiation in the asteroidal regolith cannot lead to the observed solar flare irradiation features in these meteorites. Goswami and Lal (1979) considered the difference between the exposure ages based on cosmogenic stable isotopes and radionuclides as the measure for pre-compaction irradiation duration. Such an approach is appropriate since the stable isotope age of a gas-rich meteorite will represent both the pre-compaction irradiation duration and the recent exposure duration of the meteorite as a small object in space, while the radionuclide exposure age will represent only the recent exposure duration in space.

As an alternative to the regolith scenario, Goswami and Lal (1979) have proposed that the solar flare and solar wind irradiation of individual components of gas-rich carbonaceous chondrites took place while they were residing in the surface or near surface regions of centimetre to metre size objects, prior to the formation of asteroidal size parent bodies. This must have happened in the very early stages of the evolution of the solar system. Lack of evidence for irradiation of individual grain in space requires that the pressure in the solar nebula was sufficient ($> 10^{-10}$ Atm.) to shield the grains from solar flare and solar wind particles until their incorporation into cm to metre size objects. Some of our recent studies (Goswami and Lal, unpublished) indicate that it is probable that some individual grains received direct solar flare irradiation, while being partially shielded by the gas pressure in the nebula itself. The centimetre to metre size bodies must coalesce to form larger size objects ($\geqslant$ km), within a short duration of $10^{4\pm1}$ yr, to effectively cut-off further solar flare and galactic cosmic ray irradiation, so that the constraint on the short pre-compaction irradiation duration can be satisfied. Collision among these large objects will finally lead to the formation of larger size parent bodies of CI and CM chondrites, which will thus form out of an irradiated swarm of objects, and shall contain ' irradiated ' material throughout its entire volume. This feature can readily explain the high percentage of gas-rich meteorites among the CI and CM chondrites. While impact-induced regolithic activity will definitely be present in the parent bodies of these meteorites and may lead to excavation, fragmentation and redistribution of material, the solar-wind and solar flare records seen in individual components from the gas-rich members in these groups were essentially those imprinted prior to the formation of the parent bodies.

In view of the above development, a re-evaluation of our present understanding of the irradiation features seen in gas-rich meteorites as due to their exposure in asteroidal regoliths is becoming necessary. Work is currently in progress (Goswami and Nishiizumi, unpublished) to accurately determine the pre-compaction irradiation durations of gas-rich meteorites belonging to other chondritic and achondritic groups, based on measurements of noble gas and radionuclide exposure ages (on aliquots of the same sample). This approach, however, is feasible only in the case of meteo-

rites with low exposure ages (*e.g.* H chondrites) since for meteorites with recent space exposure age exceeding 10 m.y., the radionuclides (^{26}Al, ^{53}Mn) generally used for exposure age determination suffer from saturation effect. Additional experiments to determine the possibility of very different exposure histories of the irradiated and un-irradiated components in gas-rich meteorites are also necessary to get insight into the finer details of the exposure history of these meteorites. Future work along these directions could be expected to give us valuable information on the accretionary and evolutionary history of small objects in the early solar system.

References

Anders E 1975 *Icarus* **24** 363

Anders E 1978 in *Asteroids: an exploration assessment*, NASA Conf. Publ. 2053, p. 57

Arnold J R, Honda M and Lal D 1961 *J. Geophys. Res.* **66** 3519

Arnold J R 1975 *Proc. Lunar Sci. Conf. 6th* (New York: Pergamon Press) p. 57

Bagolia C, Bhandari N, Sinha N, Goswami J N, Lal D, Lorin J C and Pellas P 1980 *Bull. Astr. Soc. Czech.* **31** 51

Bagolia C, Doshi N, Gupta S K, Kumar S, Lal D and Trivedi J R 1977 *Nucl. Track Detection* **1** 83

Bagolia C, Lal D, Sinha N and Sears D 1978 *Nucl. Track Detection* **2** 29

Baldwin B and Sheaffer Y 1971 *J. Geophys. Res.* **76** 4653

Bhandari N 1981 *Proc. Indian Acad. Sci.* (*Earth Planet. Sci.*) **90** 359

Bhandari N, Lal D, Rajan R S, Arnold J R, Marti K and Moore C B 1980 *Nucl. Tracks* **4** 213

Bhandari N and Potdar M B 1981 *Earth Planet. Sci. Lett.* (in press)

Bhattacharya S K, Goswami J N and Lal D 1973 *J. Geophys. Res.* **78** 8356

Bhattacharya S K, Imamura M, Sinha N and Bhandari N 1980 *Earth Planet. Sci. Lett.* **51** 45

Bull R K and Durrani S A 1976 *Earth Planet. Sci. Lett.* **32** 35

Cantelaube Y, Pellas P, Nordemann D and Tobailem J 1969 in *Meteorite research*, ed. P M Millman (Holland: D Reidel) p. 705

Crabb J and Schultz L 1981 *Geochim. Cosmochim. Acta* (in press)

Crozaz G 1980 in *The ancient sun* (New York: Pergamon Press) p. 331

Eberhardt P, Eugster O, Geiss J and Marti K 1966 *Z. Natuurforsch.* **A21** 414

Fleischer R L, Price P B, Walker R M, Maurette M and Morgan 1967 *J. Geophys. Res.* **72** 355

Gault D E, Horz F, Brownlee D E and Hartung J B 1974 *Proc. Lunar Sci. Conf. 5th* (New York: Pergamon Press) p. 2365

Goswami J N, Lal D, Rao M N, Sinha N and Venkatesan T R 1978 *Meteoritics* **13** 481

Goswami J N and Lal D 1979 *Icarus* **40** 510

Goswami J N, Lal D and Macdougall J D 1980 in *The ancient sun* (New York: Pergamon Press) p. 347

Gupta S K and Lal D 1978 *Nucl. Track Detection* **2** 37

Housen K R, Wilkening L, Chapman C R and Greenberg R 1979 *Icarus* **39** 317

Imamura M, Nishiizumi K and Honda M 1979 *Mem. Natl. Inst. Polar Res.* **15** 227

Jha R and Lal D 1981 (in preparation)

Lal D 1972 *Space Sci. Rev.* **14** 3

Lal D, Lorin J C, Pellas P, Rajan R S and Tamhane A S 1969 in *Meteorite research*, ed. P Millman (Holland: D Reidel) p. 275

Lal D and Rajan R S 1969 Nature (London) **223** 269

Langevin Y and Arnold J R 1977 *Annu. Rev. Earth Planet. Sci.* **5** 449

Langevin Y and Maurette M 1980 in *Lunar Planet. Sci.* 11 (Houston: Lunar Sci. Inst.) p. 602

Lorin J C and Pellas P 1975 *Meteoritics* **10** 445

Macdougall J D and Kothari B K 1976 *Earth Planet. Sci. Lett.* **33** 36

McCrosky R E 1968 in Research in space science, Smithsonian Astrophys. Observatory Sp. Report No. 280, p. 1

Opik E J 1958 *Physics of meteor flight in the atmosphere* (New York: Interscience)

Pellas P 1972 in *Proc. Noble Symp.* 21: *From plasma to planets* (New York: John Wiley) p. 65
Pellas P, Poupeau G, Lorin J C, Reeves H, Audoue J 1969 *Nature* (*London*) **223** 272
Poupeau G and Berdot J L 1972 *Earth Planet. Sci. Lett.* **14** 381
Poupeau G, Kirsten T, Steinbrunn F and Storzer D 1974 *Earth Planet. Sci. Lett.* **24** 227
Price P B, Rajan R S and Tamhane A S 1967 *J. Geophys. Res.* **72** 1377
Price P B, Hucheon I D, Braddy D and Macdougall J D 1975 *Proc. Lunar Sci. Conf. 6th* (New York Pergamon Press) p. 3449
Rajan R S 1974 *Geochim. Cosmochim. Acta* **38** 777
Rajan R S, Huneke J C, Smith S P and Wasserburg G J 1979 *Geochim. Cosmochim. Acta* **43** 957
Reedy R C, Arnold J R and Lal D 1981 Preprint
Revelle D O 1978 in Carnegie Institution, Department of Terrestrial Magnetism, Washington D.C Annual Report, p. 475
Schultz L and Signer P 1977 *Earth Planet. Sci. Lett.* **36** 363
Singhvi A, Sengupta D and Bhandari N 1981 (in preparation)
Suess H E, Wanke H and Wlotzka F 1964 *Geochim. Cosmochim. Acta* **28** 595
Turner G 1979 *Proc. Lunar Planet Sci. Conf.* 10*th* (New York: Pergamon Press) p. 1917
Walker R M 1975 *Annu. Rev. Earth Planet. Sci.* **3** 99
Wanke H 1966 *Fortschr. Chem. Forsch.* **7** 322
Wetherill G W 1980 in Carnegie Institution, Department of Terrestrial Magnetism, Washington D.C. Annual Report, p. 546
Wilkening L 1971 in *Particle track studies and the origin of gas-rich meteorites* (Tempe: Arizona State Univ.) p. 1

Records of ancient cosmic radiation in extraterrestrial rocks

NARENDRA BHANDARI
Physical Research Laboratory, Ahmedabad 380 009, India

Abstract. Recent results on cosmic ray interactions in lunar samples and meteorites resulting in production of stable and radionuclides, particle tracks and thermoluminescence are reviewed. A critical examination of ^{26}Al depth profiles in lunar rocks and soil cores, together with particle track data, enables us to determine the long term average fluxes of energetic solar protons (> 10 MeV) which can be represented by $(J_S, R_0) = (125, 125)$. The lunar rock data indicate that this flux has remained constant for 5×10^5 to 2×10^6 years.

Production rates of stable and radionuclides produced by galactic cosmic rays is given as a function of size and depth of the meteoroid. Radionuclide (^{53}Mn, ^{26}Al) depth profiles in meteorite cores, whose preatmospheric depths are deduced from track density profiles are used to develop a general procedure for calculating isotope production rates as a function of meteoroid size. Based on the track density and ^{22}Ne/^{21}Ne production rates, a criterion is developed to identify meteorites with multiple exposure history. ^{22}Ne/^{21}Ne ratio $< 1{\cdot}06$ is usually indicative of deep shielded exposure. An examination of the available data suggests that the frequency of meteorites with multiple exposure history is high, at least 15% for LL, 27%for L and 31% for H chondrites. The epi-thermal and the thermal neutron density profiles in different meteorites are deduced from ^{60}Co and track density data in Dhajala, Kirin and Allende chondrites. The data show that the production profile depends sensitively on the size and the chemical composition of the meteoroid.

Cosmic ray-induced thermoluminescence in meteorites of known preatmospheric sizes has been measured which indicates that its production profile is nearly flat and insensitive to the size of the meteoroid.

Some new possibilities in studying cosmic ray implanted radionuclides in meteorites and lunar samples using resonance ionisation spectroscopy are discussed.

Keywords. Solar cosmic rays; meteorites; particle tracks; thermoluminescence; lunar samples; radioactivity; resonance ionisation spectroscopy.

1. Introduction

The chemical and mineral constituents of rocks, exposed to cosmic radiation undergo atomic and nuclear transformations, which are now well established. The cosmic ray interactions thus result in the following effects:

(i) Nuclear species, both stable and radioactive, produced in nuclear reactions, mainly by cosmic ray primary and secondary protons, alpha particles and neutrons with target elements present in the rock material.

(ii) Particle tracks produced in crystalline material due to intense ionisation produced by heavy nuclei ($Z > 20$).

(iii) Thermoluminescence produced by charged particles, mainly low energy protons, in crystalline material.

In addition, a heavy dose of charged particles, due to exposure to solar wind and solar flares, produces radiation damage which can be easily identified in the surface regions of mineral grains.

Characteristics of cosmic rays in the remote past have been deduced from a study of such records in meteorite, lunar and terrestrial samples. In this way, the energy spectra, composition and their spatial and temporal variation in the interplanetary space have been deduced. Several exhaustive reviews of the work done in this field exist (Lal 1972, 1977; Reedy *et al* 1981; Walker 1975; Bhandari and Rao 1980) and therefore we confine our discussion to a critical assessment of some new results obtained in the last few years. The subject of cosmic ray production of tracks in lunar and meteorite minerals and their implications to the exposure history of meteorites has been covered in another paper appearing in this issue (Goswami 1981).

As all these samples are subjected to a number of natural processes, occurring simultaneously while the cosmic ray effects are accumulating, the resultant records are complex composites of several components which depend upon the exposure history and exposure geometry of individual samples. Here we describe some of the basic features of these records in meteorites and lunar samples and their limitations in deducing the characteristics of ancient cosmic rays.

2. Solar cosmic rays

Rocks and soil exposed on the lunar surface serve as excellent detectors for some components of solar and galactic cosmic rays. However, a large number of processes occur in the lunar regolith such as erosion by micrometeorites and solar wind, fragmentation of rocks, repeated burial and excavation, shock heating and collisional melting, which modify these records to an extent that it is difficult to use them directly to deduce cosmic ray fluxes. After examining a large number of the most favourable cases, it has now been realised that there are no lunar rocks which have had a simple one-stage exposure on the moon. Thus the geometry in which the rocks are found on the moon represents only the terminal phase of their exposure. Since almost all the rocks have either been fragmented, multiply exposed at various times in different geometries at different depths or have been shocked, it is difficult to use them as cosmic ray detectors until their exposure history is fully understood. This complex exposure is the main cause for the fact that exposure ages of rocks obtained by different methods *i.e.* tracks, radioisotopes, raregases, microcraters, neutron effects etc. are not concordant (Lal 1977). A rock with a simple one-stage exposure will be characterised by concordant exposure ages by all these methods but no such case has been found so far. Also rocks lying on the lunar surface undergo change in geometry, typically on time scales of a million years so that the earlier solar cosmic ray (SCR) records are usually disturbed in the lunar rocks and cannot be easily understood.

In order to deduce solar flare fluxes using lunar rocks it is therefore not adequate to measure any of the cosmic ray produced effects mentioned above; rather several types of studies have to be conducted simultaneously on carefully selected samples. In our laboratory we have adopted a procedure for understanding the exposure history of a sample, determination of erosion effects and surface exposure ages (Bhandari *et al* 1975; Bhattacharya and Bhandari 1975). This approach seems to be quite satisfactory for selecting a proper sample for cosmic ray studies and is described below.

The surface orientation of a large number of lunar rocks on the moon's surface is well documented from lunar surface photography of these samples. Of these, low

exposure age rocks (5 m.y. or less), as determined by rare gas data, were selected. Track density profiles in several sections of surface chips were measured. The track density at various depths (X) within a lunar rock ρ (X) divided by the track production rate $\dot{\rho}$ (X) gives a curve such as shown in figure 1. The steeply rising part of this curve at shallow depths (< 1 mm) allows us to estimate the erosion rate of the rock on the moon and the flatter part at depths > 1 mm reflects the exposure history which, in some favourable cases of a single-stage exposure on the lunar surface, develops into a plateau and enables us to estimate the surface exposure age of the rock to *galactic cosmic rays* (GCR) (Bhattacharya and Bhandari 1975). In the case of rocks which show a well-defined plateau, the solar flare exposure age equals the galactic cosmic ray exposure age. The error in the estimate of such an exposure age is mainly due to the uncertainty in the *average* track production rates in the past. Various estimates of the production rates (Yuhas and Walker 1973; Bhandari *et al* 1971; see also Goswami 1981) agree within about 20% at the depths of interest. Only rocks where tracks and rare gas exposure ages are (nearly) concordant were then considered suitable for further analysis of radioisotopes.

In this way, we were able to select five lunar rocks 61016, 64435, 66095, 75035 and 79215 with known solar flare exposure history and orientation on the lunar surface. These are listed in table 1. Also included are rocks 12002, 14310, 14321 and 68815, studied by other groups (Wahlen *et al* 1972; Kohl *et al* 1978) for solar flare records. Of these the rock 61016 is the most suitable because it has the closest concordance of He, Ne, and track ages. Others like 75035, 12002, 14321 have discordant exposure ages as determined by various methods.

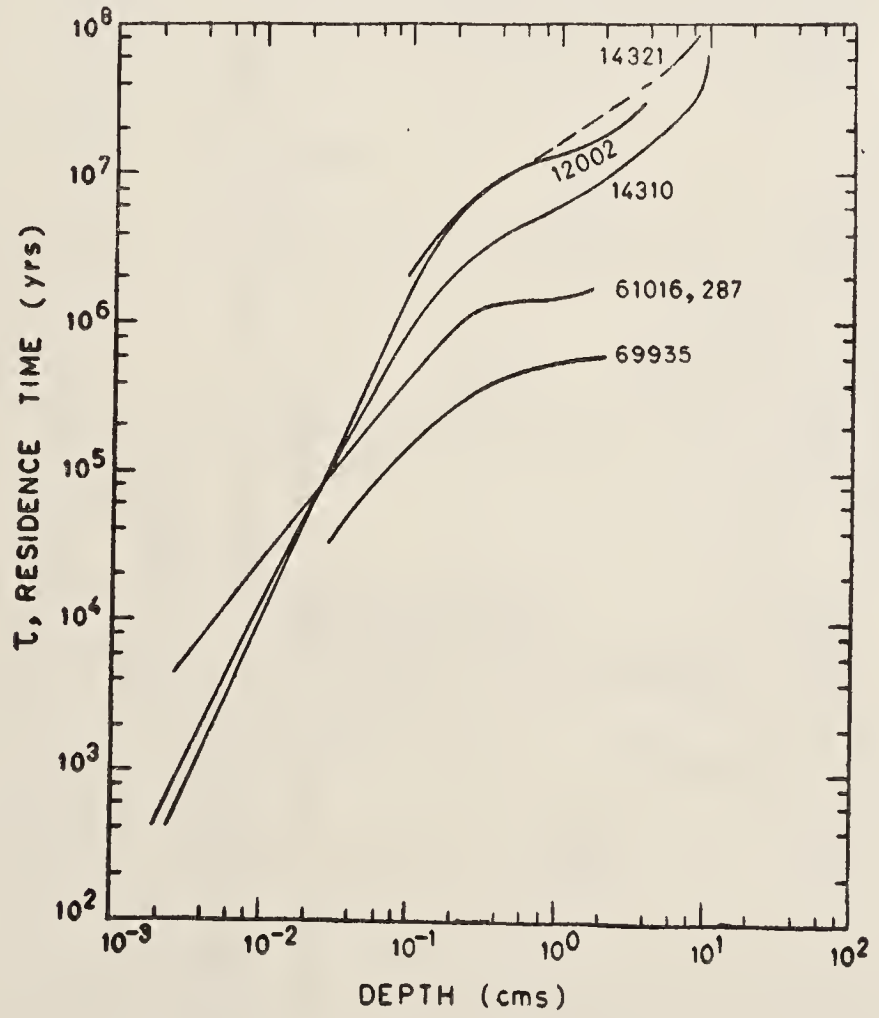

Figure 1. The exposure age plateau curve. The apparent residence time for various rocks is plotted as a function of depth. 61016 shows a good plateau in 0·2-2 cm range showing a simple exposure history with surface exposure age of 1·5 m.y. Other rocks 12002, 14310 and 14321 do not show any plateau indicative of complex exposure history with short surface residence time. (After Bhandari *et al* 1975)

Table 1. Lunar rocks studied for solar flare fluxes and their exposure systematics (1).

Rock	Exposure age (m.y.) based on					Erosion rate mm/m.y.	Exposure history	^{26}Al activity (dpm/kg)	Deduced J_s based on	
	^{3}He	^{21}Ne(6)	^{38}Ar(6)	^{81}Kr	track density				^{26}Al	^{53}Mn
12002		92			1·5(4)	0·5(5)	Complex	210(3)	90	210
14310		262			1·0(4)	—	Complex	80(3)	—	400
14321		20			2·0(4)	2·2(5)	Complex	160(3)	70	150
68815	0·06	1·2	2·2	2±0·1	2	1·3(5)	2 stage	334(3)	100	110
61016	1	1·3/4	1·7/3.7		1·5	1	1 or 2	735±75(2)	125	—
64435		0·6/1·2	0·8/1·4		0·5	1	Simple	375±65(2)	145	—
66095		1·1			1·0	0·5	—	415±70(2)	115	—
79215	180	~4/180	170		3·7	0·8	Complex	735±110(2)	140	—

(1) The data are from various sources mentioned in Bhattacharya (1979), Kohl *et al* (1978), Bhandari *et al* (1975), Dust and Crozaz (1977), Nautiyal *et al* (1981) and Venkatesan *et al* (1980).

(2) Surface activity in 0-0·3 mm depth interval.

(3) In these cases, the activity refers to 0-0·5 mm or 0-1 mm depth interval.

(4) In the absence of a plateau in the exposure age (figure 1), the approximate SCR exposure age is determined from track density and production rate at 1 mm.

(5) Assumed to match solar flare fluxes (Kohl *et al* 1978).

(6) The first value refers to SCR exposure age and the second value to GCR exposure age.

The slope (β) of the curve shown in figure 1 gives the erosion rate (Bhattacharya and Bhandari 1975). This has been calculated for each rock studied by our group and the values are given in table 1. For others the *assumed* erosion rates are given. The plateau region is nearly flat in some of these rocks as shown by the typical case of 61016. In other cases *e.g.* 12002, 14310 and 14321 there is no plateau indicative of a complex exposure history and *short* ($\leqslant$ 1 m.y.) exposure age on the lunar surface.

The surface chips of these rocks were microscopically examined for microcraters and it was found that only a part of the surface had remained well preserved and some areas had apparently suffered attrition. The well-preserved areas can also be easily distinguished by surface albedo, particularly in the case of anorthositic rocks. The well preserved area were selected for ^{26}Al measurements as described below (Bhandari *et al* 1975).

The ^{26}Al activity produced in the top layer (mean thickness 90 mg/cm^2) of rocks 61016, 64435, 66095, 75035 and 79215 were measured by the non-destructive β-γ coincidence technique (Bhandari 1977). This technique not only offers a very high depth resolution, determined by the half thickness of ^{26}Al decay positrons, but also allows selection of the surface area to be counted. The surface activity of ^{26}Al determined by this method is given in table 1.

Two of the rocks 61016 and 66935 were chosen for a more detailed depth profile using radiochemical separation techniques for ^{26}Al. The observed depth profile in rock 61016 is shown in figure 2. This has been determined nondestructively by β-γ counting as well as after radiochemical separation of ^{26}Al (Potdar 1981; Bhandari *et al* 1981b). These data can be used to determine the solar flare proton energy spectrum, which is responsible for ^{26}Al production, after taking into account the target element abundance, erosion rate and the lunar orientation of the sample. The solar flare flux $J(> 10$ MeV) as a function of rigidity R of the particles is usually represented in the form

$$dJ_s = K_s \exp(-R/R_0)\, dR,$$

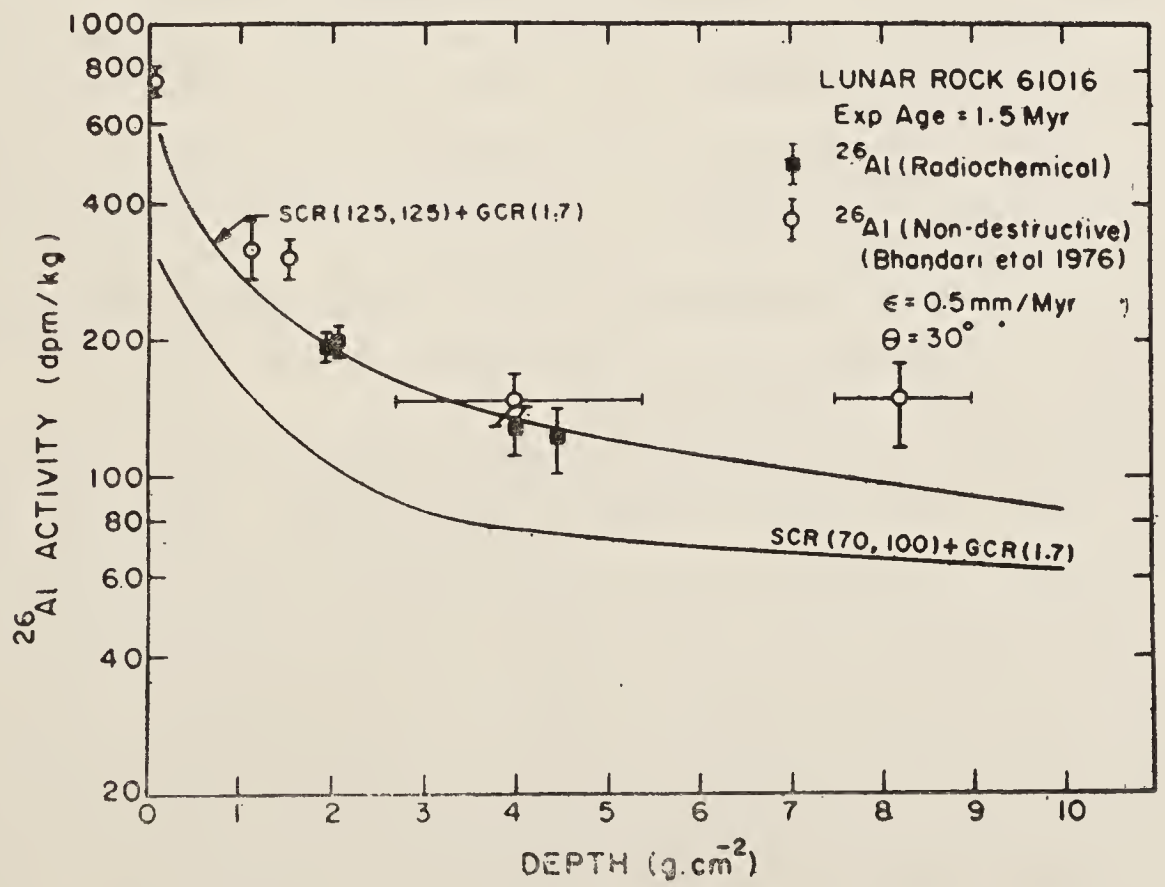

Figure 2. The measured ^{26}Al activity in rock 61016 is plotted as a function of depth. The thick curves are production profiles expected for SCR and GCR parameters as indicated (Bhandari, Potdar and Shukla, in preparation). ϵ is the erosion rate and η is the zenith angle of the rock chip on the moon.

where R_0 is the characteristic rigidity. We have calculated production rates with various sets of J_s and R_0 to find the best match with the observed values. The results as shown in figure 2 indicate that $(J_s, R_0) = (125, 125)$ best reproduce the observed profiles. It should be noted, as pointed out by Wahlen *et al* (1972), that the estimation of J_s or R_0 individually is not unique but other combinations with higher J_s and lower R_0 or *vice versa* would reproduce the observations equally well.

Some other groups (Boeckl 1972; Begemann *et al* 1972; Kohl *et al* 1978 and others) have also made attempts to determine the solar flare fluxes in the past based on radionuclides ^{26}Al, ^{53}Mn, ^{14}C and rare gas isotopes *e.g.* ^{3}He (Venkatesan *et al* 1980), and deduced flux parameters which ranged between $(J_s, R_0) = (70–200, 80–150)$. Whether such a large range of parameters represents actual time variations in solar flare fluxes or due to inherent uncertainties in the technique applied or due to improper sample studied as discussed above, has been a matter of intense debate. Time variations in solar flare and radiation fluxes have important implications to the stellar structure and affects the planetary climates and interplanetary medium (Eddy 1976). We should, however, exclude other possible causes for this wide range of parameters before they are attributed to solar variations. As pointed out earlier, there are several problems in deducing the correct flux from lunar rock data. These include corrections for exposure geometry, exposure history and erosion rate applicable to each rock which have to be independently inferred. In the radioisotopic work the most serious error arises from the assumption usually made that the rocks are saturated *i.e.* exposed for a time long enough to bring the radioisotope production in secular equilibrium with its decay. Though this assumption is usually valid for short-lived nuclides like ^{14}C, it is clear from the vast amount of work on microcraters, tracks and rare gases that no rocks are exposed for so long ($> 10^7$ years) on the lunar surface as to let ^{53}Mn to be saturated. The assumption is also not valid for ^{26}Al except in some rare cases where the surface exposure age of the rock is $\gtrsim 5 \times 10^6$ years. Most of these estimates therefore tend to give lower fluxes which should be corrected for undersaturation. The rocks 12002, 14310, 14321, etc. (Wahlen *et al* 1972; Kohl *et al* 1978) have had a short surface exposure as determined by track density profiles. The flux of (70, 100) deduced from the ^{26}Al and ^{53}Mn profile in these rocks, which has not been corrected for exposure age, is therefore in error. In the case of rare gas isotopes the diffusion losses during micrometeorite impacts and shock melting are serious as pointed out by Yaniv (1981). Furthermore the rare gases produced in pre-surface expsoure, which are sometimes partially retained by the rock may lead to serious uncertainties in estimating correct depth profile due exclusively to solar flare production.

Unfortunately there is no independent method, which gives an accurate estimate of the exposure ages, other than the track density profiles. The track method also works only in some favourable cases of simple exposure as discussed earlier. The rock 68815, whose exposure age is determined by ^{81}Kr–^{83}Kr method to be 2 m.y. (Behrmann *et al* 1973) has been studied in detail for ^{26}Al and ^{53}Mn (Kohl *et al* 1978). The ^{81}Kr–^{83}Kr age refers to the GCR age and not to the surface exposure or the sun-tan age. The track density profiles measured by Behrmann *et al* (1973) and Dust and Crozaz (1977) indicate that small-scale chipping of the rock cannot be ruled out. The plateau method indicates two-stage irradiation, probably due to a minor fragmentation event during the past 2 m.y. It is difficult to estimate the sun-tan age of this rock but this should be smaller than 2 m.y.

Lunar soil cores offer another set of samples for the estimation of solar flare fluxes. Except for the top few millimetres where the stratigraphy is disturbed by micrometeorite gardening, the soil column is generally static on a million year time scale and the uncertainty of short exposure age, as in the case of rocks, can be eliminated. The ^{26}Al data in Apollo 15 drive core tube (Fruchter *et al* 1976) are shown in figure 3. Similar measurements have been made in other drive tubes and Fruchter *et al* (1981) found that the observed integral flux is 60% more than the value calculated from SCR flux $(J_s, R_0) = (70, 100)$ and the GCR flux of 1·7 p/(cm^2 sec 4π) . The radioactivity integrated over the length of the core must match the production rate, irrespective of gardening, unless the top soil is physically transported to or away from the sampling site by some mechanism. The flux of (70, 100) is therefore clearly inadequate to explain the observed activity. If we ignore the top few millimetres which may have been accumulated from deep cratering event recently or disturbed by gardening, it is clear from figure 3 that a good match between the observed and calculated fluxes is obtained if (J_s, R_0) is taken to be (125, 125). We thus find the core tube data support the flux estimates of (125, 125) deduced from rock 61016. This flux would also explain the activity level observed in rock 14310 which has a sun-tan age of 1 m.y. (Kohl *et al* 1978).

The short-lived isotopes ^{14}C (meanlife 8200 yr) and ^{81}Kr (meanlife 3×10^5 yr) yield fluxes of $(J_s, R_0) = (200, 100)$ (Begemann *et al* 1972; Regnier *et al* 1979; Reedy 1980). Assuming (70, 100) to be flux values over $10^6 - 10^7$ yr., Reedy (1980) and Zook (1980) have argued that the ^{14}C, ^{81}Kr and TL data support time variation of the average solar flare fluxes and indicate that the flux over the past $10^3 - 10^5$ years has been higher than during $10^6 - 10^7$ yrs. Although from the arguments presented above, it appears that all the nuclides are consistent with $(J_s, R_0) = (125, 125)$ or probably with somewhat higher fluxes. Therefore the proposed variations need to be confirmed by better cross-section and activity measurements.

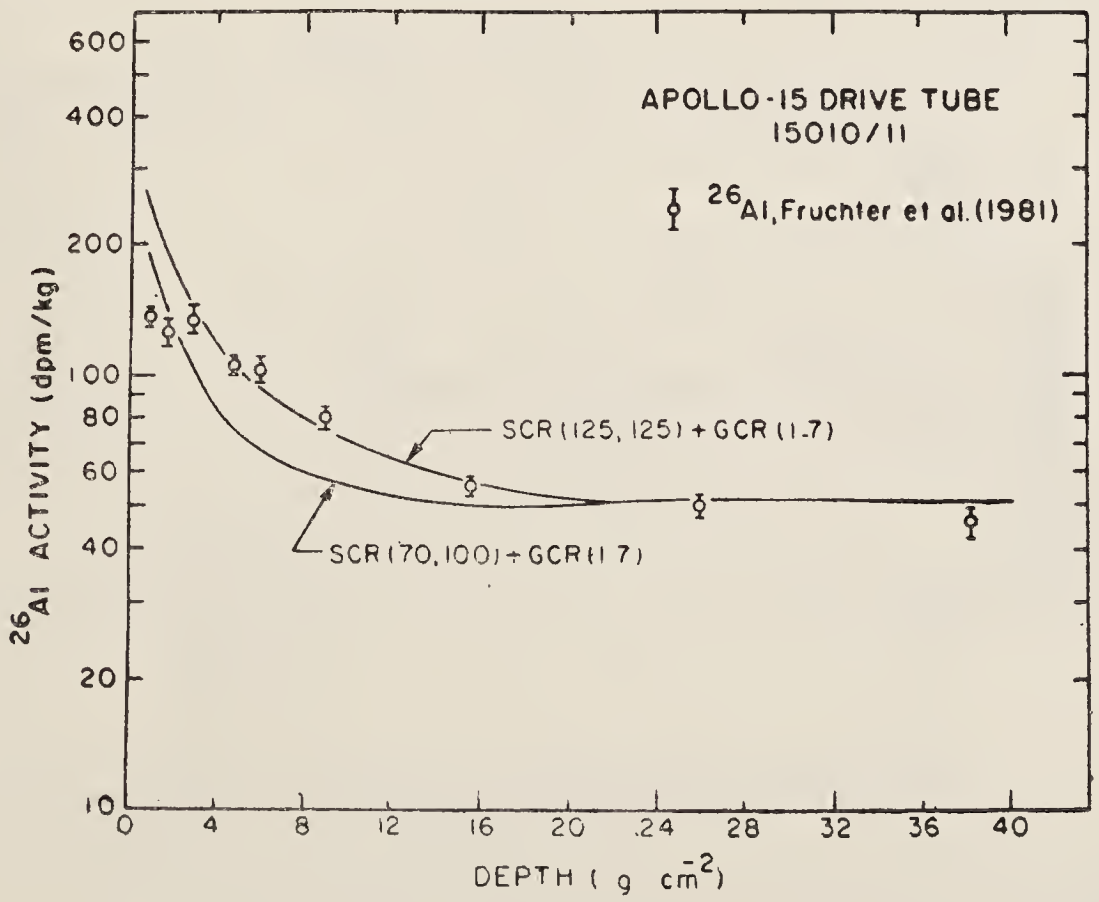

Figure 3. The measured ^{26}Al activity in Apollo 15 drive core tube 15010/11. The solid curves indicate the expected profiles for the SCR and GCR parameters as indicated (Bhandari, Potdar and Shukla, in preparation).

3. Constancy of solar flare particle fluxes

Variations in the frequency and intensity of solar flares with the sun spot cycle are well established. The *average* solar flare fluxes over the solar cycle 19 was (378, 100–130), this being the most active sun spot cycle recorded in the last two centuries with sun spot number $R_{max} = 210$. Compared to this, solar cycle 20 had, $R_{max} = 110$ and average $(J_s, R_0) = (90, 85)$ (Reedy 1977; Goswami *et al* 1981; Potdar 1981). This has led to speculations about long term variations in the solar activity. Because of the immense influence the sun has on the terrestrial climate, there has recently been a renewed interest to examine the relationship of major climatic changes on the earth in the past and the variations in the energy out-flux from the sun. Experimentally, it is an extremely difficult problem. At least for the past few decades where reliable data are available, the solar *radiation* output has been found to be remarkably constant, within about 1% (Kondrateyev and Nikolsky 1970) even as the particle flux from the sun has changed significantly as mentioned above (Reedy 1980; Potdar 1981). Statistically, the solar constant seems to be related to the sunspot number (Kondrateyev and Nikolsky 1970). If the radiation and corpuscular flux are related, it appears from these data that the variations in the radiation flux from the sun are magnified by several orders of magnitude in the corpuscular flux. Solar corpuscular flux, particularly of the high energy components, is easy to estimate from its nuclear effects in rocks. Lunar rocks thus provided an opportunity to determine variation in the time averaged ($5 \times 10^5 - 2 \times 10^6$ yr) energetic proton flux in the past (Bhandari *et al* 1976).

The rocks, listed in table 1, were exposed for different periods of time on the lunar surface. The activity of ^{26}Al was measured in the top layer of the rock, selectively in a thin layer (mean thickness 300 μ) defined by the range of aluminium-26 decay positrons as discussed earlier. The results are shown in figure 4. The activity in all rocks cluster around the expected level defined by ($J_s = 125$, $R_0 = 125$), thus showing

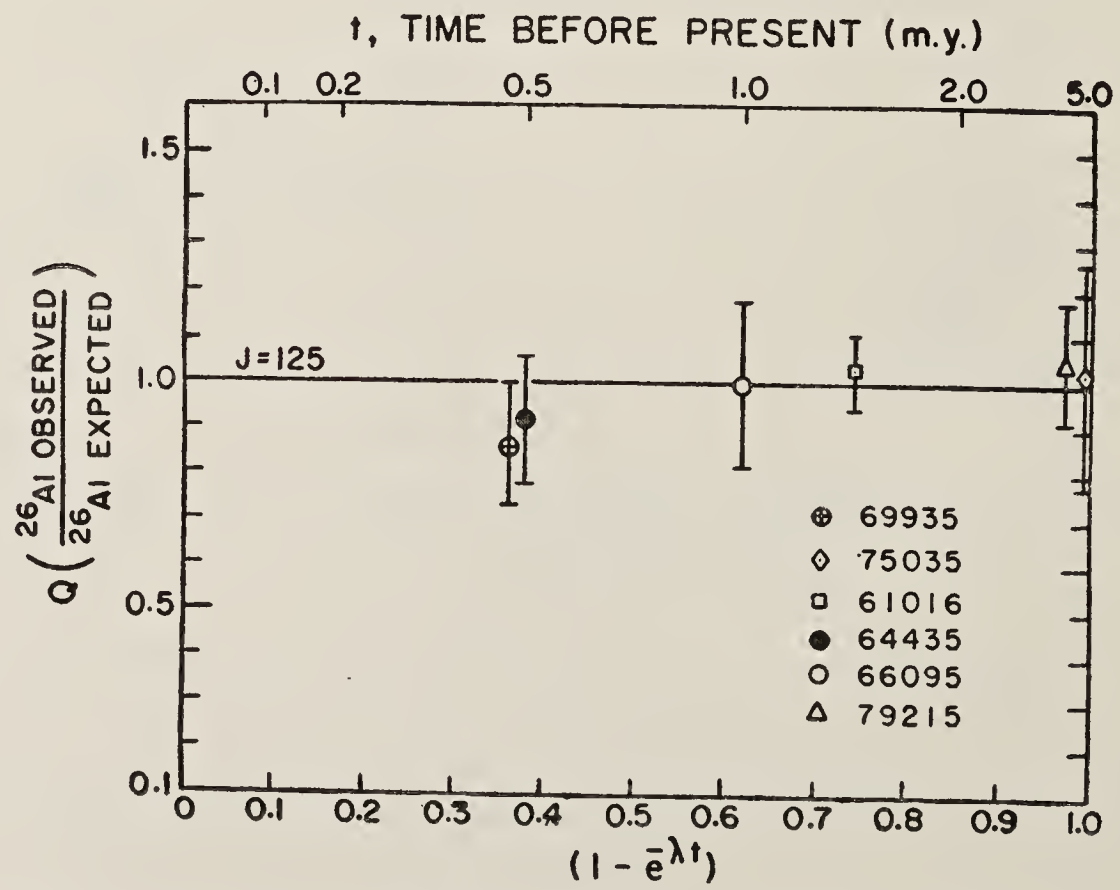

Figure 4. Ratio of the observed to expected ^{26}Al activity (based on $J_s = 125$, $R_0 = 125$.) $Q(t)$, as a function of time, measured in Apollo rocks (After Bhandari *et al* 1975). The deviation of Q from unity is small which rules out major changes in solar flare activity in the past.

that the *average* solar proton fluxes (> 10 MeV) integrated over the exposure age of the rocks have not varied beyond a level which is well within the errors of measurement.

4. Cosmic ray effects in meteorites

4.1 *Production of spallation products*

Meteorites are excellent monitors of cosmic ray intensity in the remote past since they are exposed to the cosmic rays in the inner solar system for time periods usually ranging from 10^6 to 10^9 years. The main difficulty arises from the fact that (i) their shape is significantly modified due to ablation during their atmospheric transit so that their geometry of exposure in space is not known and (ii) the dependence of production rates $P(X, R_E)$ as a function of depth (X) and size (R_E) on the primary cosmic ray spectrum is not known accurately.

The production P_i of a nuclide, from target nuclei j at a depth X in a spherical body of radius R_E depends on the target element abundance, N_j, excitation function σ_{ij} and flux of energetic nucleons $\phi(E, X, R_E)$ above the threshold energy E_T and is given by

$$P_i(X, R_E) = \sum_j \int_{E_T}^{\infty} N_j \cdot \sigma_{ij}(E) \cdot \phi(E, X, R_E)\, dE. \tag{1}$$

The excitation function σ_{ij} is known for several reactions (Tobailem 1977; Reedy and Arnold 1972) but still not available for many important reactions of interest, particularly for those induced by neutrons. $\phi(E, X, R_E)$ is also not known accurately although several attempts have been made to calculate the energy spectrum by Lavrukhina and Ustinova (1972), Kohman and Bender (1967) and Reedy and Arnold (1972). The accuracy of these calculations for production rates of various nuclides has however not yet been established although the measured concentrations of spallation products in most meteorites lie in the predicted range. Only in the case of Marjalhati pallasite, Bhattacharya *et al* (1980a) found that the measured profile of ^{53}Mn agrees with the calculated profile given by Kohman and Bender (1967). Recently Bhattacharya *et al* (1980b) and Bhandari and Potdar (1981) applied the Reedy-Arnold approach, as first used for calculating isotope production in the moon, to the case of meteorites and calculated the production rates of several stable and radionuclides. In the Reedy-Arnold formulation, the energy spectrum (primary + secondary) within the meteorite of radius R_E at any depth X is *assumed* to have the form

$$\phi(E, X, R_E) = k(X, R_E)\{\alpha(X, R_E) + E\}^{-2.5}, \tag{2}$$

where α is the spectral hardness parameter and k is the normalizing constant given by

$$k(X, R_E) = \frac{^3J_G(>1000 \text{ MeV}, X, R_E)}{2}\{\alpha(X, R_E) + 1000\}^{1.5}, \tag{3}$$

where J_G is the integral flux (above 1000 MeV) calculated from the attenuation of nucleons and fragmentation of alpha particles (and heavier nuclei) based on the primary flux

$$F_0 = J_G\,(X = 0,\ R_E = 0) = 1{\cdot}7\ \text{p/cm}^2.\ \text{sec}\ 4\pi sr.$$

At any depth X,

$$J_G\,(X, R_E) = \int_0^{2\pi} d\phi \int_0^{\pi} \Big[F_0 \exp\,(-\,r/\lambda_P) + a\,F_0 \exp\,(-r/\lambda_a) + \frac{ab\,Fo}{d}\{\exp\,(-r/\lambda_P) - \exp\,(-\,r/\lambda_a)\}/\left(\frac{1}{\lambda_a} - \frac{1}{\lambda_P}\right)\Big] \sin\,\theta\,d\,\theta, \quad (4)$$

where θ and ϕ are the zenith and azimuth angles and $r = r\ (X, R_E, \theta)$, distance of any point P from the surface along θ (Bhattacharya *et al* 1973a).

$$r = -\,(R_E - X)\cos\,\theta + \{R_E^2 \cos^2\,\theta + 2\,R_E\,X \sin^2\,\theta - X^2 \sin^2\,\theta\}^{1/2}, \quad (5)$$

where a = fraction giving the flux of alpha particles relative to protons, b = coefficient expressing the contribution to the flux from fragmentation of the alpha particles, d = interaction mean free path of alpha particles and

$$\frac{1}{\lambda_P} = \frac{1}{A} + \frac{1}{B}, \quad \text{and} \quad \frac{1}{\lambda_a} = \frac{1}{C} + \frac{1}{D},$$

where A and C are attenuation mean free paths and B and D ionisation mean free paths of protons and alpha particles respectively (Reedy and Arnold 1972).

We have experimentally determined the depth profiles of ^{53}Mn in meteorites whose preatmospheric sizes were determined by studying heavy ion tracks (Bhattacharya *et al* 1980b; Bhattacharya 1979). Assuming that these meteorites have been exposed to " normal " flux of galactic cosmic rays (1·7 p/cm^2.sec $4\pi sr$) and the energy spectrum of primary and secondary nucleons in the meteoroid is determined by the spectral shape parameter $\alpha\,(X, R_E)$ as in the Reedy-Arnold formulation, the values of α were calculated from equations 1, 2 and 3. The values of α (figure 5) and $\sigma(E)$ can then be used to deduce the production rates of other isotopes of interest such as ^{26}Al, ^{21}Ne, ^{22}Ne, ^{22}Na as a function of depth and size of the meteoroid (Bhattacharya *et al* 1980b; Potdar 1981; Bhandari and Potdar 1981). The calculated production profiles of some isotopes are shown in figure 6.

In general, it appears that the production rates increase with depth for ($R_E < 25$ cm). For larger meteoroids the isotope production rates increase steeply with depth near the surface giving a broad maximum at about 50 g cm^{-2}, followed by a slow decrease in the production rate thereafter as shown in figure 6. Measurements of particle tracks and radionuclides in several meteorites show a reasonable agreement

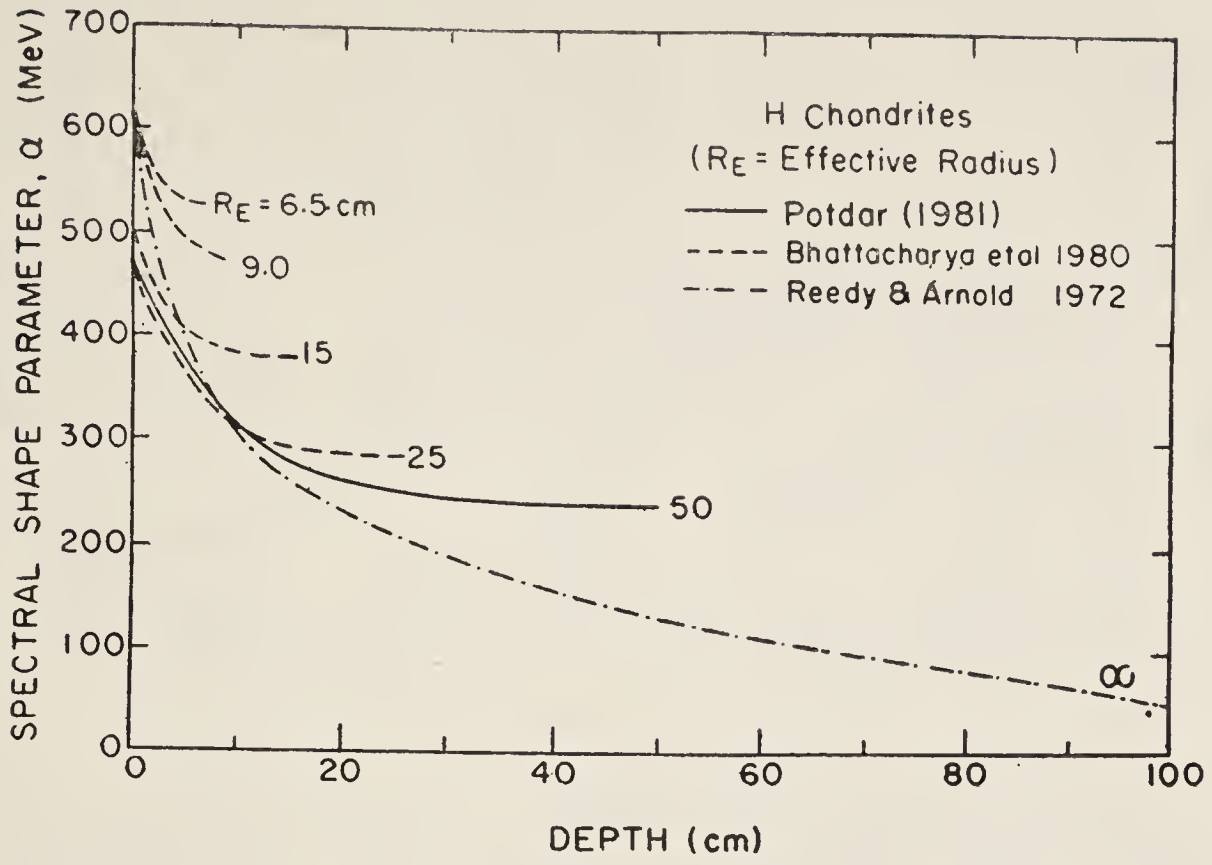

Figure 5. The spectral shape parameter α for meteoroids of various sizes (effective radius R_E) as a function of depth as determined by the observed ^{53}Mn profiles (Bhattacharya *et al* 1980) and ^{26}Al profile (Potdar 1981)

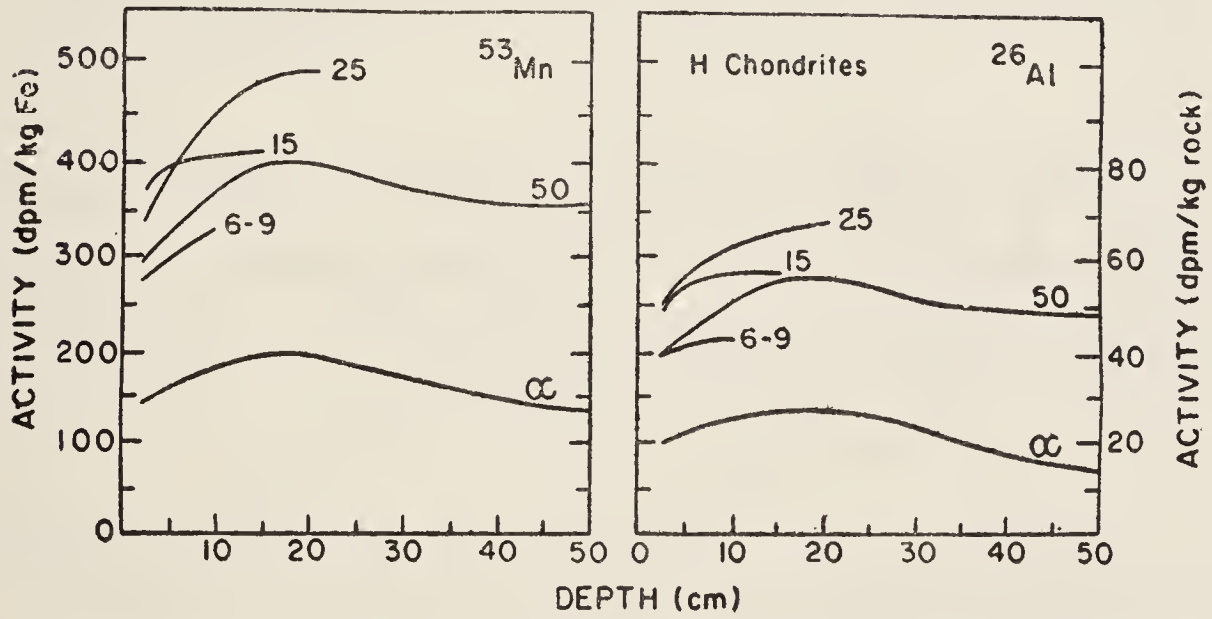

Figure 6a. Calculated production profiles for ^{53}Mn and ^{26}Al in H-chondrites of various sizes as a function of depth based on the α values given in figure 5. The production in the top 2 cm is not given as it is predominantly due to solar cosmic rays.

with the calculated production profiles given in this figure (Potdar 1981; Bhattacharya 1979; Bhandari and Potdar 1981).

By comparing the observed values with the calculations, we can identify meteorites having anomalous radioactivity. Anomalous cases can arise from time variations or intensity variations of GCR in different regions of the interplanetary space. The only well-established variations are due to sunspot cycle. We have calculated (Potdar and Bhandari 1979) the flux ($J_G > 1$ GeV) of GCR protons measured by balloon and satellite-borne detectors by various workers during the past few decades. During the last solar cycle the GCR flux (> 1 GeV) varied between 1·32 p/cm^2 sec 4π sr in 1970 to 2·36 p/cm^2. sec 4π sr in 1976 and the data indicate that it is anticorrelated with sunspot numbers with a small phase difference (figure 7). Using the model described above, and the high energy (> 1 GeV) fluxes, the production rates of ^{22}Na and ^{54}Mn were calculated for meteoroids of different sizes as a function of time of fall of meteo-

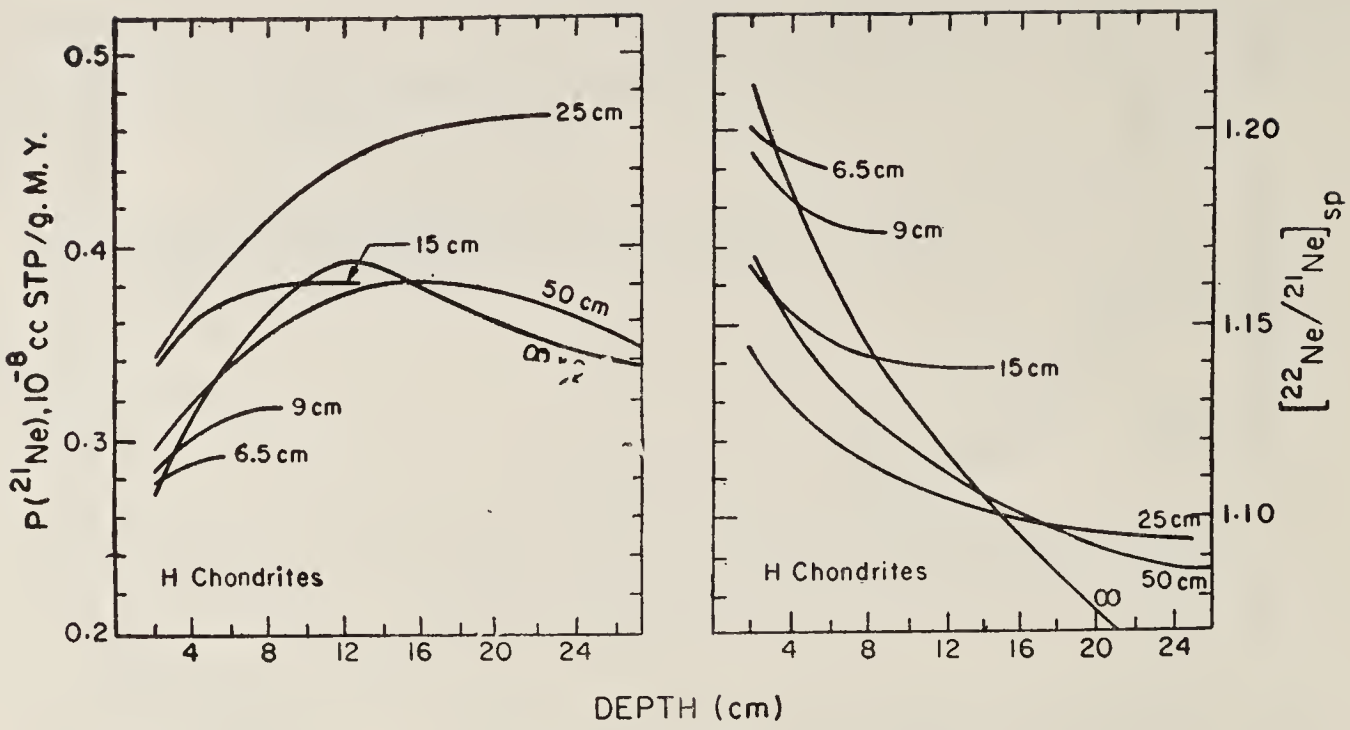

Figure 6b. Calculated depth profiles of ^{21}Ne, ^{22}Ne and NeR in H-chondrites of various sizes (Bhandari and Potdar 1981). The production in the top 2 cm is not given as it is predominantly due to solar cosmic rays. The solar production has been discussed by Bhandari and Potdar (1981).

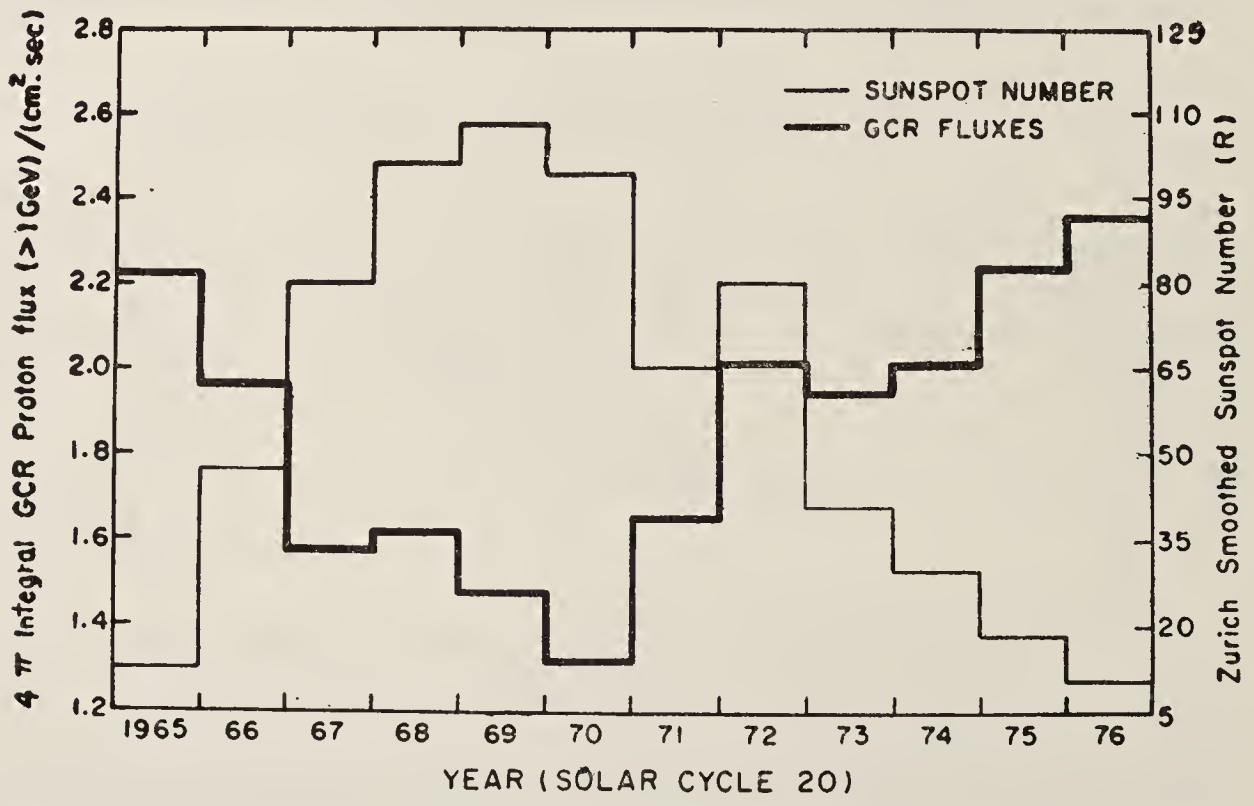

Figure 7. Correlation between sun spot number and the measured GCR flux (> 1 GeV), used in calculation of isotope production rates (Potdar and Bhandari 1979).

rites during the solar cycles 19 and 20. Activity of these radionuclides expected for a meteoroid of 50 cm radius at 15 cm depth as a function of time of fall is shown in figure 8. The curves are in qualitative agreement with the measured profile in several meteorites reported by Evans *et al* (1979). For a better comparison target abundance, depth and size effect in production must be considered for each sample.

Even when these corrections are applied, some meteorites show significant departure from the expected level for certain nuclides. ^{26}Al and ^{53}Mn are in good agreement in Dhajala chondrite but ^{22}Na and ^{54}Mn (Bhandari *et al* 1978; Potdar 1981) show anomalously high activity. The activity of ^{22}Na and ^{54}Mn was found to be 25% and 45% above the expected level at solar minimum, corresponding to the time of fall of Dhajala. Bhandari *et al* (1978) have considered the orbital parameters of Dhajala (Ballabh *et al* 1978) and suggest that relatively low GCR modulation at high

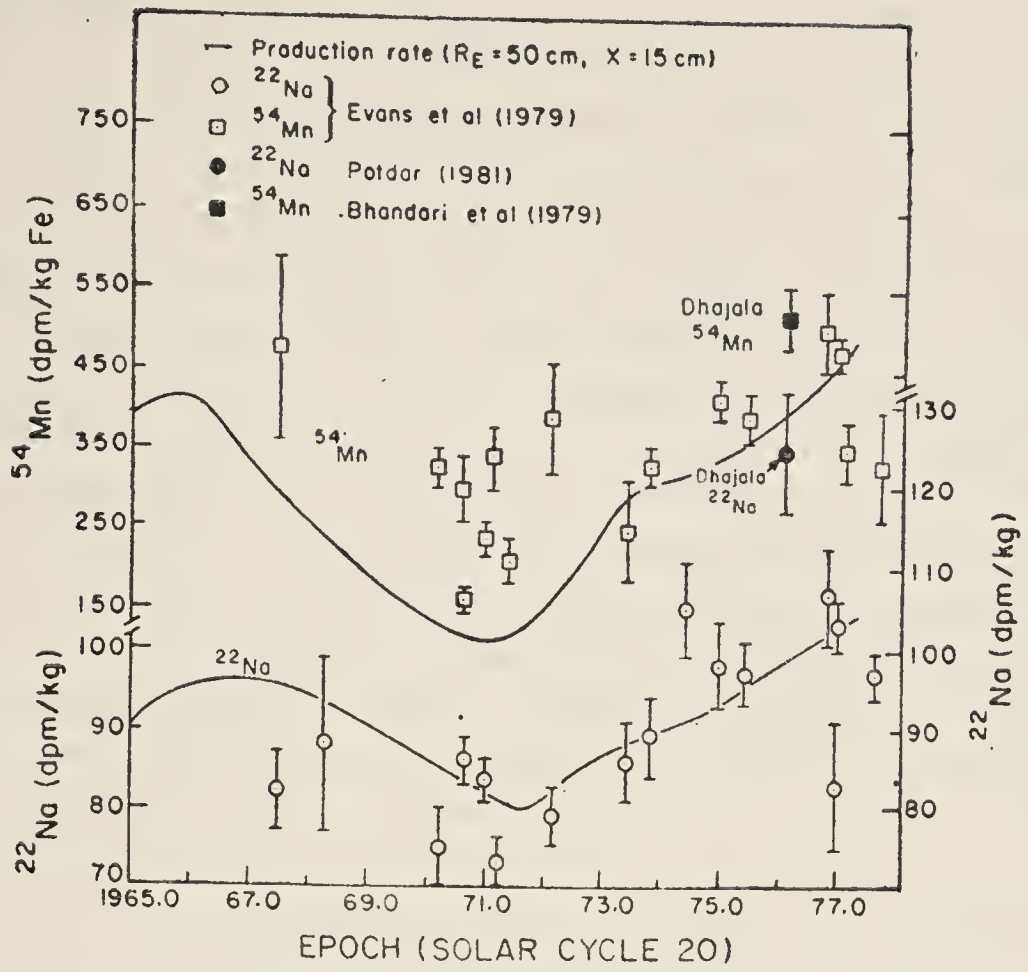

Figure 8. Solar cycle variation of ^{22}Na and ^{54}Mn. The calculated curves are from Potdar and Bhandari (1979) and experimental data are from Evans *et al* (1979) and Bhandari *et al* (1979).

helioaltitudes during solar minimum can explain the observed activity. There are some otherc hondrites which show marginally anomalous activity and such observations have been usually interpreted as due to time variation of cosmic ray intensity or due to multiple exposure of meteorites. None of these is definitely established so far. We shall discuss the possibility of identifying meteorites with multiple exposures later on.

4.2 *Neutron capture nuclides in meteorites*

Thermal neutron capture reactions produce a large number of stable and radionuclides in meteorites. Eberhardt *et al* (1963) have shown that low energy neutron source function in meteorites is very different from that of other nucleons and consequently, nuclides produced in neutron capture reactions have production profiles different from spallation nuclides like ^{26}Al, ^{21}Ne etc. as shown in figure 6. The calculations of Eberhardt *et al* (1963) are however based on ^{4}He production contours in iron meteorites. An attempt to deduce the depth profiles of neutron capture isotopes in chondrites has been made by Bhandari *et al* (1978) and Potdar (1981). They made a simultaneous measurement of a neutron capture nuclide *e.g.* ^{60}Co produced in ^{59}Co (n, γ) ^{60}Co reaction and track density, which provides the preatmospheric depth of a sample, and obtained the depth profile of neutron capture nuclides and the neutron source function. Two chondrites Dhajala (H3) and Allende (C3) have thus been studied in our laboratory. The observed profiles are shown in figure 9 where other available data on these meteorites are also included (see Potdar (1981) for source of data). Dhajala was a small meteoroid in space ($R_E = 50$ cm) whereas Allende was bigger, probably having a radius of about a metre. In addition, many fragments

of the Kirin (H5) chondrite have been extensively studied for track density as well as for several isotopes (Bourot-Denise and Pellas 1981; Honda *et al* 1980). The ^{60}Co depth profiles in Kirin chondrite and lunar cores (Wahlen *et al* 1973) are also included in figure 9. The lunar data (Wahlen *et al* 1973) as well as the calculated profiles (Lingenfelter *et al* 1972) have been normalized to cobalt abundance of 700 ppm, the value used in the meteorite calculations of Eberhardt *et al* 1963. Allende has cobalt content of 700 ppm, Dhajala 730 ppm and Kirin 840 ppm. Even after correcting for cobalt abundance the observed depth profiles in the three meteorites are found to be, significantly different. Dhajala has lower activity of ^{60}Co (peak value 80 dpm/kg) than expected from the calculations of Eberhardt *et al* (1963) whereas the peak activity of Allende and Kirin is similar (225 dpm/kg) to the expected values, although the peak positions do not match. The peak in Allende occurs at a much shallower depth (15 cm) than in Kirin (30 cm) although their preatmoshperic sizes may be comparable. This is a manifestation of different neutron slowing down lengths in carbonaceous chondrite and H chondrite because of their different chemical composition. The spallation component in ^{60}Co is very small ($\sim$ 2 dpm/kg) and thus can be neglected. The discrepancy between the observed and the calculated production profiles of ^{60}Co (Eberhardt *et al* 1963) is thus quite significant. The available data on other meteorites (Potdar 1981) also support the conclusion that the observed activity of ^{60}Co in small meteorites ($\leqslant$ 20 cm) is much smaller than the values predicted by Eberhardt *et al* (1963). It must be emphasized here that ^{60}Co production is very sensitive to the shape of the meteoroid. The calculations are for spherical bodies and we do not know the shapes of the various meteoroids discussed here. Since an accurate knowledge of the production rates of neutron capture nuclides is essential to determine the preatmospheric sizes (Potdar 1981) and to identify the meteorites with complex exposure, a more detailed study of such nuclides e.g. ^{60}Co, ^{36}Cl and ^{59}Ni is desirable.

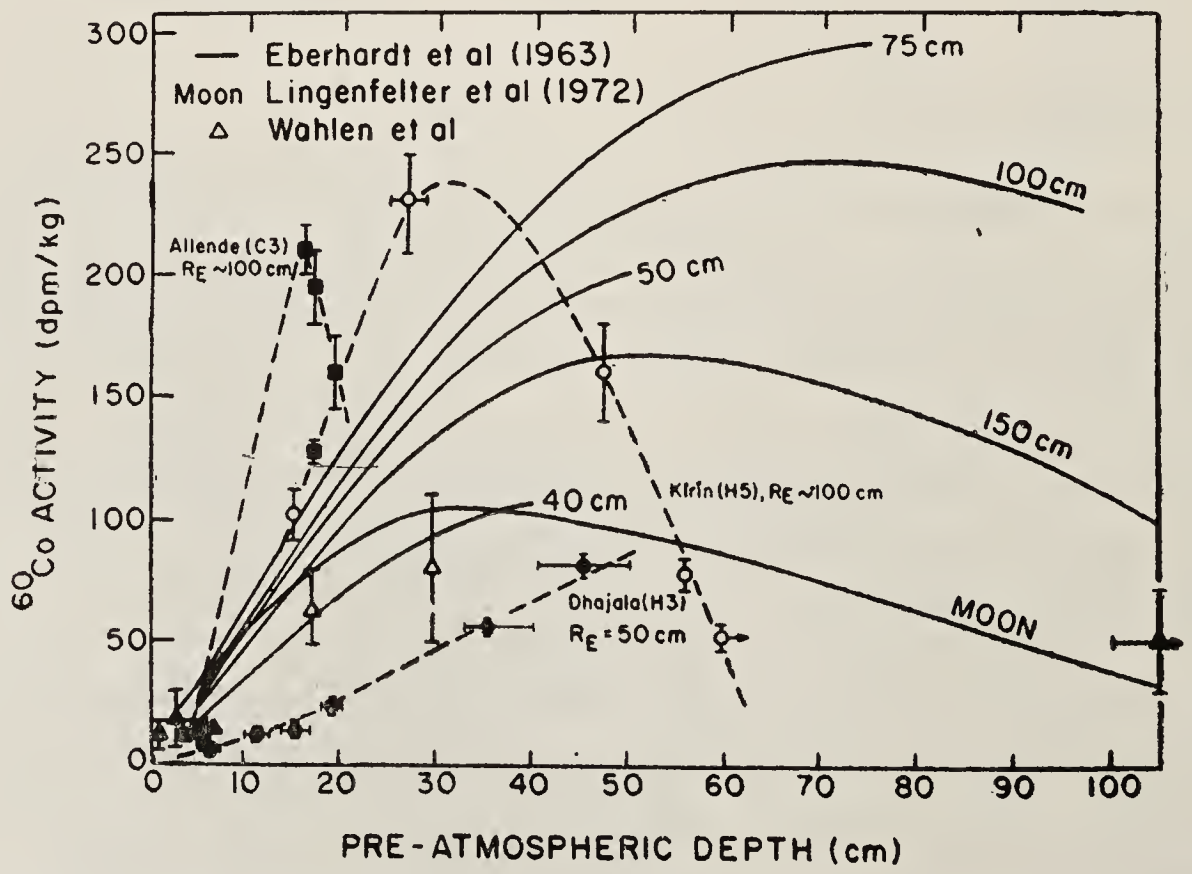

Figure 9. The measured depth profile of ^{60}Co in Dhajala (H3, $R_E = 50$ cm), Kirin (H5, $R_E \cong 100$ cm) and Allende (C3, $R_E \cong 100$ cm) meteorites. Calculated depth profiles are shown by soild curves (After Eberhardt *et al* 1963). Dhajala data are from Potdar 1981).

5. Multiple exposure of meteorites

The depth dependence of production rates of cosmic ray tracks, spallation products and neutron capture nuclides is so different that any change in exposure conditions (like geometry, shielding depth etc.) as due to fragmentation in space or reorientation in asteroidal regolith results in easily recognisable effects which are inconsistent with a simple single stage exposure. Such discrepancies have been, in fact, used to describe multiple exposure history of lunar rocks, soils and meteorites. Uncertainty in production rates of nuclides in meteorites, however, has not allowed identification of many cases of marginal multiple exposure.

Bhandari *et al* (1980a, b), based on the fact that the decrease in track production rate (TPM) with depth in a meteorite is steep compared to $^{22}Ne/^{21}Ne$ production ratio (NeR), suggested that for a simple exposure, TPM and NeR are correlated, depending mainly on the size of the meteoroid. A quantitative relationship has been obtained by Bhandari and Potdar (1981) and this allows identification of meteorites with complex exposure history as described below.

5.1 *Track production rate—NeR correlation and parent body exposure of chondrites*

The NeR-TPM correlation diagram based on the production profiles of NeR (figure 6, §3, Bhandari and Potdar 1981) and track density profiles (Bhattacharya *et al* 1973b; Goswami 1981, figure 1) is shown in figure 10.

Neon ratio and track density have been measured in the same aliquot sample in 41 meteorites. These data are shown in figure 10. Of these we consider here 22 chondrites whose preatmospheric sizes are known. In the case of 11 meteorites the measured NeR agree with the calculated values indicating that these meteorites (Bishunpur, Ensisheim, Finney, Kiel, Miller, Monze, Paragould, Pulsora, Ramsdorf, Sitathali and Tennasilm) have had single-stage exposure. Grady and Horace have

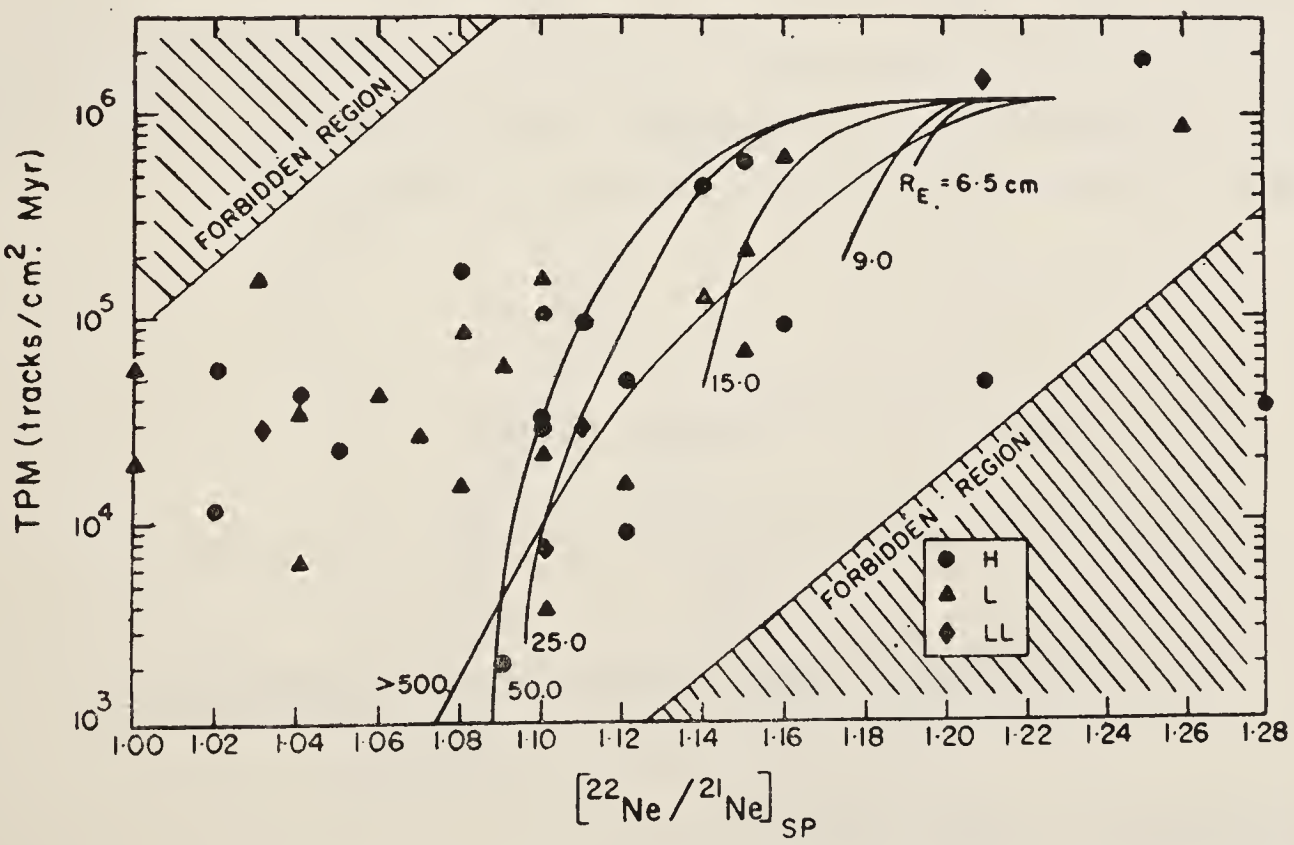

Figure 10. $^{22}Ne/^{21}Ne$ (NeR) *vs* track production rates in H chondrites of various sizes as a function of depth (Bhandari and Potdar 1981). The data points are from Bhandari *et al* (1980).

higher NeR ratios than expected and may represent cases of track annealing. Nine meteorites (De Nova, Gilgoin, Hayes Center, Kesen, Roy, Temple, Ulysses, Walters and Wellman) have lower NeR ratios than expected (Bhandari and Potdar 1981). Since NeR is independent of exposure age and its measurement is precise, usually within $\pm 2\%$, the discrepancy between the calculated and measured values is significant. Based on the calculations of production ratio of NeR (Bhandari and Potdar 1981), only a deep-shielded exposure can result in ratios lower than the expected value which is $\geqslant 1{\cdot}08$ in these cases. Two possibilities of deep-shielded exposure can be visualised (i) in the asteroid regolith, prior to the exposure of the meteoroid as a small body in the interplanetary space or (ii) due to fragmentation in space, in which case the meteoroid is exposed as a part of a larger body for sometime. In both the cases the meteoroid is exposed to cosmic rays for time T_1 at a shielding depth of $<$ 5m (the cosmic ray penetration depth) before it is exposed as an independent body for time T_2 in the interplanetary space. In view of the current mechanisms for production of meteoroids, such processes must occur frequently as pointed out by Wetherill (1980). Experimentally, however, they can be resolved only if the two exposures produce comparable amounts of spallation neon but significantly different track densities. Since the track production rate decreases steeply with depth, the track density acquired in stage T_1 will, in general, be orders of magnitude smaller than in stage T_2. Therefore TPM value will correspond to the final size of the meteoroid. Production rate of rare gas and NeR, on the other hand, decreases slowly with depth and hence, in the case of multiple exposures, the data points will lie to the left of the predicted curves (figure 10) as seen in the case of the nine meteorites listed above.

5.2 *Parent body exposure ages of meteorites and statistical analyses*

Under some plausible assumptions of shielding depths during parent body exposure, it is possible to calculate T_1, the cosmic ray exposure period in the parent body (or prior to fragmentation) from the observed NeR by using a two-component model.

If T is the exposure age of a meteorite as calculated from ^{21}Ne concentration and P (^{21}Ne) corresponding to its preatmospheric size (R_E) (figure 6), then, in the case of a complex exposure we can write (Bhandari and Potdar 1981)

$$T = T_2 + T_1 \times P_R, \tag{6}$$

where T_1 = parent body exposure age, (m.y.),

T_2 = meteoroid exposure age, (m.y.) and

$$P_R = \frac{P\,(^{21}\text{Ne})\,T_1}{P\,(^{21}\text{Ne})\,T_2}$$ *i.e.* the ratio of ^{21}Ne production rate during exposure T_1 to that during T_2.

Then $$R_m = (T_2/T)\,R_2 + (P_R\,T_1/T)\,R_1, \tag{7}$$

where R_m = measured ratio NeR = $(^{22}Ne/^{21}Ne)_{sp}$,

R_1 = NeR during the exposure T_1 and

R_2 = NeR during the exposure T_2.

Based on this simple two-stage irradiation model in which the depth of irradiation on the parent body is assumed to be 1 metre *i.e.* $P_R = 0{\cdot}15$, Bhandari and Potdar (1981) have calculated the approximate values of parent body exposure. These calculations reveal that in about 40% cases of meteorites, the parent body exposure is significant, and 50% cases belong to simple exposure. It is possible that some of the simple exposure cases include marginal cases of multiple exposure which cannot be resolved by the technique discussed above.

Although it is ideal to have $^{21,22}Ne$ and track density measurements in aliquot samples, a statistical analysis can be made from the NeR data alone since according to Bhandari *et al* (1980b) most meteoroids are small ($R_E < 25$ cm). Schultz and Kruse (1978) have compiled the available rare gas data in meteorites. Figure 11 shows a histogram of NeR for 354 ordinary chondrites which include 166 L group, 26 LL group and 162 H group chondrites. The histogram shows a peak at NeR = 1·07 for H chondrites and at 1·08 for L chondrites. Chondrites with NeR below 1·06 probably represent cases of multiple exposure as these values cannot be attained in small

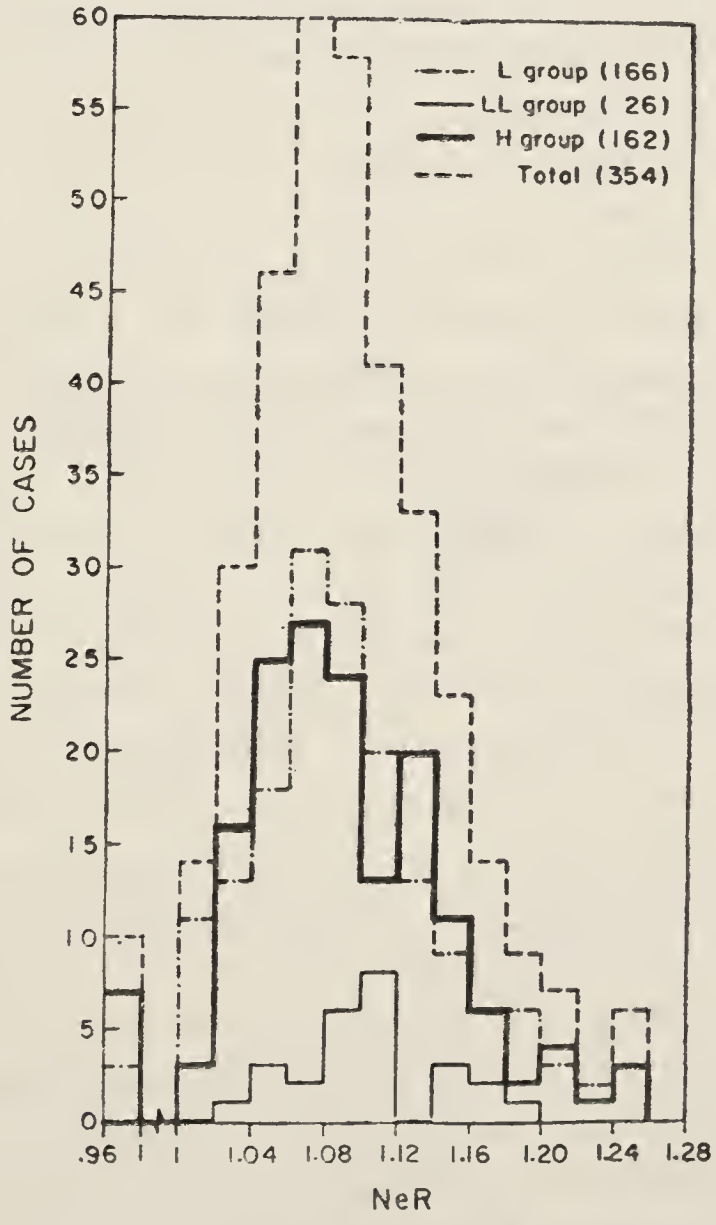

Figure 11. Distribution of spallation $^{22}Ne/^{21}Ne$ (NeR) in chondrites based on the compilation of Schultz and Kruse (1978).

($<$ 50 cm radius) meteoroid bodies. Hundred out of 354 chondrites (28 %) included in this histogram have NeR $\leqslant$ 1·06. Thus 51 out of 162 H chondrites, 45 out of 166 L chondrites and 4 out of 26 LL chondrites show multiple exposures (Bhandari *et al* 1981c). If we include other marginal cases, the actual number of meteorites with complex exposure may be larger.

The methods described above clearly indicate that a significant fraction of chondrites has been irradiated to cosmic rays in two or more stages. It should be possible to confirm some of these cases from measurements of radionuclide pairs with short and long half life *e.g.* $^{26}Al/^{53}Mn$ or from neutron effects in rare gases (Fireman 1966). Only a few such measurements are available at present and attempts are being made to include this study in future analyses.

6. Thermoluminescence of meteorites and lunar samples

Thermoluminescence has been studied in several meteorites mainly to understand the fading processes associated with atmospheric ablation, proximity of the meteoroid orbits to the sun and terrestrial age or degree of metamorphism (Singhvi *et al* 1981; Sears 1975; Melcher 1981; Vaz 1972; Sears *et al* 1980). Similarly the penetration of the diurnal thermal wave on the lunar surface and the flux of solar flare protons have been investigated from a study of TL in lunar rocks and soils (Hoyt *et al* 1971 1973). The application of TL to these processes requires the knowledge of cosmic ray induced TL gradient or equilibrium dose (ED) as a function of depth in meteoroids of different sizes. It is known that most chondrites, with a few exceptions, show a mean ED of 125 $\pm$ 25 krads but the depth dependence of ED has not been evaluated so far. We have therefore undertaken a systematic study of TL (ED) profile in meteorite cores in order to evaluate its dependence on the size and the depth of the rocks (Sen Gupta *et al* 1981). The same meteorites were studied for cosmic ray induced tracks, radionuclides *e.g.* ^{26}Al or ^{53}Mn and low and high temperature TL. All these data in case of Bansur core are shown in figure 12. The measured TL profiles in Bansur and several other meteorites covering a preatmospheric size range of 6–30 cm are shown in figure 13. The two opposite faces of Bansur meteorite, labelled SA and SC showed different low temperature TL gradient but high temperature TL was nearly the same except near the fusion crust. Keyes chondrite had negligible dose of low temperature TL, probably due to its long terrestrial age. Thus whereas the low temperature TL (LT) shows depth variation due to heating in the earth's atmosphere and can be related to atmospheric ablation (Singhvi *et al* 1981), the data indicate that the cosmic ray induced TL (HT) depth profile, (except near the fusion crust) is rather flat. All the four meteorites *i.e.* Madhipura ($R_E = 6{\cdot}5$ cm), Bansur (15 cm), St. Severin (25 cm) and Keyes (30 cm), however, show different equilibrium doses. St. Severin shows the highest ED of about 200 krads. The production rate of spallogenic nuclides also is not very sensitive to depth (figure 6a, b) but there is a systematic dependence on the size of the meteoroid (§ 3). The dependence of ED on the size does not show any systematic trend. Bar and Herr (1979) have already shown by studying radionuclides and thermoluminescence in thick target bombarded by high energy protons that their production profiles are not identical. Thus although the finer variation of ED for different meteorites, which may depend on the cosmic ray flux and hence the meteorite orbit, is not fully understood, it is clear that the depth dependence and

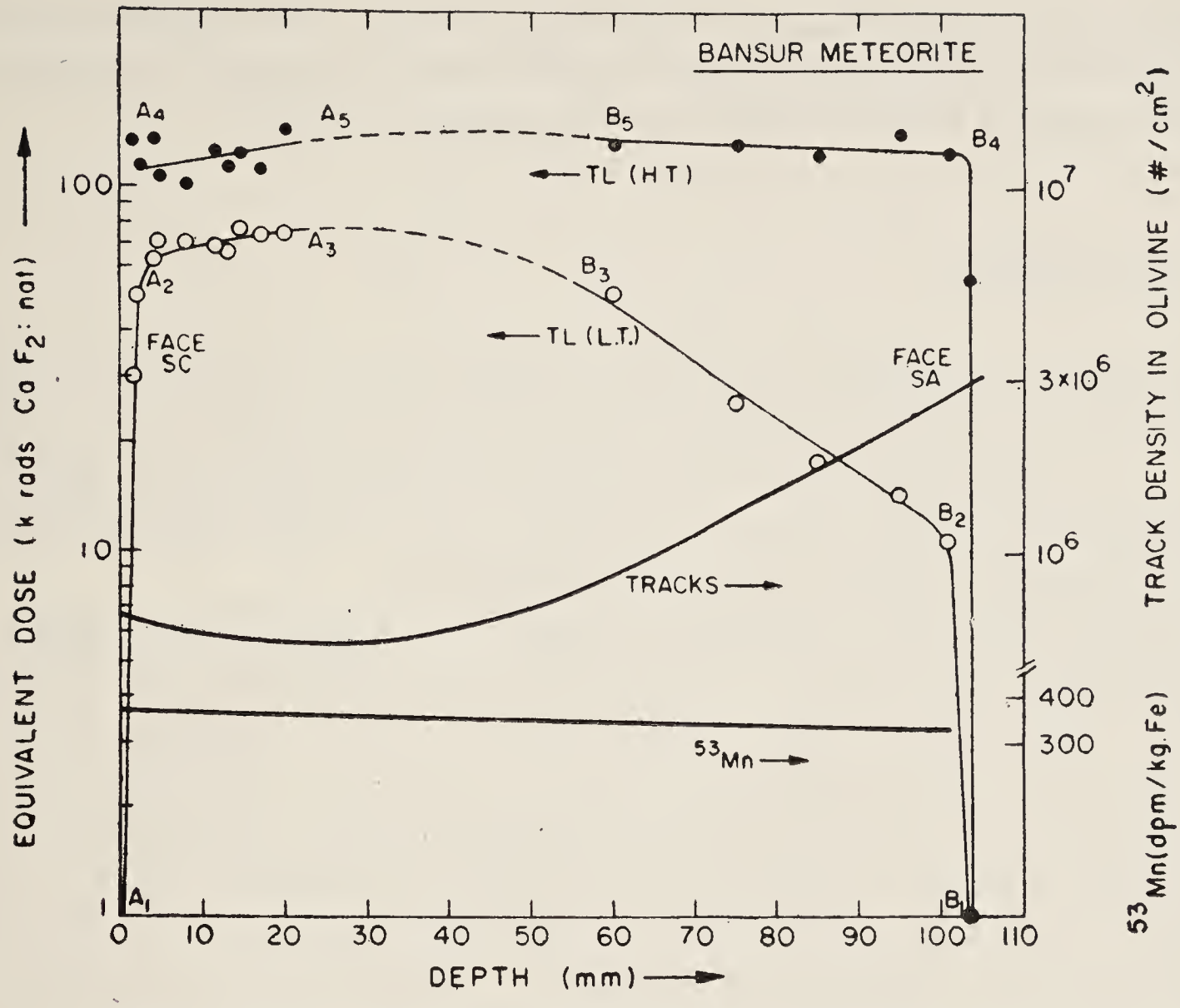

Figure 12. Thermoluminescence (HT and LT) equivalent dose, cosmic ray track density and ^{53}Mn depth profiles in Bansur chondrite core (Singhvi *et al* 1981).

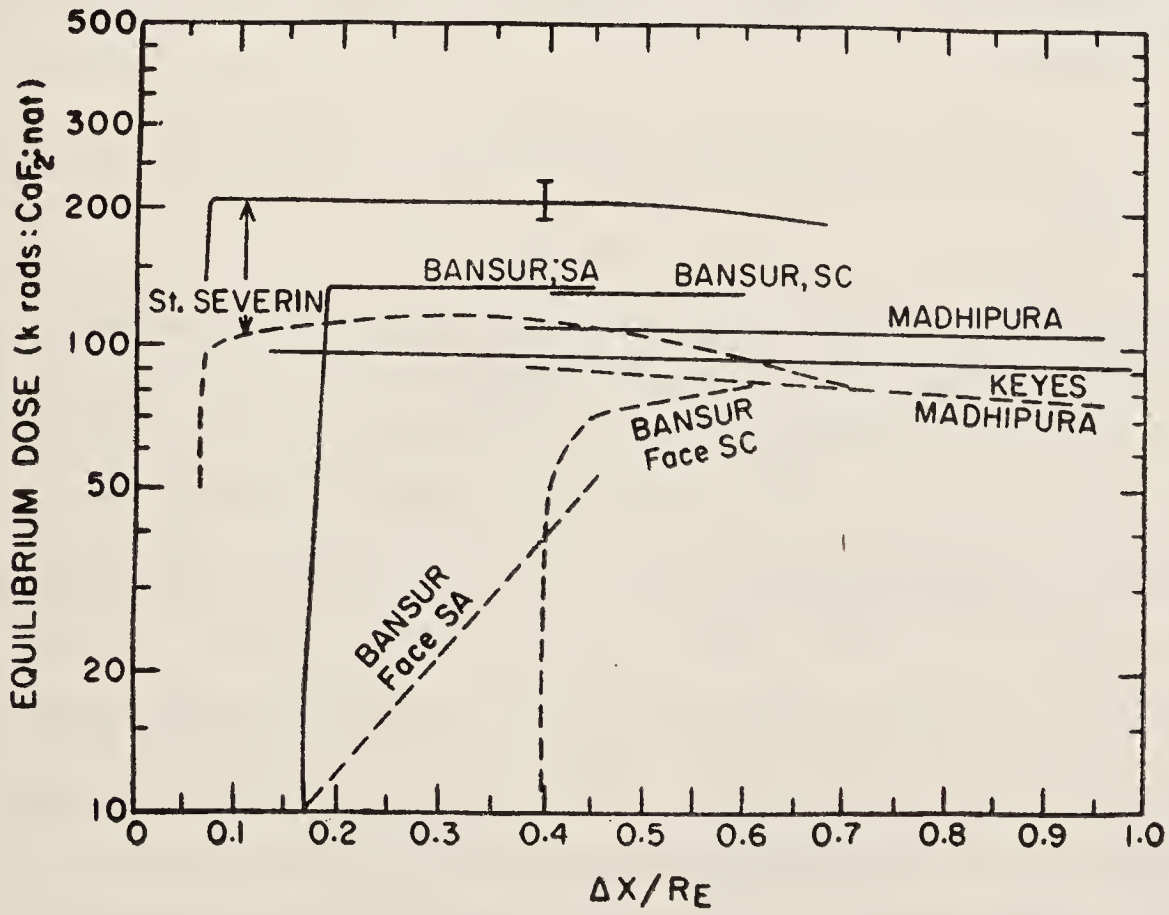

Figure 13. Thermoluminescence equilibrium dose depth profile solid line = high temp. ($\sim$300°C) and dotted line=low temp. ($\sim$175°C) in cores taken from St. Severin (R_E = 25 cm), Bansur (15 cm), Madhipura (6·5 cm) and Keyes (30 cm) chondrites. ΔX is the preatmospheric sample depth in the core and R_E is the effective radius (Sen Gupta *et al* 1981; Singhvi *et al* 1981). The opposite faces of Bansur meteorite, labelled SA and SC show different low temperature TL gradient. Typical error bar is shown on St. Severin curve. Low temperature TL is absent in Keyes chondrite.

possibly the size dependence are unimportant ($< 10\%$). The thermoluminescence is induced by low energy (eV) charged particles and photons and the data thus indicate that the flux of such particles is *nearly* constant with depth.

7. Future prospects

The results summarised above show that the work carried out in the past two decades has given us a general idea about several characteristics of cosmic rays *e.g.* flux of solar and galactic cosmic rays, their time and spatial variations and some aspects of their composition (Lal 1972, 1977; Schaeffer 1975; Bhandari and Rao 1980). More quantitative information with better time resolution is, however, necessary to understand the processes related to the origin of cosmic rays.

The basic alternatives proposed for the origin of GCR are still being debated. The contribution due to *r*-process synthesis in supernovae explosions, in *s*-process synthesis in stellar interiors or due to acceleration of interstellar material is still not resolved. Some isotopic and elemental abundances are so characteristic of these processes that the nucleosynthetic processes responsible for production of cosmic rays can be resolved, if the isotopic ratio of certain elements can be measured. Enormous effort is being made currently in this direction using particle detectors, aboard satellites and spacecrafts (Mewaldt *et al* 1979; Garcia-Munoz and Simpson 1979). Recent advances in experimental techniques for single atom detection (Hurst *et al* 1979) now make it possible to look into this problem much more effectively by taking advantage of the high cosmic ray dose received by lunar samples and meteorites. One of the possibilities is to study Pu and Cm isotopes in cosmic rays which we discuss in detail below.

7.1 *Resonance ionisation spectroscopy* (RIS) *of Pu and Cm isotopes using meteorite and lunar samples*

Relative abundances of heavy ions, particularly transuranic nuclei, in cosmic rays hold clue to their origin, acceleration and propagation. Some of these elements are produced exclusively in *r*-process nucleosynthesis and others in *r*, *s*, *p* and *n* processes or explosive nucleosynthesis, their abundances depending sensitively on the density, temperature and seed nuclei present in the stellar shell where they are believed to be formed. Direct measurements of cosmic ray composition using nuclear detectors indicate the presence of heavy nuclei, probably upto uranium, but the presence of transuranic nuclei, although expected, is still inconclusively demonstrated (Fowler *et al* 1979). Isotopic ratios of light nuclei, *e.g.* Ne, Mg. etc. have been measured (Garcia-Munoz *et al* 1979; Mewaldt *et al* 1979) but they are not so distinctly characteristic of different nucleosynthetic processes. Of the various nuclei formed in nucleosynthesis we consider here Pu, Cm (and possibly Tc) isotopes, whose relative abundances are characteristic of nucleosynthetic processes and which can be measured using RIS technique as described below, using lunar and meteorite samples.

Meteorites and lunar samples are exposed to cosmic rays for long periods of time ($10^6 - 10^9$ yr) so that they contain the implanted cosmic ray nuclei in the most enriched form found anywhere in the solar system.

Pu, Cm and Tc (in addition to Pm) are unstable nuclei and their natural abundance on earth is zero. Tc and Pm can be produced in some rare nuclear interactions on the earth at extremely low levels but Pu and Cm cannot be produced. Thus although the solar system abundance of these nuclei is negligible, the cosmic ray abundance may be significant. Considering only isotopes with half life greater than a year, we find that Pu has several such isotopes: ^{236}Pu (2·85 y), ^{238}Pu (87·8 y), ^{239}Pu ($2{\cdot}4\times10^4$ y), ^{240}Pu, (6540 y), ^{241}Pu (15 y), ^{242}Pu ($3{\cdot}8\times10^5$ y) and ^{244}Pu ($8{\cdot}3\times10^7$ y); Cm isotopes ^{243}Cm (28 y), ^{244}Cm (17·9 y), ^{245}Cm ($4{\cdot}8\times10^3$ y), ^{246}Cm ($4{\cdot}7\times10^3$ y), ^{247}Cm ($1{\cdot}5\times10^7$ y), ^{248}Cm ($3{\cdot}5\times10^5$ y), ^{250}Cm ($1{\cdot}1\times10^4$ y); Tc isotopes ^{97}Tc ($2{\cdot}6\times10^6$ y), ^{98}Tc ($1{\cdot}5\times10^6$ y), ^{99}Tc ($2{\cdot}13\times10^5$ y) and Pm isotopes ^{145}Pm (18 y), ^{146}Pm (4·4 y) and ^{147}Pm (2·62 y) are other isotopes with half life greater than a year.

Cosmic ray abundance of Pu and Cm can be calculated from nucleosynthetic yield and meteorite data. U:Pu:Cm are expected to be produced in about equal quantities in freshly synthesised material (Hillebrandt 1978). Since Fe abundance is known accurately in the solar system and in cosmic rays, we will calculate other abundances relative to Fe. U/Fe in solar system is $2{\cdot}5\times10^{-8}$ (Cameron 1970). Taking cosmic ray abundance of U and Fe to be the same as in solar system we expect Pu/Fe and Cm/Fe to be of the order of 10^{-8}. The iron group nuclei of galactic cosmic ray origin observed in stone meteorites with typical exposure age of 10^7 yr (*e.g.* St. Severin) (Bhandari *et al* 1980b) range upto 10^7/cm^2. Using the range of Fe group nuclei in silicate minerals as 15 μm, their concentration is expected to be 7×10^9 Fe/cc or 2×10^9 Fe nuclei/g rock. Pu and Cm therefore should occur at the level of 20 atoms/g in such meteorites. Some of these nuclei might undergo fragmentation in the rock material. The fragmentation is energy-dependent and only $\simeq 20\%$ particles may survive unfragmented. Thus we expect a few atoms of Pu and Cm in stony meteorites and lunar samples. Their number may be somewhat larger (factors of 2 to 10) in iron meteorites because of their longer exposure ages. The calculated values of $\mathrm{Tc/Fe} = 5\times10^{-5}$ and $\mathrm{Pm/Fe} = 10^{-6}$ lead to concentration of $10^2 - 10^4$ atoms/g for Tc and Pm.

All these nuclei do not survive the time galactic cosmic rays take in reaching the earth. The mean propagation time is $1{\cdot}6\times10^7$ years in the interstellar space as determined from the isotopic ratios of Be (Garcia Munoz and Simpson 1979). Although local contribution from freshly synthesised material in cosmic rays is possible, of the isotopes mentioned above only ^{244}Pu and ^{247}Cm are likely to survive the average life time of cosmic rays.

The three nuclides mentioned above can be easily detected using schemes 1 and 3 of Hurst *et al* (1979) as shown in table 2. The experimental technique involves a

Table 2. Expected concentration of cosmic ray implanted isotopes in meteorites and lunar samples.

Isotope	Cosmic ray abundance relative to iron	Expected (1) concentration atom/g rock	RIS scheme (2)
Cm (247)	$1{\cdot}8\times10^{-8}$	~5	1
Pu (244)	2×10^{-8}	~5	1
Tc (97, 98, 99)	5×10^{-5}	10^2-10^3 (3)	3

(1) In shallow samples of meteorites with GCR exposure age of $\geqslant$ 10 m.y.
(2) Hurst *et al* (1979).
(3) Assuming fresh injection at time scales comparable to the half life of isotopes.

suitable step by which either the meteorite or lunar sample atoms can be directly introduced into a proportional counter or the elements of interest can be first chemically enriched and then introduced in the chamber. Scheme 1 A (ω_1, ω_1 e^-) A^+ is the simplest of all, using a single frequency laser and the time coincidence is assured Pu and Cm can thus be selectively and unambiguously ionised and identified using this scheme. Scheme 3 for Tc A (ω_1, ω_2, ωe^-) A^+ is comparatively more complicated requiring two or more lasers.

Thus it appears that RIS can be effectively used to detect Cm and Pu atoms implanted in meteorites and lunar samples. Their concentration should provide parameters relating to the origin of cosmic rays and enable us to distinguish various channels of their synthesis. Although these are difficult experiments, they appear feasible and will provide a new insight into the ancient records of cosmic rays in extraterrestrial rocks.

Acknowledgements

The author is indebted to Dr G S Hurst and Dr J N Goswami for useful discussions and to Dr P N Shukla, Dr A K Singhvi, Mr M B Potdar and Mr D Sen Gupta for providing unpublished results and valuable help in writing this article. Thanks are due to Mr K M Suthar for assistance.

References

Ballabh G M, Bhatnagar A and Bhandari N 1978 *Icarus* **33** 361

Bar K and Herr W 1974 *Earth Planet. Sci Lett.* **22** 188

Begemann F, Born W, Palune H, Vilcsek E and Wanke H 1972 *Proc. Lunar Sci. Conf.* 3*rd*. (New York: Pergamon Press) p. 1963

Behrman C, Crozaz G, Drozd R, Hohenberg C, Ralston C, Walker R and Yuhas D 1973*Proc. Lunar Sci. Conf.* 4*th*. (New York: Pergamon Press) p. 1957

Bhandari N 1977 *Proc. Lunar Sci. Conf.* 8*th*. (New York: Pergamon Press) p. 3607

Bhandari N, Bhat S, Lal D, Rajagopalan G, Tamhane A S and Venkatavaradan V S 1971 *Proc. Lunar Sci. Conf. 2nd* (Massachusetts: MIT Press) p. 2611

Bhandari N, Bhattacharya S K and Padia J T 1975 *Proc. Lunar Sci. Conf.* 6*th*. (New York: Pergamon Press) p. 1913

Bhandari N, Bhattacharya S K and Padia J T 1976 *Proc. Lunar Sci. Conf.* 7*th*. (New York: Pergamon Press) p. 513

Bhandari N, Bhattacharya S K and Somayajulu B L K 1978 *Earth Planet. Sci. Lett.* **40** 194

Bhandari N, Lal D, Goswami J N 1976 Unpublished

Bhandari N, Lal D, Nautiyal C M, Padia J T, Potdar M B, Rao M N and Venkatesan T R 1980a *Meteoritics* **15** 265

Bhandari N, Lal D, Rajan R S, Arnold J R, Marti K and Moore C B 1980b *Nucl. Track* **4** 213

Bhandari N, Potdar M B and Shukla P N 1981b *Lunar Planet. Sci. XII* (Houston: Lunar Planet Inst.) p. 62

Bhandari N, Potdar M B and Suthar K M 1981c *Meteoritics* **16** 293

Bhandari N and Rao M N 1980 *Proc. Indian Acad. Sci.* (Earth Planet. Sci.) **89** 121

Bhandari N and Potdar M B 1982 *Earth Planet. Sci. Lett.* **57** 143

Bhattacharya S K 1979 *cosmic ray characteristics based on induced radioactivity in lunar samples and meteorites*, Ph. D Thesis, Gujarat University, Ahmedabad.

Bhattacharya S K and Bhandari N 1975 *Proc. Lunar Sci. Conf.* 6*th*. (New York: Pergamon Press) 1901

Bhattacharya S K, Bhandari N and Perelygin V P 1980a *J. Geophys. Res.* **85** 1439

Bhattacharya S K, Imamura M, Sinha N and Bhandari N 1980b *Earth Planet. Sci. Lett.* **51** 45
Bhattacharya S K, Goswami J N and Lal D 1973b *J. Geophys. Res.* **78** 8356
Bhattacharya S K, Goswami J N, Gupta S K and Lal D 1973a *The Moon* **8** 253
Boeckl R S 1972 *Earth Planet. Sci. Lett.* **16** 26
Bourot-Denise M and Pellas P 1981 *Meteoritics* **16** 297
Cameron A G W 1970 *Sp. Sci. Rev.* **15** 121
Clayton D D, Fowler W A, Hull T E and Zimmerman B A 1961 *Ann. Phys.* **17** 331
Cressy P J Jr and Bogard D D 1976 *Geochim. Cosmochim. Acta* **40** 749
Dust S and Crozaz G 1977 *Proc. Lunar Sci. Conf. 8th.* (New York: Pergamon Press) p. 2315
Eberhardt P, Geiss J and Lutz H 1963 In *Earth science and meteoritics*, (ed.) J Geiss and E D Goldberg, (Amsterdam: North Holland) p. 143
Evans J C, Rancitelli L A, Reeves J H and Bogard D D 1979 Abstracts of papers presented at the Conf. on Ancient Sun (Houston: Lunar Planet. Inst.) p. 28
Finkel R C 1972 *Depth profiles of galactic cosmic ray produced radionuclides in lunar samples* Ph.D. Thesis, University of California San Diego
Fireman E L 1966 *Z. Naturforsch.* **A21** 1138
Fowler P H, Clapham V M, Henshaw D L, Thompson A and O'Sullivan D 1979 *Proc. 16th. Int. Conf. on Cosmic Rays*, **6** (Tokyo: Univ. of Tokyo) p. 370
Fruchter J S, Rancitelli L A and Perkins R W 1976 *Proc. Lunar Sci. Conf. 7th.* (New York: Pergamon Press) p. 127
Fruchter J S, Evans J C, Reeves J H and Perkins R W 1981 *Lunar and Planet. Sci. XII* (Houston: Lunar Planet. Inst.) p. 774
Garcia-Munoz M and Simpson J A 1979 *Proc. 16th. Int. Conf. on Cosmic Rays* **1** (Kyoto: Univ. of Tokyo) p. 270
Goswami J N, Jha R and Lal D 1981 *J. Astrophys. Astr.* **2** 201
Goswami J N 1981 *Proc. Indian Acad. Sci. (Earth Planet. Sci.)* **90** 345
Hillebrandt W 1978 *Space Sci. Rev.* **21** 639
Honda M, Horie R, Imamura M, Nishiizumi K, Takaoka N and Konura K 1980 *Geochem. J.* **14** 82
Hoyt H P Jr, Miyajima M, Walker R M, Zimmerman D W and Zimmerman J 1971 *Proc. Lunar Sci. Conf. 2nd.* (New York: Pergamon Press) p. 2245
Hoyt H P Jr, Walker R M and Zimmerman DW 1973 *Proc. Lunar Sci. Conf. 4th.* (New York: Pergamon Press) p. 2489
Hurst G S, Payne M G, Kramer S D and Young J P 1979 *Rev. Mod. Phys.* **51** 767
Kohl C P, Murrel M T, Russ G P III and Arnold J R 1978 *Proc. Lunar Sci. Conf. 9th.* (New York: Pergamon Press) p. 2299
Kohman T P and Bender M L 1967 in *High energy nuclear reactions in astrophysics* (ed.) B S P Shen, (New York: Benjamin) p. 169
Kondrateyev K Y and Nikolosky G A 1970 *Q. J. R. Met. Soc.* **5** 69
Lal D 1972 *Sp. Sci. Rev.* **14** 3
Lal D 1977 *Philos. Trans. R. Soc. London* **A285** 69
Lavrukhina A K and Ustinova G K 1972 *Earth Planet Sci. Lett.* **15** 347
Lingenfelter R E, Canfield H and Hampel V E 1972 *Earth Planet. Sci. Lett.* **16** 355
Melcher C L 1981 *Earth Planet. Sci. Lett.* **52** 39
Mewaldt R A, Spalding J D, Stone E C and Vogt R E 1979 *Proc. 16th. Int. Conf. on Cosmic Rays* 7 (Tokyo: Univ. of Tokyo) p. 382
Nautiyal C M, Padia J T, Rao M N, Venkatesan T R 1981 *Proc. Lunar and Planet. Sci. Conf. 12th.*
Nishiizumi K and Arnold J R 1981 *Lunar and Planet. Sci. XII* (Houston: Lunar Planet. Inst.) p. 3061
Potdar M B 1981 *Nuclear interactions of the solar and galactic cosmic rays with interplanetary materials* Ph.D. Thesis, Gujarat University, Ahmedabad
Potdar M B and Bhandari N 1979 *Proc. Indian Natl. Sci. Acad.* **A45** 32
Rancitelli L A, Fruchter J S, Felix W D, Perkins R W and Wogman N A 1975 *Proc. Lunar. Sci. Conf. 6th.* (New York: Pergamon Press) p. 1891
Reedy R C 1977 *Proc. Lunar Sci. Conf. 8th* (New York: Pergamon) p. 825

Reedy R C 1980 *Proc. Conf. on Ancient Sun*, (eds.) R O Pepin, J A Eddy and R M Merrill (New York: Pergamon Press) p. 365
Reedy R C and Arnold J R 1972 *J. Geophys. Res.* **77** 537
Reedy R C, Arnold J R and Lal D 1981 *Science* (in press)
Regnier S, Hohenberg C M, Marti K and Reedy R C 1979 *Proc. Lunar Sci. Conf.* 10*th.* (New York: Pergamon) p. 1565
Schaeffer O A 1975 *Proc.* 14*th Int. Cosmic ray conf.* **11** (Munich: Max-Plank Inst.) p. 3508
Schultz L and Kruse H 1978 *Nucl. Track Detection* **2** 65
Sears D W 1975 *Mod. Geol.* **5** 155
Sears D W, Grossman J N, Melcher C L, Ross L M and Mills A A 1980 *Nature* (*London*) **287** 791
Sengupta D, Bhandari N and Singhvi A K 1981 in preparation
Singhvi A K, Pal S and Bhandari N 1981 *Proc. Conf. on TL Symposium* (Oxford) PACT (in press).
Tobailem J 1977 Note CEA–N–1466 (4) 45 Centre d'Etudes Nucleaires de Saclay, France
Vaz J E 1972 *Meteoritics* 7 77
Venkatesan T R, Nautiyal C M, Padia J T and Rao M N 1980 *Proc. Lunar Sci. Conf.* 11*th.* (New York: Pergamon Press) p. 1271
Wahlen M, Honda M, Imamura M, Fruchter J S, Finkel R C, Kohl CP, Arnold J R and Reedy R C 1972 *Proc. Lunar Sci. Conf.* 3*rd.* (New York: Pergamon Press) p. 1719
Wahlen M, Finkel R C, Imamura M, Kohl C P and Arnold J R 1973 *Earth Planet. Sci. Lett.* **19** 315
Walker R M 1975 *Annn. Rev. Earth Planet. Sci.* **3** 99
Wetherill G W 1980 *Meteoritics* **15** 386
Woosley S E, Arnett W D and Clayton D D 1978 *Astrophys. J.* **26** 231
Yaniv A 1981 *Nature* (*London*) **292** 866
Yaniv A and Marti K 1981 *Astrophys. J. Lett.* **247** L143
Yuhas D and Walker R 1973 *Proc.* 13*th Int. Conf. on Cosmic Rays* **2** (Denver: Univ. of Denver) p. 1116
Zook H A 1980 *Proc. Conf. on Ancient Sun* (eds.) R O Pepin, J A Eddy and R M Merrill (New York: Pergamon Press) p. 245

Fission tracks and cooling rates of meteorites

GHISLAINE CROZAZ
Department of Earth and Planetary Sciences and The McDonnel Center for Space Sciences, Washington University, St. Louis, Missouri 63130, USA and Physical Research Laboratory, Ahmedabad 380 009, India

Abstract. Recent work on fission track studies of meteorite samples to obtain cooling rates of meteorite parent bodies is reviewed. The cooling rates of chondrites are in excess of 1°K/10^6 yr. Fission track studies of phosphate grains in mesosiderites do not support the extremely slow cooling rates of 0·1°K/10^6 yr for these meteorites, inferred from metallographic studies. The accumulating evidence from fission track studies indicates a gross underestimation of the cooling rates of meteorites as determined by the metallographic techniques.

Keywords. Fission tracks; chondrites; mesosiderites; metallography; cooling rates.

1. Introduction

Fission tracks have been used to gain insight into the thermal history of meteorites of various types. This history is related to the places and modes of origin of these objects. Meteorites are divided into three major groups: stony (less than 25% Fe-Ni), stony-iron (50% Fe-Ni, 50% silicate material), and iron (essentially made of Fe and Ni) meteorites. The stony meteorites are further sub-divided into chondrites (containing rounded inclusions called chondrules) and achondrites (which contain no chondrule and most closely resemble terrestrial basalts). Stony-iron meteorites include pallasites (mainly olivine and Fe-Ni) and mesosiderites (which are complex breccias). The parent bodies from which the meteorites came were, in some cases, melted due to heat generated by radioactive heat sources within these bodies. Immiscible zones of pure metal liquid, pure silicate melt, and more complex mixtures of liquid metal and solid silicate minerals were formed during this melting event. Upon solidification, such zones served as the source of iron meteorites, achondrites and many of the stony-iron meteorites. Although the constituent chondrules were probably once molten, the chondrite themselves constitute a non-igneous assemblage of materials. Some chondrites have been heated severely enough to undergo various degrees of recrystallization. All these heating events are assumed to have occurred early in the history of the solar system, in bodies of asteroidal dimensions.

2. Cooling rates of meteorites

Cooling rates of meteorites were first inferred from their metal alloy compositions, and a large number of papers have been published on this subject; the results have been recently summarized by Wood (1979). From 900°K to 650°K, two iron-nickel

alloys (kamacite and taenite) are stable but their compositions and proportions vary with temperature and can be used to determine cooling rates. These are usually found to be of the order of 1-10°K/10^6 yr with occasional values upto 1,000°K/10^6 yr. All types of meteorites have been studied in this manner. In the case of irons and pallasites, there is no independent way to measure cooling rates but, in the case of chondrites, achondrites, and mesosiderites, which all contain a U-rich phosphate phase, it is possible to use fission tracks to evaluate their thermal history. This is particularly important because there is an inconsistency between the metallographic results and the measured radiometric ages of the meteorites of all groups. This fact led Wood (1979) to suggest that metallographic cooling rates might be systematically underestimated by a factor of ~6.

2.1 *Cooling rates of chondrites*

Pellas and Storzer, in 1977, undertook a study of fission tracks in the U-rich minor phosphate phases (Whitlockite and chloroapatite) of chondrites. They also studied silicate grains (feldspar, pyroxene and olivine) which are deficient in uranium, but contain tracks on their surfaces which were assumed to be produced when these grains were in contact with the U-rich phosphate grains. The phosphate abundance in chondrites is very low (less than 1 %) and thus the search for grains (from the major constituent phases of chondrites) which once were in contact with phosphate grains is both difficult and a lengthy process. A summary of this work has been recently reported by Pellas and Storzer (1981). Using the fission track densities they observed and the previously measured annealing properties for these various minerals, cooling rates in excess of 1°K/10^6 yr were inferred for the chondritic meteorites analysed

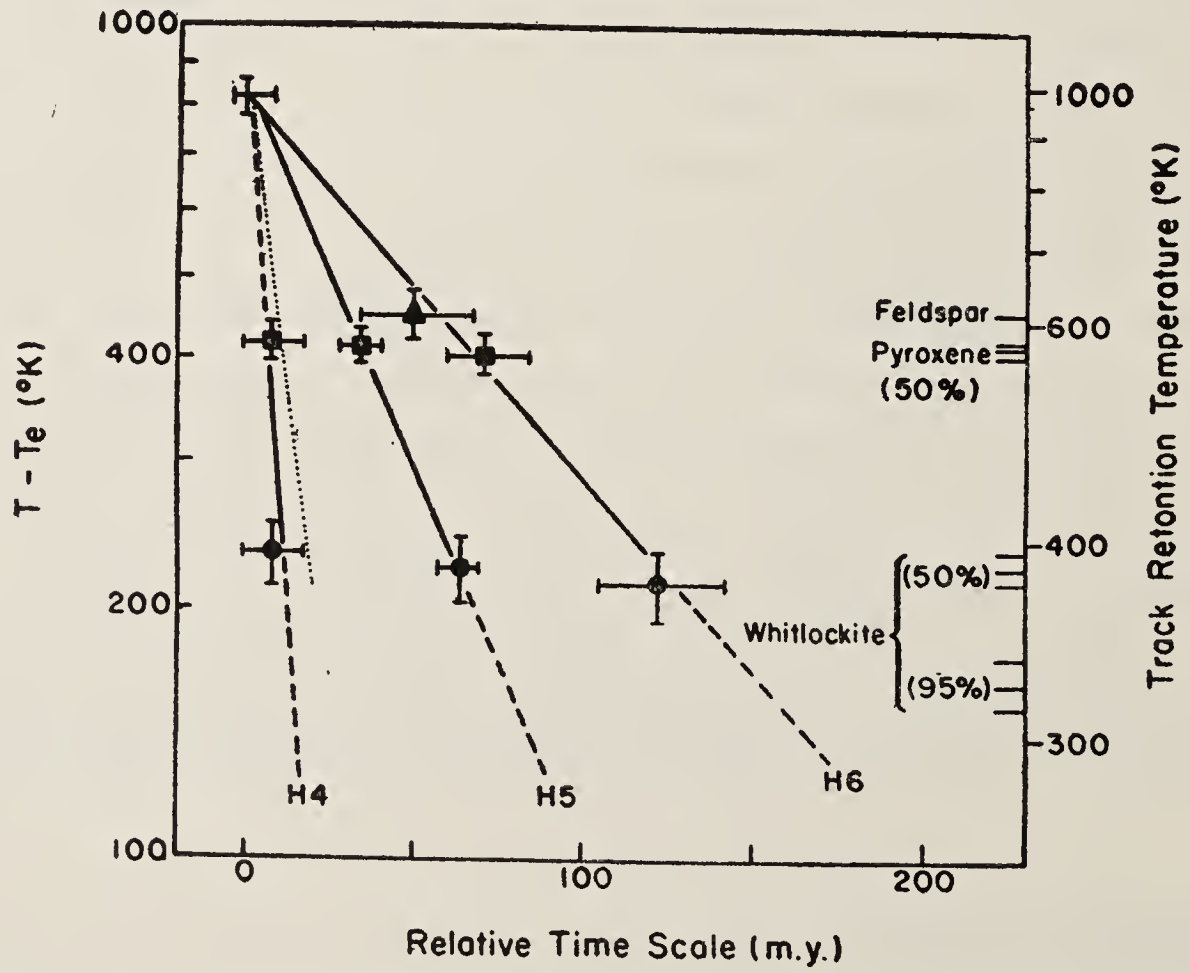

Figure 1. Cooling curves of H chondrites in the temperature interval 1000 to 375°K. Solid lines follow experimental data, dotted lines are extrapolated values. The left ordinate is the temperature reduced by the surface temperature T_e of the parent body of H chondrites. Assumed value of T_e = 160°K. (Figure taken from Pellas and Storzer 1981).

by them. For each subgroup of meteorites, the values seem to cluster pointing towards a common mode of origin. Figure 1 (taken from Pellas and Storzer 1981) shows the cooling curves determined for four different chondrites of the same group (H group), but which differ in their degrees of metamorphism (lowest in H4 and highest in H6 chondrites). According to Pellas and Storzer (1981) the cooling rates are given by the slopes of the various experimental lines and are highest for the least metamorphosed chondrites (H4) and lowest for the H6 chondrites, while the H5 chondrites seem to be intermediate. They conclude that these cooling rates are consistent with an onion-shell model for the parent bodies of these chondirtes (see figure 3) in which petrologic type 6 materials resided near the central region, and types 5, 4 and 3 were located successively in the outer shells.

Scott and Rajan (1981) have recently published a combined metallographic and fission track study of four chondrites, including two so-called gas-rich chondrites, Weston and Fayetteville. The other two ' ordinary ' chondrites analysed by them are Bhola and Mizo-Madaras. Gas-rich chondrites contain inclusions which were once, prior to the compaction of the meteorite, irradiated by the solar wind. They also contain crystals with solar flare tracks which were also acquired when these grains were residing at the very surface of an atmosphereless parent body prior to their incorporation into the meteorite.

The results obtained from metallographic studies of the Bhola chondrite is shown in figure 2, where the central nickel concentrations of taenite grains are plotted against the apparent distance from the edge of the grains for different types of materials sampled from this meteorite, within which these grains resided. All points plot coherently giving cooling rates of 0·1°K/m.y. in the temperature range 750 to 600°K. The metallographic cooling rates thus seem to be underestimated by at least a factor of 5, when compared to cooling rates obtained by fission track method (Pellas and

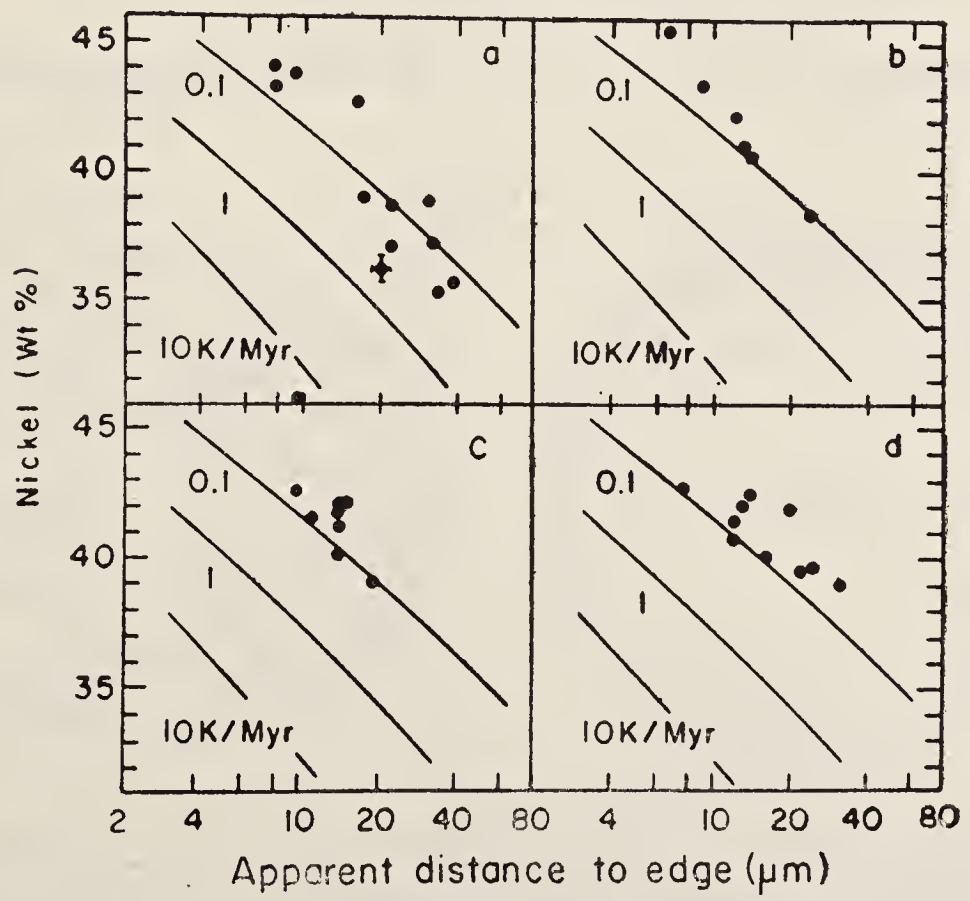

Figure 2. Central Ni concentrations and dimensions of taenite grains in host (**a**), shock-blackened (**b**), lightly shaded (**c**), and LL4 (**d**) xenoliths in Bhola. The data define a cooling rate of 0·1°K/m.y. The uniformity of the cooling rate in the host and the clasts suggests that this slow cooling occurred after the meteorite's compaction (Figure reproduced from Scott and Rajan 1981).

Storzer 1981). The metallographic studies of the two gas-rich meteorites, on the other hand, showed that they include components which cooled at different rates (extremes differ by up to a factor of ~100), and thus in different environments, prior to the compaction of the meteorites. Although these data do not invalidate the onion-shell model proposed by Pellas and Storzer (1981), Scott and Rajan (1981) favour a model (see figure 3) in which maximum metamorphic temperatures were reached in planetesimals with a radius smaller than 10 km which were then accreted to form chondritic parent bodies. This is an interesting and new model which has not yet been fully tested.

2.2 *Cooling rates of mesosiderites*

Of all the meteorites for which metallographic cooling rates have been determined, the entire group of mesosiderites seems to have cooled extremely slowly. Powell (1969) suggested that mesosiderites might have cooled as slowly as $0{\cdot}1°K/10^6$ yr. This cooling rate, if correct, has profound consequences as it implies that the mesosiderites must have evolved in a parent body appreciably larger than the largest asteroid currently observed.

We recently undertook (Crozaz and Tasker 1981) a fission track investigation of the U-rich whitlockites of mesosiderites with the objective of setting additional constraints on the thermal history of this group of meteorites. If the cooling rate of $0{\cdot}1°K/10^6$ yr is correct, the fission track ages of the whitlockites should be definitely lower than 3×10^9 years, the time by which the parent body of the mesosiderites will cool down to reach an effective track retention temperature.

We investigated eleven of the twenty one known mesosiderites including representatives of all the metamorphic groups. This study was complicated by the fact

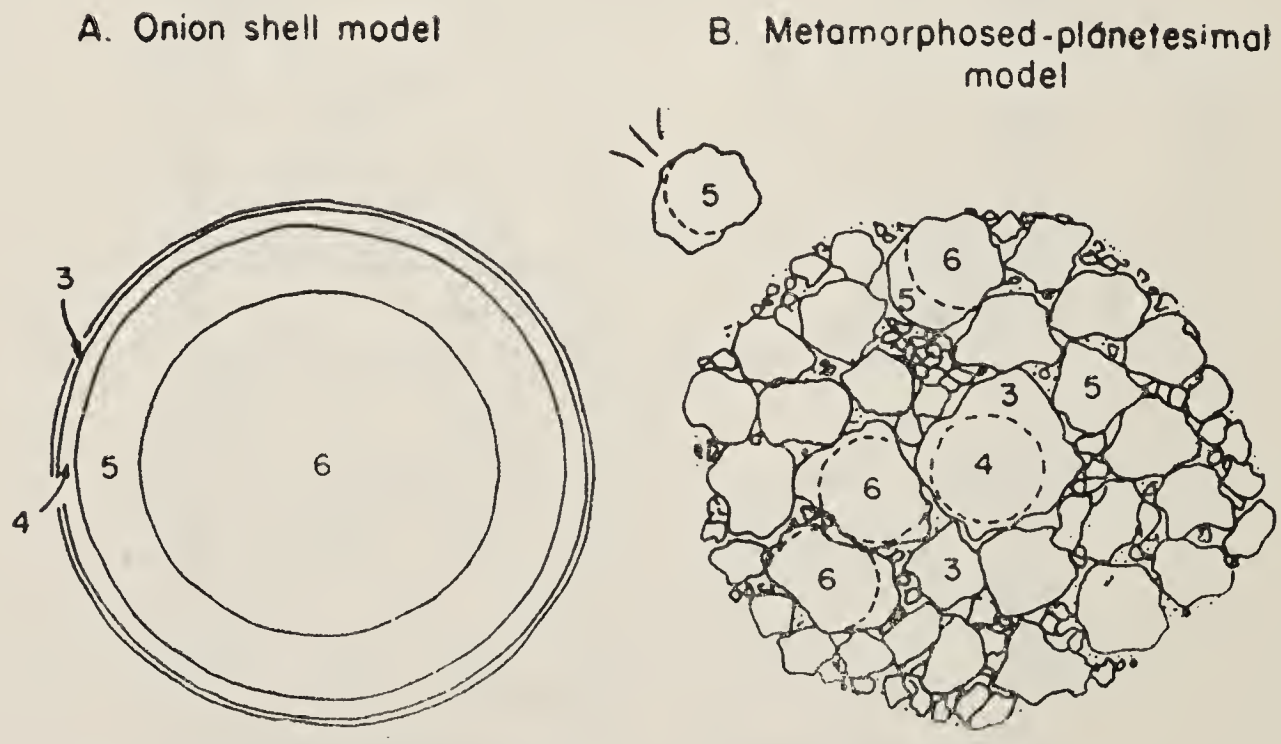

Figure 3. Schematic model for ordinary chondrite parent bodies. (A) Conventional onion-shell model in which radioactive heating *after* accretion produces a radial distribution of metamorphic types 3-6 (drawn to correspond the observed H group fall frequencies). (B) Metamorphosed-planetesimal model in which maximum metamorphic temperatures are reached in small planetesimals (~ 10 km in radius) *before* the chondritic parent body has accereted. Abundant mixing of types 3 to 6 in xenolithic chondrites (specially in LL chondrites) suggests that if (A) ever existed, it must hve been thoroughly mixed by subsequent collisions; (B) seems to fit the data better. (Figure reproduced from Scott and Rajan 1981).

that meteoritic whitlockite can potentially register tracks from the following sources: (i) the spontaneous fission of ^{238}U, (ii) the spontaneous fission of ^{244}Pu, (iii) heavy particles in the cosmic rays, (iv) induced fission of U and Th, and (v) nucler reactions induced mainly by high energy protons (short spallation recoil tracks). Various techniques were used to identify tracks from these sources, and to determine a fission track-age. Cosmic ray track densities were measured in adjacent U-poor grains, the uranium concentration in whitlockite was determined after neutron irradiation, and all track measurements were made using replicas studied in a scanning electron microscope. Our criteria were very conservative leading to *lower limits* for the actual fission track densities. Table 1 (from Crozaz and Tasker 1981) compares the measured fission track densities (column 2) in the whitlockite of mesosiderites of various metamorphic groups with the fission track densities expected from the decay of ^{238}U alone over a time period of $4{\cdot}5 \times 10^9$ yr. Some mesosiderites have large excesses of fission tracks (presumably due to the decay of ^{224}Pu); others have more modest excesses, whereas some do not have track excesses but still have apparent fission track ages, older than 3×10^9yr. Based on these new results it appears that the previously inferred low cooling rates determined by metallographic techniques were much too low. With the lifting of the requirement of extremely low cooling rates, a number of asteroids with radii equal or less than 150 km, which are concentrated in the inner portion of the asteroid belt and which have spectral reflectance characteristics compatible with the mesosiderite mineralogy (Gaffey and McCord 1977), are possible parent bodies for this group of meteorites.

Table 1. Fission tracks in the whitlockite of mesosiderite (Crozaz and Tasker, 1981)

	Measured fission track density (cm^{-2})	Expected fission track density (cm^{-2})*
Group 1		
Crab Orchard	2×10^6	$1{\cdot}6 \times 10^6$
Mount Padbury	4×10^6	$3{\cdot}0 \times 10^6$
Patwar	2×10^7	$2{\cdot}2 \times 10^6$
Vaca Muerta	10^7	$2{\cdot}8 \times 10^6$
Group 2		
Veramin	2×10^5	$5{\cdot}4 \times 10^6 - 1 \times 10^7$
Group 3		
Emery	$1{\cdot}4 \times 10^6$	$1{\cdot}6 \times 10^6$
Estherville	$2{\cdot}6 \times 10^6$	$4{\cdot}5 \times 10^6$
Morristown	$1{\cdot}8 \times 10^6$	$8{\cdot}0 \times 10^5$
Group 4		
Hainholz	$4{\cdot}3 \times 10^6$	$1{\cdot}7 \times 10^6$
Pinnaroo	$4{\cdot}9 \times 10^6$	$3{\cdot}0 \times 10^6$

*Calculated from the measured U concentration and for a meteorite's age of $4{\cdot}5 \times 10^9$ years.

The accumulating evidence from fission track studies thus points towards a gross underestimation of the cooling rates of meteorites as determined by the metallographic techniques.

References

Crozaz G and Tasker D R 1981 *Geochim. Cosmochim. Acta.* (in press)
Gaffey M J and McCord T B 1977 *Proc. Lunar Sci. Conf. 8th* (New York: Pergamon Press), p. 113
Pellas P and Storzer D 1977 *in Comets, asteroids, meteorites* (ed.) A H Delsemme (Toledo, Ohio: Univ. of Toledo Press) p. 355
Pellas P and Storzer D 1981 *Philos. Trans. R. Soc. London Ser.* **A347** 253
Powell B N 1969 *Geochim. Cosmochim. Acta.* **33** 789
Scott E R D and Rajan R S 1981 *Geochim. Cosmochim. Acta* **45** 53
Wood J A 1979 *in Asteroids* (ed.) T Gehrels (Tucson: Univ. Arizona Press) p. 849

Fission track geochronology of India

K K NAGPAUL
Department of Physics, Kurukshetra University, Kurukshetra 132 119, India

Abstract. The fission track ages of cogenetic/co-existing minerals namely garnet, muscovite and apatite from three mica belts *i.e.*, Bihar, Rajasthan, Nellore of peninsular India and Himalayan region, coupled with the corresponding closing temperatures of the minerals have been used to reveal the thermal and uplift histories of these regions. The data show that the extra-peninsular part of the subcontinent during Himalayan orogenic cycle (upper cretaceous-tertiary) witnessed the highest cooling and uplift rates in comparison to the older cycles in peninsular India.

Keywords. Fission tracks; geochronology; closing temperature; cooling and uplift rates; orogenic belts.

1. Introduction

The term geochronology, used earlier for geological time estimates by sedimentation rates, is now commonly applied to geological dating based on the radio-active decay of elements. The field of geochronology is of interdisciplinary nature involving earth scientists, physicists and chemists and is therefore an ideal discipline for team-work. The science of geochronology, in general, is associated with two types of problems: (i) technical and (ii) correct interpretation of the age data. The primary answer to geochronological work is time, the date of the geological event. However, the question of whether a mineral or rock reacted to a later event, and to what extent, can also be answered by geochronology. The most important parameters that control the age results are temperature and the presence of fluid phases. Therefore, these parameters can be evaluated by geochronological work and geochronological data can be used for the construction of metamorphic isograde.

It is widely accepted that radiometric ages determined on metamorphic minerals from orogenic belts generally reflect their cooling history rather than their primary crystallisation. Armstrong (1966) first developed this concept in detail, while Harper (1967) pioneered its application to the British cadenonian. Its general acceptance, however, stems largely from the investigations of the Central Alps by Prof. Jager and her colleagues at Bern. The time span over which the thermal history of any geological region can be built up will depend upon whether (i) different minerals have been dated by the same method, (ii) the same mineral if possible is dated by different techniques, or (iii) different minerals are dated by different methods.

In this paper we discuss the first possibility in detail as we have dated different minerals collected from various mica belts and the Himalayan region of India by the same fission track etch technique.

2. Age equation

The speed of radioactive decay, and thus the speed of the geochronological clock, depends only on the stability of the radioactive nucleus; it cannot be changed by outside parameters such as pressure and temperature. Actually, the nature of chemical bond has been found to exert a slight influence on the decay constants of several radioactive isotopes, but this influence is much smaller than the precision of age measurements. Thus we can state that the radioactive clock has a constant speed, independent of the different geological conditions.

We know that the radioactive decay is governed by the well-known formula

$$N = N_0 \exp(-\lambda t).$$

This equation leads to the age formula

$$t = \frac{1}{\lambda} \ln \frac{N_0}{N}.$$

At time $t = 0$, only the parent isotopes are in the system, the number being N_0; after time t, a certain number of parent isotopes P are left and the daughter isotopes D have been formed. Thus we can write

$$P + D = N_0 \ (N = P),$$

$$t = \frac{1}{\lambda} \ln \left(1 + \frac{D}{P}\right).$$

In fission track dating technique, D is measured in terms of fossil fission tracks which are produced due to the spontaneous fission of U^{238} whereas P is estimated in terms of the uranium present in the mineral. The equations used are as given below:

$$\rho_s = \frac{\lambda_F n^{238} F (\exp(\lambda_D T - 1)}{\lambda_D}, \tag{1}$$

$$\rho_i = n^{235} \phi \sigma F. \tag{2}$$

Combining equations (1) and (2), we obtain

$$T = \frac{1}{\lambda_D} \ln \left(1 + \frac{\rho_s}{\rho_i} \frac{\lambda_D}{\lambda_F} \phi \sigma I\right),$$

where ρ_s = fossil track density, ρ_i = induced track density, λ_D = total decay constant of uranium, λ_F = spontaneous decay constant of uranium, n^{238} = number of U^{238} atoms/cm^3 of the mineral, n^{235} = number of U^{235} atoms/cm^3 of the mineral, F = a constant depending upon the etchable range of fission tracks, etching efficiency and geometry etc., ϕ = thermal neutron dose, σ = thermal neutron cross-section for fission of U^{235}, and I = isotopic abundance ratio of uranium.

Fission track age determination thus requires essentially the fission track densities before and after the thermal neutron irradiation of the samples and thermal neutron dose measurements.

3. About various constants

The values of the constants are listed below:

$$I = 7{\cdot}25 \times 10^{-3},$$

$$\lambda_D = 1{\cdot}55 \times 10^{-10}\text{yr}^{-1},$$

$$\sigma = 580 \times 10^{-24}\ \text{cm}^2.$$

The value of λ_F *i.e.* the spontaneous fission decay constant is still a matter of debate among trackologists. The values used by various workers are:

$(6{\cdot}9 \pm 0{\cdot}2) \times 10^{-17}\ \text{yr}^{-1}$, (Fleischer and Price 1964);

$(7{\cdot}03 \pm 0{\cdot}11) \times 10^{-17}\ \text{yr}^{-1}$, (Roberts *et al* 1968);

$(7{\cdot}00 \pm 0{\cdot}28) \times 10^{-17}\ \text{yr}^{-1}$, (Hurford and Gleadow 1977);

$(8{\cdot}42 \pm 0{\cdot}10) \times 10^{-17}\ \text{yr}^{-1}$, (Spadvechhia and Hahx 1967);

$(8{\cdot}7 \pm 0{\cdot}6) \times 10^{-17}\ \text{yr}^{-1}$, (Wagner *et al* 1975).

Though we have been calculating the ages using the value of λ_F by Roberts *et al* (1968), yet this point is a matter of controversy and it should be resolved to assign a single value to λ_F. (See discussion in the article by Poupeau 1981).

4. Experimental procedure

4.1 *Optimization of etching conditions*

In progressive etching, there exists a considerable time difference when the tracks, intersecting the surface under investigation, are just revealed and are fully revealed. Prolonged etching widens these channels to sizes that may adversely affect resolution either because of their large size or overlapping due to higher number of track events. It is therefore necessary to use those etching times at which the optical detection efficiency for all the etched events is maximum. Optimum etching conditions to meet this requirement can be obtained from the plots of track density variation with etching time by choosing the etching times corresponding to peak revelation or plateau of tracks (Nagpaul and Nand Lal 1980).

4.2 *Dating methods*

There are various dating methods employed by various workers in the field. These methods are summarised by Gleadow and Lovering (1975), and also discussed by Poupeau (1981). In our laboratory we have mostly used the subtraction method. The details of the technique are given in Nagpaul and Nand Lal (1980).

4.3 *Annealing studies of minerals*

4.3 a *The concept of closing temperatures:* The idea of closing temperatures is very important from the interpretation point of view of fission track ages. An elaboration of this concept is given below:

The concept of closing temperature is applicable only if the rocks have cooled slowly. In fast cooling rocks the fission track ages give the formation time of the samples. When co-existing minerals from such rocks are dated, concordant ages are found. The fast cooling model is characteristic of volcanic rocks.

The concept of closing temperature is illustrated in figure 1. It is assumed that, while the system is near the temperature of crystallization, the daughter nuclide diffuses out as fast as it is produced by radioactive decay. As the system cools, it enters a transitional temperature range within which some of the daughter product accumu-

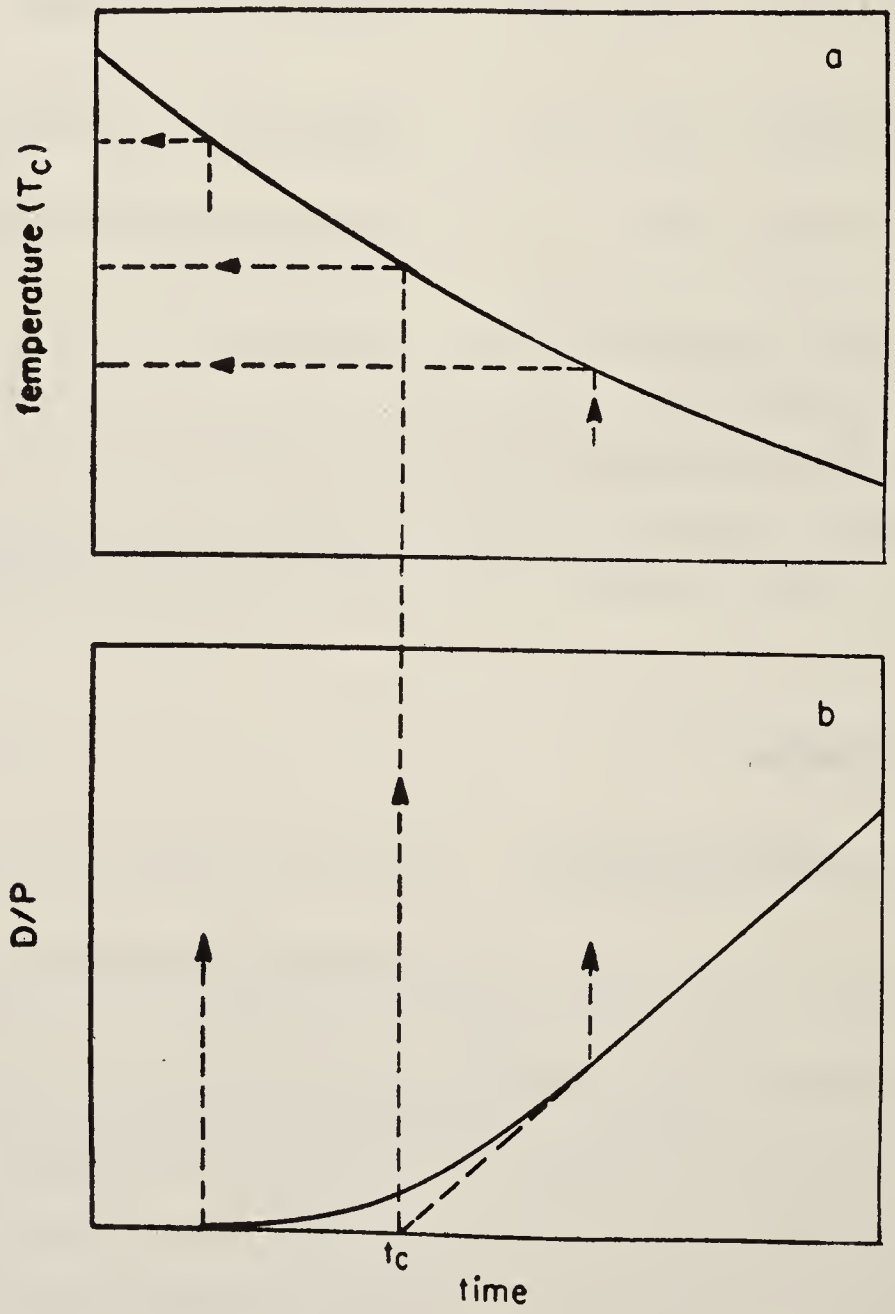

Figure 1. Definition of closure temperature; (a) cooling curve, (b) accumulation curve. *D/P* is the daughter/parent ratio. Broken lines show approximate limits of transitional time-temperature range.

lates in the mineral and some is lost. Eventually, at temperatures near ambient, the losses are negligible and the daughter product accumulates without any loss whatsoever. In calculating an ' age ' for the system, we in effect extrapolate the last portion of the curve back to the time axis, as shown by the broken line. According to this picture, the closure process is not a sharply defined event. Nonetheless closing temperature T_c can be given a simple and precise definition as illustrated in figure 1 namely the temperature of the system at the time given by its apparent age; on this basis it can be directly related to cooling history.

It is easy to imagine that closing temperature may vary with cooling rate; the slower the rate of cooling, the longer will be the time during which total or partial loss of daughter product may occur, and the lower will be both the apparent age and the corresponding closure temperature. Incorporating the idea of cooling rates, Haack (1977) proposed a model to calculate the closing temperatures of various minerals. He has integrated the opposing effects of track production and fading over time for a series of cooling rates. We have obtained the track growth curves *vs* temperature for various minerals for different cooling rates and estimated T_c following the approach of Haack (Sharma *et al* 1980). These are given in table 1.

According to Wagner (1972), the fission track age can be taken to represent the time when the rock cools down to a temperature at which 50% of the tracks are stable. In reality the stable conditions for the tracks to be recorded arrive progressively over a wide range of temperatures called partial stability zone. The simplest estimate of the effective closing temperature can be obtained by extrapolating the results of laboratory annealing data to the times of the order of $10^7 - 10^8$ years and taking the temperatures at which 50% of the tracks are stable. Using this procedure the T_c values obtained are given in table 1. If we compare T_c by two approaches we find that the two values agree only if the cooling rates are of the order of 100°C/m.y. which are rarely encountered in geological set-ups.

Table 1. Closing temperature of various minerals

Mineral	Fission track closing temp. (°C) for cooling rates					Closing temp. by other radiometric methods*		
	0.1°C/m.y.	1°C/m.y.	10°C/m.y.	100°C/m.y.	**	Rb-Sr	K-Ar	U-Pb
Apatite	83	100	117	134	130±30	—	—	—
Biotite	22	39	56	73	100±20	300	300	—
Epidote	165	185	205	225	240±25	—	—	—
Garnet	258	276	296	317	350±50	—	—	—
Hornblende	99	117	135	155	145±25	—	—	—
Muscovite	105	125	145	165	170±25	500	350	—
Monazite	—	—	—	—	—	—	—	530
Phengite	—	—	—	—	—	500	350	—
Sphene	282	302	322	342	340±25	—	—	—
Zircon**	—	—	—	—	350	—	—	—

*Data from Wagner *et al* (1977).

**Temperature corresponding to 50% track-retention for 10^6–10^7 years (Saini 1978).

***The closing temperatures at various cooling rates for zircon could not be calculated as its annealing characteristics are available only for 0% and 100% track retention (Krishnaswami *et al* 1973).

4.3 b *Age correction due to geological annealing of fossil tracks:* There are two methods to assess the age correction due to shortening of fossil tracks over geological times at low ambient temperatures. One which is mostly followed by our group is to measure the length reductions of fossil tracks with respect to induced tracks and then convert this length reduction to density reduction through translation curves obtained in the laboratory (Nagpaul and Nand Lal 1980). Another method for finding out the model ages is due to Poupeau *et al* (1980) and is known as plateau age method. Though the plateau method is more accurate, a large number of analysis is required to calculate the plateau age. Poupeau (1981) has discussed the age correction method in detail.

4.4 *Cooling and uplift rates*

The uplift rates in the present work have been derived according to the equation:

$$\text{Uplift rate} = \frac{\text{Cooling rate}}{\text{Geothermal gradient}},$$

where cooling rates are calculated from the closing temperatures and apparent ages of the various minerals, and an average geothermal gradient of the order of 30°C/km has been adopted. The above relation gives only an average uplift rate, and may not be valid if the uplift is not a continuous one but related to tectonic pulses of short durations. However, as a first order approximation, the results obtained using this relation are extremely useful for understanding the thermal and tectonic history of the various orogenic belts in the Indian subcontinent.

5. Geochronology and cooling rates of various geological regions

Although the available geochronological data, particularly the mineral ages, for the peninsular and the extra-peninsular India are far too meagre for arriving at the final conclusion regarding the cooling and the uplift rates of different geological regions, an attempt has been made to synthesize and correlate the information available from various pegmatitic belts *viz*. Bihar, Nellore, Rajasthan, South India and the Himalayan region.

5.1 *Rajasthan mica belt*

A large number of pegmatites from which the samples were collected which have been dated by fission track method, occur in the region around Gangapur in Bhilwara district. The salient features of the tectonic-metamorphic history of this region which has been investigated in detail by Sharma (1978) are as follows:

The metasediments represented by staurolite-kyanite schist, sillimanite-kyanite schist, garneti-ferrous mica schist, gneisses, calc-silicate rocks and crystalline limestone belonging to Aravalli Group have been intruded by granites, pegmatites and quartz veins. Originally, these rocks might have been argillaceous, arenaceous and calcareous sediments which through regional folding and associated metamorphism have resulted into the present form of metasediments. Three phases of folding have

been recognised in the area. The tectonic history of the area began with the formation of first generation F_1 folds which have a regional NNE-SSW trend. The most prevalent planar structure associated with this folding was the axial plane foliation. Simultaneous to the development of this foliation, the regional metamorphism also progressed to a high grade amphibolite facies. The pegmatites and quartz veins which represent a differentiated fraction of the granite magma intruded along the structurally favourable locales formed during this tectonic episode, particularly the axial plane foliation and F_1 folds. Most of the pegmatites in the present area belong to this period and have been affected by subsequent deformations.

The second tectonic event which closely followed the F_1 resulted in the development of a set of second generation folds designated as F_2 which are tight and isoclinal and plunge at moderate angle towards NE or SW. This fold movement caused the development of fractures in partially or completely solidified pegmatites emplaced during the first tectonic phase.

The third and the last tectonic episode in the area is represented by broad open cross folds F_3 which are accompanied by fracture cleavages that occur roughly parallel to the axial plane of these folds. Otherwise, this movement was not intensive enough and did not result in any recrystallization of minerals, nor of any intensive foliation.

5.1a *Fission track age data and their interpretation:* The fission track age data of garnet, muscovite and apatite, analysed in our laboratory are disucussed by Nagpal and Nagpaul (1974) and Sharma *et al* (1975). The apparent fission track ages of garnet from pegmatites lie between 960 m.y. and 1100 m.y., muscovite between 745 m.y. and 835 m.y. and apatite between 410 m.y. and 555 m.y. The mean f.t. ages of the cogenetic minerals are given in table 2. The errors in the age data represent the standard error of the mean.

Three major orogenic cycles have been recognised in Rajasthan—The Delhi Cycle, the Aravalli Cycle and the Banded Gneissic Group Cycle, which are assigned different ages by different workers (Holmes 1949, 1955; Aswathanarayana 1956; Rama Rao 1964; Sarkar *et al* 1964; Vinogradov *et al* 1964; Crawford 1970; Pichamuthu 1971; Balasundram and Balasubrahmanyan 1973).

The ages of Untala granite, Erinpura granite and muscovite from Lower Alwar Schists ($\sim$ 900 m.y.) by Rb-Sr method (Crawford 1970); uraninite from the Danta mine (906 $\pm$ 20 m.y.) and monazite from the Soniana pegmatite (735-865 m.y.) by U-Th-Pb method (Holmes 1949; Chauduri *et al* 1967) and those of cogenetic minerals from the pegmatites of this region by f.t. method are comparable and suggest that all of them may be related to the same tectonic episode. The discrepancy in the fission

Table 2. Fission track age data of minerals from mica belts

Region	Number of samples analysed for			Mean fission track ages (m.y.) of		
	garnet	muscovite	apatite	garnet	muscovite	apatite
Rajasthan mica belt	4	7	5	982±78	793±31	493±71
Bihar mica belt	6	7	8	834±35	763±30	454±52
Nellore mica belt	5	—	5	1065±55	—	424±8

track ages of these minerals from the same pegmatite is attributed to the differences in their thermal track stability and has been elaborated in the following paragraph.

As is evident from the above discussion the granite magma and its differentiated pegmatitic melt after its emplacement into the Aravalli metasediments during the closing stage of the first tectonic episode started crystallizing around 1000–1100 m.y. The temperature-pressure conditions during that period had sufficiently increased resulting in a high grade regional metamorphism (amphibolite facies) and anatectic magmatism in the area. A fall in the temperature after the emplacement of the melt resulted in crystallization of the pegmatitic bodies. The second tectonic episode which fractured these pegmatites and albitized the already consolidated primary zones, might have been active between 900–950 m.y. as indicated by dating of uraninite and monazite of the replacement zones. After this tectonic event, the pegmatite bodies gradually cooled down so as to reach firstly the closing temperature of garnet and subsequently to that of muscovite and apatite. The cooling and uplift rates of the pegmatites calculated by using the closing temperatures and the corresponding mineral ages, are given in table 3.

5.2 *The Bihar mica belt*

The geology of these pegmatites has been described in detail by Mahadevan (1965) and Anandalwar and Mahadevan (1968).

The Bihar mica belt and the adjoining areas of eastern India have been affected by various orogenies such as Older Metamorphics, Iron-Ore, Singhbhum, Satpura and Monghyr. The imprint of the oldest orogeny in the area is recorded by muscovite ($\sim$ 3035 m.y.) from pegmatite near Jorapokar emplaced into the metamorphic rocks older than those of the Iron-Ore series from which it differs in higher degree of metamorphism (Sarkar *et al* 1964). According to Sarkar *et al* (1964), the Iron-Ore Orogeny, regional metamorphism and emplacement of the Singhbhum Granite and Soda Granite from Bihar took place around 2100 m.y.

A number of minerals from pegmatites of the Bihar mica belt dated by various workers (Holmes 1950; Sarkar 1941; Sarkar and Sen Sharma 1946; Nandi and Sen 1950 a, b; Aswathanarayana 1956; Venkatasubramanian and Krishnan 1960; Sarkar and Saha 1962) suggest that these pegmatites were emplaced during the closing stage of the Satpura Orogeny which is considered by Holmes (1950) to be around 950 m.y.,

Table 3. Cooling and uplift rates of various mica belts.

Region	Time span (m.y.)	Cooling rate* (°C/m.y.)	Uplift rate (m/m.y.)
Rajasthan mica belt	982—793	1.7	57
	793—493	0.8	2·8
Bihar mica belt	834—763	2.1	70.9
	763—454	0.8	2.8
Nellore mica belt	1065—424	2.7	90

*Cooling rates have been calculated by using the closing temperatures corresponding to cooling rate of 1°C/m.y.

and they are genetically related to the Chotanagpur granite-gneiss, a part of which has been dated at 1000 m.y. (Crawford 1968). According to Sarkar *et al* (1964), the age data from the Bihar mica belt is comparable with that of the Muri (890–970 m.y.) Singhbhum (934–940 m.y.), Gangapur (912–993 m.y.) and Ranchi (980 m.y.) belts and all belong to the Satpura cycle.

A mild metamorphism followed by emplacement of granite in the Monghyr district (located $\sim$ 200 km NE of the area under study) around 400 m.y. has also been reported by Sarkar *et al* (1964). The f.t. age data of all the three cogenetic minerals analysed in our laboratory by Nand Lal *et al* (1976) and given in table 2 suggest the emplacement of pegmatites in the Hazaribagh district of the Bihar mica belt during the Satpura orogeny. Further the data also indicate that the fission tracks even in the most sensitive mineral (apatite) were not affected by the Monghyr orogeny ($\sim$ 400 m.y.), thus suggesting it to be of mild nature and local extent.

The discordance of f.t. ages of the three cogenetic minerals is attributed to the uplift and cooling of rocks in which these pegmatites were emplaced and is discussed below:

Since the pegmatites were emplaced in the rocks of the upper amphibolite facies, the temperature of about 595 $\pm$ 10°C might have been reached in the region (Winkler 1967) though the initial temperature of the pegmatitic melt at the time of emplacement may be higher. After their emplacement the pegmatitic bodies started crystallizing and cooling down. The rate of initial cooling might have been greater until the temperature of the pegmatites reached the regional temperature prevailing in the area (*i.e.* $\sim$ 600°C) which was not favourable for retention of tracks in any of the minerals. The pegmatite bodies along with country rocks started uplifting and cooling simultaneously. The spectrum of cooling and uplift rates for the region is indicated in table 3.

The model f.t. age of apatite has tectonic significance in relation to the development of the Narmada-Son deep-seated fracture lineament which cuts across the Indian Peninsula and passes adjoining to the Bihar mica belt. This lineament is believed to be of different ages; Proterozoic by Auden (1949), and Naqvi *et al* (1974); Permian by Fox (1931) and Tertiary by Ahmed (1966). Our data (Nand Lal *et al* 1976) suggest that there was no significant tectonic activity along this fracture lineament, at least subsequent to 600 m.y., the model f.t. age of apatite.

5.3 *The Nellore mica belt*

A number of minerals from pegmatites of the Nellore mica belt have been dated by various workers by mass spectrometric method. Venkatasubramanian *et al* (1968) have reported the age value of 1500 m.y. for muscovite from the Nellore mica belt, which is in good agreement with lead ages for Samarskites from associated pegmatites (Holmes 1955). From this data, the pegmatitic intrusion of the Nellore mica belt is regarded as associated with the cooling stages of the Eastern Ghats Orogeny (1500–1600 m.y.).

A metamorphism, folding and uplift of the Eastern Ghats around 500 m.y. ago has been reported by Aswathanarayana (1964). The model f.t. age of 440 m.y. for apatite (Parshad *et al* 1979) indicates that the thermal event associated with metamorphic cycle affected this mineral and set a new fission clock. The new f.t. age of 1065 m.y. for garnet (table 2, Parshad *et al* 1979) indicates that during the metamorphic event

around 500 m.y., though the temperature crossed the closing temperature of apatite (100°C), it was below the closing temperature of garnet (276°C). The cooling and uplift rates calculated for these pegmatites are given in table 3.

5.4 *The Himalayan orogenic belt*

This orogenic belt, unlike other orogenic belts of India, is geologically and geochronologically less understood. The occurrence of pre-cambrian gneisses as old as 2,030 m.y. (Wangtu gneiss), 1,890 m.y. (Munsiari gneiss), 1,430 m.y. (Baragaon gneiss) and 1,220 m.y. (Bandal gneiss) in the crystalline basement suggests some possible magmatic correlation with the adjoining regions of the Aravalli orogenic belt (Bhanot *et al* 1973, 1978, 1979).

The presence of a pronounced unconformity marked between the Martolis and the Ralamas in Kumaun (Heim and Gansser 1939), the Haimantas and the Jadha in Garhwal (Auden 1949) and the Dogras and the Tanawals in the Vihi, Sindh and Banihal areas of Kashmir (Wadia 1957) suggest diastrophic movements towards the end of the Purana Era. The dating of granitic rocks from Mandi, Manali and Rohtang regions around 500–600 m.y. (Jager *et al* 1971; Bhanot *et al* 1973; Mehta 1977) suggests magmatism associated with the closing phase of this episode; however, the information on metamorphism and deformation related to this event is not clear so far. The presence of Caledonian and Hercynian epiorogenic movements in the Himalayas has also been suggested by Valdiya (1964) besides the Tertiary Orogeny which brought about the evolution of the Himalyas in at least four successive phases.

The first diastrophic phase of the Himalayan Orogeny took place towards the Upper Cretaceous during which period marine conditions in Karakoram and Tibet Plateau, marine transgression by the Nummulitic sea in the lesser Himalayan region and emplacement of ophiolites in the Indus-Suture zone took place. This phase has been designated the " Karakoram Orogeny " by De Terra (1933) and Valdiya (1964).

Valdiya (1964) considers that the second phase, known as the " Post Kirthar Orogeny ", took place towards the end of the Eocene and culminated in the Oligocene period. As a result, the Tibetan Plateau emerged from the cradle of the sea, the crystalline basement started ridging up along the Indo-Tibetan border, followed by possible development of exotic nappes of the Kumaun-Tibet border and emplacements of tourmaline-bearing granites of batholithic dimensions.

During the third phase, which took place towards the Middle Miocene period, the Himalayan Orogenic Belt witnessed the strongest upheaval; this brought about tight isoclinal folding, overturning and thrusting and was designated the " Sirmurrian Orogeny ". Recently, Sharma and Nagpaul (1980) have dated the thrusting event in the Satluj Valley at around 15 m.y.

The fourth phase in the tectonic evolution of the Himalayas commenced in the Pliocene and continued down to Middle Pleistocene time. This phase, called the " Siwalik Orogeny ", brought about folding and faulting of the Siwaliks, formation of the Main Boundary Fault, reactivation of the lesser Himalayan thrusts, elevation and tilting of Karewas of Kashmir and development of the Indo-Gangetic depression.

5.4a *Cooling and uplift rates*

The geodetic surveys carried out by the Survey of India (6th Gen. Assembly Meeting IUGG, Grenoble) have revealed that the Himalayas has been rising at a rate of 0·8 mm/year (800 m/m.y. during the past 75 years). Sharma *et al* (1978), using fission-track techniques, calculated a tectonic uplift of 550 m/m.y. for the past 8 m.y. from the Mandi region of the northwest Himalayas. Saini *et al* (1979) have suggested uplift rates of 0·04 mm/year, 0·08 mm/year and 0·15 mm/year for the period 200–46 m.y.; 31–20 m.y. and 20–11 m.y., respectively for the Kinnaur region of the Higher Himalayas. These authors also suggested that this region uplifted at a comparatively much faster rate of 0·8 mm/year between 15–7 m.y. ago during Miocene thrusting. Mehta using Rb-Sr muscovite and biotite ages from Kulu-Manali area, has calculated an uplift rate of 800 m/m.y. during the period 25–10 m.y. (Mehta 1979). The information on the cooling rates from the Himalayan Orogenic Belt is limited to the fission-track data reported by Saini *et al* (1979) and Saini (1978). Sharma *et al* (1978) suggested a cooling rate of 2–3°C/m.y. and 4°C/m.y. for the periods between 200–46 m.y.; 31–20 m.y. and 20–11 m.y., respectively for the Kinnaur region. They also suggested rapid cooling ($\sim$ 25°C/m.y.) subsequent to thrusting in the area. Frank *et al* (1977), using Rb-Sr age data, aiso suggested rapid cooling in the vicinity of the thrust zone in the Kulu area. The above data obviously suggest faster uplift and rapid cooling after the Middle Miocene (Sirmurian Orogeny) which brought about folding, overturning and thrusting in the Himalayas. The cooling and uplift rates for this region are given in table 4.

An important fact which emerges from the cooling and uplift histories of various geological regions of India discussed above is that the Himalayan Orogenic Cycle (Upper Cretaceous-Tertiary) witnessed the highest uplift and cooling rates as compared to older cycles of the peninsular India and may be attributed to large-scale horizontal shift of the Indian plate from 40°S lattitude to 8°N latitude in the past 71 m.y as suggested by Molnar and Tapponier (1975) at an average rate of about 50 mm/year (Le Pichon 1968; Minster *et al* 1974).

Table 4. Uplift and cooling rates of Himalayan orogenic belt

Locality/region	Method	Age span	Uplift rate (m/m.y.)	Cooling rate (°C/m.y.)
Outer Himalayan region	geodetic	past 75 years	800	—
Kulu	Rb-Sr-mineral ages	25-10 m.y.	800	—
Mandi	fission track	32-16 m.y.	—	2·0–3·0
		16-8 m.y.	—	3.0–6.0
		past 8 m.y.	550	—
Kinnaur	fission track	200-46 m.y.	30	1.0
		31-20 m.y.	80	2·0
		20-11 m.y.	150	4.0
		15- 7 m.y.	800	25.0

References

Ahmed F 1966 Post-Gondwana Faulting in Peninsular India and its bearing on the tectonics of the Subcontinent *Ann. Geol. Dep. Aligarh Muslim Univ.* (Aligarh) **2** 1

Anandalwar M A and Mahadevan T M 1968 *Rec. Geol. Surv. India* **95** 347

Armstrong R L 1966 in *Pottasium argon dating* (Heidelberg: Springer Verlag) p. 117

Aswathanarayana U 1956 *Am. J. Sci.* **254** 19

Aswathanarayana U 1964 *J. Geophys. Res.* **69** 3479

Auden J B 1949 *Rec. Geol. Surv. India* **76** 74

Balasundram M S and Balasubrahmanyan M N 1973 *Geol. Soc. Malaysia Bull.* **6** 213

Bhanot V B, Bhandari A K, Singh V P and Kausal A K 1973 *Him. Geol. Seminar* (*Abstract*) *held in Delhi in* 1972

Bhanot V B, Kwatra S K, Kausal A K and Pandey B K 1978 *J. Geol. Soc. India* **19** 224

Bhanot V B, Pandey B K and Singh V P 1979 *Seminar Abstract* (Nainital: Nainital University)

Chouduri R, Kosztolanyi C and Coppens R 1967 *Bull. Soc. Mines. Crystallogr.* **90** 77

Crawford A R 1968 *Geochronology of Pre-Cambrian rocks of Peninsular India and Ceylon* (Ph.D. Thesis) Australian National University

Crawford A R 1970 *J. Earth Sci.* **7** 91

De Terra H 1933 16th Int. Geological Cong. **2** 859

Fleischer R L and Price P B 1964 *Geochim. Cosmochim. Acta* **23** 1705

Fox C S 1931 *Mem. Geol. Surv. India* **58** 241

Frank W, Thoni M and Purtoscheller F 1977 *Colloq. Int. CNRS* 268

Gleadow A J W and Lovering J F (1975) *Fission track dating methods* (Publication Number 3: Univ. of Melbourne)

Haack U 1977 *Am. J. Sci.* **277** 459

Harper C T 1967 *Scott. J. Geol.* **3** 46

Heim A and Gansser A 1939 *Mem. Soc. Helv. Sci. Nat.* **73** 1

Holmes A 1949 *Geol. Mag.* **86** 288

Holmes A 1950 *Am. Mineral.* **35** 10

Holmes A 1955 *Ceylon. Proc. Geol. Ass. Can.* **65** 81

Hurford A J and Gleadow A J W 1977 *Nucl. Track Detection* **1** 41

Jager E, Bhandari A K and Bhanot V B 1971 *Ecologae Geol. Helv.* **64** 521

Krishnaswami S, Lal D, Prabhu N and Tamhane S A 1973 *Earth Planet. Sci. Lett.* **22** 51

Le Pichon X 1968 *J. Geophys. Res.* **73** 3661

Mahadevan T M 1965 *Mining, Geological and Metallurgical Institute*, Wadia Commem. Vol. 1, 480

Mehta P K 1977 *Geol. Rundsch* **66** 156

Mehta P K 1980 *Tectonophysics* **62** 311

Minster J B, Jordan T H, Molnar P and Haines E 1974 *Geophys. J.R. Astron. Soc.* **36** 541

Molnar P and Tapponier P 1975 *Science* **189** 419

Nagpal M K and Nagpaul K K 1974 *Can. J. Earth Sci.* **11** 519

Nagpaul K K and Nand Lal 1980 Report No. PL-480/NBS(G)-182/80/1, Kurukshetra University, India (Unpublished)

Nandi S K and Sen D N 1950 *J. Sci. Ind. Res.* **B9 124**, 156

Nand Lal, Saini H S, Nagpaul K K and Sharma K K 1976 *Tectonophysics* **34** 163

Naqvi S M, Divakara Rao V and Narain H 1974 *Precambrian Res.* **1** 345

Parshad R, Lal N and Nagpaul K K 1979 *J. Geol. Soc. India* **20** 31

Pichamuthu C S 1971 *J. Geol. Soc. India* **12** 265

Poupeau G 1981 *Proc. Indian Acad. Sci.* (*Earth Planet. Sci.*) **90** 403

Poupeau G, Carpena J, Chankaudet A and Romary Ph 1980 *Solid State nuclear track detectors* (New York: Pergamon Press) 965

Rama Rao B 1964 *J. Geol. Soc. India* **5** 56

Roberts J H, Gold R and Armani R J 1968 *Phys. Rev.* **174** 1482

Saini H S 1978 *Solid state nuclear track detectors and their applications to earth sciences Ph.D. Thesis*, Kurukshetra University, Kurukshetra, India

Saini H S, Waraich R S, Malhotra N K and Nagpaul K K 1979 *Him. Geol.* **9** (in Press)

Sarkar S N, Polkanov A R, Gerling E K and Chukrov F V 1964 *Proc. 22nd Int. Geol. Cong. X* 102
Sarkar S N and Saha A K 1962 *Geol. Min. Metall. Soc. India* **34** 97
Sarkar S N and Sen Sharma R N 1946 *Sci. Cult.* **11** 569
Sarkar T C 1941 *Proc. Indian Acad. Sci.* **A13** 245
Sharma K K 1978 *Rec. Res. Geol.* **7** 118
Sharma K K and Kumar S 1978 *Him. Geol.* **8** 252
Sharma K K, Nagpaul M K, Nagpaul K K and Jhingran A G 1975 *Chayanica. Geol.* **1** 196
Sharma K K and Nagpaul K K 1980 *Proc. fission track dating workshop*, Pisa (in Press)
Sharma Y P, Nand Lal, Bal K D, Parshad R and Nagpaul K K 1980 *Contrib. Mineral. Petrol.* **72** 335
Spadeavecchia A and Hann B 1967 *Helv. Phys. Acta* **40** 1063
Valdiya K S 1964 *Proc. 22nd Int. Geol. Congr. New Delhi* **11** 269
Venkatasubramanian V S, Gopalan S S, Iyer Pal S and Krishnan R S 1968 *Can. J. Earth Sci.* **5** 601
Venkatasubramanian V S and Krishnan R S 1960 *Proc. Natl. Inst. Sci.* **A26** (*Suppl. II*) 89
Vinogradov A P, Tugarinov A I, Zhikov C I, Stupinokov N I, Bikikov B V and Ktorre K G 1964 *Proc. 22nd Int. Geol. Congr.* (*New Delhi*) **10** 553
Wadia 1957 *The geology of India* (London: MacMillan) p. 536
Wagner G A 1972 *Fortschr. Mines* **49** 114
Wagner G A, Reimer G M, Carpenter B S, Faul H, Vander Linder R and Gijbels R 1975 *Geochim. Cosmochim. Acta* **39** 1279
Wagner G A, Reimer G M and Jager E 1977 *Mem. Ist. Geol. Mineral Univ. Padova* **30** 1
Winkler H G 1967 *Petrogenesis of metamorphic rocks* (New York: Springer) p. 237

Precision, accuracy and meaning of fission track ages

G POUPEAU
Centre des Faibles Radioactivities Laboratoire Mixte CNRS/CEA 91190 Gif-sur Yvette, France
Present Address:
Centro Brasileiro de Pesquisas Fisicas, Av. Wenceslau Braz, 71 Rio de Janeiro, Brazil

Abstract. The precision, meaning, and accuracy of the fission track (FT) dating method are reviewed from an examination of the recent literature as well as previously unpublished data from the author's laboratory.

It is concluded that for *apparent* FT ages (*i.e.* ages derived from the canonical age equation) a precision (2σ level) of the order of $\pm$ 4% to $\pm$ 5% can be reached provided that (i) uranium is sufficiently homogeneously distributed in the dated samples, at least locally; and (ii) a large enough number of tracks can be counted.

Model FT ages, *i.e.* ages for which partial geological track annealing is taken into account, have variable degrees of precision. While model ages obtained with the track-size method seem, as evaluated from the literature, to have usually a limited precision of the order of $\pm$ 30% (2σ), plateau ages usually have a precision better than $\pm$ 5% at a 2σ confidence level. Because it provides an objective test on the accuracy of track identification, as well as some insight of the variability of closing temperatures between various samples of a given mineral phase, the Isochronal Plateau (ICP) method, when applicable, will be preferred (Poupeau *et al* 1980a). However, for phases which could be damaged by heating at relatively high temperatures, as for example hydrated glass shards from tephra, an Isothermal Plateau (ITP) approach is to be preferred.

Due to uncertainties about the value of the ^{238}U spontaneous fission decay constant λ_f, as well as difficulties inherent in the dosimetry of thermal neutrons in nuclear reactors, the FT method of dating is not an independent one. Presently, it relies on the existence of geological standards (volcanic rocks) of known age, allowing to determine an *operational* 'λ_f' value (Naeser *et al* 1980). Accordingly, the accuracy of an FT age is limited by the accuracy on the age of the standard. It should be better than $\sim$ 5%.

For volcanic, hypovolcanic rocks, and shallow intrusives, the FT method dates the time of formation, provided they were not further reheated. More generally, the track method provides *cooling* ages. Closing temperatures calculated from laboratory experiments vary from $\lesssim$ 300°C to 100°C, according to minerals, for slow cooling rates ($\sim$ 1°C/m.y.). For apatites, recent geological calibrations (Naeser *et al* 1980; Gleadow and Duddy 1980) confirmed laboratory extrapolations. The association of the FT method with other geochronometers is therefore critical to the study of the cooling history of old cratons as well as to the evaluation of uplift/erosion rates in recent belts.

Keywords. Fission tracks; fission track dating; track annealing; fission decay constant; neutron dosimetry; model ages; plateau ages; cooling and uplift rates.

1. Introduction

The fission track (FT) method of dating proposed in 1963 by Price and Walker has been shown to apply to a variety of problems from anthropology to plate tectonics and cosmochronology (Fleischer *et al* 1975). Methods have been devised in order to take into account in age determinations the effect of partial fading of fossil tracks (Storzer and Wagner 1969; Storzer and Poupeau 1973a). However, the FT ages reported in the literature are too often difficult to use and compare with other radiometric

methods, either because their quoted precision is unclear or due to uncertain choices of parameters in the equation used for deriving FT ages.

There is an urgent need of standardization in FT dating; specifically, it should include both the use of recognized standards for interlaboratory calibrations and the adoption of widely accepted models for evaluating the precision of the measured ages. It is the aim of this paper to give the present status of FT dating from the point of view of precision, accuracy, and meaning of ages. Model ages will be specially considered. In this context, we present here the first set of analytical data obtained in minerals by plateau methods of dating (preliminary accounts were given in Poupeau *et al* 1978a, b; 1980a, b, and Carpena *et al* 1980). Recent general accounts of the FT dating method can be found in Naeser (1978, 1979), Wagner (1978, 1979), Poupeau (1981a), and Poupeau and Rajan (1981).

2. Relevant relationships

Any FT age t is obtained basically by counting two track densities (expressed as number of tracks per unit area), respectively, the densities D_f of fossil tracks from the spontaneous fission of ^{238}U and D_i from ^{235}U induced fission tracks, the latter ones produced by irradiation of the sample by thermal neutrons in a nuclear reactor. In order to discuss the precision and meaning of an FT age, it is convenient to write the age equation (Price and Walker 1963) in the form* (Poupeau *et al* 1980b):

$$t = A \ln \left\{ 1 + B \frac{\eta^{235}}{\eta^{238}} \frac{D_f}{D_i} \right\}, \qquad (1)$$

where $A = 1/\lambda_t$ and $\lambda_t = 1{\cdot}55125 \times 10^{-10}$ yrs^{-1} total decay constant of ^{238}U (Jaffey *et al* 1971),

$$B = \frac{\sigma I \phi \lambda_t}{\lambda_f} \frac{\bar{R}^{235}}{\bar{R}^{238}}, \text{ with}$$

$\sigma = 580$ barns (Table of isotopes, 1978), cross-section of ^{235}U fission by thermal neutrons,

$I = 7{\cdot}235 \times 10^{-3}$ (Cowan and Adler 1976), natural $^{235}U/^{238}U$ isotopic ratio,

ϕ = thermal neutron dose (neutrons cm^{-2}),

λ_f = ^{238}U spontaneous fission decay constant. Two values of λ_f are principally in use (see § 6): $\lambda_f = 7{\cdot}03 \times 10^{-17}$ yrs^{-1} and $\lambda_f = 8{\cdot}46 \times 10^{-17}$ yrs^{-1},

$\bar{R}^{235}/\bar{R}^{238}$ = mean track length ratio of thermally unaffected fossil and induced fission tracks. From theoretical calculations (see Bhandari *et al* 1971) as well as experimental evidences, this ratio is taken as equal to one, and B simplifies to:

$$B = \sigma I \phi \lambda_t / \lambda_f,$$

*This form holds for the internal method of dating (§ 3 and figure 1). In the external detector geometry, D_i would have to be replaced usually by $2D_i$ (see Gleadow and Lovering 1977).

η^{235} and η^{238} = registration efficiency factors. They are measures of the fraction of tracks intersecting the external surface of a solid state track detector (SSTD) that can be made observable by chemical etching (Fleischer *et al* 1975).

In practice, however, as one cannot measure directly the η parameters, one always uses, for FT age calculations, the following reduced form:

$$t = A \ln \left\{ 1 + B \frac{D_f}{D_i} \right\}, \tag{2}$$

which assumes $\eta^{235}/\eta^{238} = 1$*. This can lead to a meaningful FT age only when *no* partial geological annealing affects the fossil tracks. This ideal situation occurs only in limited circumstances, *e.g.* mineral dating of volcanic rocks and shallow intrusives. A η^{235}/η^{238} ratio higher than one is almost the rule in volcanic and impact glasses and not infrequent in minerals from metamorphic rocks.

When the fossil tracks are partially faded η^{238} and thus D_f are correlatively lowered, the age given by equation (2) is then an *apparent age* without geological significance (Poupeau 1981a, Wagner 1979). Therefore, for *each* FT age measurement it is absolutely necessary (i) to determine whether or not D_f has been affected by environmental conditions during the geologic time of track storage, and (ii) to quantitatively take this effect into account to 'correct' the apparent age given by equation (2) (see § 2 below).

The precision of an FT age obtained by equation (2) is given by (Johnson *et al* 1979):

$$\frac{\sigma_t}{t} = C \left\{ \left(\frac{\sigma_f}{D_f}\right)^2 + \left(\frac{\sigma_i}{D_i}\right)^2 + \left(\frac{\sigma_\phi}{\phi}\right)^2 - 2r\left(\frac{\sigma_f}{D_f}\right)\left(\frac{\sigma_i}{D_i}\right) \right\}^{1/2}, \tag{3}$$

where σ_t, σ_f, σ_i, and σ_ϕ are the standard errors on t, D_f, D_i, and ϕ respectively, r is the correlation coefficient between D_f and D_i

and $$C = \frac{A}{t}[1 - \exp(-t/A)], \tag{4}$$

For practical purposes $C \approx 1$ if $t < 10^8$ yrs. Equation (3), as expressed in percent errors, then reduces to:

$$E_t = C(E_f^2 + E_i^2 + E_\phi^2 - 2rE_f E_i)^{1/2}, \tag{5}$$

where the E's are the percent errors on t, D_f, D_i and ϕ. Estimates of E_t are discussed below considering the various methods of track dating.

*Incidentally, this also assumes that the neutron dose used to produce D_i has no effect on the track recording and etching properties of the dated phase.

3. Dating techniques

As the calculations of E_t are somewhat dependent on the way D_f and D_i are measured, it appears relevant to recall briefly the main techniques used for FT dating.

As shown in figure 1, two methods can be used, either the external detector (ED) or internal detector (ID) method. In the ID method, D_f and D_i are most often measured on different samples—either two fragments of the same crystal (figure 1A), as often done for micas (where large crystals are available), or on two different groups of crystals, as typically practised for apatites (figure 1B). The method is called the internal detector method, since the surfaces on which track counts are made are surfaces internal to the mineral. The internal surfaces are generated, prior to etching, either by fracturing along cleavage planes (micas) or polishing (other minerals and glasses). Alternatively (figure 1C), both D_f and D_i can be counted on the same piece of mineral provided that a repolishing after neutron irradiation reveals a new internal surface. The thickness of the removed layer must be greater than, or equal to, the range of one fission fragment.

In the external detector method, the induced fission tracks are either etched on the same face as the fossil tracks (figure 1D) or on an external detector placed against a polished surface of the sample to be dated during irradiation (figure 1E).

Whereas any procedure in principle can be applied to samples where the uranium distribution is uniform, procedures 1C to 1E are more appropriate to those samples where the U distribution is irregular on a small scale.

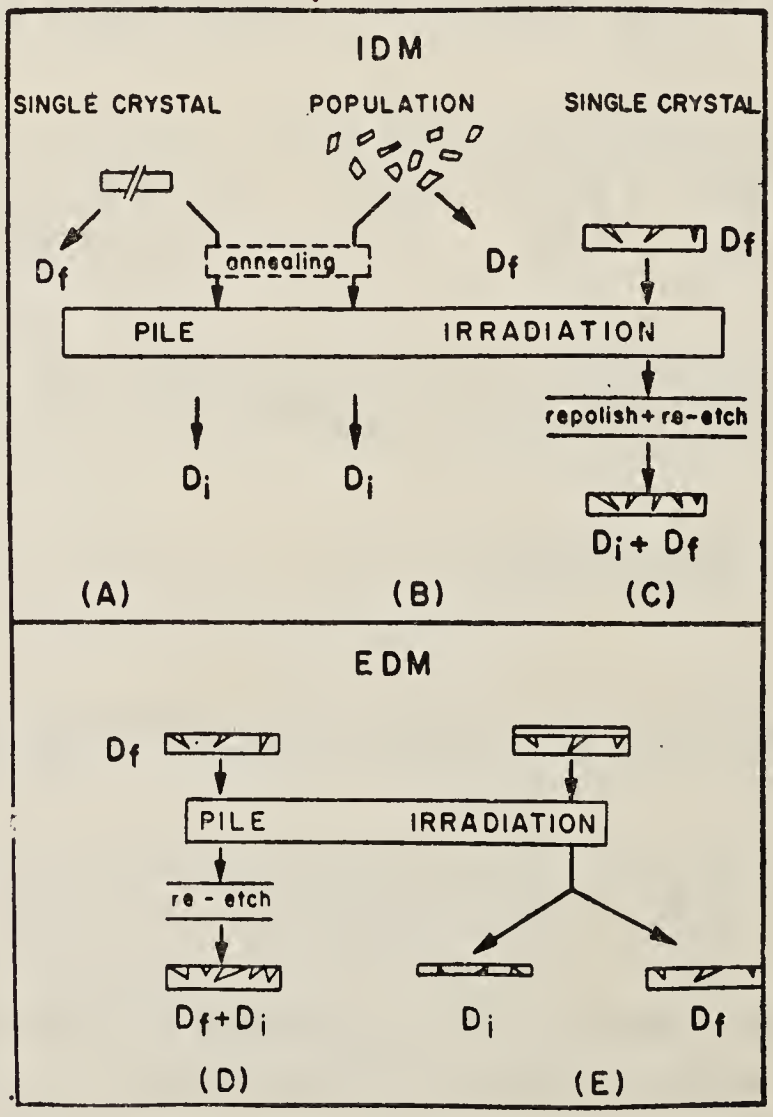

Figure 1. Fission track dating methods (see text). IDM and EDM, respectively, refer to internal detector and external detector methods; D_f and D_i, fossil and thermal neutron induced fission track densities.

4. Precision on apparent ages

The precision on *apparent age*, *i.e.* an FT age directly derived from equation (1), depends primarily on the parameters D_f, D_i, r, and ϕ.

4.1 *Precision on* ϕ

The neutron dosimetry in FT dating is usually carried out by radioactive countings of metal monitor foils (Co, Cu, Au, etc.) or by irradiating a uranium glass standard simultaneously with the sample and then counting the induced fission tracks produced in the standard. These standards are usually intercalibrated to metal foils (Carpenter and Reimer 1974).

With metal foils, a statistical precision of 1 % (2σ) can be achieved without difficulty. With uranium glass standards, a precision of the order of 4% (2σ) can be reached if about 2,500 fission tracks are counted.

4.2 *Precision on* D_f, D_i, r *and the apparent age* t

The precision of D_f and D_i is usually calculated from poisson or gaussian statistics. Since the uranium distribution in samples is often not perfectly homogeneous, the latter statistical approach generally is considered to give a more realistic evaluation of the uncertainty in track counting (Naeser 1978). However, regrettably, no justification (statistical test results) for the choice of a particular statistics is given in the published literature on FT dating. Often the use of a poissonian law results in a lowering of the counting uncertainty estimates.

The evaluation of the correlation coefficient r of equations (3) and (5) is easy only in the ED method when several minerals from a given rock are dated separately. It is suggested (McGee and Johnson 1979) that, in order to avoid the high sensitivity of r with the number of measurements if only a few samples are used, at least 10 different samples must be analysed to calculate an FT age with this method. With the ED procedure (E) in figure 1, a precision on the apparent age t of the order of $\pm$ 4% (2σ) can be achieved (figure 2).

In the ID method, where the correlation coefficient cannot be calculated numerically, McGee and Johnson (1979) suggest to adopt a value of 0·8 as a 'conservative guess.' In these conditions, assuming $E_f = E_i = E_\phi = 2\%$ (1σ), a precision of $\pm$ 5% (2σ) can be obtained for the dating procedures (A) and (B) of figure 1.

When the induced tracks are measured on a sample where the fossil tracks were not thermally annealed before neutron irradiation, the net track density D_i is deduced from the total track density D^* after irradiation by:

$$D_i = D^* - D_f. \tag{6}$$

In this case, the precision on D_i given by

$$\sigma^2_{(D_i)} = \sigma^2_{(D_f)} + \sigma^2_{(D^*)}, \tag{7}$$

is larger than the statistical counting error.

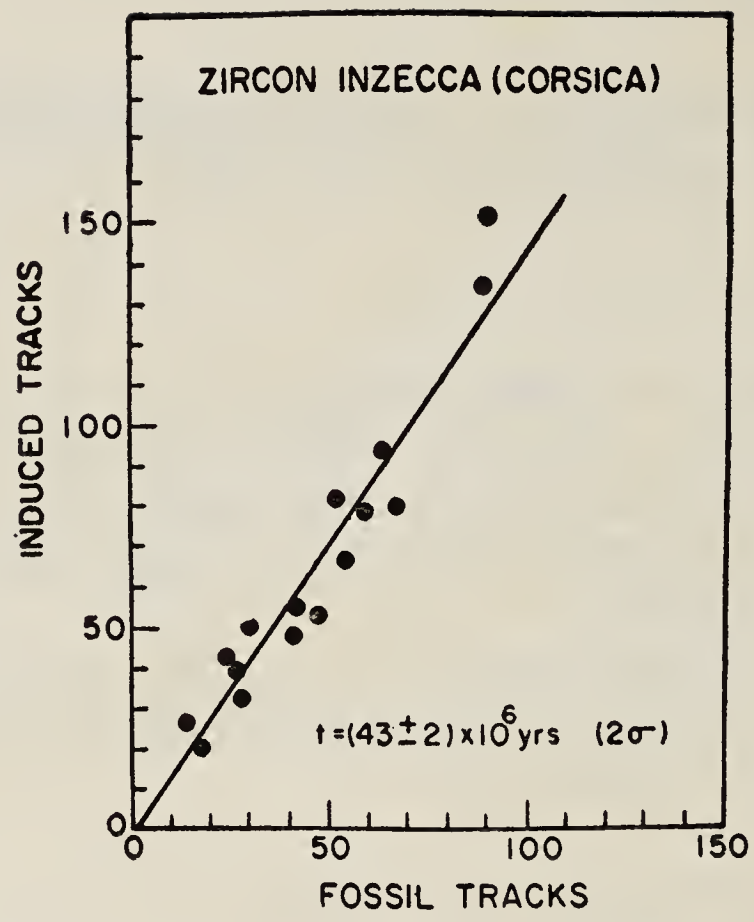

Figure 2. Isochrone age of 16 zircons from a trondjhemite (Corsica) dated by the external detector method. $E_f = 3.66\%$; $E_i = 3.13\%$; $\sigma_\phi = 2\%$; $r = 0.96$ (all errors are 1σ; from Carpena *et al* 1979). The numbers on axis are the number of fossil and induced tracks counted per crystal.

The determination of errors on apparent ages, derived as discussed above, deals only with random error measurements. This approach does not take into account other sources of errors in the age such as counting geometry, adequacy of statistical laws applied to measured track distribution to calculate statistical counting errors, identification of tracks, actual value of the correlation coefficient r (in the ID method), etc. The effect of track annealing and choice of constants are considered in the next two sections.

5. Precision on model FT ages

When fossil tracks are partially annealed, the ratio η^{235}/η^{238} of equation (1) is no longer equal to one and correspondingly the condition of applicability of equation (2) is no more fulfilled. Therefore, a meaningful FT age cannot be derived directly from this equation unless partial track annealing effect is taken into account. This can be done either by correcting the term D_f of equation (2) for track density loss, in the ' track-size ' correction method (Storzer and Wagner 1969), or by reducing the ratio η^{235}/η^{238} to unity by a series of laboratory annealing steps in the ' plateau ' method (Storzer and Poupeau 1973a). These two methods are based on the assumption that although partial track annealing results in a lowering of the etchable track density, it does not affect significantly—at least for fossil track density reduction* of $\lesssim$ 50-70 %—the volumic density (*i.e.* the number of etchable fission events per volume unit) of fossil tracks.

*As estimated from the literature [cf. for glasses Storzer (1970a) and minerals (biotite) Nagpaul *et al* (1974)].

5.1 *FT ages corrected using the ' track-size ' method*

5.1*a The model.* The track-size method of correcting apparent FT ages is based on the observation that, with increasing degree of annealing, both the density of etchable tracks and their diameter (for glasses, where tracks present a characteristic ellipsoid etch pit shape) or length (in minerals) decrease (see Storzer and Wagner 1969).

In order to correct an apparent FT age by this method, one first has to establish from a series of thermal annealing experiments a calibration curve between the fractional reduction of the etchable track length and track density of thermal neutron induced ^{235}U fission tracks. Then, from the measurement of the ratio $\bar{L}^{238}/\bar{R}^{235}$ (figure 3), one can graphically deduce the value of the correction factor X to D_f. The corrected value of the fossil track density to be incorporated in equation (2) is:

$$D_f \text{ (corrected)} = \frac{D_f \text{ (measured)}}{X} \times 100. \tag{8}$$

The introduction of the factor X in equation (2), with its large associated uncertainty, will ultimately control the precision on the corrected age.

5.1*b Precision on corrected FT ages.* Although the ' track-size ' correction method was introduced as early as 1969 (Storzer and Wagner 1969) and systematically applied later on by several groups, it is not yet clear how the precision on corrected FT ages is calculated as no account of its derivation has yet been given. However, some tentative estimate can be drawn from published data.

The precision on any age corrected by the size method depends, in addition to the precision on D_f, D_i, and ϕ, on the uncertainties on X, *i.e.* on the ratio $\bar{L}_f/\bar{R}^{235}$ and on the calibration curve (figure 3).

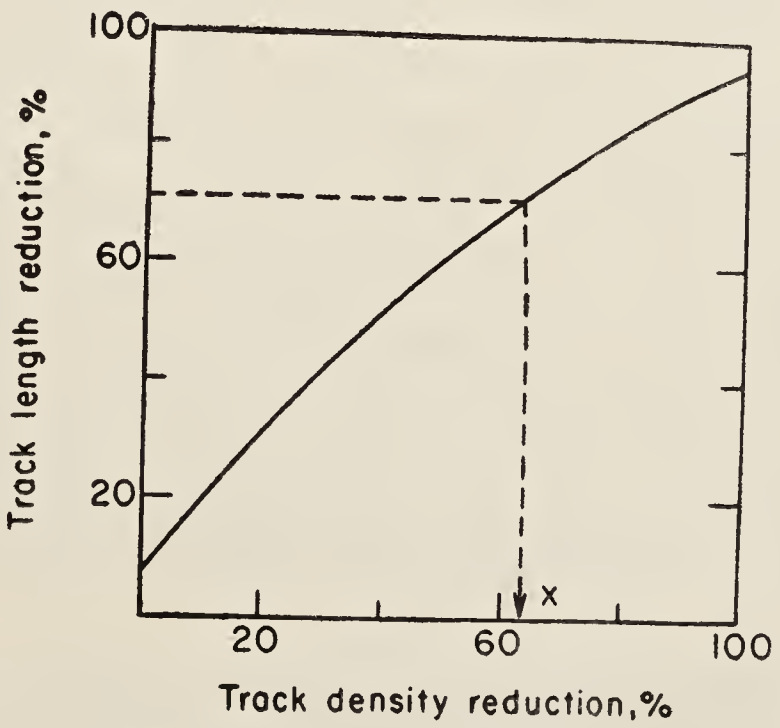

Figure 3. Correction of an apparent FT age with partially faded fossil tracks using the 'track-size' correction method. The ratio of the mean track length (or diameter, in glass) $\bar{L}_f/\bar{R}^{235}$ (see text) is used to deduce the percentage of track density loss. The corrected fossil track density is D_f (corrected) $= 100/x \; D_f$ (measured). $\bar{R}_f$ and $\bar{R}^{235}$ are mean length of fossil and induced fission tracks, respectively.

The mean track lengths (or diameter for glass) $\bar{L}_f$ and $\bar{R}^{235}$ seem to be usually calculated from only some 100 to 200 individual tracks (Storzer and Wagner 1969, Saini and Nagpaul 1979; Arias *et al* 1981). Moreover, it is seen from the track length/diameter distribution histograms published in the literature that, except for unannealed track length in minerals, as measured by the track-in-track method (Bhandari *et al* 1971), the distribution of track length or diameter does not generally follow a gaussian distribution. Therefore, the uncertainty on any mean track length is best taken as the standard deviation of the distribution (Saini and Nagpaul 1979):

$$\sigma = \left(\frac{\Sigma (L_j - \bar{L})^2}{n-1}\right)^{1/2}$$

where n is the total number of tracks measured, L_j and $\bar{L}$, respectively, the length of the jth track and the mean track length $\bar{L} = \Sigma L_j/n$.

The precision on the ratio $\bar{L}_f/\bar{R}^{235}$ is then given by:

$$\sigma^2 = \sigma^2_{\bar{L}_f} + \sigma^2_{\bar{R}^{235}}.$$

Calculations of $\sigma^2_{\bar{L}_f}$ and $\sigma^2_{\bar{R}^{235}}$ from histograms reported in the literature show that, in general, the standard error σ^2 is of the order of 10%. As a result, the error on X is of about 15%.

Assuming the error on the calibration curve as comparatively negligible, the precision on an FT age corrected by the track-size method can be derived using a modified form of equation (5):

$$E_t^2 = C(E_f^2 + E_i^2 + E_\phi^2 + E_x^2 - 2r\, E_f E_i). \tag{9}$$

Assuming D_f, D_i and ϕ can be obtained with a precision (1σ) of 2% and taking the parameter C of equation (3) as equal to one, it appears that whatever the value of r (between 0 and 1) the precision on an FT age corrected with the track-size value cannot be better than $\sim$16% (1σ). This evaluation is of the same order as the one suggested in the initial article by Storzer and Wagner (1969).

The preceding discussion was based on the assumption that the fossil track length distribution was unimodal, which is generally the case. When bimodality is present, *i.e.* when two populations of fossil tracks show different degrees of fading (see Storzer 1970a; Nagpaul *et al* 1974), an additional error has to be taken into account, linked to the demodulation of these two peaks, which date different events. The extent of this additional error could be of the order of 20% (Storzer 1970 a).

Therefore, as useful as it may be, the size correction method does not allow a fine time resolution, as its overall precision ($\pm 2\sigma$) seems to be, at best, of the order of $\pm$ 30%.

5.2 *FT ages corrected using the plateau method*

The major source of uncertainties in the track-size correction method comes from track length (or diameter) measurements. The pleateau methods are aimed at giving FT ages *directly* corrected for partial geological track fading. Since no detailed

analytical data have yet been published, a few examples of plateau age dating of micas and apatites will be given below after a discussion of the precision of these methods.

5.2*a Principle and precision of plateau age dating.* The plateau method represents an attempt to fulfill the condition $\eta^{235}/\eta^{238} = 1$ of applicability of equation (2). In order to do so aliquots of the mineral phase to be dated, with latent fossil and induced fission tracks, respectively, are annealed under various conditions (time, temperature) to reduce η^{235} to the same value as (the eventually geologically lowered) η^{238}, with the presupposition that, once this is realized, the η^{235}/η^{238} ratio will remain constant and will be equal to one upon further annealing (figure 4). Two procedures have been proposed to achieve this goal: the isochronal plateau (ICP) method (Storzer and Poupeau 1973a; Popeau *et al* 1980*a*) and the isothermal plateau (ITP) method (Dakowski *et al* 1974).

In each of these methods, a series of apparent FT ages is measured on aliquots

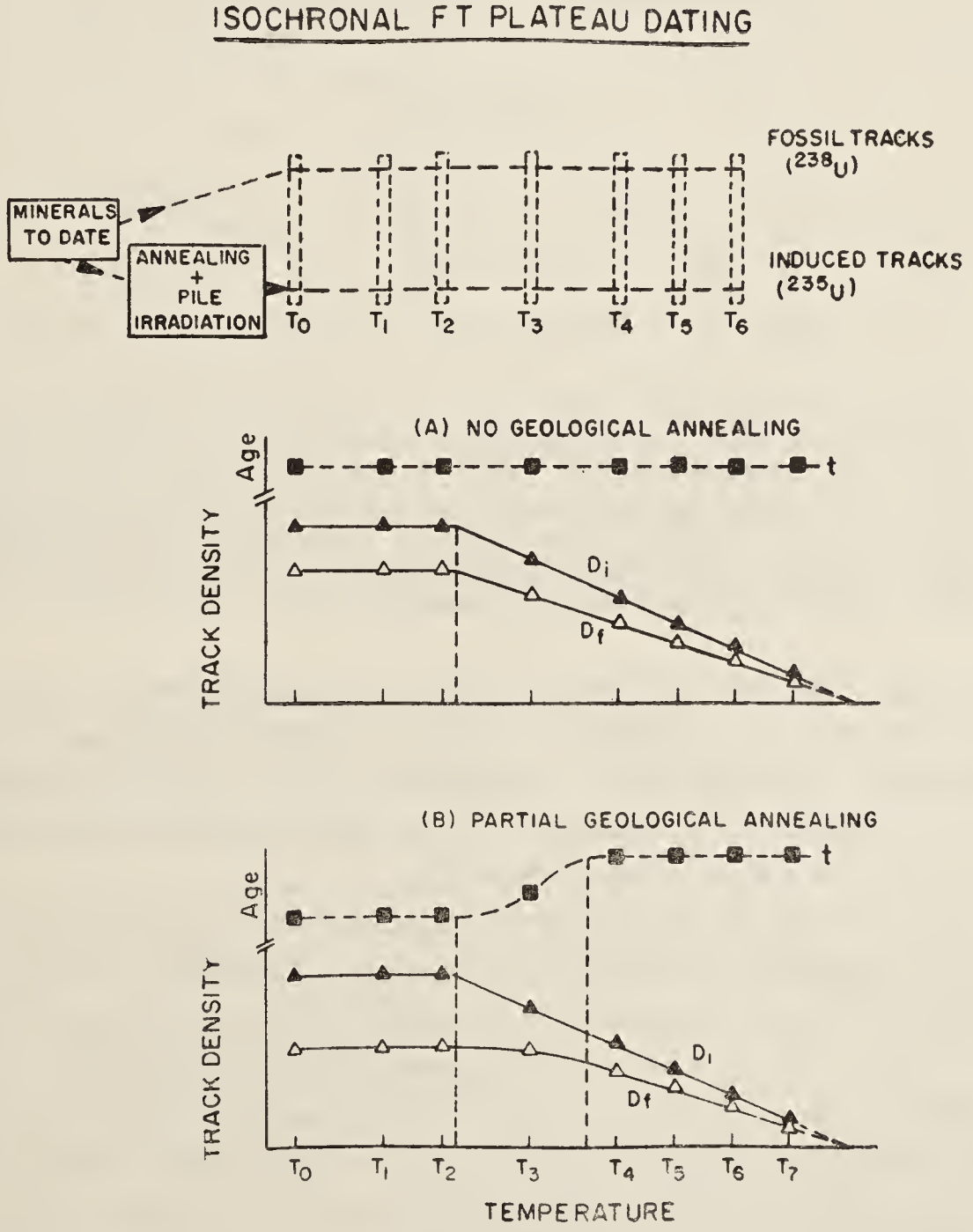

Figure 4. Principle of isochronal FT plateau age dating. The minerals to date are split into two sub-samples for the measure of fossil and induced fission tracks. Annealing is optional and to be avoided if suspected to modify the physical state of the dated mineral phase (f.i. glass). After irradiation, aliquots respectively with fossil and induced fission tracks are heated for a standard time at a given temperature and then dated. Depending on the absence or presence of geological annealing (figures A and B, respectively), different behaviour of the fossil track population is expected (Poupeau *et al* 1980a).

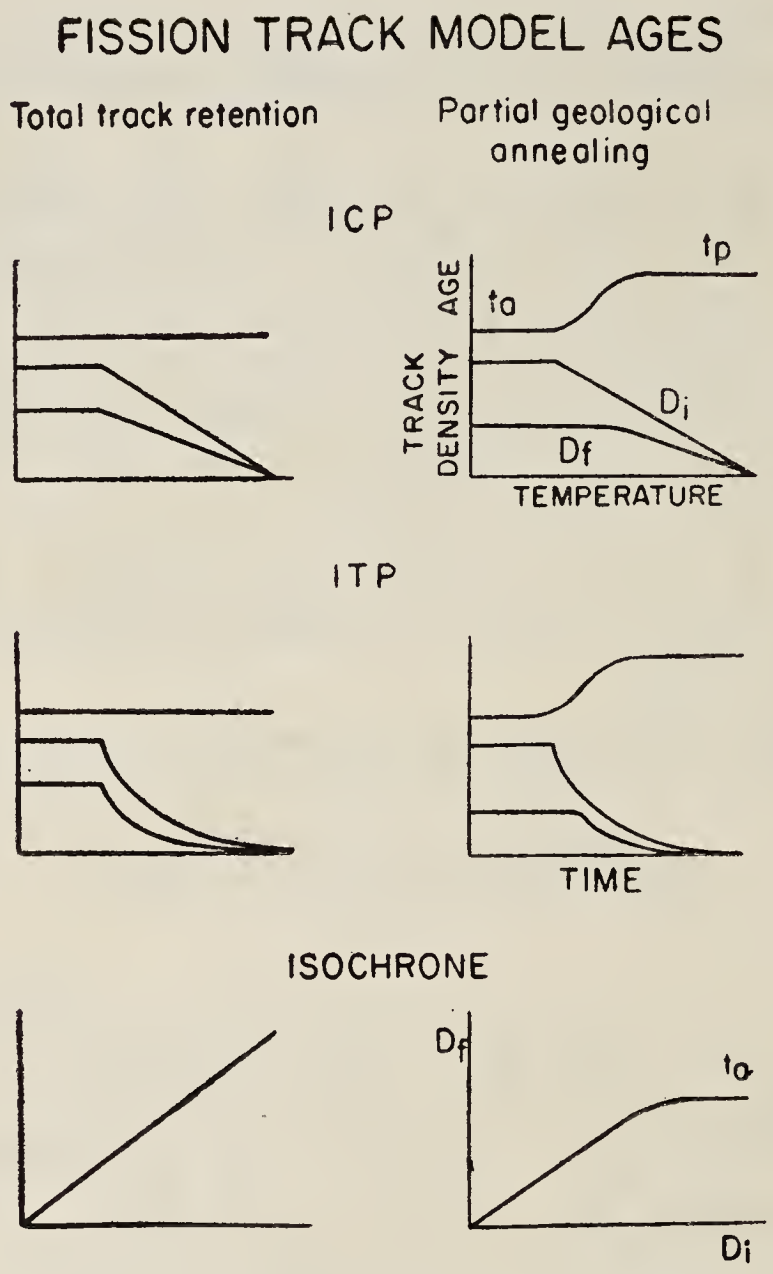

Figure 5. Comparison of the behaviour of D_f, D_i and the apparent age t with temperature in the isochronal plateau (ICP) method (top), or with time, in the isothermal plateau (ITP) method (middle). With increasing temperature and/or time, D_f and D_i decrease; and their ratio (hence t) reaches eventually a constant value (isochrone representation of data, bottom figure). Eventually, if some geological annealing affects the fossil tracks, the FT age will evolve from a low apparent age t_a to a higher plateau value t_p. Scales in all diagrams are linear.

subjected to various thermal treatments before age measurements. In the ICP method (figure 4), the aliquots are submitted to annealing steps for a standard time (one hour in our routine procedure), each aliquot being dated after a single annealing step. In the ITP method, the aliquots are submitted to a *cumulative* series of annealing steps at a given temperature, but for increasing durations.

In the absence of geological fossil track fading, both D_f and D_i are supposed to react similarly to laboratory thermal treatment. Therefore, the ratio D_f/D_i and, consequently, the FT age t are expected to remain constant along the heating procedure (figures 4, 5). On the contrary, if geological fading is present, D_f will not be affected as much as D_i in the first annealing steps (as fossil tracks are already partially annealed) up to a point where $\eta^{235} = \eta^{238}$; and beyond this point both track populations are expected to have similar annealing characteristics. Accordingly, the FT age t would increase from a low value to a stable high temperature value. If several age measurements are made at the plateau, the final age t_{pl} and its precision $\sigma_{t_{\mathrm{pl}}}$ are calculated as weighted averages (Bevington 1969):

$$t_{\mathrm{pl}} = \frac{\Sigma\,(t_i/\sigma_i^2)}{\Sigma\,(1/\sigma_i^2)},$$

$$\sigma^2_{t\,\mathrm{pl}} = \frac{1}{\Sigma\,(1/\sigma_1^2)}. \qquad (10)$$

The errors (2σ) on plateau ages calculated from relations (10) are usually smaller than $\pm$ 5%. Some illustrations are given below.

5.2*b Examples of FT plateau ages.* Although the applicability of the plateau method of Storzer and Poupeau (1973a) for minerals was questioned at first (Naeser and Fleischer 1975), it was later shown to give significant ages in micas and apatites from a variety of environments (Poupeau *et al* 1978a, b; Carpena *et al* 1979; Mailhe *et al* 1980). Typical examples of micas and apatites analysed by plateau methods are presented in tables 1 to 3. Analytical data for three phlogopites and five apatites are given in tables 1 and 2, respectively; and plateau ages are compiled in table 3. The geological meaning of these ages was discussed elsewhere (Poupeau *et al* 1978a; Carpena *et al* 1980; Poupeau 1981b). All ages and their quoted precision have been recalculated (as in Poupeau 1981b) using (3) and (10). All minerals in tables 1 and 2 have been dated by the ICP method. In addition, two apatite samples (# 2520 and Nages) have also been treated by the ITP method.

In micas, where uranium is homogeneously distributed, the errors on track densities were calculated as Poisson errors. From table 1, it appears that none of these micas has been affected by geological partial annealing: for each sample, the apparent age determined at ambient temperature is indistinguishable from those measured after some thermal treatment. As an expected consequence (see figure 5), annealing of both fossil and induced tracks start at about the same temperature in these micas as illustrated in figure 6 for the Ampandrandava and Mahanela samples. Similarly, in the isochrone mode of representation (figure 7), no geological fading of the fossil tracks is discernible. In this case, plateau ages have been calculated (table 3) from all apparent age values giving a precision on the weighted ages of better than $\pm$ 4% (2σ).

In apatites, where uranium is generally less homogeneously distributed than in micas, the error on D_f and D_i has been evaluated with gaussian statistics rather than poissonian (Naeser 1978). The apatites were dated with the population method. Usually, track densities were measured from measurement on at least $\sim$ 40 crystals, giving apparent ages with a precision of $\lesssim$ 10% and plateau ages of the order of $\pm$ 5% (2σ). In sample 70242, where few crystals were available and track densities rather low (table 2), a precision on the plateau age of $\pm$ 9% (2σ) was still achievable.

Two apatite samples (## 2520 and M44), do not present any detectable geological annealing. Some annealing could be present in two others, M 34 and 70242, but the limited precision on the apparent ages of these samples prevents any definitive conclusion to be reached on this matter. Only the Nages apatites present a clear-cut case of geological track fading, with an apparent age of 197 $\pm$ 14 m. y., significantly lower than its ICP plateau value of 283 $\pm$ 14 m. y. (figure 8).

In principle, ICP and ITP treatments are supposed to produce similar results when applied to a given sample. This has been tested on the Nages and 2520 samples. On the Nages sample, both ICP and ITP ages were determined by the same observer. The plateau values of 283 $\pm$ 14 m.y. and 281 $\pm$ 22 m.y. are in remarkable agreement. When all analytical data are combined together, they provide an age of 282$\pm$12 m.y.

Table 1. Fission track plateau ages in micas: Analytical data*

Sample	Etching time (min.)	Annealing temperature (°C)	ϕ (10^{15}cm^{-2})	D_f (10^4/cm^2)	N_f	D_i (10^5/cm^2)	N_i	$t \pm 1\sigma$** (10^6 yrs)
Ampandrandava 132206	8	Ambient	0·98	4·37	344	0·615	463	404 ± 14
	,,	300	6·09	5·90	354	5·31	470	392 ± 13
	,,	400		4·74	677	4·22	642	397 ± 10
	,,	450		4·61	264	4·02	319	405 ± 16
	,,	480		4·03	195	3·57	2000	399 ± 20
	,,	500		3·91	721	3·38	2007	408 ± 10
	,,	550		3·85	202	3·37	1997	403 ± 12
Mahanela 103 794	8	Ambient	6·09	2·84	730	1·72	670	575 ± 14
	,,	200		2·87	472	1·80	1110	556 ± 17
	,,	400		2·63	808	1·59	531	576 ± 16
	,,	490		2·45	600	1·49	531	572 ± 16
	,,	530		2·35	300	1·39	600	588 ± 21
Monroe 55250	10	Ambient	6·09	1·53	300	1·86	250	293 ± 12
	,,	300		1·57	508	1·79	627	312 ± 9
	,,	440		1·09	253	1·27	300	305 ± 12
	,,	480		1·02	250	1·16	280	312 ± 12

*All track density measurements were made with a scanning electron microscope, but for the Ampandrandava sample with a short neutron dose exposure. The use of various magnifications with the SEM is responsible for the departures from linearity in the decrease of D_f and D_i with temperature (figure 6). This, however, does not affect either the isochron diagram (figure 7) of the age calculations (similar magnifications were used for the measurement of the D_f and D_i of a given apparent age).

ϕ, thermal neutron fluence; D_f and D_i, fossil and induced fission track densities; N_f and N_i, total number of fossil and induced tracks counted; t, apparent age.

**Calculated with $\lambda_f = 7{\cdot}03 \times 10^{-17}$ yrs^{-1} (see § 6). The errors on D_f and D_i were calculated from a poissonian statistics. The error on ϕ is taken as ±1 % (2σ) from statistical counting error on a cobalt foil monitor. The errors on t have been calculated from equation (5) with $r = 0{\cdot}8$.

Table 2. Plateau age-fission track dating of apatites: Analytical data+

Sample	T (°C)	Time (hours)	N	n	$D_f \pm 1\sigma$	N	n	$D_i \pm 1\sigma$	$t \pm 1\sigma$* (10^6 yrs)
1	2	3	4	5	6	7	8	9	10
					$10^6 cm^{-2}$			10^6 cm^{-2}	
2520	270	0·66	450	20	2·25 ± 0·13	874	20	4·37 ± 0·27	244 ± 10
(ITP)	,,	2	675	30	2·25 ± 0·17	1750	40	4·37 ± 0·18	243 ± 6
	,,	4	892	40	2·23 ± 0·11	1729	40	4·28 ± 0·15	247 ± 6
	,,	8	758	40	1·91 ± 0·074	1140	31	3·67 ± 0·13	246 ± 6
	,,	16	437	25	1·75 ± 0·077	712	21	3·39 ± 0·035	244 ± 8
	,,	32	665	40	1·67 ± 0·060	1294	40	3·23 ± 0·062	243 ± 6
	,,	64	612	40	1·53 ± 0·099	595	20	2·97 ± 0·019	244 ± 7
	,,	126	523	40	1·31 ± 0·062	1010	40	2·52 ± 0·012	245 ± 7
	,,	260	310	40	0·775 ± 0·035	603	40	1·51 ± 0·062	243 ± 9
	,,	504	121	54	0·22 ± 0·022	173	40	0·43 ± 0·035	241 ± 13
	,,	840	7	51	(0·014)	13	50	(0·026)	(249)
2520	Ambient	1	122	50	1·22 ± 0·13	228	48	2·38 ± 0·19	243 ± 16
(ICP)	285	,,	90	43	1·04 ± 0·11	189	48	1·96 ± 0·15	251 ± 16
	300	,,	82	53	0·773 ± 0·082	124	43	1·44 ± 0·13	254 ± 16
	310	,,	41	37	0·554 ± 0·12	74	35	1·06 ± 0·14	247 ± 35
	320	,,	49	52	0.432 ± 0·066	74	47	0·787 ± 0·091	259 ± 24
M34	Ambient	1	886	84	5·27 ± 0·22	1452	79	9·19 ± 0·36	271 ± 8
(ICP)	285	,,	644	79	4·07 ± 0·24	1236	91	6·79 ± 0·28	283 ± 11
	300	,,	515	68	3·78 ± 0·24	957	83	5·76 ± 0·30	309 ± 12
	310	,,	444	75	2·96 ± 0·16	849	90	4·72 ± 0·22	296 ± 10
	320	,,	368	70	2·62 ± 0·13	593	71	4·17 ± 0·26	296 ± 12

1	2	3	4	5	6	7	8	9	10
					10^5/cm²			10^5/cm²	
M44	Ambient	1	144	35	5·25 ± 0·40	137	20	8·74 ± 0·79	284 ± 16
(ICP)	285	,,	108	30	4·59 ± 0·49	172	30	7·31 ± 0·62	296 ± 19
	300	,,	122	40	3·89 ± 0·43	180	37	6·21 ± 0·48	296 ± 20
	310	,,	124	45	3·52 ± 0·34	146	34	5·48 ± 0·39	302 ± 18
	320	,,	96	40	3·06 ± 0·34	124	35	4·52 ± 0·52	318 ± 23
70242	Ambient	1	28	17	1·05 ± 0·15	75	24	1·99 ± 0·18	250 ± 24
(ICP)	285	,,	34	20	1·08 ± 0·15	67	25	1·71 ± 0·14	298 ± 27
	300	,,	28	20	0·893 ± 0·12	58	26	1·42 ± 0·12	297 ± 24
	310	,,	24	20	0·765 ± 0·11	40	20	1·27 ± 0·14	284 ± 24
	320	,,	29	30	0·616 ± 0·15	31	20	0·98 ± 0·14	294 ± 45
Nages	Ambient	1	111	43	0·79 ± 0·09	139	33	1·29 ± 0·11	197 ± 14
(ICP)	230	,,	129	50	0·79 ± 0·10	126	34	1·13 ± 0·10	223 ± 17
	240	,,	85	33	0·78 ± 0·10	109	33	1·01 ± 0·10	247 ± 19
	260	,,	99	45	0·67 ± 0·10	104	40	0·79 ± 0·07	272 ± 26
	270	,,	85	39	0·67 ± 0·05	89	35	0·78 ± 0·06	274 ± 13
	280	,,	68	33	0·63 ± 0·05	75	32	0·72 ± 0·06	286 ± 15
	290	,,	80	45	0·55 ± 0·06	83	40	0·64 ± 0·05	272 ± 18
	300	,,	49	31	0·48 ± 0·06	60	37	0·50 ± 0·05	310 ± 23
	310	,,	43	30	0·44 ± 0·05	47	30	0·45 ± 0·05	290 ± 21
Nages	280	20	114	41	0·85 ± 0·07	96	31	0·90 ± 0·07	286 ± 15
(ITP)	,,	60	65	45	0·44 ± 0·05	50	30	0·51 ± 0·06	275 ± 20
	,,	120	18	42	0·13 ± 0·03	21	41	0·15 ± 0·03	269 ± 38

+Analysts: V. K. Ceylan for sample 2520 ITP (isothermal plateau age); J. Carpena (Poupeau *et al* 1980b; Carpena 1980) for the Nages sample; D. Chaillou for other measurements (ICP = isochronal plateau ages).

*The apatites were dated with the population method (Naeser 1979); N is the number of tracks counted and n the number of crystals. The errors on D_f and D_i are taken as standard error of the mean. The neutron fluence measured with a cobalt foil, was $8{\cdot}07 \times 10^{15}$ n/cm² for the 4 first samples and $5{\cdot}43 \times 10^{15}$ n/cm² in the case of Nages, with a statistical error of ± 1% (2σ). Errors on t were calculated using equation 5 with $r = 0{\cdot}8$.

Table 3. Apparent and plateau ages of phlogopites and apatites ($\times 10^6$yrs)

Sample	'Ambient' temperature age+ ($t \pm 2\sigma$)	Plateau age+ N*	$t \pm 2\sigma$	
Phlogopites				
Ampandrandova	404 ± 28	7	401 ± 10	
Mahanela	575 ± 28	5	572 ± 14	
Monroe	293 ± 42	4	306 ± 11	
Apatites				
MOR 34	271 ± 16	5	287 ± 9	
MOR 44	284 ± 32	5	296 ± 17	
70242	250 ± 48	4	292 ± 27	
2520 (ICP)	243 ± 32	5	250 ± 34	245 ± 4
2520 (ITP)		10	244 ± 5	
Nages (ICP)	197 ± 28	6	283 ± 14	282 ± 12
Nages (ITP)	—	3	281 ± 22	

+The 'ambient' temperature age is the apparent age obtained without preannealing treatment (table 1). The plateau ages and their precision have been calculated from equation (11). In all cases except for sample 70242, the plateau ages were calculated from the apparent age measurements (see text).

*No. of plateau steps.

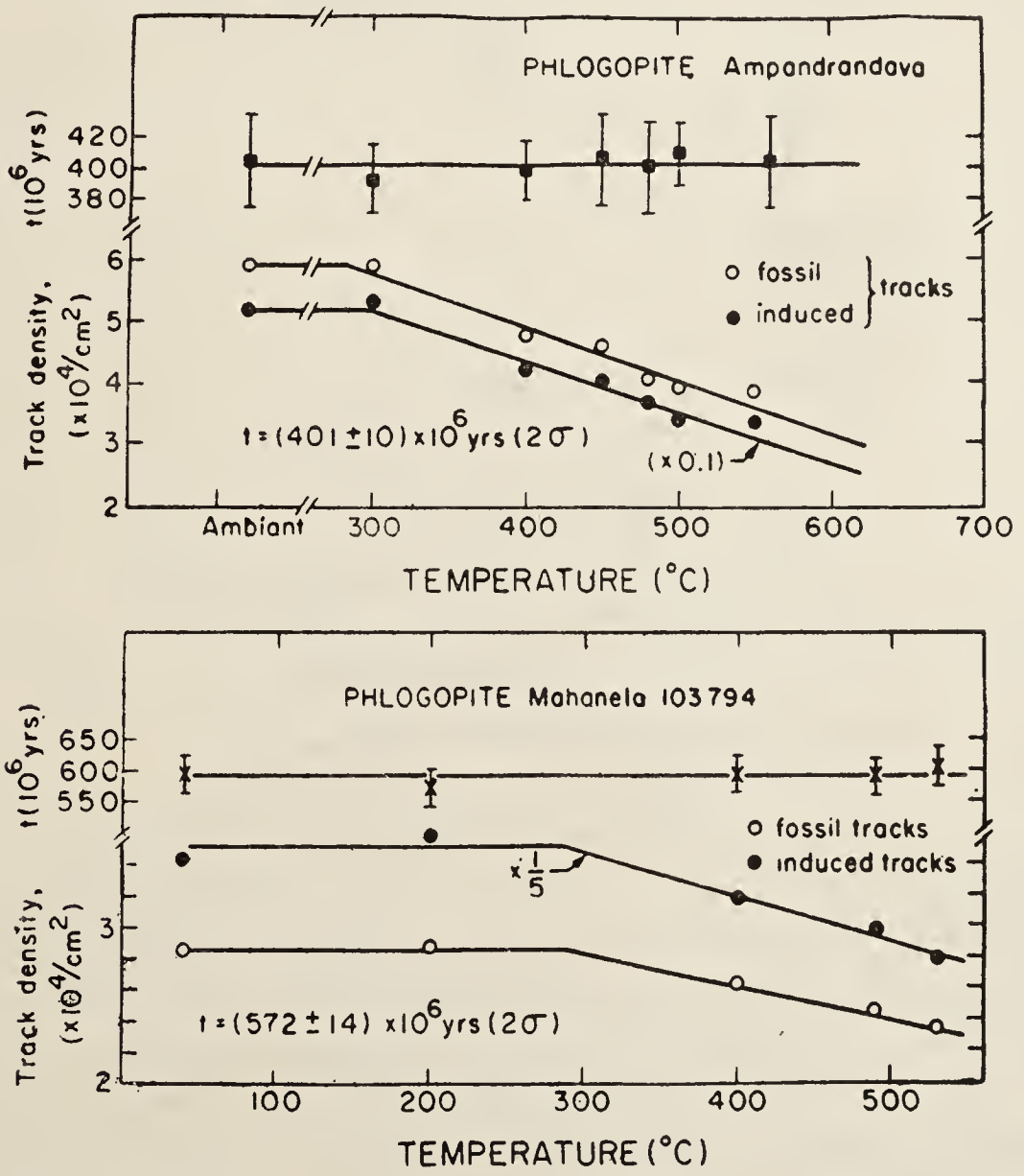

Figure 6. Isochronal plateau ages of the Ampandrandava (Malagasy) and Mahanela (Ceylon) phlogopites (see table 1).

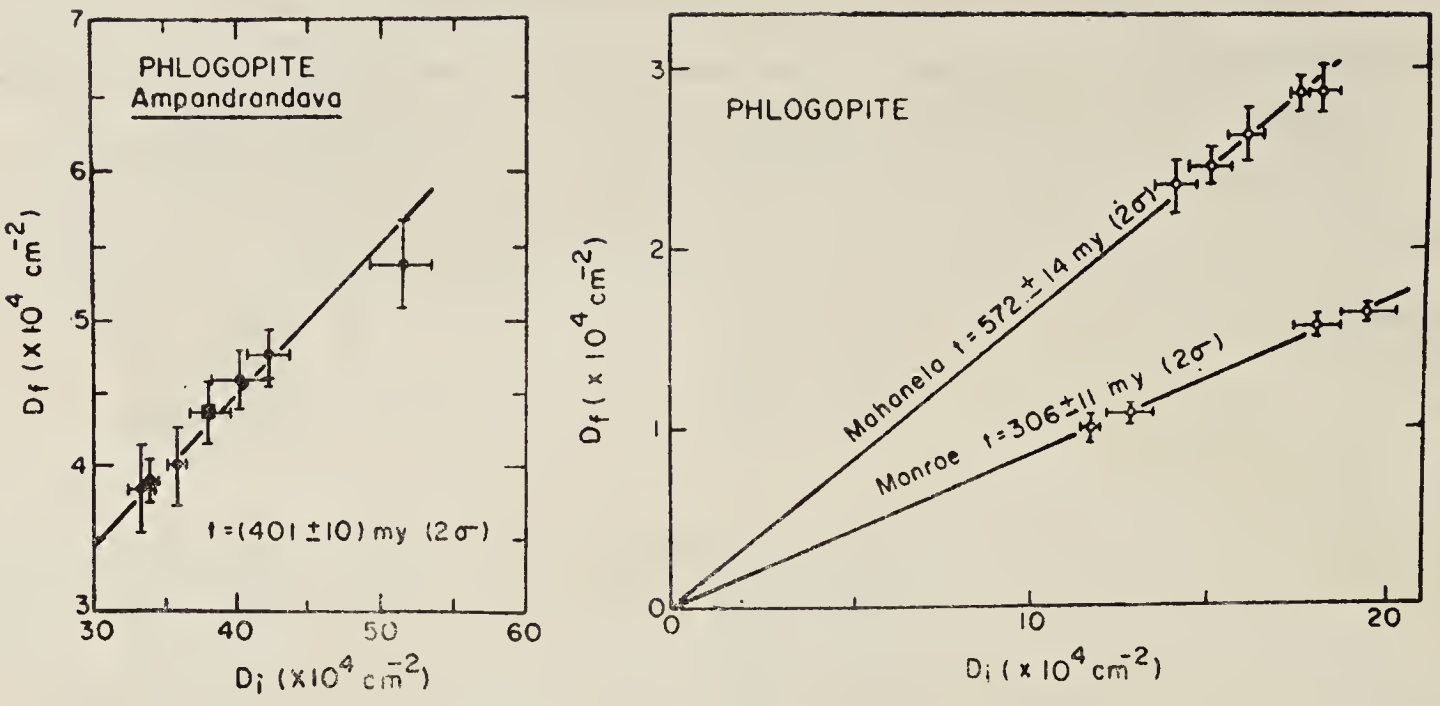

Figure 7. Isochrone representation of the phlogopite data from table 1. All track density measurements were made with a scanning electron microscope, except for one measurement of Ampandrandava sample (rectangle in figure); this last age was also determined with a neutron dose lower than for other measurements (table 1). The track densities have been normalized to a neutron fluence of $6{\cdot}09 \times 10^{15}$ n/cm^2.

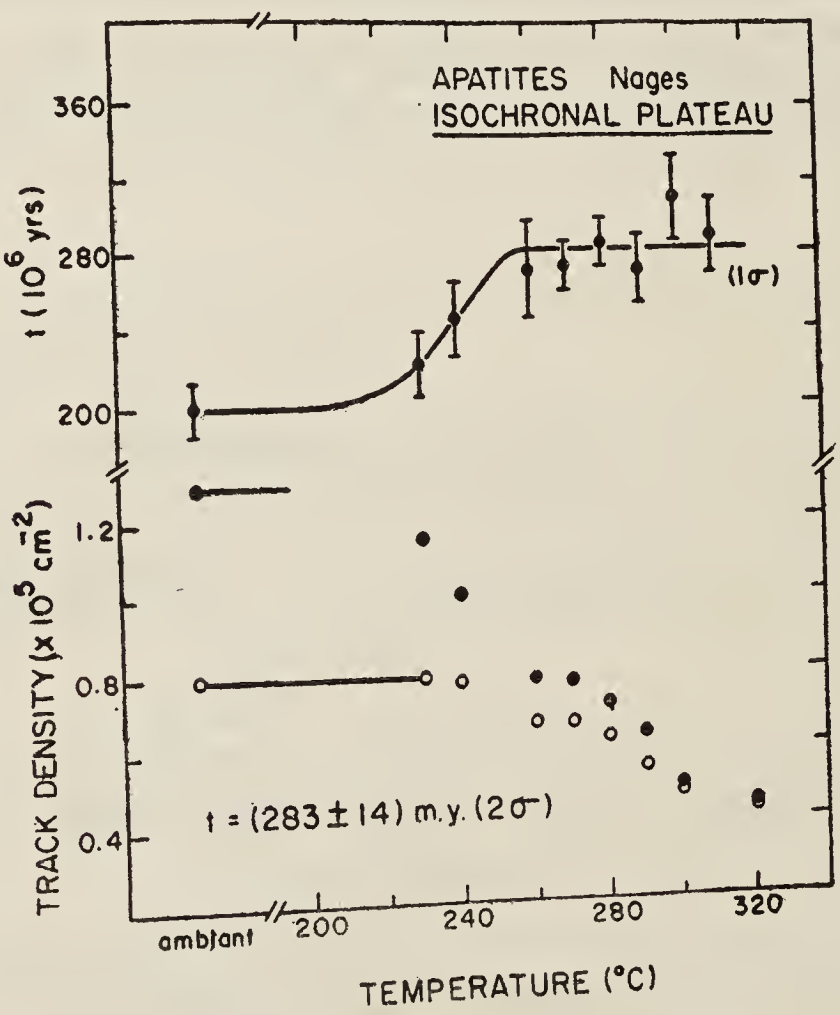

Figure 8. Isochronal plateau age of the Nages apatites.

(figure 9). Sample 2520 (figures 10 and 11) illustrates the effect of both the number of tracks counted and the number of apparent age determinations on the plateau age values. In this sample, the ICP and ITP data were obtained, respectively, by two different observers. Whereas the ages obtained by both of them are concordant, it appears that an effort on improving counting statistics (as in the ITP age determination of this sample) results in a much higher final precision. In particular, the effect of choosing a grid unit for countings, allowing a larger number of tracks per crystal to be counted, is to reduce considerably the scatter among individual determinations of D_f and D_i (figure 12).

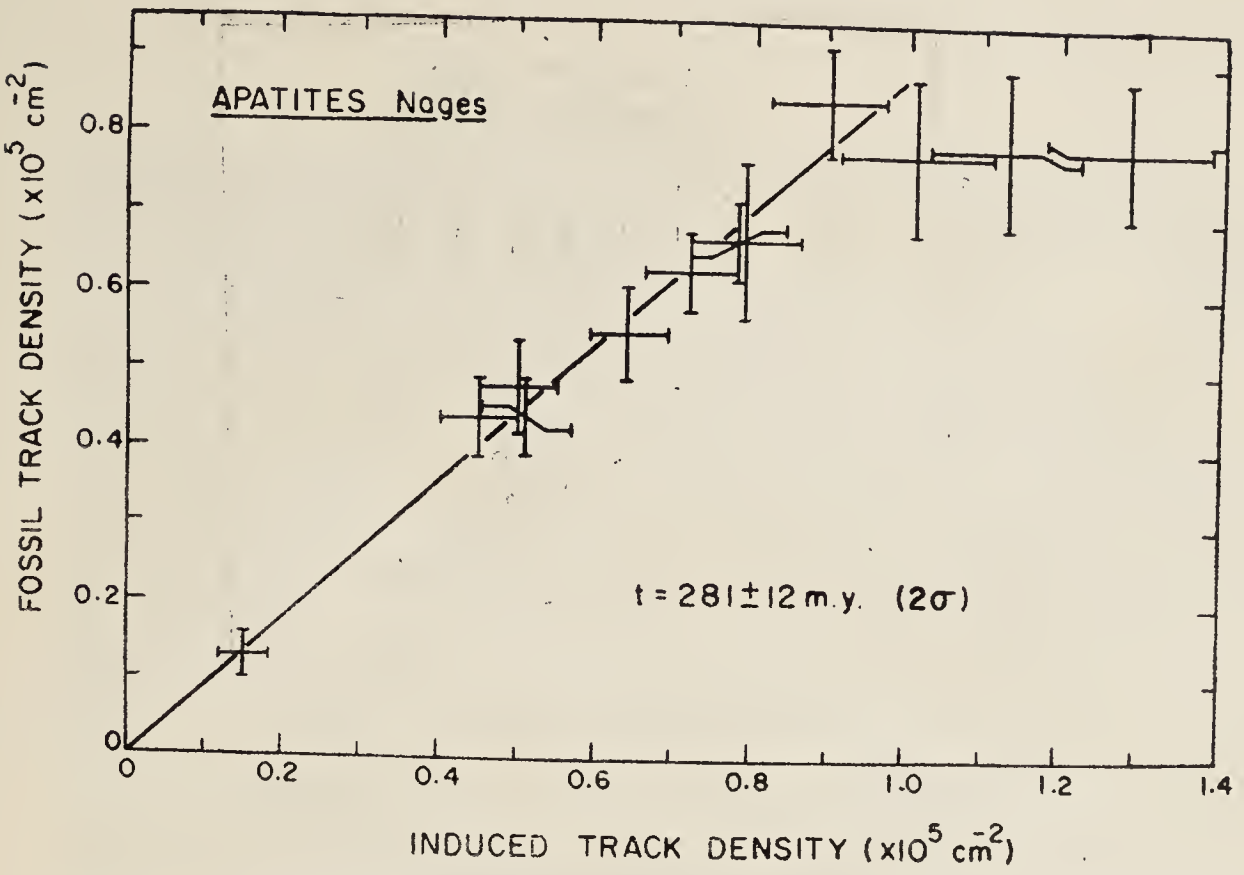

Figure 9. Isochrone representation of the ICP and ITP data for the Nages apatites.

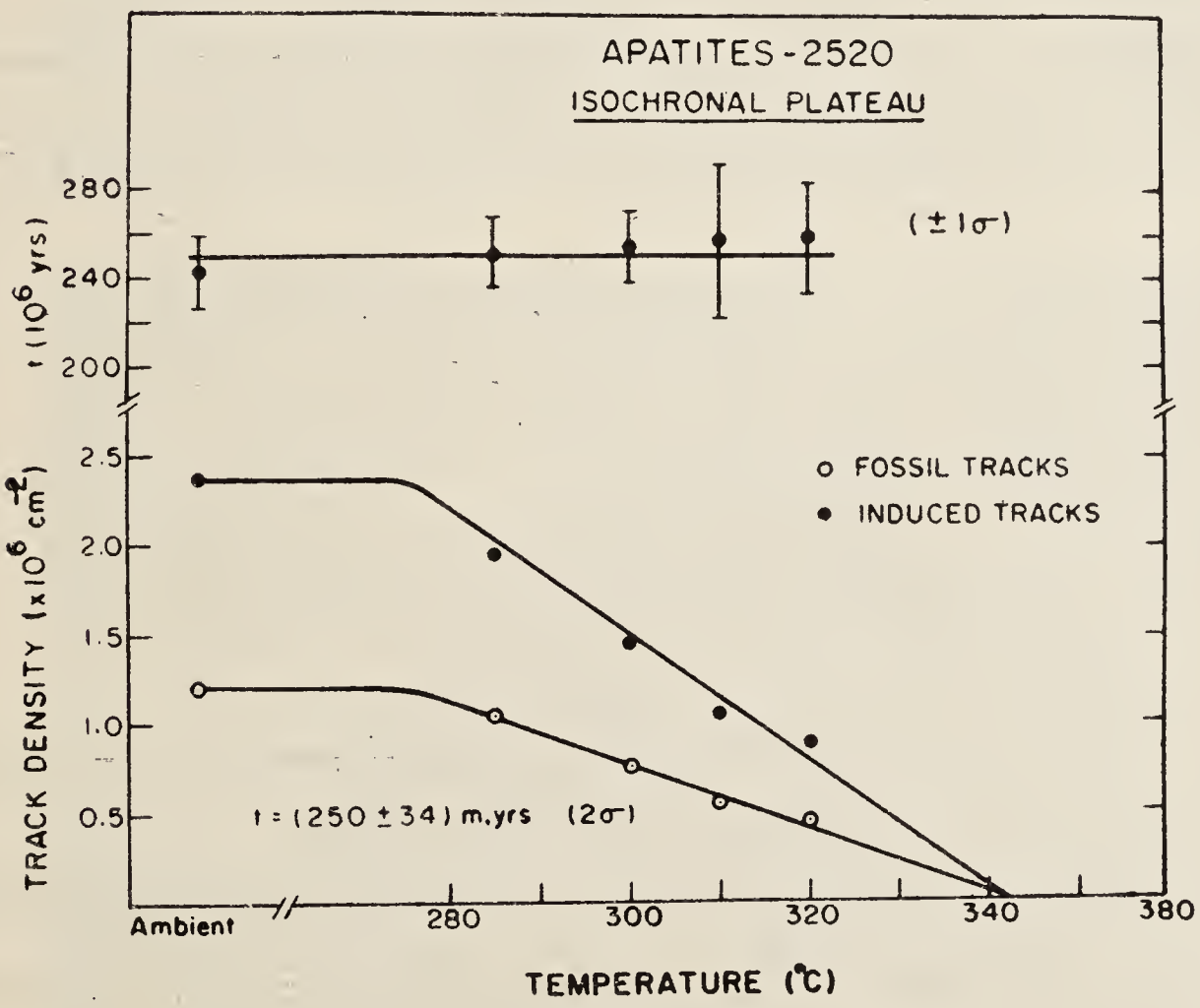

Figure 10. Isochronal plateau age of apatites 2520.

Finally, as in the case of micas, it appears from tables 2 and 3 that a precision on apparent ages of the order of ± 5% to ± 10% (2σ) results on a plateau value determined to within ± 5% (2σ). It might be added here that the plateau age values of these apatites are in excellent agreement with the values expected from geological considerations (Carpena *et al* 1980; Poupeau 1981b).

The results in tables 1 and 2 having been obtained by the internal method of dating of the subtype 1A of figure 1 for micas and 1B for apatites, the correlation coefficient r of equation (3) could not be calculated from the analytical data (McGee and Johnson

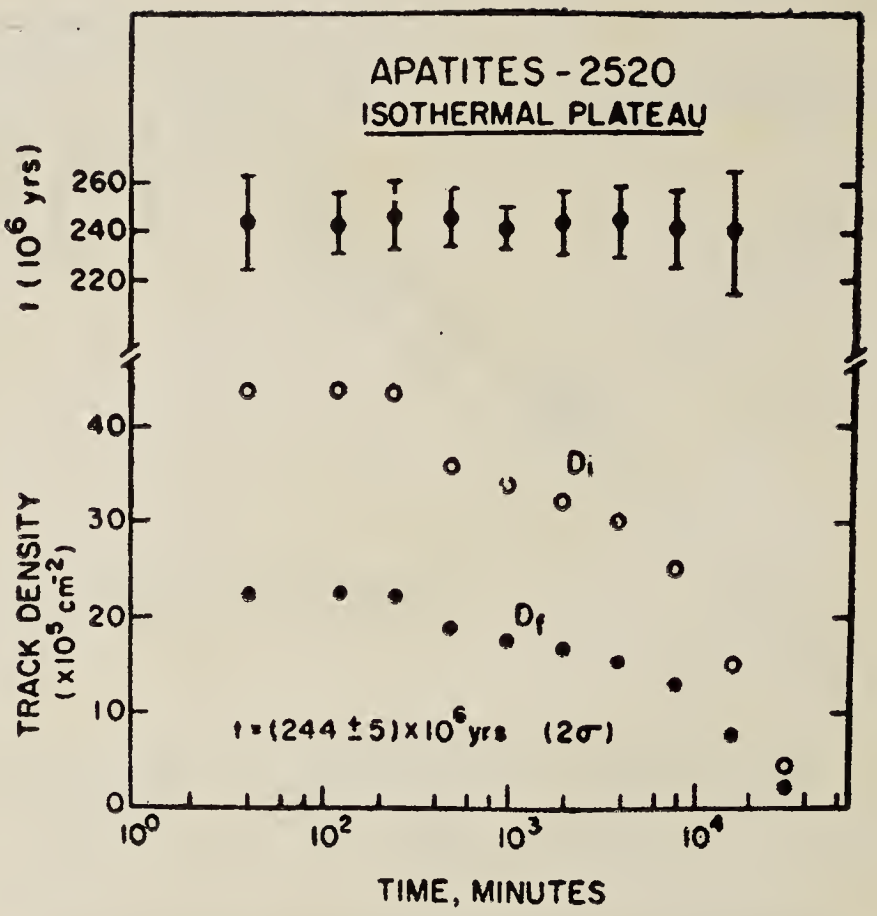

Figure 11. Isothermal plateau age of apatites 2520.

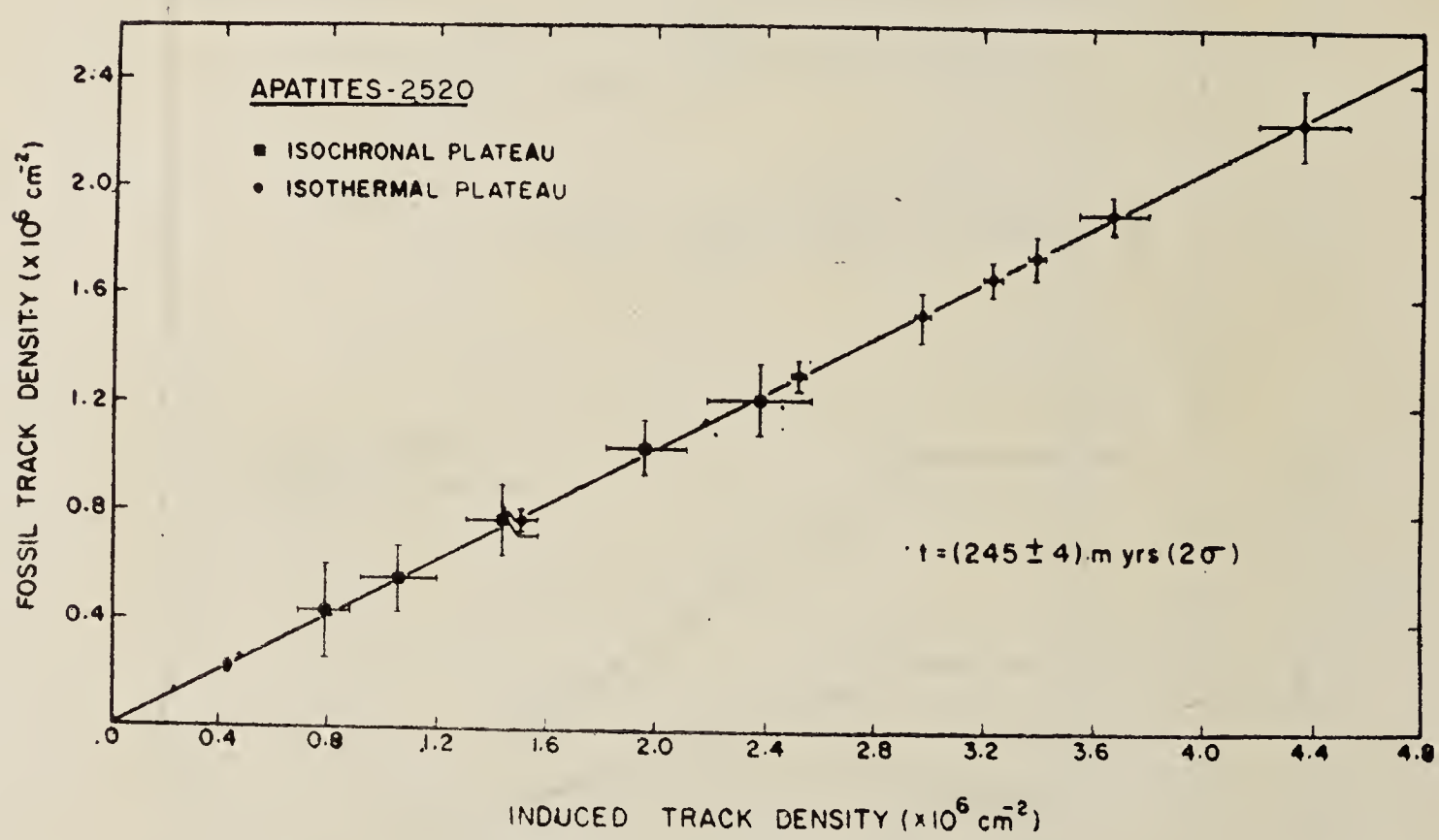

Figure 12. Isochrone representation of the ICP and ITP data for the 2520 apatites.

1979). As suggested by McGee and Johnson we have adopted in this case the ' conservative value ' of $r = 0{\cdot}8$. A comparison (tables 1 and 2) between the errors calculated on individual ages and the dispersion of these ages for a given sample demonstrates a posteriori that an 0·8 value for the correlation coefficient between D_f and D_l gives, in effect, a conservative estimate of the precision on t and, therefore, on the plateau ages themselves.

5.2*c Remarks on the ITP method.* Although equivalent from the point of view of plateau age precision, as seen above for apatites, the ICP and ITP methods cannot be indifferently applied to any mineral phase. For instance, thermal treatments at even moderate temperatures can modify the physical structure of certain mineral phases

Figure 13. Effect of fission track etching (HF 40% 20°C, 15 seconds) on hydrated glass shards from the Middle Park tephra (Colorado). (**a**) Sample heated for 1 h at 220°C before etching, (**b**) unheated sample. Whereas in (b) the etching treatment does not affect the shards, all of those in (a) exhibit large etching figures. Scale bar, 100 microns.

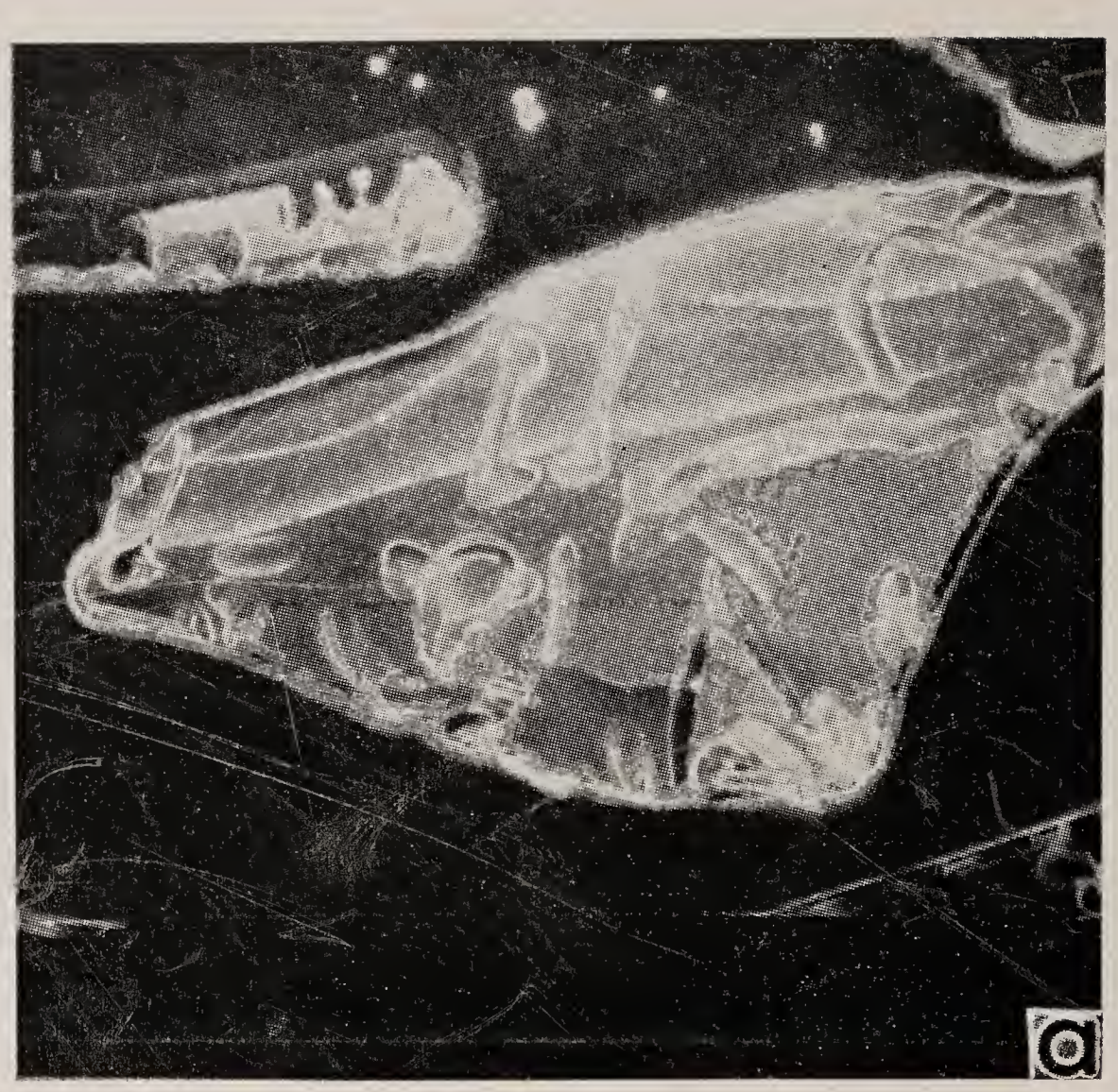

Figure 14. **a** and **b**

Figure 14. **c** and **d**

Figure 14. Enlarged views of a few Middle Park tephra glass shards treated as in (a) from figure 13. Fission tracks can still be counted on some parts of shards like in (a), (b), whereas it has become impossible due to the large extent of etched corrosion figures, as in (c), (d). Scale bar, 100 microns (Observation, as in figure 13 in scanning electron microscopy).

as in the case of metamict minerals (*e.g.* zircon) or volcanic glasses. For those phases, an ITP treatment is to be preferred, if not the only one possible. In order to illustrate these different properties of the ITP and ICP methods, we give below some data obtained on the FT dating of tephra glass shards.

Volcanic ash projections, or tephras, are very useful stratigraphic markers in sedimentary series. For instance, our knowledge of the timing of early hominoid evolution in the eastern African rift is basically obtained by the dating of tephra materials. The dating of these materials by the K-Ar or FT methods, especially for recent projections, is often extremely difficult (see Hay 1980) because of either (i) problems in K-Ar dating, due to potassium leaching or contamination by crustal materials; or (ii) rarity of mineral phases convenient for FT dating, as zircons. Recently Naeser *et al* (1980) attempted FT dating of the main component of the tephras themselves, *i.e.*, glass shards. The conclusion of these authors was that, although unhydrated glass shard dating was relevant with the plateau method, no reliable age could be obtained with altered (hydrated) glass shards due to some disruption upon track etching of these particles when submitted to thermal treatments above $\sim 200°C$*.

Naeser and colleagues had been using an ICP method. Naeser kindly provided us with some of his samples on which we have been working with the ITP and ICP modes. We (Poupeau and Vincent, unpublished) effectively found that hydrated glass shards heated above $\sim 200°C$ reacted badly to track etching, as can be seen in figure 13: large channels and gulfs opened by etching are present in practically all shards from a heated (1 h at 220°C) aliquot, whereas these are practically absent on the untreated sample. In figure 14, typical etch figures are displayed at higher magnification showing the details of shard behaviours. Samples from other localities may behave even worse.

In order to date the Middle Park shards of figures 13 and 14, the fossil tracks were not annealed. Our results, as well as those of Naeser *et al* (1979) are reported in table 4. The relatively limited damage caused by the corrosion figures of figures 13 and 14 still allowed, although painfully, to use the ICP method, for which we found—as for the ' ambient temperature ' age—results in good agreement with those of the

Table 4. Apparent and plateau ages of the Middle Park tephra (Colorado) glass shards ($\times 10^6$ yrs)

'Ambient' temperature age ($\pm 2\sigma$)	'High' temperature age ($\pm 2\sigma$)	Source	Other ages†	Source
9·4 ± 1·4	14·5 ± 4·2	(a)	13·5 ± 2·2	(a)
10·0 ± 1·7	17·1 ± 2·05	(b)	13·3 ± 1·2	(a)
	15·4 ± 1·0	(c)		

†FT ages for zircons.

(a) Naeser *et al* 1980. The 'high' temperature age has been measured on a sample heated for 1 hour at 290°C.

(b) and (c), Poupeau and Vincent (unpub. data). Age (b) was obtained on a sample heated for 1 hour at 220°C; age (c) was calculated from three individual ages determined on samples heated between 100°C and 170°C for times up to 20 days. Errors on D_f and D_i calculated from fission track statistics.

*The disruption upon track etching of glassy shards was interpreted as a consequence of dehydration during thermal treatment.

Denver group. However, we found that working in the ITP mode at 170°C allowed us to work comfortably without dealing with etch-damaged glass shards. Thus, we believe from these preliminary results that the ITP mode for the dating of tephra glass shards will ease in the future the use of this material for FT dating.

6. Accuracy and standardization in FT dating

The accuracy in FT dating is mainly controlled by the systematic errors on the ^{238}U spontaneous fission decay constant λ_f and the neutron dosimetry. The other parameters in equation (1): λ_t, I and σ^{235} are known with an accuracy of better than 2%.

6.1 *The λ_f problem and thermal neutron dosimetry*

Since the discovery of the spontaneous fission of ^{238}U about 40 years ago, λ_f has been determined more than 40 times (see compilation by Bigazzi 1981) ranging from $0{\cdot}7 \times 10^{-17}$ yrs^{-1} to 28×10^{-17}yrs^{-1}. Most values, however, are grouped in the interval $6{\cdot}6 \times 10^{-17}$ yrs^{-1} to $11{\cdot}55 \times 10^{-17}$ yrs^{-1}, with two major peaks at 7×10^{-17} yrs^{-1} and $8{\cdot}5 \times 10^{-17}$ yrs^{-1}, and a lesser one toward $11{\cdot}7 \times 10^{-17}$ yrs^{-1} (figure 15). Values of λ_f determined by direct determination counters and radio-chemical or mass spectrometric analysis are evenly distributed in this interval. However, the values obtained by geological calibrations are strongly peaked around 7×10^{-17} yrs^{-1} and $8{\cdot}5 \times 10^{-17}$ yrs^{-1}, as do the determinations of λ_f with nuclear emulsions or solid state track detectors when a thermal neutron irradiation in a nuclear reactor is performed. There is, therefore, some suggestion that neutron dosimetry might introduce a bias in the geological calibration of λ_f.

The thermal neutron dosimetry in FT dating is usually carried out either by the means of fission track counting in uranium-bearing glass standards, calibrated against

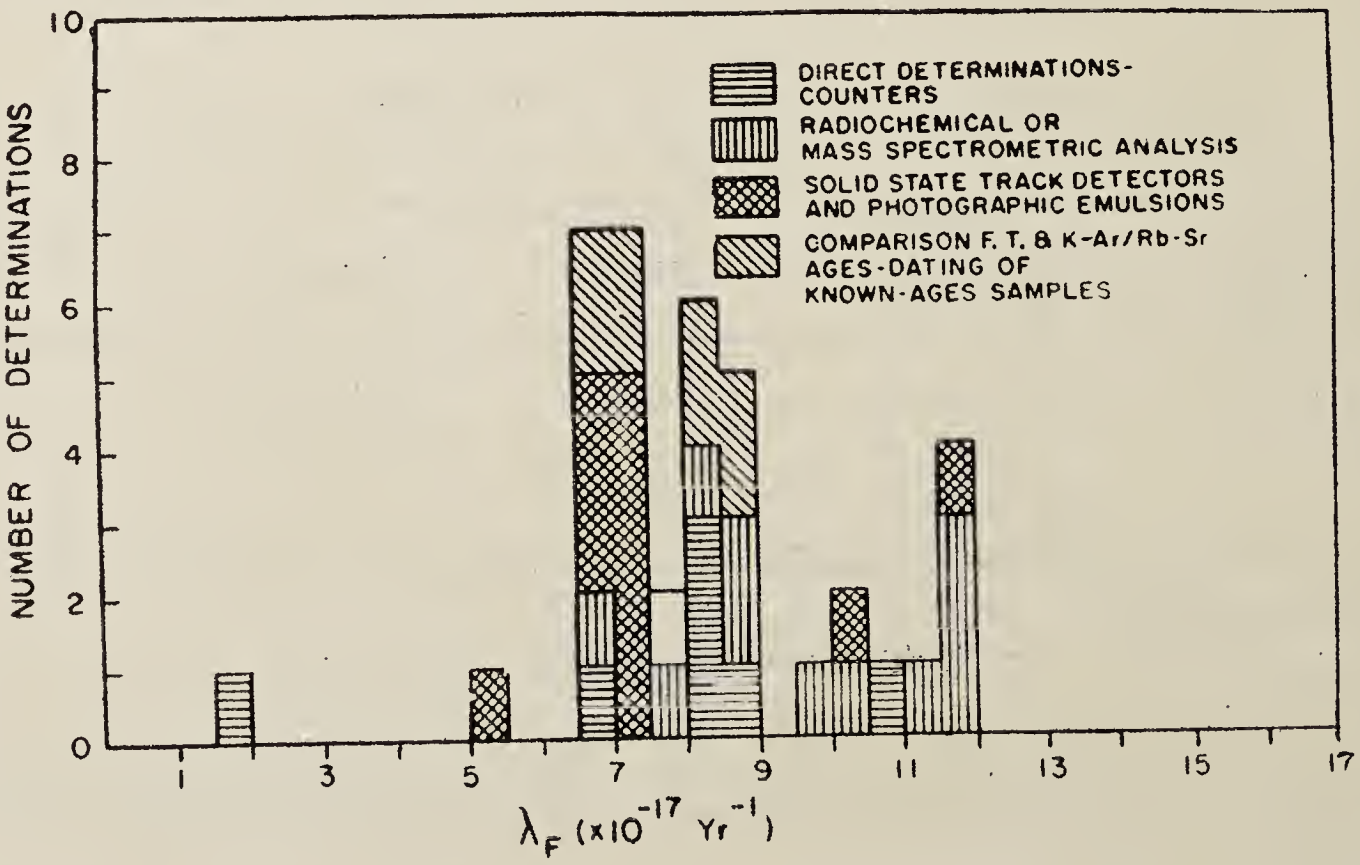

Figure 15. Histogram showing the distribution of λ_f (^{238}U spontaneous fission decay constant) as determined since 1950. A few earlier values in the range (22-28) $\times 10^{-17}$ yrs $^{1-}$ have not been reported (courtsey, Bigazzi, 1981).

metal foil monitors, or directly by measuring the activity induced in the metal foils. In the latter case, the thermal neutron flux ϕ_{th} is obtained from the total induced activity A_{tot} as:

$$\phi_{th} = \frac{A_{th}}{N\sigma_m}[1 - \exp(-\lambda_m t)]^{-1}, \tag{11}$$

where $A_{th} = A_{tot}\ (1-1/R_{cd})$; ϕ_{th} is the thermal neutron fluence (n.cm^{-2}); A_{th}, the thermal activity; N, the number of target atoms in the metal foil; σ_m and λ_m are, respectively, the thermal neutron capture cross-section for the target nuclide (cm^{-2}) and the decay constant of the daughter nuclide; t, the duration of irradiation; and R_{cd} the cadmium ratio.

Therefore, given a well-dated geological sample (see below), λ_f can be determined from* :

$$\lambda_f = \frac{D_f}{D_t} \cdot \frac{\sigma I \phi_{th}}{t}, \tag{12}$$

where t is the age of the sample.

However, disappointing results were obtained following this approach for determination of λ_f. For instance, in two carefully designed experiments, Hurford and Gleadow (1977) and Wagner *et al* (1975) attempted to derive λ_f from equation (12) using, respectively, minerals from volcanic rocks dated by K-Ar and man-made glasses whose year of manufacture was known. From their measurements, the two groups were led to recommend for fission track work two different values of λ_f, differing from each other by as much as 20%. Such a difference could not be explained either in terms of the uncertainty in the real ages of the samples selected or by partial track annealing of the fossil tracks (see, in particular, the further work of Naeser *et al* 1981, on some of the material studied by Hurford and Gleadow). The two groups had used different methods of neutron dosimetry; and, as suggested by Hurford and Gleadow (1977) the differences in evaluation of λ_f might be attributed to some ' unexplained systematic discrepancies ' in the neutron dose measurements.

It may be stressed here how difficult it is to evaluate the proper thermal neutron fluence to the sample using metal foils. The accuracy of this neutron fluence depends not only on the parameters σ_m and λ_m (equation 11), but also on the particular shape of the neutron energy distribution at the place and time of irradiation in a given reactor, as the excitation functions of ^{235}U for neutron-induced fission and the monitor metal foil for neutron capture reactions have different neutron energy dependance.†

A large majority of FT-dating laboratories use glass standards for thermal neutron dosimetry. In this case, the thermal neutron fluence ϕ_{th} is deduced from the track

*This supposes also that the sample be irradiated in the reactor at a place where the ratio of thermal to epithermal neutrons is larger than 100, so that the contribution of ^{235}U−induced fission from epithermal neutrons is $< 1\%$ to that of thermal neutrons.

†Other factors include neutron flux spatial inhomogeneities; sample neutron self absorption, itself a function of chemistry and geometry of samples, all parameters not amenable easily to quantification.

density D_ϕ in the glass*, or better, in an external detector fixed against it during irradiation, following the relationship

$$\phi_{th} = K\, D_\phi. \tag{13}$$

In this case, any FT age is affected by an additional systematic error attached to the factor K (this factor being determined through a joint irradiation of a metal monitor foil allowing the determination of ϕ_{th} and the glass standard†).

Clearly, therefore, the situation about thermal neutron dosimetry is presently far from satisfactory, and improvements are urgently needed. Some suggestions in this direction are reported in § 6.3. However, the examination of the present status of an interlaboratory comparison programme initiated by Naeser suggests that many FT laboratories have, through internal calbiration, reached the points where their data are geologically reliable.

6.2 *The Fish Canyon Tuff interlaboratory programme*

The Fish Canyon Tuff is a well-dated volcanic formation from Colorado. Its K-Ar age, as determined from sanidine, biotite, hornblende, and plagioclase (*i.e.* from mineral phases whose potassium content may differ by as much as more than one order of magnitude) is $27{\cdot}9 \pm 0{\cdot}7$ m. y. Naeser separated apatite and zircon crystals from an initial sample of 280 kg and distributed concentrates of these minerals to more than 50 laboratories, of which 19 reported data for apatites and 9 for zircons.

The main results of this programme (Naeser *et al* 1981) were to show that all laboratories using a λ_f value near to 7×10^{-17} yrs^{-1} found apatite and zircon FT ages concordant with the K-Ar value, respectively, at $28{\cdot}5 \pm 0{\cdot}4$ m. y. ($\pm$ 1 standard error of the mean) and $23{\cdot}7 \pm 1{\cdot}0$ m. y. On the other hand, the few laboratories using a λ_f value $\sim 20\%$ higher ($8{\cdot}4 \times 10^{-17}$ yrs^{-1}) found discordant ages of $24{\cdot}7 \pm 1{\cdot}0$ m. y. $\sim 20\%$ lower than the K-Ar ages, a difference not explainable in terms of fossil track annealing (Naeser *et al* 1981). This report unfortunately does not precisely describe the methods for neutron dosimetry used by each laboratory.

In May 1981, a new extensive sampling of the Fish Canyon Tuff has been made (Naeser, personal communication), and separated apatites and zircons will be made available through the National Bureau of Standards (Washington, D. C.). It would be worthwhile that, in this further step of interlaboratory comparisons on the Fish Canyon Tuff, data concerning the neutron dosimetry are provided by the participating groups and made available to the whole community.

6.3 *Toward a standardization in FT dating?*

From the preceding discussion, it results that neither the spontaneous fission decay constant λ_f nor the thermal neutron dosimetry are accurately known or measured. However, as shown in many publications, and especially on the systematic study of

*The induced fission tracks in the glass itself may be subject to partial annealing during irradiation, especially for long duration irradiations.

†Moreover, there are indications that the factor K itself may vary slightly with the reactor operating conditions (Hurford and Gleadow 1980; Carpenter, pers. comm. 1981).

the Fish Canyon Tuff, significant FT ages can be obtained. This is due to the fact that in practice, according to its own method of neutron dosimetry, each laboratory defines an operational 'λ_f' value allowing to find the adequate 'age' for well-dated geological standards.* Accordingly, the ultimate accuracy of any FT, age is limited by the accuracy on the age of the geological standard rock, *i.e.* about 3% with the Fish Canyon Tuff standard. In order to facilitate the problem of age intercomparisons between different laboratories, several standards were proposed for neutron dosimetry (Fleischer *et al* 1975). The most widely used at present are the NBS glass standards series set up by Carpenter and Reimer (1974). The laboratories using these glasses, as can be judged from the literature and personal contacts, tend to favour a λ_f value around 7×10^{-17} yrs^{-1}; and the value of $7{\cdot}03 \times 10^{-17}$ yrs^{-1} given by Roberts *et al* (1968) is currently being adopted by an increasing number of groups (Naeser *et al* 1979; Hurford and Gleadow 1977; Poupeau *et al* 1978a; Virk and Koul 1977; Parshad *et al* 1979) as replacing the widely used older values of $6{\cdot}85 \times 10^{-17}$ yrs^{-1} and $6{\cdot}9 \times 10^{-17}$ yrs^{-1}, determined earlier by Fleischer and Price (1964).

Another value, of $8{\cdot}46 \times 10^{-17}$ yrs^{-1} (Galliker *et al* 1970) has been adopted by a few groups (*e.g.* Wagner *et al* 1976). It is based on λ_f determinations from U-rich man-made glasses of known ages (Wagner *et al* 1975; Thiel and Herr 1976) as well as on geological calibrations with K-Ar dated impact and volcanic glasses (Storzer 1970b; Storzer and Popeau 1973b).

Recently, Carpenter (1980) showed that, provided uranium isotopic composition and content in glass dosimeters are well known (which is the case of the NBS standards), the measure of the neutron fluence can be avoided. Still, an operational λ_f value remains to be determined following the above lines.

The only way to eliminate the problems linked to λ_f and ϕ would be (as in ^{40}Ar-^{39}Ar dating) to irradiate with each sample, x, to date, a geological sample of known age t_{st}. The age equation then reduces to (Hurford and Green, 1980)

$$t_x = \frac{1}{\lambda_D} \ln \left\{ 1 + \lambda_D \, t_{st} \frac{\left(\frac{D_F}{D_l}\right)_x}{\left(\frac{D_F}{D_l}\right)_{st}} \right\}, \tag{14}$$

for which the percent error on t_x would be given by a modified form of equation (5):

$$E = C \left\{ E_{fx}^2 + E_{ix}^2 + E_{fst}^2 + E_{ist}^2 - 2r \left(E_{fx} \, E_{ix} + E_{fst} \, E_{ist} \right) \right\}^{1/2}. \tag{15}$$

The advantage of the two latter procedures would be that they avoid any systematic errors and eventual fluctuations in the factor K of equation (13) without losing the precision of the dated phase.

*This assumes that both the FT method and the reference isotopic method date the *same* event. In recent volcanic rocks dated by K-Ar, this event is reasonably assumed to date the time of extrusion.

7. Meaning of FT ages

An FT age dates the time since which the tracks are recorded in a mineral (Price and Walker 1963). Laboratory experiments have shown that even moderate temperature increases are able to reduce the etching efficiency factor η to zero: one hour of heating between 50°C and 700°C (according to the mineral considered) is sufficient to completely erase fission tracks (Fleischer *et al* 1975). Extrapolation of laboratory thermal track annealing data (Arrhenius curves) have shown that in geological formations, fission tracks should not be recorded in minerals at temperatures above ~300°C* (Fleischer *et al* 1975; Wagner 1979). As a consequence, FT ages can be interpreted as *formation ages* only for rocks with a very rapid cooling history**: volcanic and hypovolcanic rocks and eventually shallow intrusives. Thus, in most of the cases, FT ages should be considered as *cooling ages*, *i.e.* as dating the time since which the mineral cooled below a threshold temperature (temperature of track retention, or ' closing temperature ', Dodson 1979). However, the interpretation of FT ages as cooling ages is also often complicated by the fact that, for a certain temperature range below the temperature T_0 at which fossil tracks start to be recorded (and, therefore, for a certain amount of time in the cooling history), the fission tracks are only partially recorded. This problem, which has been a source of confusion for years, deserves further comment.

7.1 *FT ages as cooling ages*

In order to discuss the meaning of FT ages as cooling ages, we have represented in figure 16 the evolution with time of the etchable track density in one mineral phase from a rock with differing cooling histories.

For a rock with a very rapid cooling (*e.g.* volcanic rocks) even the first tracks formed below the threshold temperature T_0 are fully recorded and have the same etch-

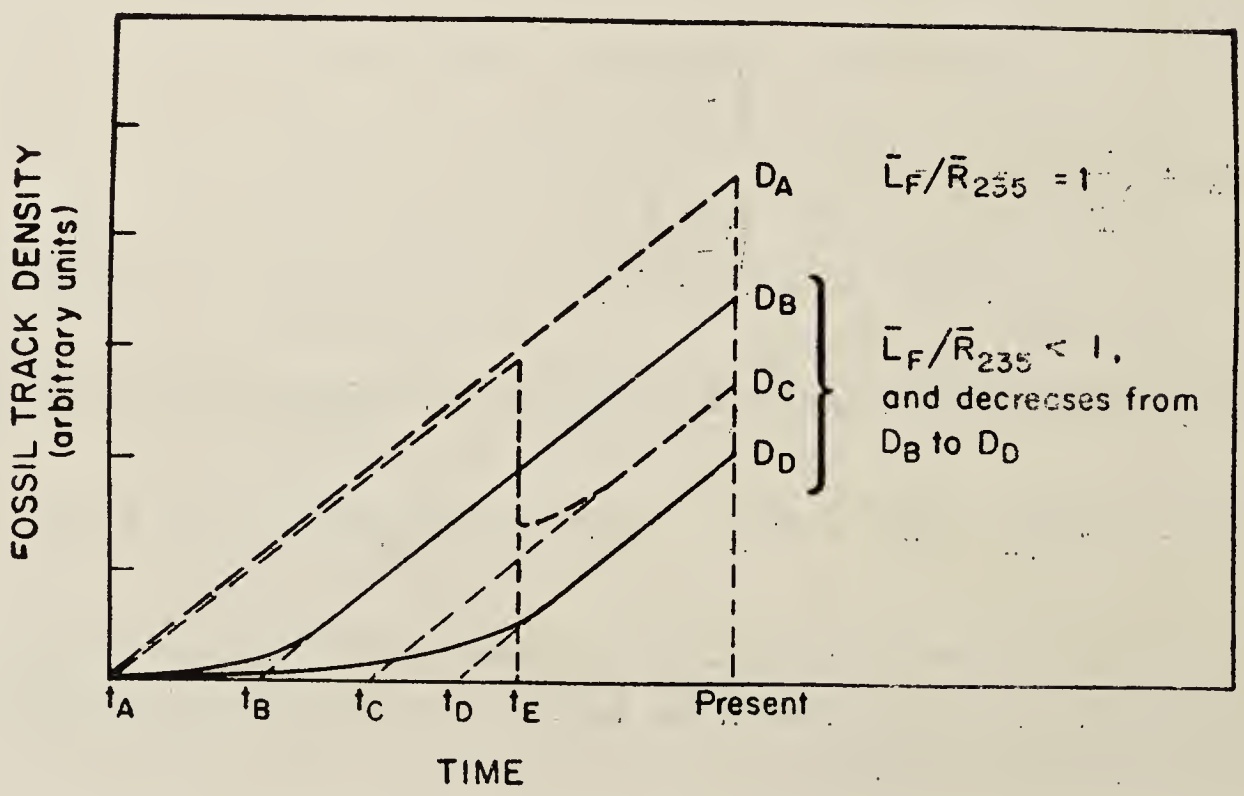

Figure 16. Evolution of the etchable fossil fission track density with time in a geological sample with different cooling histories (see text).

*Quartz is a possible exception.

**As far as they have not been further reheated.

ing efficiency as the recently formed tracks. In this case (if the time t_A since which the rock cooled below T_0 is $< 10^8$ yrs), D_f increases linearly with time (Price and Walker 1963) to reach the present day value of D_A (figure 16).

For rocks whose cooling rates below T_0 were ' slow,' the first tracks formed were only partially recorded and have an etching efficiency lower than the most recently formed track. This is reflected in figure 16 by the progressing increase of D_f with time in the initial build-up of the etchable track density before reaching linearity. Depending on the cooling rate, the apparent ages measured from the etchable fossil track density can be considerably lower than the time of the beginning of track registration. For instance, the apparent fission track age for a sample having followed the $t_A - D_B$ path will be calculated at t_B; and with a still lower cooling rate, along $t_B - D_D$, the apparent age would even be much less (t_D). Obviously the times t_A, t_B and t_D refer to different temperature histories.

Using Arrhenius plots for fission-track thermal annealing from the literature, Haack (1977) calculated the ' effective closing temperatures ' corresponding to ages like t_B and t_D, assuming different cooling rates. He showed that the closing temperature varies slowly with the cooling rate. For instance, in apatites, the calculated effective closing temperature changes from 95°C to ~ 70°C for constant cooling rates between 10°C/m.y. and 0·1°C/m.y. Similar results were reported by Dodson (1979).

However, if only the apparent ages are available, these results are of limited use to interpret fission track data. In effect, the cooling rate not only may have varied with time, but may also present discontinuities due to thermal pulses as in the path $t_A - D_C$ of figure 16, where a thermal event at time t_E may result in a meaningless apparent age, t_C.

It is these uncertainties in the meaning of any apparent age which led several authors to try to get model ages taking into account the partial geological track fading effects. The basic assumption of *all* model ages (' track-size ' corrected ages or plateau ages) is that partial track fading affects only the *etchable* track density, but not the volumic (number per volume unit) density of recorded events. In other words, whatever the degree of partial fading in a sample, *i.e.* whatever may be the present-day etchable fossil track density between D_A and less than D_D in figure 16, it should be possible to date with model-ages the time t_A since which fossil tracks started to be recorded. Model ages, therefore, would refer to the time of beginning of track retention.

The track retention temperatures can be obtained from extrapolated laboratory annealing data (Arrhenius plots). One can, however, question if the extrapolation of annealing curves obtained from short duration laboratory experiments to times longer than 10^6 yrs is valid. Recent geological calibrations (Naeser 1979; Naeser *et al* 1980; Gleadow and Duddy 1980) tend to lend some support in favour of this hypothesis. Taking advantage of favourable geological situations and samplings (f.i., geothermal drill holes), these authors were able to obtain a geological control of isothermal heating effects on fission track stability in apatites. For annealing times extending from ~ 10^5 yrs to 10^8 yrs (figure 17), Naeser *et al* (1980) demonstrated that (i) the 50% geological annealing points for apatites, plot on the laboratory extrapolated curve; and (ii) the 100% and 0% annealing points plot, respectively, on 75% and 25% laboratory curves. In other terms, the range

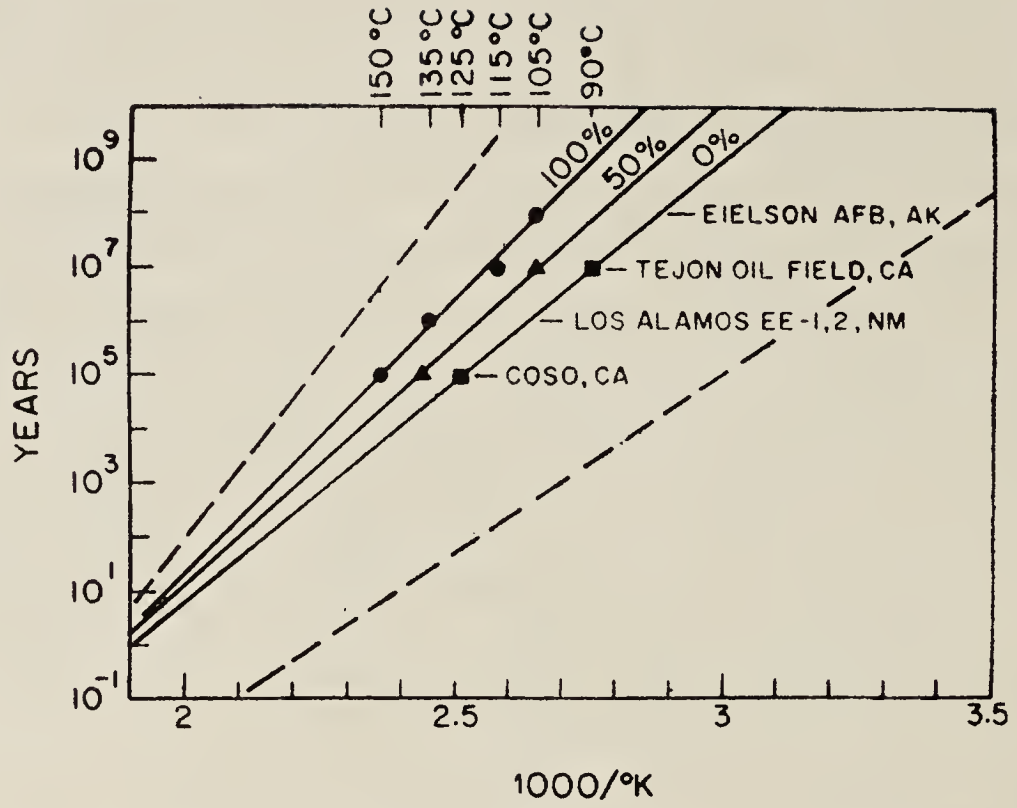

Figure 17. Arrhenius plots for thə thrmal slability of tracks in apatites. Full lines, 0%, 50% and 100% track annealing curves as geologically calibrated from the fossil track record in four different apatite samples. Dotted lines, extrapolated laboratory Arrhenius annealing curves for 0% and 100% annealing. The 50% laboratory annealing curve coincides with the 50% geological calibration curve (courtesy, Naeser 1981).

of temperatures in which partial track retention would occur appears to be smaller than expected. These results are confirmed by those of Gleadow and Duddy (1980).

From figure 17, it can be deduced from the 100% annealing plot that, in rapidly cooling basement rocks, the threshold temperature for apatites is of the order of 135°C (corresponding to 10^6 yrs isothermal annealing). For a rock with a model age of 10^8 yrs, whatever its further cooling history, a direct reading of the 100% annealing curve indicates its closing temperature must be in the range 105-135°C; the uncertainty in this range increases with increasing model age.

At present, apatites are the only mineral phase for which geological calibration of the closing temperature exists. Preliminary data exist for other phases as sphene and zircons, but they are yet too few to allow valuable comparisons with laboratory annealing data.

7.2 *FT ages and evaluation of uplift rates*

The concept of cooling age is by no means new in geochronology (see Faure 1979, and references therein); and it is well known that while some isotopic clocks start from the time of mineral crystallization or rock formation, others behave as closed systems for specific minerals below a certain ' closing ' (or ' blocking ') temperature upon cooling. Therefore, different isotope dating methods can, in principle, give an overview of the cooling history of a geological unit. It must be kept in mind, however, that this history will effectively describe a succession of thermal events with decreasing intensity. This may obviously be an oversimplification of the real thermal history of a rock, as sketched in figure 18. Discontinuities in the cooling history of a rock can thus be smoothed away by considering only the isotopic age distribution. Similarly, moderate thermal events can reset some geochronometers and, therefore, erase any memory of low temperature stages of the rock history, as shown for the case of apatites in figure 18.

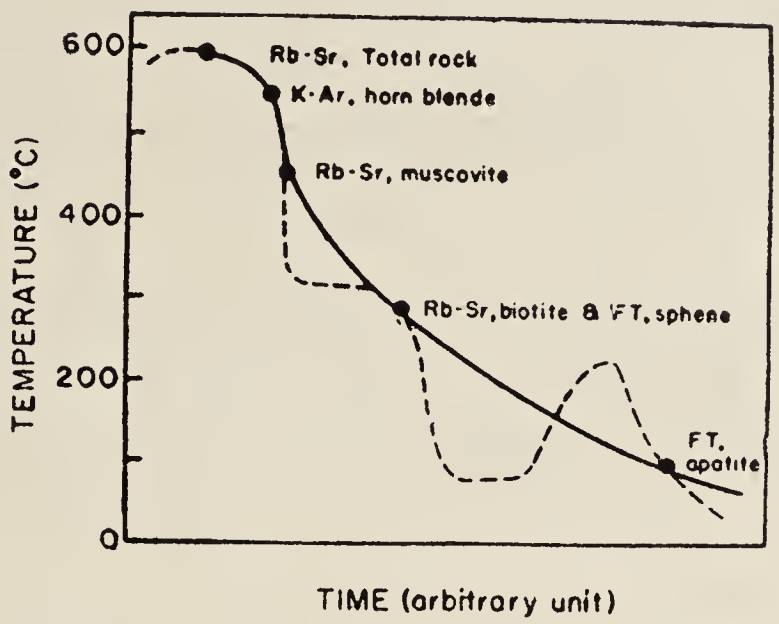

Figure 18. Hypothetical cooling history (dotted line) of a granitic body formed at 600°C and the smoothed cooling curve (solid line) that could be deduced from geochronological studies.

Certainly, the best way to define the past crystallization thermal history of a rock is to combine several geochronological approaches (K-Ar, Rb-Sr, etc.) with the FT method. In doing this it must still be remembered that the geochemical 'closing temperatures' are mostly meaningful for low cooling rates and that, at any rate, they are, whatever geochronometer is considered, generally slightly dependent on the cooling rate itself (Dodson 1979; Turner *et al* 1979).

With this limitation in mind, it is, however, possible to derive from any age difference Δt between two geochronometers having a ΔT difference in closing temperature an uplift (or erosion) rate, following the equation (Sharma *et al* 1981):

$$\text{uplift rate} = \frac{\text{cooling rate}}{\text{geothermal gradient}}, \tag{16}$$

where a (generally constant) value of the geothermal gradient has to be guessed. It is to be kept in mind that the 'uplift rate' so deduced depends only on the initial and final states of the system. This average value is not automatically representative of the actual cooling history. For instance, in many cases it is very difficult to decide whether or not the erosion (or uplift) was a continuous process with a constant rate in a given time interval Δt (equation 16) or was mainly linked to tectonic pulses of short duration (figure 18). Moreover, differences of cooling ages between different minerals of a rock do not refer necessarily to any uplift. This may happen when the settling of intrusions at depth may reset (to zero) the most thermally sensitive geochronometers in their thermal aureoles.

Finally, in recent mountain belts with still elevated reliefs, as the Alps or Himalayas, the FT cooling ages of minerals with low closing temperatures (*e.g.* apatites with $\sim$100°C) are very sensitive to geomorphology. It is well known that samples taken horizontally below a massif (in tunnels) show youngest apatites FT ages where the rock cover is most important. In these conditions, only a careful and detailed sampling can lead to meaningful interpretation of cooling ages in terms of tectonic and uplift history of a given area (Wagner *et al* 1977).

In conclusion, provided that precautions are taken in the handling of geochronological data (Baksi and Poupeau 1981), the FT method can contribute usefully to the deciphering of the cooling history of segments of the terrestrial crust.

8. Summary and conclusions

An analysis of the fission track dating method has been made through a survey of the recent literature from the point of view of precision, accuracy, and the meaning of FT ages. The results of this work can be summarized as follows:

(i) The use of a stepwise dating plateau method allows a high degree of precision on FT ages to better than $\pm 5\%$ (2σ) to be obtained, regardless of the presence or not of partial fossil track fading. From our experience, the isochronal plateau method, when applicable, is to be preferred, as it gives additional information on (a) the accuracy of fission track identification, and (b) indirectly, the variability of the geological closing temperature of a given mineral phase (Poupeau 1981a; Poupeau *et al* 1980a). The isothermal plateau method is very useful for metamict minerals which may degrade upon heating at relatively high temperatures, as may be the case for volcanic glasses. This method proved to be the best way to date hydrated glass shards (Carpena *et al* 1981; this work and in preparation), otherwise found to be difficult or impossible to treat with a conventional plateau method (Naeser *et al* 1979).

(ii) The accuracy of FT age is strongly dependent on the choice of λ_f and neutron dosimetry, both affected by unknown systematic errors. Accordingly, it has been recommended that (Naeser *et al* 1979; Poupeau 1981a), once a neutron dosimetry system is chosen, λ_f should be considered as an operationally adjustable parameter obtained by geological calibration with well-dated volcanic rocks. Under these conditions, an accuracy of better than 5% is achievable. In order to adopt a common set of parameters in the age equation, a standardization of the neutron dosimetry would be highly desirable. The already widely distributed NBS glass standards series (Carpenter and Reimer 1974) may fulfil this role, even though suggestions were made (Workshop on Fission Track Dating, Pisa, 1980) to improve future standards.

(iii) Very often, reported FT ages cannot be used meaningfully due to the lack of appropriate information. Some suggestions for improvements of data presentation were recently made (Naeser *et al* 1979). We would recommend for each FT age determination that (a) both the neutron dosimetry and 'λ_f' value be specified (with proper reference); (b) sufficient statistical data are provided: number of counting cells, total number of tracks, statistical law (and its justification) used to derive counting error, level of confidence interval on D_f, D_i, ϕ, etc. These data are needed to compare sets of FT ages obtained with different irradiations and in different laboratories and also for comparing FT and other isotopic ages.

(iv) In volcanic rocks FT ages can generally be interpreted as formation ages. Their correct interpretation in other samples requires that partial track fading is taken into account in the age determination process. When a plateau method cannot be applied (due to an inhomogeneous fission track distribution or a low track density in the samples to date), some control on the geological track annealing can still be obtained through track length or track diameter measurements. The closing temperatures of minerals for FT dating are lower ($\sim$ 300°C to 100°C) than for most other nuclear geochronometers. Therefore, when used in conjunction with other dating methods, the FT ages may allow us to gain

some insight into the last stages of the cooling history and thermal stabilization of orogenic belts and cratons. It seems that a fine time resolution can be achieved at present with the FT method. Further improvements might include the extension of model ages to new mineral phases, a better determination of the closing temperature of minerals especially with geological calibrations following the line of Naeser (1979, 1980), and the search for minerals with a track retention temperature higher than 300°C, which would allow more complete studies of the cooling history of geological systems. In this respect, quartz seems to be a good candidate (Fleischer *et al* 1975, table 2.4) if used as a natural external detector.

Acknowledgements

The author is grateful to Drs G Bigazzi and C W Naeser, who allowed him to reproduce some of their still unpublished data. Several graduate students, J Carpena, V K Ceylan, D Chaillou, and D Vincent, and Dr Ph Romary helped in track measurements. He thanks Drs A Baksi, S Carpenter, Prof. K K Nagpaul, and Dr K K Sharma for discussions and Drs S Carpenter, J N Goswami, R S Rajan, and A S Tamhane for their comments on the manuscript.

This article was written in Ahmedabad during a stay at the Physical Research Laboratory. The author wishes to thank Prof. D Lal, Director of PRL, and his colleagues in the Geophysics Group for their hospitality and very stimulating discussions.

The final version of this manuscript was prepared at the Department of Terrestrial Magnetism, Carnegie Institution of Washington, D. C. The author wishes to thank its Director, Dr G Wetherill, and Dr R S Rajan for their encouragements and for having provided him all facilities for his work at DTM.

This work was supported by the Centre National de la Recherche Scientifique (France) and the Council of Scientific and Industrial Research (India).

References

Arias C, Bigazzi G and Bonadonna F P 1981 *Nuclear Tracks* **5** 129
Baksi A K and Poupeau G 1981 submitted to *Tectonophysics*.
Bhandari N, Bhat S G, Lal D, Rajagopalan G, Tamhane A S and Venkatavaradan V S 1971 *Nature* **230** 219
Bigazzi G 1981 *Nuclear Tracks* **5** 35
Bevington P R 1969 *Data reduction and error analysis for the physical sciences* (New York: McGraw Hill) p. 336.
Carpena J 1980 3rd Cycle Thesis Montpellier University p. 112
Carpena J, Mailhe D, Naeser C W and Poupeau G 1979 *C. R. Acad Sci. Paris* **D289** 829
Carpena J, Chaillou D, Chambaudet A and Poupeau G 1980 In *Solid state nuclear track detectors* (New York: Pergamon) p. 961
Carpena J, Mailhe D, Poupeau G and Vincent D 1981 *Nuclear Tracks* (in press)
Carpenter B S 1980 Preprint
Carpenter B S and Reimer G M 1974 NBS Special Publication 260-49 P. 1.
Cowan G A and Adler H H 1976 *Geochim. Cosmochim. Acta* **40** 1487
Dakowski M, Burchart J and Galaska J 1974 *Bull. Acad. Pol. Sci.* **22** 11

Dodson M H 1979 in Lectures in isotope geology (Berlin: Springer Verlag) p. 207
Faure 1979 Principles of Isotope geology (New York: John Wiley), p. 464
Fleischer R L and Price P B 1964 *Phys. Rev.* **B133** 63
Fleischer R L, Price P B and Walker R M 1975 *Nuclear tracks in solids: Principles and applicaitions* (Berkeley: University of California Press), p. 605
Galliker D, Hugentobler E and Hahan B 1970 *Helv. Phys. Acta* **43** 593
Gleadow A J W and Lovering J F 1977 *Nuclear Track Detection* **1** 99
Gleadow A J W and Duddy I R 1980 Workshop on fission track dating Pisa Sept. 10-12 (Abstract).
Haack U 1977 *Am. J. Sci.* **277** 459
Hay R L 1980 *Nature (London)* **284** 401
Hurford A J and Gleadow A J W 1977 *Nuclear Track Detection* **1** 41
Hurford A J and Green S 1980 Workshop on fission track dating Pisa September 10-12 (Abstract)
Jaffey A H, Flynn K F, Glendenin L C, Bentley W C and Essling A M 1971 *Phys. Rev.* **C4** 1889
Johnson N M, McGee V E and Naeser C W 1979 *Nuclear Tracks* **3** 93
McGee V E and Johnson N M 1979 *Math. Geol.* **11** 255
Mailhe D, Carpena J and Poupeau G 1980 Instituto Geografico Nacional Madrid Special Publication No. 201 p. 149
Naeser C W 1978 U S Geol. Surv. Open File Report 76–190.
Naeser C W 1979 in *Lectures in isotope geology* (Berlin: Springer Verlag) p. 154
Naeser C W 1980 Preprint
Naeser C W and Fleischer R L 1975 *Geophys. Res. Lett.* **2** 67
Naeser C W, Izett G A and Obradovitch J D 1980 *U.S. Geol. Surv. Bull.* (in press)
Naeser C W Gleadow A J W and Wagner G A 1979 *Nuclear Tracks* **3** 133
Naeser C W, Zimmerman R A and Cebula G T 1981 *Nuclear Tracks* **5** 65
Nagpaul K K, Mehta P P and Gupta M L 1974 *Pure Appl. Geophys.* **112** 140
Parshad R, Lal N and Nagpaul K K 1979 *J. Geol. Soc. India* **20** 31
Poupeau G 1981a *Cienc. Cult.* **33** 325
Poupeau G 1981b Preprint
Poupeau G and Rajan S R 1981 *Nucl. Sci. Appl.* (submitted)
Poupeau G, Romary Ph and Toulhoat P 1978a U.S. Geol. Survey Open File Report No. 78-701 p. 339
Poupeau G, Toulhoat P and Romary Ph 1978b *C. R. Acad. Sci. Paris* **D287** 971
Poupeau G, Carpena J, Chambaudet A and Romary Ph 1980a in *Solid state nuclear track detectors* (New York: Pergamon) p. 965
Poupeau G, Carpena J, Mailhe D and Ceylan V K 1980b *C.R Acad. Sci. Paris* **D290** 1189
Price P B and Walker R M 1963 *J. Geophys. Res.* **68** 4847
Roberts J H, Gad R and Armani R J 1968 *Phys. Rev.* **174** 1481
Saini H S and Nagpaul K K 1979 *Int. J. Appl. Radiat. Isot.* **30** 213
Sharma K K, Bal K D, Prashad, R, Lal N and Nagpaul K K 1981 *Tectonophysics* **70** 135
Storzer D 1970a *Earth Planet Sci. Lett.* **8** 55
Storzer D 1970b Ph.D. Thesis (Heidelberg Univ.: West Germany)
Storzer D and Poupeau G 1973a *C.R. Acad. Sci. Paris* **D276** 137
Storzer D and Poupeau G 1973b *Revnion Anuelle des Sciences de la Terre* (ed. Soc. Geol. France) p. 387
Storzer D and Wagner G A 1969 *Earth Planet Sci. Lett.* **5** 463
Thiel K and Herr W 1976 *Earth Planet. Sci. Lett.* **30** 50
Turner G, Enright M C and Cadogau P H 1978 *Pro. Lunar Planet. Sci. 9th* (New York: Pergamon) p. 989
Virk H S and Koul S L 1977 *J. Phys. Earth* **25** 177
Wagner G A 1979 in *Lectures in isotope geology* (Berlin: Springer Verlag), p. 170
Wagner G A 1978 *Nuclear Track Detection* **2** 51
Wagner G A, Storzer D and Keller J 1976 *N. Jb. Minner Mh* **84**
Wagner G A, Reimer G M, Carpenter B S, Faul H, Van Der Linden R and Gijbels R 1975 *Geochim. Cosmochim. Acta.* **39** 1279
Wagner G A, Reimer G M and Jayer E 1977 *Mem. 1st Gəol. Min.* (Univ. Padova) Italy, p. 27

Application of solid state nuclear track detectors in fission studies

R H IYER
Nuclear Materials Accounting Cell, Bhabha Atomic Research Centre,
Bombay 400 085, India

Abstract. Solid state nuclear track detectors (SSNTD) were introduced as an important research tool in nuclear science and technology in the early 1960s. In this paper an attempt is made to give an overview of some of the important applications of SSNTD in the study of fission-related phenomena. The areas covered are: (a) spontaneous fission half-lives, (b) compound nuclear life-time measurements, (c) fission cross-section, excitation functions and fission fragment angular distributions, (d) fission isomers, (e) search for superheavy elements and (f) absolute fission yield measurements. In each case a few examples of experimental work carried out in various laboratories including the Bhabha Atomic Research Centre (BARC), Bombay are discussed to highlight the significant contributions these studies have made to our understanding of nuclei and nuclear fission. The important role played by SSNTD in each of the above areas of fission studies is illustrated. Some specific cases are cited where the innovative use of SSNTD has lead to results of profound significance in fission physics. A general review of the impact of these studies on our present understanding of nuclei and nuclear fission as well as a brief outline of the problems and future prospects are also given in the paper.

Keywords. Tracks; fission; half-lives; cross-section; excitation function; isomers; superheavy elements.

1. Introduction

Solid state nuclear track detectors (SSNTD) were introduced as an important tool in nuclear science and technology in the early 1960s (Fleischer *et al* 1965). They are dielectric materials such as mica, glass, synthetic plastics etc. which record and permanently store the trajectory of fast-moving charged particles. The stored information contained in the trajectory of the charged particles can be conveniently retrieved by the experimenter by selective chemical etching and observation under an optical microscope. The extreme simplicity of the technique coupled with the lack of dependence on costly electronics on the one hand and the availability of a variety of detectors with different sensitivities to charged particles on the other make them particularly useful in the investigation of rare and low cross-section events in an essentially background-free situation. By merely counting the number of tracks (recorded on a detector) of charged particles ejected from a nuclear reaction, one can do experiments in nuclear physics and chemistry, particle dosimetry and microanalysis (Fleischer *et al* 1972). There is hardly any branch of science and technology where SSNTDs do not have an actual or potential application. Today, the technique has developed from a mere laboratory curiosity into one of the cheapest and most powerful expeirmental tools in the study of a number of nuclear phenomena (Fleischer *et al* 1975). Its growth in the last

15 years, both in size and applications has been spectacular. Over fifty laboratories around the world make use of this technique for various experimental work which has led to the growth of fundamental knowledge and technological applications. Many review articles cataloging the diverse applications of the technique are available in the literature (Fleischer *et al* 1965, 1972, 1975).

Precision measurements in scientific research have generally come through the use of expensive instruments. But the SSNTD technique, also called track-etch technique has made precision measurements on the detection and measurement of neutron and charged particle-induced nuclear reactions so inexpensive that even small laboratories with some basic facilities can take up R & D work using this technique.

In this paper we shall discuss some of the important applications of the technique to fission-related studies by citing examples of experimental work carried out in various laboratories including those carried out at our research centre and highlight the significant contributions these studies have made to our understanding of nuclei and nuclear fission. The topics covered are: (a) measurement of spontaneous fission half-lives, (b) measurement of life-times of compound nuclei, (c) fission cross-sections, angular distribution of fission fragments and fission excitation functions, (d) investigations on fission isomers, (e) search for super heavy elements and (f) absolute fission yield measurements. It is not practicable to give an exhaustive coverage of each topic for the simple reason that the experimental and theoretical data reported in the literature are too voluminous. Instead, one or two examples will be discussed in each case to illustrate how SSNTD has played a key role. A general review of the impact of these and related studies on our understanding of nuclei and nuclear fission is also given here.

2. Special features of SSNTD

Before discussing specific applications of SSNTD, let us very briefly examine some of their special features (apart from their simplicity and inexpensive nature) which make them extremely valuable for studies related to the fission process:

(i) they are insensitive to high background radiation making investigations on specific, rare and low cross-section nuclear reactions possible.
(ii) a wide variety of detectors with different sensitivities to charged particles are available for the experimenter to choose from to meet his specific experimental needs.
(iii) the integrating nature of the detectors allows events to be accumulated over large periods of time without any deterioration of the detector.
(iv) they are amenable to different geometrical arrangements such as 2π, 4π, forward and backward recoil geometry etc.
(v) they can be used in any size; small sizes allow them to be used in remote and difficult-to-reach experimental locations.
(vi) it is a non-electronic technique; so no electronic break downs to worry about.

These features of SSNTD, coupled with some ingenuity on the part of the investigator make them unique among the experimental tools that are generally employed in fission studies.

3. Applications to fission-related studies

3.1 *Measurement of spontaneous fission half-lives*

Spontaneous fission from the ground state is an important mode of decay of heavy elements with atomic number $Z90$ and above. It occurs with measurable decay rate in elements from uranium up, the half-lives decreasing rapidly with increasing Z. Table 1 shows some typical data to illustrate the wide range of spontaneous fission half-lives. A precise knowledge of the spontaneous fission half-lives of heavy elements is important from the point of view of basic understanding of nuclear structure, checking existing theories of fission and alpha decay systematics, predicting the properties of new heavy elements and extending the periodic table to regions covering the yet undiscovered superheavy elments. From purely practical considerations, the spontaneous fission decay constant of ^{238}U is a basic parameter needed in geochronology. Many current techniques of assay of heavy elements, require a knowledge of their decay properties; these are linked with nuclear safeguards, plutonium recycle, and accounting and management of nuclear materials.

Solid state nuclear track detectors have been used very effectively in the accurate measurement of both extremely large and extremely short spontaneous fission half-lives (Hulet *et al* 1971; Khan and Durrani 1973; see table 1). When one considers spontaneous fission decay of heavy elements it is important to realise that alpha

Table 1. Spontaneous fission half-lives of some heavy element isotopes—typical data*

Nuclide	Z	$t_{1/2}$ (SF)	Remarks
^{232}Th	90	$\sim 10^{21}$ y	
^{231}Pa	91	10^{16} y	
^{235}U	92	$1{\cdot}9 \times 10^{17}$ y	a
^{238}U	92	$1{\cdot}02 \times 10^{16}$ y	a
^{237}Np	93	$3{\cdot}0 \times 10^{18}$ y	a
^{238}Pu	94	$4{\cdot}6 \times 10^{10}$ y	a
^{241}Am	95	$1{\cdot}15 \times 10^{14}$ y	a
^{244}Cm	96	10^{7} y	a
^{249}Bk	97	$1{\cdot}65 \times 10^{9}$ y	a
^{248}Cf	98	3×10^{4} y	a
^{252}Cf	98	85 y	a
^{256}Cf	98	740 sec	
^{253}Es	99	$6{\cdot}3 \times 10^{5}$ y	
^{257}Fm	100	125 y	
^{258}Fm	100	380μsec.	a
^{259}Fm	100	1·5 sec.	
^{259}Md	101	5700 sec.	
^{259}No	102	8·6 sec.	a
^{256}No	102	1500 sec.	a
$^{258}104$	104	11 milli sec.	a
$^{261}105$	105	1·8 sec.	a
$^{262}105$	105	$\sim$28 sec.	a

*Source of data: Fleischer *et al* 1975; Gay and Sher 1975; Hoffman 1979.
a-SSNTDs have been used (Fleischer *et al* 1975.)

decay is a competitive process. Consequently, the heavy element isotopes are associated with intense alpha activity causing problems in handling and those arising from pile-up alpha pulses (Gay and Sher 1975). For example, the ratio of alpha to spontaneous fission decay of ^{238}Pu is about 5×10^8. The determination of long SF life-times require fairly large amounts of the isotope and large observation (exposure) times. In such situations the integrating nature of SSNTD coupled with their insensitivity to alpha particles (mica in particular) are major advantages over the conventional electronic techniques.

The principle for the conventional and simplest use of the technique for the measurement of fairly long spontaneous fission half-lives is well established (Fleischer and Price 1964; Khan and Durrani 1972; Gay and Sher 1975) . For example, in the determination of the spontaneous fission decay constant of ^{238}U, a natural uranium source in the form of a thin metal foil or in the form of an electroplated source is kept in direct contact with a track detector (usually mica) for a sufficiently long period of time to accumulate a statistically significant number of spontaneous fission tracks. The number of tracks recorded can be expressed as:

$$(\text{track})_{SF} = K \,.\, N_8 \,.\, \lambda_{SF} \,.\, t_{SF},$$

where K is the track registration efficiency for the source-detector assembly, N_8 is the number of ^{238}U atoms exposed to the detector, λ_{SF} is the spontaneous fission decay constant of ^{238}U and t_{SF} is the exposure time.

In order to eliminate the need for knowing the track registration efficiency, K, a second exposure of the source detector assembly is carried out with thermal neutrons using a fresh detector. The detector records induced fission tracks from the thermal neutron fission of ^{235}U which can be expressed as

$$(\text{tracks})_{irr} = K \,.\, N_5 \,.\, \sigma_f \,.\, \phi \; t_{irr},$$

where N_5 is the number of atoms of ^{235}U in the source, σ_f is the thermal neutron fission cross-section of ^{235}U, ϕ is the thermal neutron flux and t_{irr} is the irradiation time. Then

$$\frac{(\text{tracks})_{irr}}{(\text{tracks})_{SF}} = \frac{N_5}{N_8} \cdot \frac{\sigma_f \,.\, \phi}{\lambda_{SF}} \cdot \frac{t_{irr}}{t_{SF}}.$$

All the quantities in the above equation are known except λ_{SF} which can be determined.

A couple of illustrative examples of the ingenious uses of SSNTD to measure extremely short SF life-times and which have made a profound impact on nuclear structure, nuclear stability and fission systematics are outlined below. As already pointed out, spontaneous fission half-lives decrease rapidly with increasing atomic number. One of the serious problems associated with the study of very heavy actinide elements with $Z > 98$ is their very short half-lives and low production cross-sections. Until about 1973, the heaviest nuclide whose fission properties were studied in some detail was $^{257}_{100}$Fm (Hoffman 1979). With the availability of small quantities of isotopes of very heavy actinides through heavy ion reactions, fission properties of heavier actinide isotopes have recently been investigated particularly at the Los Alamos Scientific

Laboratory, the Lawrence Livermore Laboratory, the University of California, Berkeley and the Oak Ridge National Laboratory (Ferguson *et al* 1979).

Hulet *et al* (1971) used a 'rotating drum method' to determine the spontaneous fission half-life of $^{258}_{100}$Fm. The experimental arrangement is shown in figure 1. Atoms of ^{258}Fm were produced by bombarding a weightless target of $^{257}_{100}$Fm (about 10^9 atoms electrodeposited on a 0·013 mm thick beryllium foil) with 12·5 MeV deuterons by the ^{257}Fm (d, p) ^{258}Fm reaction. The atoms of ^{258}Fm formed, recoil out of the target and get deposited on a steel drum. The irradiation is stopped and the drum is rotated at a known high speed (1500–3275 rpm). The fission fragments resulting from the spontaneous fission of ^{258}Fm are caught in a series of mica strips which record the fission tracks. Several runs were performed to accumulate enough spontaneous fission events. From the speed of rotation of the drum and the variation of fission track density in the mica strips, the half-life was estimated. Figure 2 shows the experimental results which indicate a SF half-life of 380 $\pm$ 60 μ sec for ^{258}Fm.

An equally ingenious experimental arrangement, the 'moving belt method' was used by Flerov *et al* (1964) at Dubna to obtain possible evidence of an isotope of the element 104. Atoms of the element 104 were produced by bombarding thin (700 μg/cm$_2$ covered with 100 μg/cm^2 of nickel) targets of $^{242}_{94}$Pu with ^{22}Ne ions. The recoiling product atoms from the reaction ^{242}Pu $(^{22}$Ne, 4n$)^{260}_{104}$ were caught in a conveyer belt about 8 m long. At the end of the bombardment, the belt moves at a known high speed and the fission fragments resulting from the spontaneous fission of element 104 are caught in phosphate glass detectors which record the fission tracks. Here again, the half-life is estimated from the variation in track density and from a knowledge of the speed of the moving belt. The experimental arrangement is shown in figure 3. From this experiment a half-life of 0·3 sec was estimated for element 104.

Both the 'rotating drum—SSNTD' and the 'moving belt—SSNTD' systems have played a major role in the detection and identification of trans-fermium isotopes and are standard experimental tools in all leading research centres in the world engaged in the search for very heavy and superheavy elements.

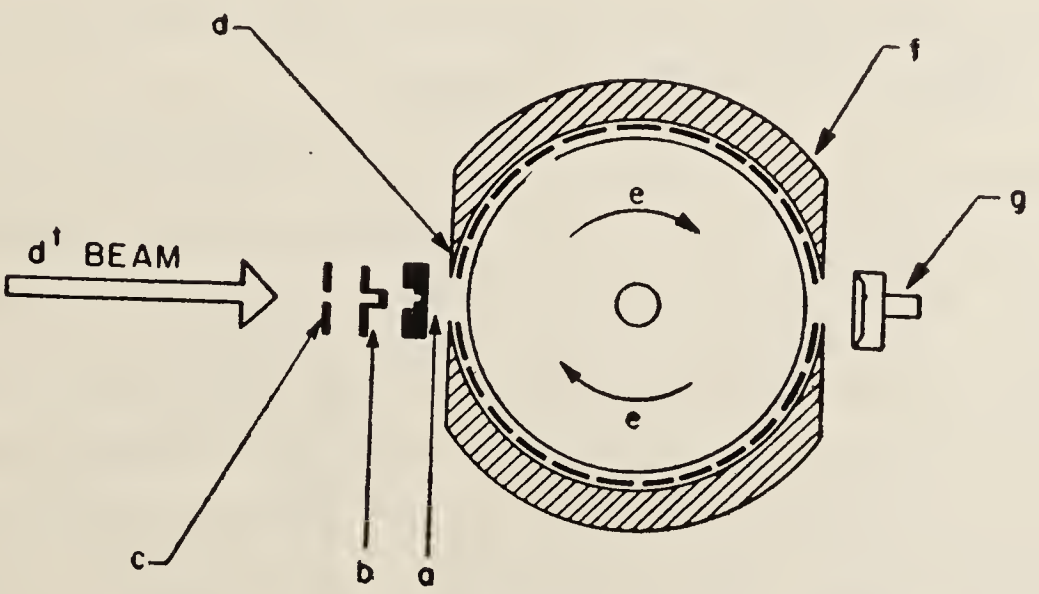

Figure 1. Schematic representation of the target and drum-mica system for measurement of short spontaneous fission (SF) half-life. Deuterons strike the ^{257}Fm target (a) after passing through aluminium degrading foils (b) and tantalum collimator (c). The atoms of ^{258}Fm recoiling from the target are caught on the surface of the rotating drum (e) and their decay by SF is recorded in short strips of mica (d) attached in a continuous band to the drum housing (f). An α-detector (g) was used for monitoring the recoil efficiency of the target (Hulet *et al* 1971).

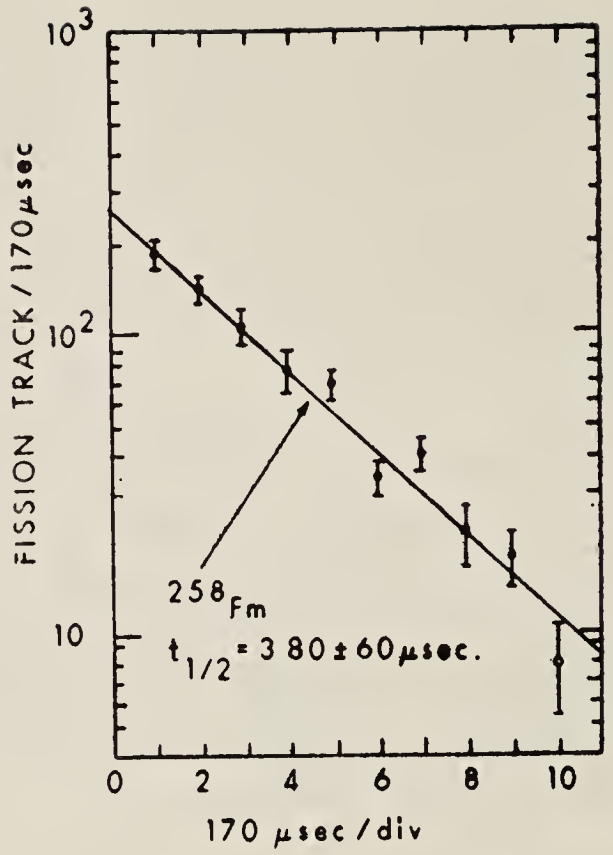

Figure 2. Decay curve for spontaneous fission assigned to ^{258}Fm. Net fission tracks from five bombardments have been summed (Hulet *et al* 1971).

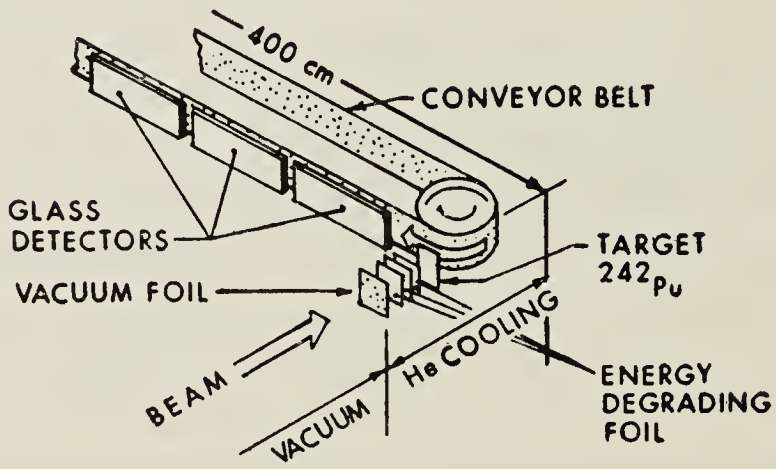

Figure 3. The scheme of the arrangement used in the experiments on the synthesis of element 104: The moving belt-SSNTD system (Flerov *et al* 1964).

Let us now briefly discuss the impact of these experiments, particularly the experimental results on ^{258}Fm, on fission physics.

The available information on the spontaneous fission half-lives of actinide and trans-actinide elements has been used to establish certain systematic trends for even-even isotopes (Nurmia *et al* 1967). While the $t_{1/2}$(SF) generally decrease with increasing Z, a definite stabilising effect for 152 neutrons has been observed, beginning with curium. These calculations reproduce the general trends very well but can show large deviations for a given nuclide (Randrup *et al* 1976; Baran 1978; Baran *et al* 1979) . The experimental value for the $t_{1/2}$(SF) of ^{258}Fm of 380 μ sec was lower than the predicted value by nearly 6 to 8 orders of magnitude. This was a completely unexpected result and the sharply decreasing trend of SF life-times of nuclei with $N > 152$ was contrary to theoretical predictions. Hulet *et al* (1971) observed that even-even nuclei with $N = 158$ are becoming catastrophically unstable towards spontaneous fission. This necessitated a thorough re-evaluation of the techniques of calculating the life-times of very heavy and superheavy nuclides. While it is recognised that the relatively long spontaneous fission half-life of 125 years for $^{257}_{100}$Fm with 157 neutrons is due to the extra hindrance associated with SF of nuclei with an odd number of nucleons

(Johansson 1959; Randrup *et al* 1973) the decrease in $t_{1/2}$ (SF) by a factor of nearly 10^{13} on adding just one more neutron to $^{257}_{100}$Fm is indeed a dramatic effect.

This rather unexpected result, prompted a determined experimental effort not only to measure the SF lifetimes of many new heavy elment isotopes with neutron numbers in the vicinity of 158, but also on other important fission characteristics such as mass distribution, total kinetic energy release etc. Some of the new and exciting results are discussed below.

Recently, the $t_{1/2}$ (SF) of $^{256}_{98}$Cf, which also has 158 neutrons as $^{258}_{100}$Fm, has been measured by Hoffman *et al* (1977) to be 12·3 minutes. This indicates a reduction by a factor of $1{\cdot}4 \times 10^{-4}$ in half-life for addition of 2 neutrons to ^{254}Cf ($T_{1/2}$=60 days) compared to the reduction factor of $1{\cdot}9 \times 10^{-3}$ in the case of $^{252}_{98}$Cf to $^{254}_{98}$Cf. Although the half-life reduction for 2 neutrons between $^{254}_{98}$Cf to $^{256}_{98}$Cf is one order of magnitude larger than between $^{252}_{98}$Cf and $^{254}_{98}$Cf, a 'disaster' for 158 neutrons appears to have been averted. Among the trans-fermium isotopes, with odd number of nucleons, $^{259}_{101}$Md is again of special interest in that it also has 158 neutrons like $^{258}_{100}$Fm but the odd nucleon hindrance effect referred to above is about 10% compared to $^{258}_{100}$Fm making the $t_{1/2}$ (SF) of $^{259}_{101}$Md to be 95 min (Wild *et al* 1979). These recent observations, suggest the possibility that for the even-even trans-fermium isotopes, the second fission barrier (Clark 1971) is absent leading to extremely short $t_{1/2}$ (SF)

The measurement of spontaneous fission half-life of $^{258}_{100}$Fm also had a profound impact on the discovery of $^{259}_{100}$Fm, a nuclide with 159 neutrons (Hoffman *et al* 1976). On the basis of SF decay systematics and the known $t_{1/2}$ (SF) of 125 years for $^{257}_{100}$Fm, the $t_{1/2}$ (SF) of $^{259}_{100}$ Fm was estimated to be in the range of 5 hr to 7·5 years. A search for $^{259}_{100}$Fm in underground nuclear tests, however, failed to give any evidence of the presence of this isotope (Hoffman 1976). The discovery of 380 microsecond for the $t_{1/2}$ (SF) of $^{258}_{100}$Fm indicating the on-set of a possible 'disaster' in spontaneous fission half-lives of nuclei with $N > 157$ promted a re-estimate of the $t_{1/2}$ (SF) of heavier trans-fermium isotopes. This led to the thinking that $^{258}_{100}$Fm and $^{259}_{100}$Fm should have about the same spontaneous fission half-lives except for the special hindrance associated with the odd neutron in $^{259}_{100}$Fm and its $t_{1/2}$ (SF) might be only a few tenths of a second. This information was valuable in designing the right type of experiments for the discovery of $^{259}_{100}$Fm by the reaction ^{257}Fm (t, p) ^{259}Fm. Its $t_{1/2}$ (SF) was found to be 1·5 sec.

Let us now quickly turn our attention to the other interesting features of fission, *viz.* mass distribution and kinetic energy release in the trans-fermium region. All previous measurements of low energy fission have shown the familiar *asymmetric mass division*, and the linear dependence of the average total kinetic energy (TKE) on $Z^2/A^{1/3}$. This is true upto and including the isotope $^{257}_{100}$Fm. However, addition of one extra neutron to $^{257}_{100}$Fm completely changes the picture. $^{258}_{100}$Fm and $^{259}_{100}$Fm show *symmetric mass division* and the TKE is about 40 MeV higher than the expected value. These results are shown in figures 4 and 5 respectively. On the basis of this, one would predict increased symmetric fission and higher TKE for heavy nuclei with neutron number $N \geqslant 158$. Surprisingly, however, the available data on the spontaneous fission of $^{256}_{98}$Cf ($N = 158$) and ^{262}105 ($N = 157$), one of the heaviest nuclide studied, do not show either increased symmetric fission or higher TKE. There is a distinct preference for mass asymmetry and normal kinetic energy release. The recent data on the spontaneous fission properties of $^{259}_{101}$Md ($N = 158$) is again somewhat perplex-

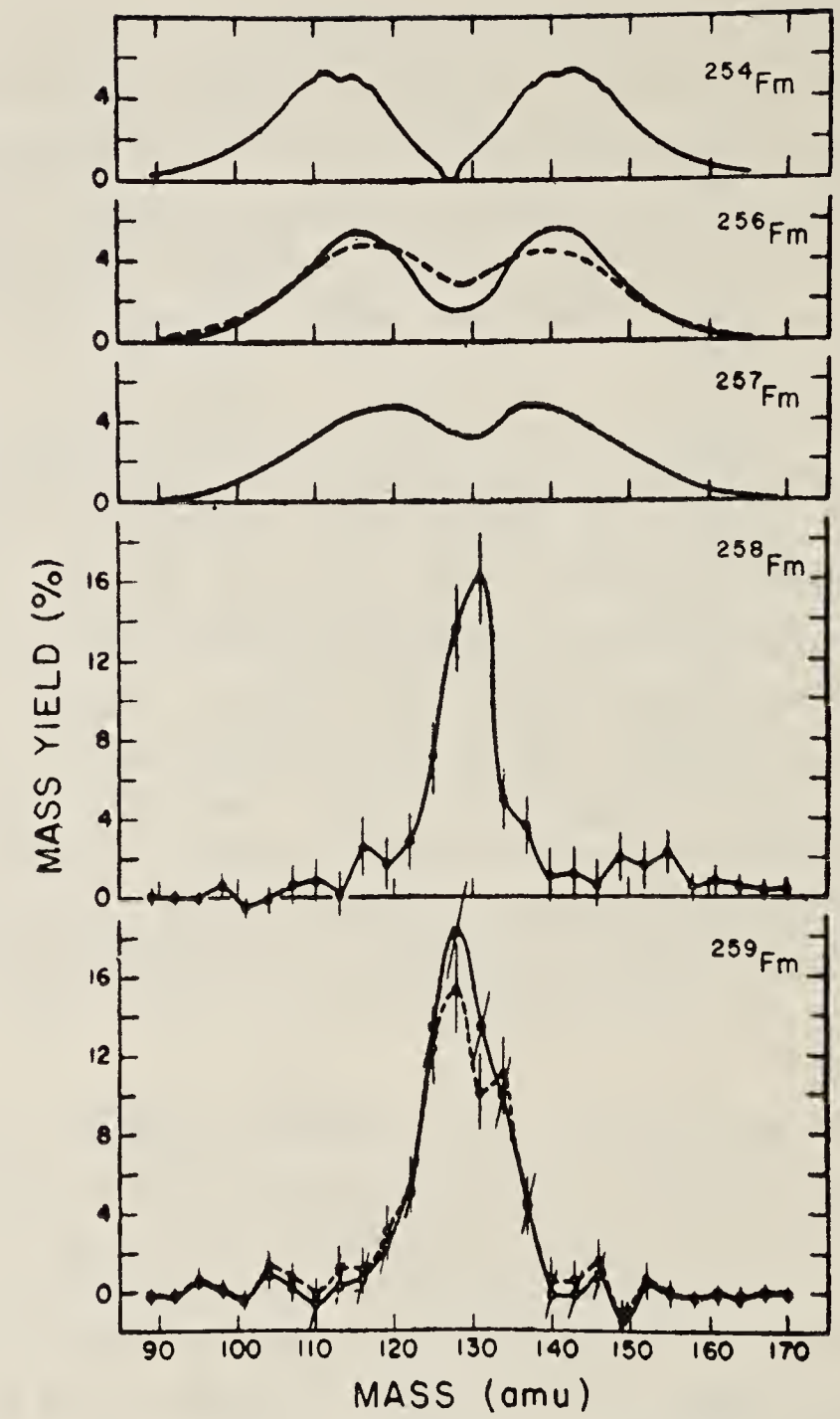

Figure 4. Trends in the mass distributions in the fission of fermium isotopes (Hoffman 1979).

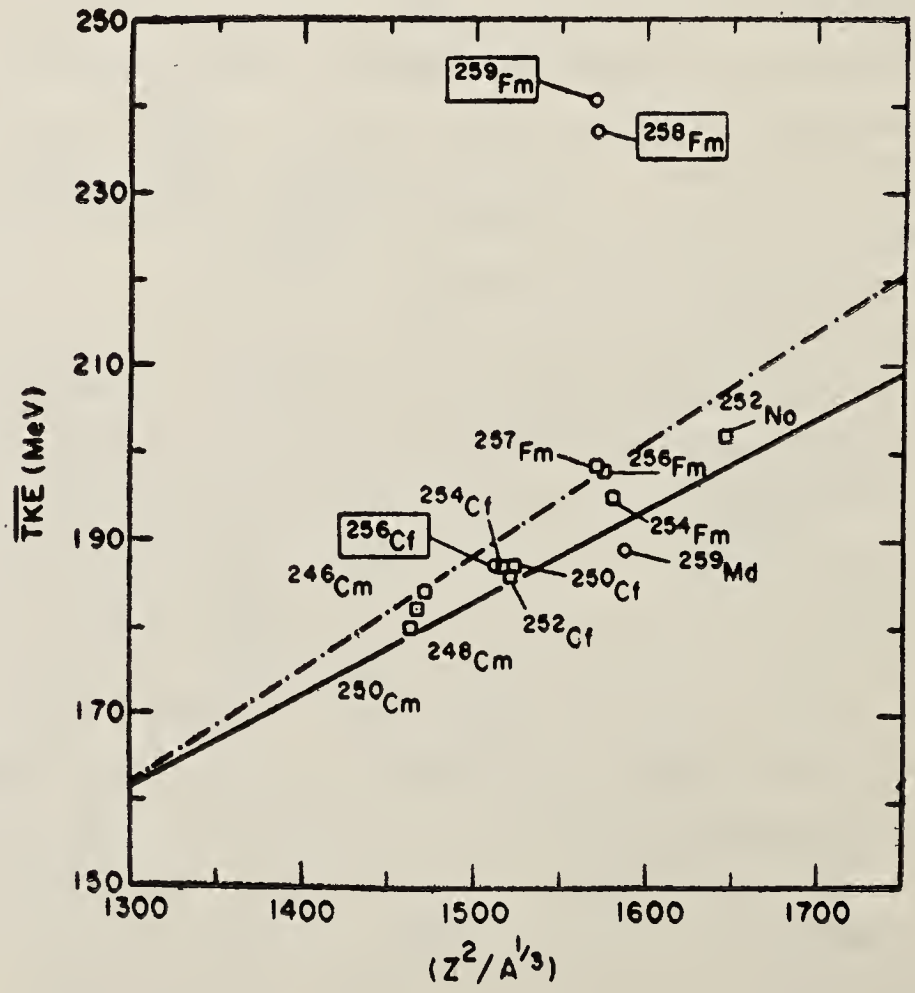

Figure 5. Trends in the total kinetic energy (TKE) release in the fission of very heavy actinides (Hoffman 1979).

ing (Hulet *et al* 1979). The most interesting observation is that while SF of $^{259}_{101}$Md and $^{259}_{100}$Fm are highly symmetric like those of $^{258}_{100}$Fm, the total kinetic energy release is somewhat less than what is expected from the linear trend (see figure 5)—an observation which is inconsistent with current fission theories in which fragment shells govern the fission process. Perhaps, the odd proton in $^{259}_{101}$Md may force a three-body break-up accounting for the low TKE leaving the nucleus to break into two fragments with $Z = 50$. Other possibilities require storing of about 60 MeV as internal energy for collective motion, internal rotation or internal heating.

Thus it would appear that $^{257}_{100}$Fm (N=157) is in a sense 'unique' and in a 'transition' region. The addition of one extra neutron to $^{257}_{100}$Fm brings about marked changes in the whole spectrum of fission properties of heavier nuclei. One key observation initially made possible by the innovative use of SSNTD—the determination of $t_{1/2}$ (SF) of $^{258}_{100}$Fm—has lead to many new and exciting results. It is clear, that further experimental efforts on the trans-fermium region are needed to check various theoretical approaches as well as to settle the issue of the suggested return to asymmetric mass division and lower TKEs.

3.2 *Life-times of compound nuclei*

Measurement of extremely short life-times of compound nuclei in the range 10^{-18} to 10^{-16} sec through the ingeneous use of SSNTD in a technique called 'crystal blocking' is another landmark in the history of application of SSNTD to nuclear physics (Brown *et al* 1968). In this technique, the reaction products (excited compound nuclei with short life-times) are produced in thin single crystals and the probability of escape of their fission fragments is measured along different crystallographic directions. This indicates the distance travelled by the fissioning nucleus in the crystal. From a knowledge of the recoil velocity of the compound nucleus and the distance travelled by it within the crystal (which is obtained from the blocking pattern of the emitted fragments) the life-times are evaluated. Figure 6 shows the experimental arrangement and the results of Brown *et al* (1968) on the measurement of life-time for the fission of ^{238}U by 12 MeV protons. Single crystals of UO_2 were used as the target. Lexan detector placed at a distance of 50 cm collected the fission fragments emitted along the

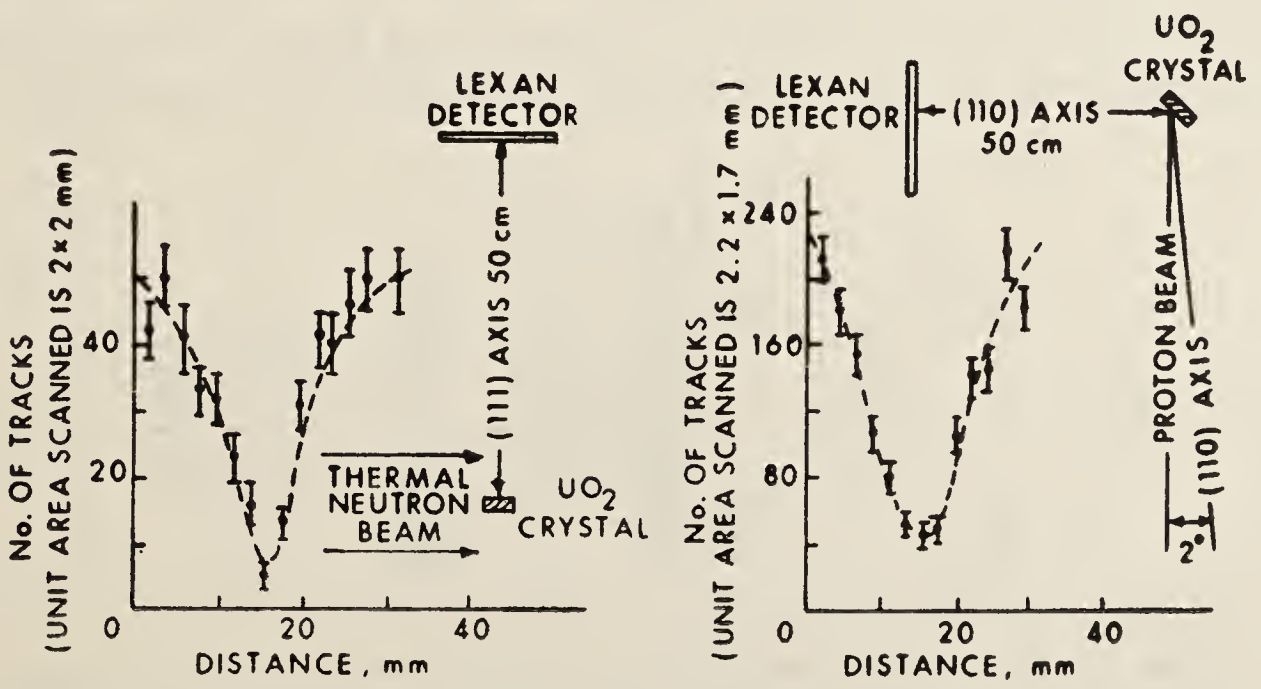

Figure 6. Extremely short life-times measurement by crystal blocking technique (Brown *et al* 1968).

[110] axis. The figure represents the angular distribution of fission fragments (the blocking patterns) along the [110] axis in a thermal neutron and 12 MeV proton irradiation. This showed that the total life time in the 12 MeV proton fission of ^{238}U is less than 2×10^{-17} sec. This technique will find important application in obtaining evidence for the formation of spontaneously fissioning superheavy elements with half-lives in the range of $10^{-14} - 10^{-18}$ seconds in heavy ion-induced nuclear reactions (see § 3.5).

3.3 *Fission cross-sections, excitation functions and angular distribution of fission fragments*

Voluminous data are available in the literature on fission cross-section and related measurements by using SSNTD. In all these studies, the extreme simplicity and sensitivity of SSNTD have been exploited. The work of Burnet *et al* (1964); on the helium ion induced fission of Au is a classic example of the use of SSNTD in low-Z element fission studies. Here the insensitivity of mica to large doses of high energy alpha particles allowed extremely low fission cross-sections—as low as 10^{-35} cm^2—to be measured and the fission barrier for the ^{201}Tl compound nucleus to be estimated. In most of these studies, a target-detector assembly is used in a 2π geometry. A typical 2π geometry experimental set-up for the determination of fission cross-sections is shown in figure 7 in which a stack of thin electrodeposited targets in contact with the detector is assembled. Using this experimental set-up the 14 MeV neutron fission cross-sections of a number of actinide elements were obtained in Trombay (Choudhuri *et al* 1979).

A very elegant use of plastic track detectors for studying the fission properties of low Z elements was demonstrated by Raisbeck and Cobble (1967). These are extremely low fission cross-section processes and in order to get even the most qualitative information on such systems, it was necessary to develop detection techniques which are not only extremely sensitive but also highly discriminating. It was also necessary to use exceedingly pure targets with respect to heavy element contamination. The fragile nature of the targets (thin layer of oxides of thulium, lutetium and rhenium deposited on high purity silverfoils) and the requirement of intense doses of alpha particles ruled out the possibility of using a 2π geometry set-up. The fission fragments recoiling out of the thin targets in the backward direction with respect to the incident beam of alpha particles were collected in a cylindrical lexan plastic detector.

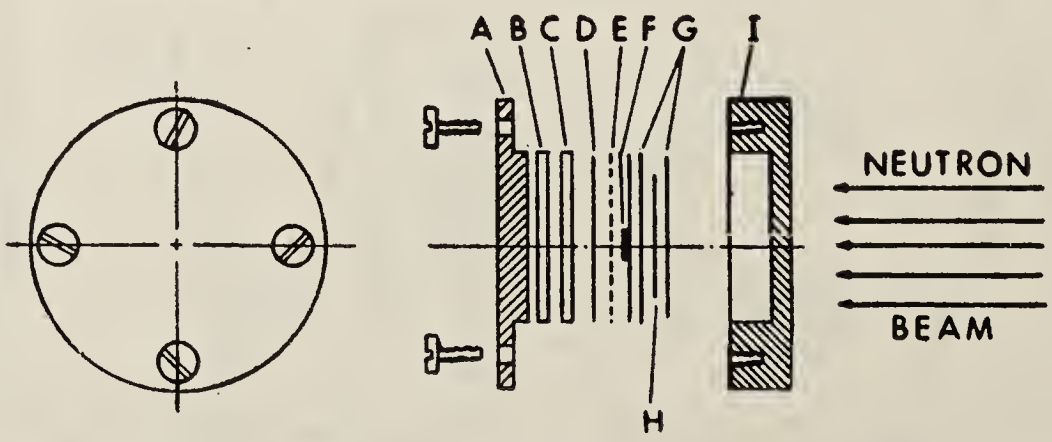

Figure 7. Schematic of irradiation assembly used for cross-section measurement: (A) perspex lid with screws, (B) and (C) perspex spacers, (D) and (G) Aluminium guard, (E) lexan detector, (F) target nuclide, (H) Al neutron monitor, and (I) perspex body (Choudhury *et al* 1979).

This arrangement provided both the sensitivity and the necessary discrimination against non-fission spallation reactions. Using such a cylindrical backward recoil geometry they measured the fission excitation functions of $^{169}_{69}$Tm, $^{175}_{71}$Lu and $^{185,187}_{75}$Re with 30–80 MeV helium ions (figure 8).

In the case of low Z elements neutron emission predominates over fission and the ratio of the fission cross-section to total reaction cross-section σ_f/σ_R is nearly equal to the ratio of the fission width to neutron emission width Γ_f/Γ_n. For example, for lutetium excited with 40 MeV helium ions, only one in 10^8 nuclear interactions leads to a fission event. The fission excitation functions were analysed, using a statistical model expression suggested by Huizenga and Vandenbosch (1962) to extract the fission barriers, E_f.

$$\frac{\sigma_f}{\sigma_R} \approx \frac{\Gamma_f}{\Gamma_n} = K_0 \frac{a_n\,[2a_f^{1/2}\,(E - E_f)^{1/2} - 1]}{4A^{2/3}\,a_f\,(E - B_n)} \times$$

$$\exp\,[2a_f^{1/2}\,(E - E_f)^{1/2} - 2a_n^{1/2}\,(E - B_n)^{1/2}],$$

where a_n and a_f are the level density parameters for neutron emission and fission respectively, E is the excitation energy, E_f is the fission barrier, B_n is the neutron binding energy, A is the mass number of compound nucleus and K_0 is a constant. The calculated fission barriers are 22·5, 23·6, 27·5 and 28·7 MeV respectively for the compound nuclei ^{189}Ir, ^{191}Ir, ^{179}Ta and ^{173}Lu. These data along with other data from the literature have been used to correlate the dependence of Γ_f/Γ_n on the fission-ability parameter Z^2/A (normalised to an excitation energy of 40 MeV) and shown in figure 9 which shows a striking exponential relationship. A marked deviation starting at $^{230}_{90}$Th (a compound nucelus formed in the reaction between $^{4}_{2}$He and $^{226}_{88}$Ra) gives conclusive evidence for the transition from predominantly symmetric fission mode for

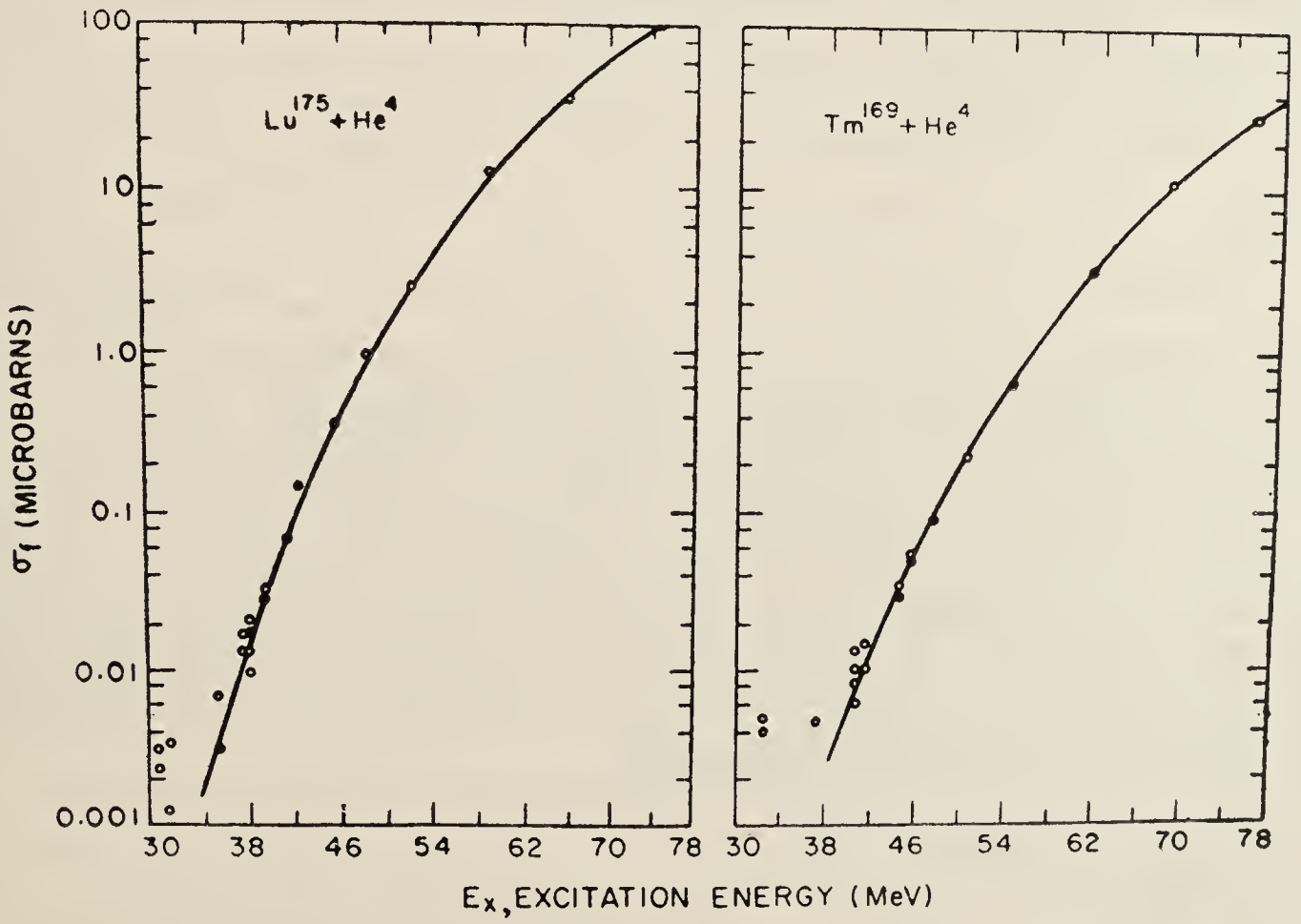

Figure 8. Helium-ion induced fission excitation functions of ^{169}Tm and ^{175}Ln (Raisbeck and Cobble 1967).

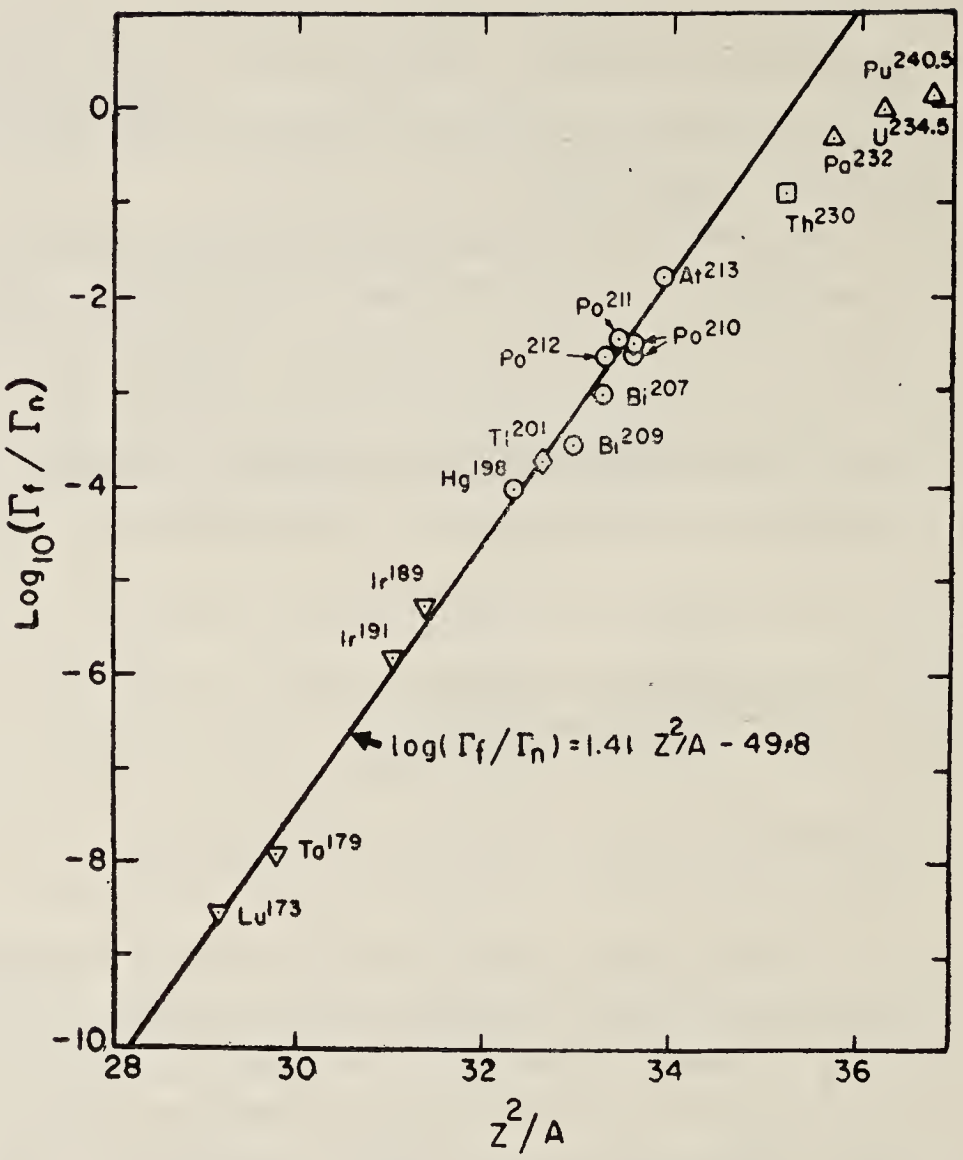

Figure 9. Correlation of Γ_f/Γ_n with fissionability parameter Z^2/A (Raisbeck and Cobble 1967).

low Z elements ($Z < 90$) to assymetric fission mode in high $Z(Z > 90)$ elements and corroborates the ' two-mode ' fission hypothesis (Turkevich and Niday 1951). It is worth pointing out here that the fission of ^{226}Ra with ^{4}He ions (compound nucleus $^{230}_{90}$Th) gives a 'triple-humped' mass distribution with nearly equal contributions from both the symmetric and the asymmetric fission modes (Fairhall *et al* 1958).

We conclude this discussion by citing one example of the innovative use of SSNTD for the measurement of fission fragment angular distributions carried out at BARC (Chaudhuri *et al* 1979). Using a novel fission recoil chamber about the size of a ' grape fruit ' evolved from considerations of neutron economy, it was possible to get the 14 MeV neutron fission fragment angular distributions of five independently fissioning actinide nuclei at a time. The fragments were collected in cylindrical lexan detectors in a forward recoil geometry. The experimental set-up and the geometry are shown in figures 10 and 11. Horizontal scans of the unfolded detector give the track density at a given angle of emission, θ, of fragments with respect to the neutron beam. The working of the recoil chamber and the method of calculation was checked by observing isotropic distribution of fragments in the thermal neutron fission of ^{235}U and ^{239}Pu (figure 12). From the measured track density, Td, and from a knowledge of the radius of the cylindrical detector, R, and the angle, θ, the angular distributions were calculated using the expression

$$\left(\frac{d\sigma}{d\Omega}\right)_\theta = \frac{\text{constant} \times R^2 \times Td}{\sin^3 \theta}$$

where the constant depends on the experimental parameters such as the neutron

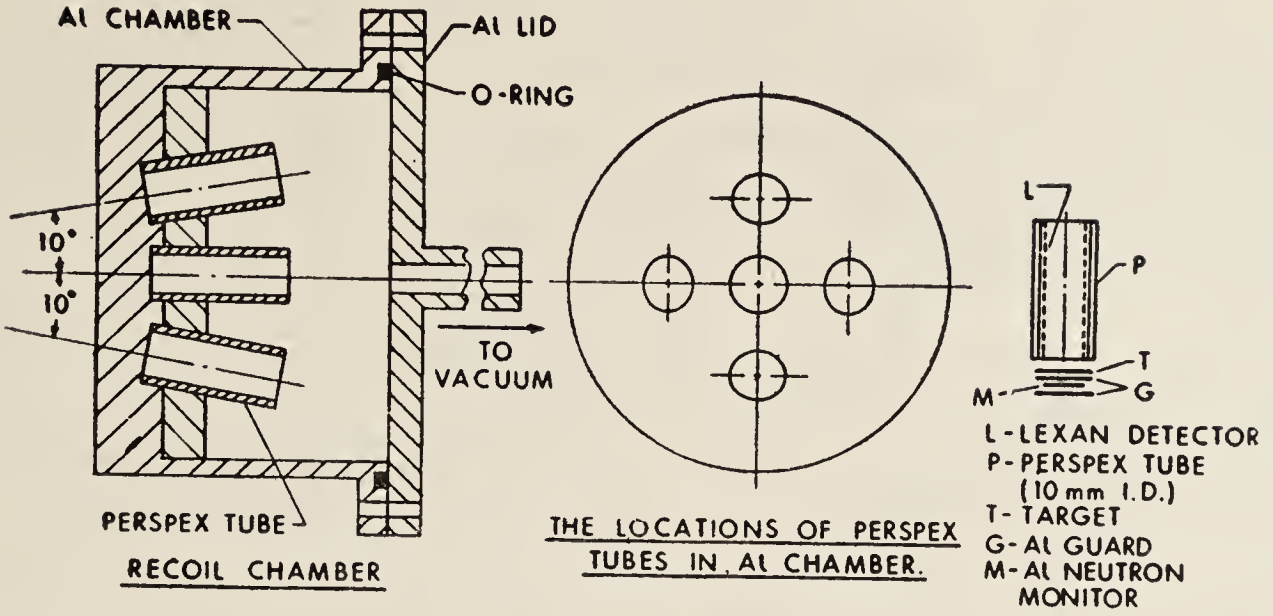

Figure 10. Schematic diagram of the recoil chamber used in angular distribution measurements (Choudhury *et al* 1979).

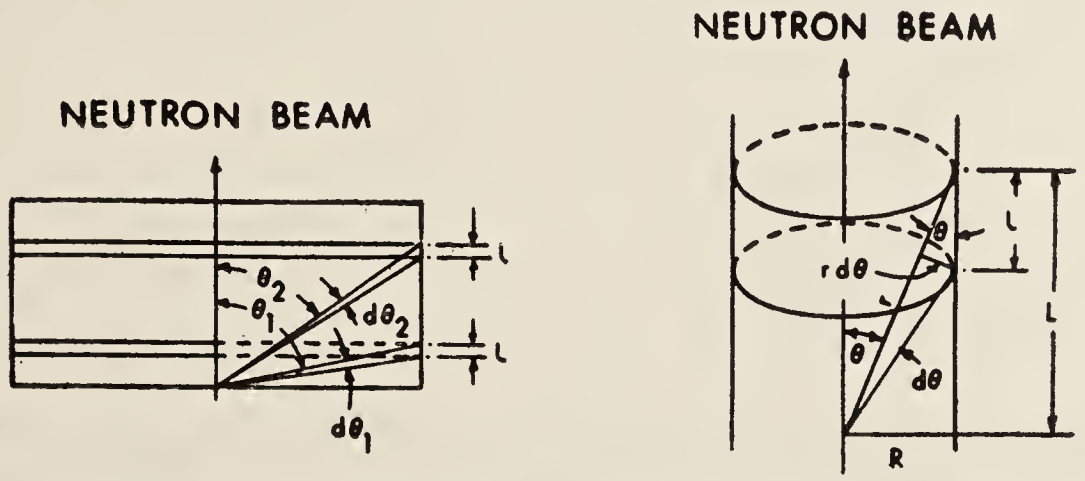

Figure 11. Schematic diagram showing the track registration geometry used for angular distribution measurements (Choudhury *et al* 1979).

flux, time of irradiation, number of target atoms etc. The expected trend of decrease of the anisotropy in the fragment angular distribution with increasing Z^2/A of the compound nucleus was observed. From an analysis of the data, the third chance fission thresholds $(n, 2n'f)$ for the fission of ^{231}Pa and ^{241}Am were evaluated to be 13·2 and 11·1 MeV respectively.

3.4 *Fission isomers*

We now turn our attention to another major area of fission studies namely fission isomers and the double-humped fission barrier which has revolutionised our understanding of the fission process in the last two decades and where SSNTD has played a key role in collecting valuable experimental information. In 1962, at Dubna, USSR, Polikanov *et al* reported the accidental discovery of a 14 millisecond spontaneous fission isotope $^{242}_{95}$Am in a reaction involving accelerated ^{22}Ne ion with ^{238}U. This was a startling result in that the ground state spontaneous fission half-life of $^{242}_{95}$Am estimated from spontaneous fission systematics was about 10^{19} times longer. Subsequent theoretical and experimental research led to the identification of the 14 millisecond spontaneous fission activity as being due to a metastable state of ^{242}Am. This new state of metastability was termed as ' shape isomerism ' to distinguish it from the familiar spin isomerism in the forbidden gamma transitions and the idea of the ' double-humped fission barrier ' was born (Clark 1971).

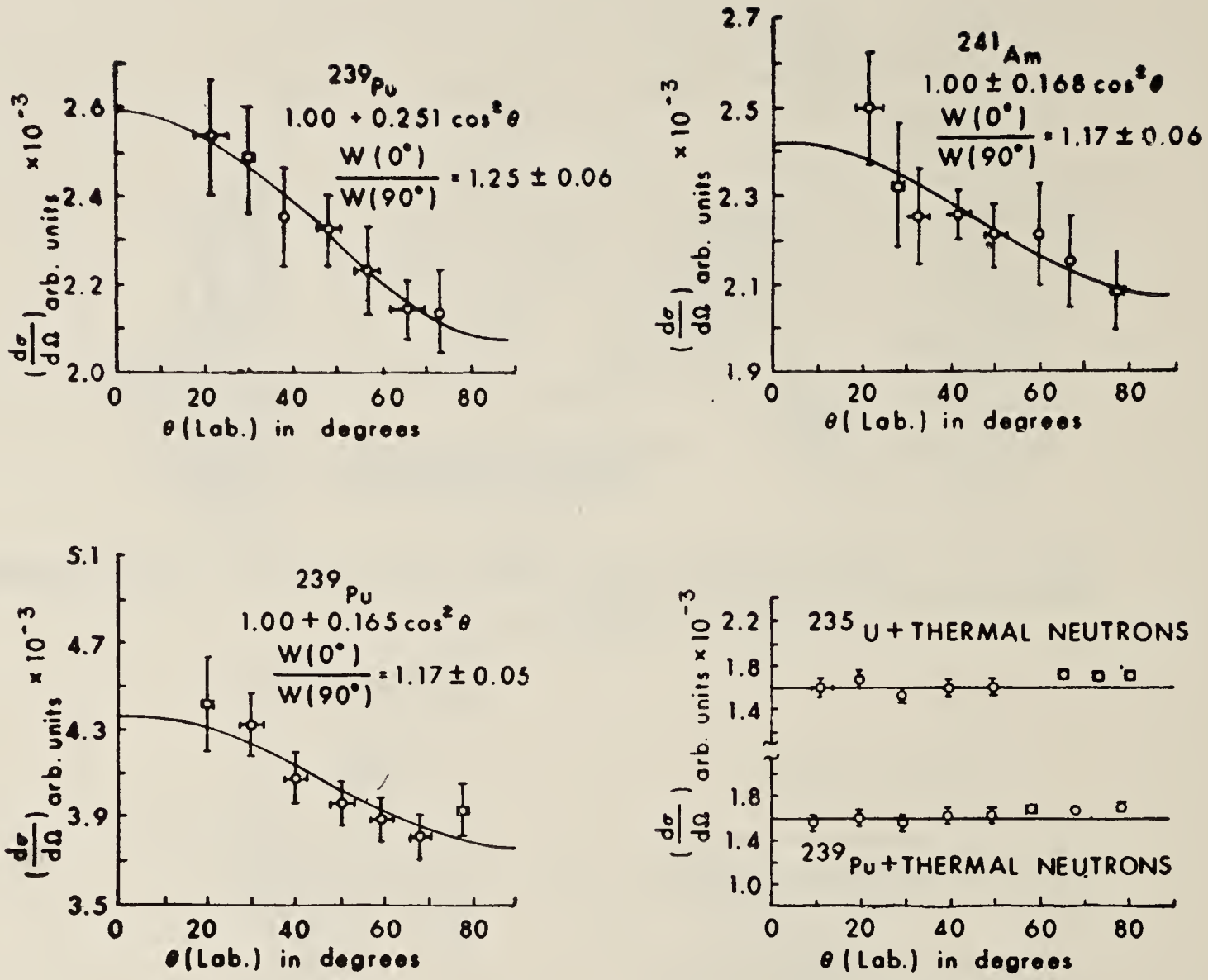

Figure 12. Experimental fission fragment angular distributions in the thermal and 14 MeV neutron induced fission of actinide isotopes (Choudhury *et al* 1979).

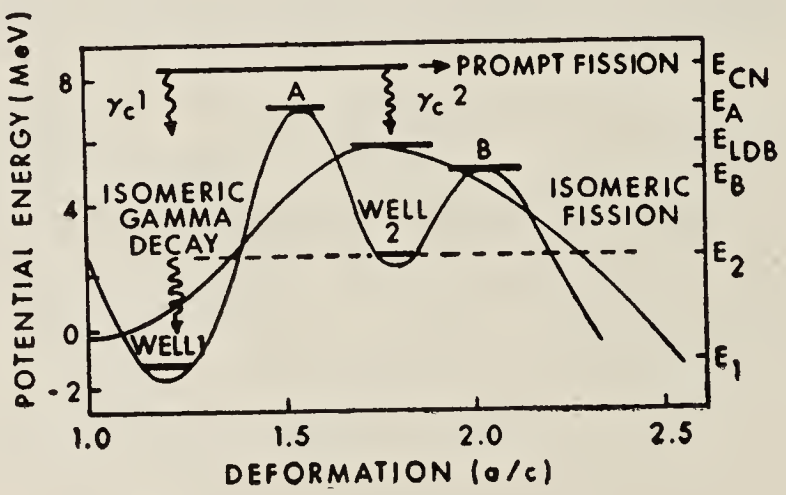

Figure 13. The double-humped fission barrier (Clark 1971).

In order to appreciate the significant role the SSNTDs have played in this area it is worthwhile considering the phenomenon in some detail. Let us do it with the help of figure 13 taken from Clark (1971). In the conventional ground state spontaneous fission, the ground state nucleus tunnels through the entire potential barrier (the single-humped barrier based on liquid drop model shown in the figure) and consequently has long spontaneous fission life-times. This is equivalent to having the nucleus trapped in well 1 with a ground state energy of E_1. On the other hand, if a nucleus is trapped in well 2 with an excitation energy E_2, then, its decay is hindered by both the inner and the outer potential barriers. In other words it is in an isomeric or meta-stable state. Decay to the right (through the smaller barrier) is by isomeric fission and decay to the left by gamma emission. E_A, E_B and E_{LDB} are the heights of the

inner barrier A, outer barrier B and the liquid drop barrier respectively. A nucleus excited to an excitation energy E_{CN} can de-excite either by prompt fission or by gamma decay into the wells 1 and 2.The enormous enhancement of the fission rate of ^{242m}Am can now be understood by assuming it as an isomeric state trapped in well 2 where the probability of tunnelling through the 2nd barrier B is much greater compared to the ground state nucleus in well 1.

The main category of experimental support for the existence of the double-humped fission barrier comes from a study of fission isomers. Another piece of experimental evidence is the occurrence of structures in the sub-threshold fission excitation functions in neutron or deuteron-induced reactions of actinide nuclei. Several experimental approaches have been evolved to identify new cases of fission isomers in order to establish the generality of the phenomenon. In these experiments, the rotating drum and the moving belt methods described in § 3·1 have been extensively used in conjunction with mica, makrafol and lexan detectors. The mechanical constraints limit the usefulness of these techniques to half-lives greater than about one millisecond.

The identification of fission isomers with much shorter half-lives (in the nano-second to microsecond region) calls for greater ingenuity on the part of the experimenter—the serious problem being the need to discriminate against the predominant prompt fission process. Using large area plastic track detectors in a geometrical arrangement that shielded prompt fission but recorded delayed fission from nuclei in flight, Lark *et al* (1969) in Copenhagen were able to observe about ten new cases of fission isomers with half-lives ranging from 5 nanosec to 1·5 micro seconds. The experimental arrangement is given in figure 14. The half-lives were calculated from the estimated recoil velocity of the nuclei in flight and the density of fission tracks as a function of distance from the target. A slightly modified approach has been employed by Mehta and coworkers at BARC to measure the isomeric fission cross-section for the ^{238}U (n, n') ^{238m}U reaction in the 14 MeV neutron induced fission of ^{238}U (Chaterjee *et al* 1981). An annular plastic track detector (makrofol) in a recoil geometry was used to register delayed fission events. The plastic detector was kept in the same plane as the target so that it does not register prompt fission events. A catcher foil was kept at a distance of 1·5 cm from the target to stop the recoiling uranium nuclei and to improve the geometrical efficiency of the detector.

As already pointed out, experimental evidence for the double-humped fission barrier comes from the existence of fission isomers as well as from the occurrence of structures in the sub-threshold fission excitation functions. In general, it is observed

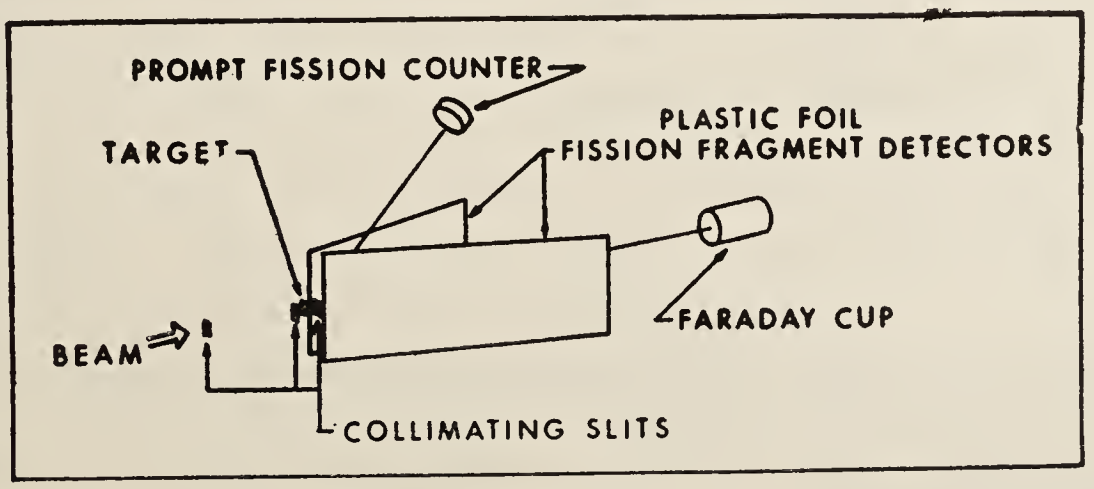

Figure 14. Experimental arrangement for the measurement of half-lives of fission isomers in the nano-second region (Lark *et al* 1969).

that for higher actinides the 2nd barrier is smaller than the 1st barrier (and even disappears with increasing Z) while for the lighter actinides such as thorium, the reverse seems to be the case making gamma decay heavily favoured over fission. This effect probably accounts for the absence of many fissioning isomers in this region. The structures seen in the sub-threshold fission excitation functions of ^{230}Th etc. are correlated with a vibrational resonance in the 2nd well.

A critical and comprehensive account of the information available on double-humped fission barrier that can be deduced from the vast amount of experimental work is given by Bjornholm and Lynn (1980). As of today 45 fission isomers with half-lives in the range of less than 5 picoseconds to 14 milliseconds have been identified in the U-BK region. These are listed in table 2. SSNTDs have played a significant role in the discovery of many of these isomers and have thus contributed to the present state of our understanding of the double humped fission barrier.

3.5 *Search for superheavy elements*

The existence of an island of stable elements beyond the present periodic table has been predicted by theoretical extrapolations of the nuclear properties (Seaborg 1969;

Table 2. Occurrence and half-lives of fission isomers in the uranium-berkelium region*

Nucleus	$t_{1/2}$	Nucleus	$t_{1/2}$
^{236}U	125 ± 15 nsec(a)	^{237}Am	5 ± 2 nsec
^{238}U	195 ± 30 nsec(a)	^{238}Am	35 ± 4 μsec
	> 1 nsec	^{239}Am	163 ± 12 nsec
^{237}Np	40 ± 12 nsec(a)	^{240}Am	0·91 ± 0·07 msec
^{235}Pu	30 ± 5 nsec	^{241}Am	1·5 ± 0·6 μsec
^{236}Pu	40 ± 15 psec	^{242}Am	14 ± 0·7 msec
	34 ± 8 nsec	^{243}Am	5·5 ± 0·5 μsec
^{237}Pu	110 ± 12 nsec	^{244}Am	1·0 ± 0·15 msec
	1·1 ± 0·08 μsec	^{245}Am	640 ± 60 nsec
^{238}Pu	0·5 ± 0·2 nsec	^{246}Am	73 ± 10 μsec
	6·0 ± 1·5 nsec	^{240}Cm	10 ± 2 psec
^{239}Pu	8·1 ± 0·8 μsec		55 ± 5 nsec
	3·0 ± 2 nsec	^{241}Cm	15 ± 1 nsec
^{240}Pu	3·8 ± 0·3 nsec	^{242}Cm	40 ± 15 psec
^{241}Pu	24 ± 1 μsec	^{243}Cm	180 ± 70 nsec
			42 ± 6 nsec
	30 ± 5 nsec	^{244}Cm	< 5 psec
^{242}Pu	3·6 ± 0·6 nsec		> 100 nsec
	50 ± 30 nsec	^{245}Cm	13 ± 2 nsec
^{243}Pu	60 ± 15 nsec	^{242}Bk	600 ± 100 nsec
^{244}Pu	0·4 ± 0·1 nsec		9·5 ± 2 nsec
^{245}Pu	90 ± 30 nsec	^{243}Bk	5 ± 2 nsec
		^{244}Bk	820 ± 60 nsec
		^{245}Bk	2 ± 1 nsec

*Taken from Bjornholm and Lynn (1980).

In a number of nuclei 2 decay periods are identified. The second one is presumably due to an excited state in the second well.

(a) gamma decay to the left competes with fission to the right of the second well.

Otto *et al* 1978). During the past 10-12 years extensive search for superheavy elements (SHE) both in nature and in the laboratory *viz.* heavy ion induced nuclear reactions has been made but without much success. In these searches, SSNTDs have played a significant role and they will continue to do so in future also. We outline some of the techniques used in this continuing search and the current thinking on where and how to look for SHE in nature and in the laboratory. Most of the information is based on the work of Seaborg, Flerov and Hermann and their colleagues in the USA, USSR and FRG respectively (Otto *et al* 1978; Flerov *et al* 1978; Hermann 1979).

The search for SHE in nature are based on two assumptions: (a) they decay either by spontaneous fission or are in secular equilibrium with a descendent which decay by SF, (b) they follow the lower homologues both in geochemical fractionation and in industrial processes. A suggestion has been made to look for eka-elements of easily volatile elements in nature (Nurmia 1974). The exciting possibility exists that SHE are produced in supernova explosion or other astrophysical processes and reach the earth's atmosphere or deep-sea sediments as cosmic fall outs (Nurmia 1974).

Let us now consider the possible modes of formation of SHE in the laboratory through heavy ion reactions. Here, three principal mechanisms are considered. The first one is exchange of a few nucleons between the two colliding nuclei in a rather distant collision called *quasi-elastic transfer*. If the collisions are closer, then two new possibilities arise, *viz.* for *complete fusion* or for the nuclei to stick together for about 10^{-21} sec to form a composite system in which the entire kinetic energy of the projectile is transferred into internal excitation or rotation. This process is called *strongly damped or deep inelastic collision*. During such a process a substantial number of nucleons from the projectile can be transferred into the target nuclei. In complete fusion, which is favoured in reactions with light heavy ions such as C, O, Ar etc., the compound nucleus will be highly excited and will decay by evaporation of several nucleons, alpha particles and gamma rays and the residual nucleus may undergo fission. In deep inelastic collisions, the system decays by emission of neutrons, protons, gamma rays or by fission. It is this process which is likely to lead to the formation of SHE. Because of the need for transferring a large number of nucleons to reach the SHE regions, reactions involving very heavy projectiles such as ^{197}Au, ^{208}Pb, ^{238}U, etc. with heavy target nuclei such as ^{238}U, ^{248}Cm, ^{249}Cf, ^{254}Fm are being considered. Table 3 gives a summary of the attempts made so far (1979) to synthesise SHE by complete fusion reactions.

We now consider the various techniques that are employed for the detection of SHE. The spontaneous fission decay with a wide range of half-lives and the large predicted kinetic energy releases essentially form the basis for their detection. In view of the extremely small formation cross-sections (of the order of nanobarns or less) the detection system should be extremely sensitive. The complex nature of the reaction products demands high specificity in addition to sensitivity. The similarity of predicted chemical properties of SHE and their lower homologues also come in handy in selecting natural samples and form the basis of devising chemical separation schemes for isolating SHE fractions from targets irradiated with heavy ions (Seaborg 1969). A general survey of techniques available to detect SHE in heavy ion induced reactions is given in table 4. The measurable half-lives range from a few seconds to about 10^{-18} sec. Of particular interest to our discussion are the mechanical transport systems like rotating drums, moving belt, etc. which

Table 3. Attempts to synthesise SHE by fusion reactions*.

System	Compound nucleus	Upper limit for production cross-section (cm^2)
$^{232}_{90}Th + ^{48}_{20}Ca$	$^{280}110^{170}$	3×10^{-35}
$^{231}_{91}Pa + ^{48}_{20}Ca$	$^{279}111^{168}$	4×10^{-35}
$^{233}_{92}U + ^{48}_{20}Ca$	$^{281}112^{169}$	7×10^{-35}
$^{248}_{96}Cm + ^{40}_{18}Ar$	$^{288}114^{174}$	2×10^{-32}
$^{242}_{94}Pu + ^{48}_{20}Ca$	$^{290}114^{176}$	1×10^{-35}
$^{243}_{95}Am + ^{48}_{20}Ca$	$^{291}115^{176}$	2×10^{-35}
$^{246}_{96}Cm + ^{48}_{20}Ca$	$^{294}116^{178}$	2×10^{-35}
$^{248}_{96}Cm + ^{48}_{20}Ca$	$^{296}116^{180}$	—
$^{208}_{82}Pb + ^{84}_{36}Kr$	$^{292}118^{174}$	1×10^{-30}
$^{208}_{82}Pb + ^{86}_{36}Kr$	$^{294}118^{176}$	6×10^{-35} $1{\cdot}5 \times 10^{-30}$
$^{238}_{92}U + ^{59}_{27}Co$	$^{297}119^{178}$	4×10^{-33}
$^{238}_{92}U + ^{(60)}_{28}Ni$	$^{298}120^{178}$	2×10^{-33}
$^{238}_{92}U + ^{(65)}_{29}Cu$	$^{303}121^{182}$	8×10^{-33}
$^{238}_{92}U + ^{65}_{29}Cu$		2×10^{-33} 4×10^{-34}
$^{232}_{90}Th + ^{76}_{32}Ge$	$^{308}122^{186}$	1×10^{-34}
$^{136}_{54}Xe + ^{170}_{68}Er$	$^{306}122^{184}$	$1{\cdot}5 \times 10^{-33}$
$^{238}_{92}U + ^{76}_{32}Ge$	$^{314}124^{190}$	1×10^{-34}
$^{243}_{95}Am + ^{68}_{30}Zn$	$^{311}125^{186}$	5×10^{-32}
$^{232}_{90}Th + ^{84}_{36}Kr$	$^{316}126^{190}$	5×10^{-30}
$^{238}_{92}U + ^{84}_{36}Kr$	$^{322}128^{194}$	8×10^{-29}

*Taken from Hermann (1979).

are applicable to species with millisecond half-lives and the crystal blocking technique which are applicable to the extreme region of 10^{-14}—10^{-18} sec.

Hundreds of natural samples including lead from old cathedrals, manganese nodules from the ocean floor, water from hot springs, meteorites and lunar samples have been investigated for possible evidence for SHE based on direct or indirect detection of fission events. Fission tracks are looked for in glass, mica or plastics in contact with the sample. Neutrons emitted in the fission process are also looked for. Assuming a half-life of 10^9 years, these detection techniques have a sensitivity of

Table 4. Techniques for detection of SHE produced in heavy ion reactions

Technique	Approximate range of half-lives (seconds)	Cross-section limit (cm^2)	Remarks
Chemical separation	1 to 10^7	10^{-36}	Combined with fission fragment detection. Corresponds to one atom of SHE per 10^{12} reactions.
Gas jet system	0.1	—	Activity is transported from production site to detector.
Mechanical transport Drums and Tapes	10^{-3} — 10^4	10^{-35}	
Magnetic and electrostatic detection	10^{-6} — 10^6	10^{-34}	
Time of flight and energy loss	10^{-8} — 10^{-3}	10^{-28}	
TOF-d*E*/dX-*E*			
Decay in flight	10^{-10} — 10^{-2}	10^{-33}	Using metal absorber foils and observing fission fragments perpendicular to the flight path, half-lives of 10^{-12} sec can be detected.
Crystal blocking	10^{-14} — 10^{-18}	10^{-30}	

10^{-12} to 10^{-14} g of SHE per gram of the sample. An exhaustive list of searches for SHE with track detectors is given by Fleischer *et al* (1975). While all these searches for SHE in nature have given negative results, there are two recently identified natural sources which deserve attention (Hermann 1979). One is the hot spring water from the Cheleken peninsula in the Caspian sea (Flerov *et al* 1978), and the other the carbonaceous chondrite meteorite Allende. The hot spring water from Cheleken peninsula is rich in volatile elements and is supposed to carry material escaping from great depths in the earth's mantle. Weak spontaneous fission activities have been detected by processing about 2000 cubic metres of water through ion exchange elution and subsequent chemical separations.

The ' superheavy element connection ' of several carbonaceous chondrite meteorites comes from the fact they they contain an excess of neutron rich xenon isotopes of fission origin (*e.g.* ^{136}Xe) as well as volatile elements such as thallium, bismuth and indium (Anders and Heyman 1969; Anders and Larimer 1972). They also contain neutron deficient xenon isotopes giving anomalous $^{136}Xe/^{132}Xe$ ratios. From a parallelism in the condensation history of fissiogenic xenon and of volatile elements it appears that the neutron-rich xenon isotopes originate from the spontaneous fission of a volatile superheavy element eka-bismuth (115), eka-lead (114) or eka-thalium (113) (Anders *et al* 1975). Flerov *et al* (1977) and Popeko and Ter-akopyan (1979) have observed weak spontaneous fission activity of the order of one event per month per kilogram in meteorite Allende. Using an evaporation-condensation technique attempts are being made to concentrate the possible superheavy fraction from Allende (Zvara *et al* 1977).

From the foregoing discussion, it is clear that the searches for SHE both in nature and in the laboratory are continuing but so far SHE has eluded detection. Current

hopes of synthesising superheavy elements are pinned down on the reaction between two colliding uranium nuclei at the Darmstadt UNILAC accelerator (Hermann 1979). With the versatility of SSNTDs coupled with the current developments and refinements in the methodology of detection systems it is hoped that track detectors will play an important role in the eventual discovery of superheavy elements.

3.6 *Absolute fission-yield measurements*

So far, we have been discussing those areas of fission physics and chemistry where the direct or indirect use of solid state nuclear track detectors have contributed immensely to the growth of fundamental knowledge. We now cite one area of fission studies where the use of these detectors has yielded results of applied interest namely, absolute fission yield measurements. This is particularly relevant in the present context when the relevance of basic research is often debated upon.

Accurate fission product nuclear data such as fission yields, cross-sections, decay schemes etc. are required to resolve a number of problems associated with the design and operation of thermal and fast reactors as well as for other applications such as nuclear safeguards. Their importance can be judged from the fact that international conferences on fission product nuclear data are periodically being organised by the IAEA. The current trend with respect to fission yield measurements is towards measurements at known neutron spectrum and *on an absolute basis*. For thermal reactors, the fission product yields of ^{239}Pu and ^{241}Pu are becoming increasingly important, but the yields are more uncertain than those of ^{235}U. Information for calculating decay heat data from fission products following a potential loss of coolant accident are urgently needed for all reactor systems for their safer design. Thes calculations (Baumung 1977) require the independent and fractional chain yields, beta and gamma energies, half-lives etc. of more than 400 short-lived fission products. At present these are estimated from theory.

Measurement of fission product yields require two basic input data: (a) the total number of fissions occurring in the target and (b) the number of fission product atoms formed. The total number of fissions is related to, n, the number of atoms undergoing fissions, σ, the fission cross-section (cm^2), ϕ, the neutron flux (cm^{-2} sec^{-1}) and the irradiation time, t (sec.) by the equation

$$F = n\,\sigma\,\phi\,t.$$

This crucial quantity is generally measured by (i) isotope dilution mass spectrometry, (ii) measuring the neutron flux in the irradiation environment, and (iii) using a fission chamber. The problems and inaccuracies associated with these methods have been reviewed by Lammer and Eder (1973) and by Ramaswami *et al* (1979).

The number of fission product atoms is determined by general radiometric methods (beta or gamma counting) or by mass spectrometry in the case of stable isotopes.

Recently, we have evolved a new approach to absolute fission yield measurements using solid state nuclear track detectors in combination with high resolution gamma ray spectrometry (Ramaswami *et al* 1979; Iyer *et al* 1974). This method is particularly suitable for measurement of absolute yields of short-lived fission products which are very important from the point of view of decay heat calculations and which are not easily amenable to measurements by many other currently available techniques.

The novelty and merit of the technique evolved at Trombay lie in the fact that it eliminates the need for the measurement of neutron flux, fission cross-section, and the exact number of target atoms, thereby eliminating the errors associated with these measurements. The total number of fission F is determined directly with a high degree of accuracy by recording in a mica strip, the number of fissions occurring in a dilute solution of the same target material. The solutions containing the mica strip and the target are irradiated simultaneously in the same irradiation environment. The experimental arrangement is shown in figure 15.

The total number of fissions F is determined from the measured fission track density, Td, (#/cm^2) in the mica strip and from a knowledge of the weight, of the target W(gm), the concentration of the dilute solution, C(g/cm^3) and the track registration efficiency in solution, K_{wet} (cm), by the equation

$$F = n\sigma\phi t = \frac{Td \,.\, W}{K_{wet} \,.\, C}$$

The accuracy of the total number of fissions F depends mainly on the value of K_{wet} which has been determined very carefully in our laboratory (Iyer *et al* 1974). The advantages of using fission track registration in track detectors immersed in solution as compared to track detectors in contact with a plachetted target (McElory *et al* 1970; Larsen *et al* 1972) have been reviewed by Iyer *et al* (1973), the most significant being increased accuracy and ease of quantitative measurements, both stemming from the uniform distribution of track density on the detector. The method has been applied to obtain a set of absolute fission yields in the neutron induced fission of ^{232}Th, ^{233}U, ^{235}U, ^{239}Pu and ^{245}Cm including the yields of fission products with half lives as short as 7 minutes (Ramaswamy *et al* 1979, 1980, 1981). Recently, the method has been extended to the spontaneous fission of ^{244}Cm as well (Raghuraman *et al* 1980). Some

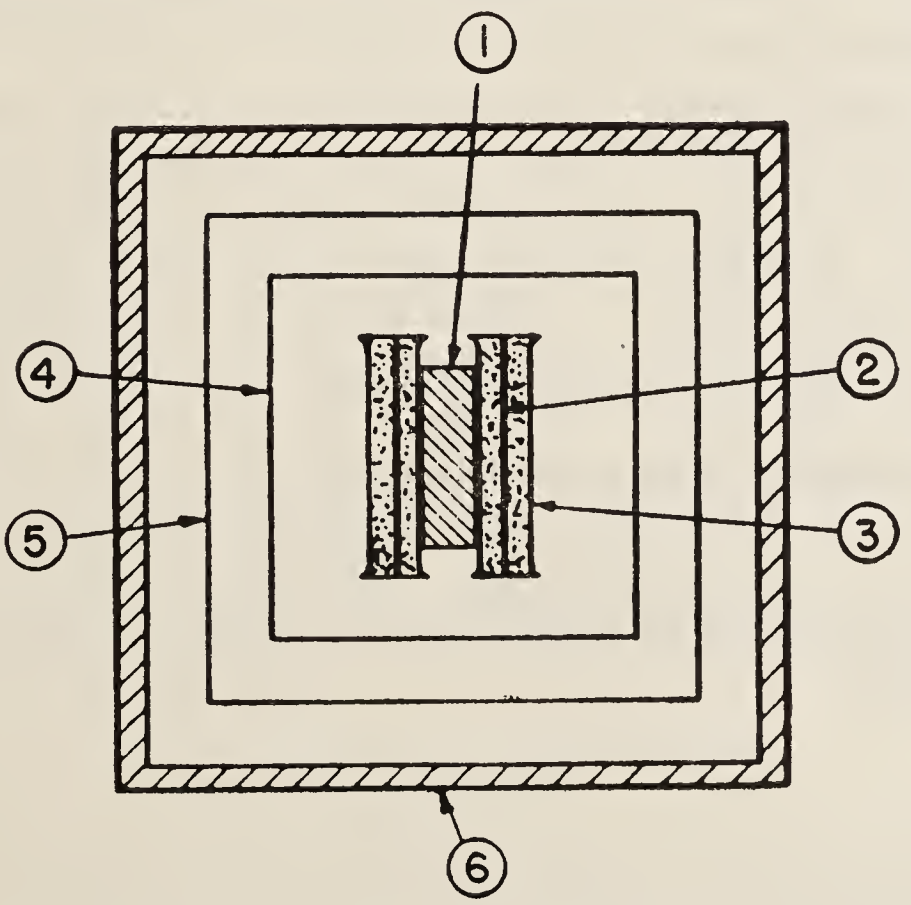

Figure 15. Target-SSNTD arrangement for absolute fission yield measurements: (1) uranyl nitrate sealed in PVC bag, (2) lexan detector immersed in uranyl nitrate solution, (3) polypropylene tube containing uranyl nitrate solution, (4) cadmium foil, (5) sealed PVC bag, (6) harwell aluminium can.

Table 5. Absolute yields of some short-lived fission products in the neutron fission of ^{233}U, ^{235}U and ^{239}Pu†

Fission product	$t_{1/2}$	Fission yield (%) ^{233}U	^{235}U	^{239}Pu
^{87}Kr	76·3 M	—	2·48	—
^{88}Kr	2·8 H	—	2·86	0·9
^{89}Rb	15·2 M	—	4·44	1·46
^{93}Sr*	7·3 M	—	6·37	3·63
^{104}Tc*	18·2 M	—	1·64	5·69
^{134}Te*	41·8 M	—	6·8	4·73
^{134}I	52·6 M	—	7·26	—
^{138}Cs	32·2 M	—	6·55	—
^{139}Ba	1·4 H	6·25	6·34	5.75
^{141}Ba*	18·0 M	—	5·96	5·52
^{142}La	92.7 M	6·58	5·22	4·37

†Source of data: Ramaswami *et al* (1979, 1980, 1981).
*First reported measurement of absolute yields.

recent data are shown in table 5. In addition to obtaining new experimental fission yield data the SSNTD technique has the potential of being extended to measurement of absolute yields of products with half-lives much shorter than those measured so far.

4. Future outlook – problems and prospects

We have had a glimpse of the immense potentialities of solid state nuclear track detectors in probing the many facets of one of the most complex nuclear phenomena, namely nuclear fission. The impact of some of the results obtained through the use of these detectors is indeed far reaching. Any new innovation brings along both promises and challenges: SSNTDs are no exception. A majority of the studies involving tracks of charged particles in SSNTDs is related to the fission process and the presence of these tracks has mainly been used to obtain unambiguos evidence for the occurrence of fission events, with very little effort to precisely identify the particles that caused them. To fully exploit the capabilities of SSNTDs we have to find answers to some of the open problems. A concerted effort on the part of trackologists is needed to precisely identify the charge (Z), mass (M) and energy (E) of the tracks of charged particles in SSNTDs. With recent success in locating newer and better particle track detectors coupled with improvements in track-etching and identification techniques, trackologists have reason to be optimistic about achieving a breakthrough in this area in the coming years. With that, a growing number of exciting new discoveries that depend on a knowledge of Z, M and E of the charged particles are bound to follow.

References

Anders E and Heyman D 1969 *Science* **164** 821
Anders E and Larimer J W 1972 *Science* **175** 981
Anders E, Higuchi H, Cros J, Takahashi H and Morgan J W 1975 *Science* **190** 1262

Baran A 1978 *Phys. Lett.* **B76** 8
Baran A, Pomovski K, Larson S E, Moller P, Nilsson S G, Randrup J, Lukasiak A and Sobiszewski A 1979 *Physics and chemistry of fission*, 4th IAEA Symposium, Julich, (Vienna: IAEA) Vol. 1, p. 143
Baumung K 1977 *Reactor Dosimetry* Proc. Second ASTM-EURATOM Symposium, Palo Alto (Washington: US Nuclear Regulatory Commission) Vol. 2, p. 563
Bjornholm S and Lynn J E 1980 *Rev. Mod. Phys.* **52** 725
Brown F, Mardsen D A and Werner R D 1968 *Phys. Rev. Lett.* **20** 1449
Burnett D S, Gatti R C, Plasil F, Price P B, Swiatecki W J and Thompson S G 1964 *Phys. Rev.* **B134** 952
Chaterjee A, Athougies A L, Kailas S and Mehta M K 1981 *Phys. Rev.* **C24** 1629
Chaudhuri N K, Natarajan V, Sampath Kumar R, Sagu M L and Iyer R H 1979 *Nuclear Tracks* **3** 69
Clark D D 1971 *Phys. Today* **24** 23
Fairhall A W, Jensen R C and Neuzil E F 1958 *Peaceful uses of atomic energy*, Proc II UN Conf., Geneva, (Geneva: UN) Vol. 15, p. 452
Ferguson R L, Bemis C E Jr, Plasil F, Silva R J, O'Kelley G D, Hahn R L, Hensely D C, Keifer M L, Mustafa M G, Hulet E K and Lougheed R W 1979 *Physics and chemistry of fission*, Proc. 4th IAEA Symp., Julich (Vienna: IAEA) p. 208
Fleischer R L, Alter H W, Furman S C, Prize P B and Walker R M 1972 *Science* **178** 255
Fleischer R L and Price P B 1964 *Phys. Rev.* **B133** 63
Fleischer R L, Price P B and Walker R M 1965 *Annu. Rev. Nucl. Sci.* **15** 1
Fleischer R L, Price P B anc Walker R M 1975 *Nuclear tracks in solids: Principle and application* (Berkeley: Univ. of Calif. Press)
Flerov G N, Oganesyan Yu Ts., Lovanov Yu V, Kuznetsov U I, Durin V A, Perelygin V P, Gavrilov K A, Tretiakova S P and Plotko V M 1964 *Phys. Lett.* **3** 73
Flerov G N, Ter-Akopyan, G M, Popeko A G, Fefilow B C and Subbotin V G 1977 *Sov. J. Nucl. Phys.* **26** 236
Flerov G N 1978 Report No. D7-11724 (Joint Inst. for Nucl. Res. Dubna)
Gay R and Sher R 1975 *Nuclear cross-section and technology*, Washington Conf., NBS Spl. Publ. 425 Vol. 2 p. 587
Hermann G 1979 Report No. GSI-79-7, Gesselschaft fur Scheverionen-Forschung, Darmstadt)
Hoffman D C 1967 *Ark Fys.* **36** 533
Hoffman D C 1979 *Physics and chemistry of fission*, 4th IAEA Symposium, Julich (Vienna: IAEA) Vol. 2 p. 275
Hoffman D C, Weber J, Wilhelmy J B, Hulet E K, Landrum J H, Lougheed R W and Wild J F 1976 Report LA-UR-76-1055 (Los Almos Laboratory)
Hoffman D C, Wilhelmy J B, Weber J, Daniels W R, Hulet E K, Landrum J H, Lougheed R W and Wild J F 1977, Report LA-UR-77-2901 (Los Almos Laboratory)
Huizenga J R and Vandenbosch R 1962 in *Nuclear reactions* (ed) P M Endt and P B Smith (Amsterdam: North Holland) vol. 2, p. 42
Hulet E K, Wild J F, Lougheed R W, Evans J E, Qualheim B J, Nurmia N and Ghiorso A 1971 *Phys. Rev. Lett.* **26** 523
Hulet E K, Wild J F, Lougheed R W, Baisden P A, Landrum, J H, Dougan R J, Mustafa M, Ghiorso A and Nitchke J M 1979 *Physics and chemistry of fission*, 4th IAEA Symposium, Julich, (Vienna: IAEA) Vol. 2, p. 299
Iyer R H, Sagu M L, Sampath Kumar R and Chaudhuri N K 1973 *Nucl. Instrum. Methods* **109** 453
Iyer R H, Sampath Kumar R and Chaudhuri N K 1974 *Nucl. Instrum. Methods* **115** 23
Johansson S A E 1959 *Nucl. Phys.* **12** 449
Khan H A and Durrani S A 1972 *Nucl. Instrum. Methods* **98** 229
Khan H A and Durrani S A 1973 *Radiat. Eff.* **17** 113
Lammer M and Leder O J 1973 *Nuclear data in scienee and technology* (Vienna: IAEA)
Lark N L, Sletten G, Pederson J and Bjornholm S 1969 *Nucl. Phys.* **A139** 481
Larsen R P, Dudey N D, Hainrich R R, Armani R J, Gold R, Oldham R D and Popek R J 1972 *Trans. Am. Nucl. Soc.* **15** 483
McElroy M N, Kellog L S, Armani R J, Tochilin E and Zimmer W H 1970 *Trans. Am. Nucl. Soc.* **13** 868

Nurmia M, Sikkeland T, Silva R and Ghiorso A 1967 *Phys. Lett.* **B26** 78
Nurmia N J 1974 Report LBL-4000 (Lawrence Berkeley Laboratory) p. 53
Otto R J, Morissey D J, Seaborg G T and Loveland W D 1978 Report No. LBL-7710 (Lawrence Berkeley Laboratory)
Polikanov S M, Durin U A, Karnavkhov V A, Mikheev V L, Pelve A A, Skobelev N K, Subbotin V G, Ter-akopyan G M and Fomichev V A 1962 *Sov. Phys. JETP* **15** 1016
Popeko A G and Ter-akopyan G M 1979 *Yad. Fiz.* **29** 604
Raghuraman K, Ramaswami A, Srivastava B K, Natarajan V, Jadhav A V, Sivaramakrishnan C K and Iyer R H 1980 *Proc. DAE Symp. on Nucl. and Radiochemistry, Waltair*, 147
Raisbeck G M and Cobble J W 1967 *Phys. Rev.* **153** 1270
Ramaswami A, Natarajan V, Srivastava B K, Sampath Kumar R, Chaudhuri N K and Iyer R H 1979 *J. Inorg. Nucl. Chem.* **41** 1531
Ramaswami A, Natarajan V and Iyer R H 1980 *J. Inorg. Nucl. Chem.* **42** 1213
Ramaswami A, Natarajan V, Srivastava B K and Iyer R H 1981 *J. Inorg. Nucl. Chem.* (in press)
Randrup J, Tsang C F, Moller P, Nilsson S G and Larson S E 1973 *Nucl. Phys.* **A217** 221
Randrup J, Larson S E, Moller P, Nilsson S G, Pomovsky K and Sobiczewski A 1976 *Phys. Rev.* **C13** 229
Seaborg G T 1969 *J. Chem. Educ.* **46** 626
Turkevich A and Niday J B 1951 *Phys. Rev.* **84** 52
Wild J F, Hulet E K, Loaghead R W, Landrum J H, Nitschke J M and Ghorso A 1979 ACS/CSJ Chemical Congress (Abstract-NUCL-64) Honolulu
Zvara L, Flerov G N, Zhuikov B L, Rutz T, Shalaevskii M R 1977 *Sov. J. Nucl. Phys.* **26** 240

Nuclear Tracks: Researches in Space Physics, Geophysics and Nuclear Physics; contains seven invited review papers presented at the second National Seminar-cum-Workshop on Nuclear Tracks held during February, 1981 at the Physical Research Laboratory, Ahmedabad. These papers, authored by both Indian and foreign scientists, deal with topics of current research interest in the field of use and application of nuclear track technique, and include researches in lunar samples and meteorites, fission track geochronology, contemporary and ancient cosmic rays in the interplanetary space, and fission studies. This volume should serve as an excellent source book for research workers involved in these fields of research, and will be invaluable for scientists and research students interested in understanding the developments taking place in the different fields of research using the nuclear track technique.